Crustal thickening in the early Mesoarchaean? Insight from ancient high-pressure metamorphism in SW India

Thesis submitted in accordance with the requirements of the University of Adelaide for an Honours Degree in Geology

Mitchell Jae Bockmann

November 2017

THE UNIVERSITY of ADELAIDE

CRUSTAL THICKENING IN THE EARLY MESOARCHAEAN? INSIGHT FROM ANCIENT HIGH-PRESSURE METAMORPHISM IN SW INDIA

RUNNING TITLE: CRUSTAL THICKENING IN THE EARLY MESOARCHAEAN

ABSTRACT

Eoarchaean–Mesoarchaean crust typically registers uniformly high *T/P* metamorphism, thought to reflect a stagnant lid tectonic regime in the primitive Earth. However, we report evidence for high-pressure granulite metamorphism from the early Mesoarchaean in south-west India. Garnet-kyanite-rutile-bearing assemblages in felsic granulites record minimum peak metamorphic conditions of 13.1 kbar and 940 ^{o}C. LA–ICP–MS analysis of zircon and monazite U–Pb isotopes and trace elements indicate high-pressure granulite facies metamorphism took place at *ca.* 3.15 Ga. Apparent thermal gradients of 72°C/kbar correspond to burial beneath ~45km of continental crust. The preservation of crust under these conditions is not expected this early in the Earth's history under the conditions proposed for the stagnant lid regime. This implies that the transition toward a more modern style tectonic regime may have taken place earlier than what is currently recognised.

KEYWORDS

Crustal thickening, Mesoarchaean, metamorphism, high-pressure, India, U–Pb geochronology, pseudosection

TABLE OF CONTENTS

LIST OF FIGURES AND TABLES

INTRODUCTION

Evidence for high-pressure metamorphism within Archaean crustal rocks is rare (Brown, 2007a). This absence is generally perceived as a reflection of the Earth's thermal structure before the onset of secular cooling (Brown, 2007a, 2007b). It is proposed that during this time, typical Archaean crustal thicknesses of 45km would undergo basal delamination when brought into contact with suggested mantle temperatures of up ~1600°C (Johnson, Brown, Kaus, & VanTongeren, 2014). Furthermore, this suggests that subduction, if present at all, had different dynamics to the modern day and could have only occurred at shallow angles due to the effect of greater mantle temperatures on crustal strength and buoyancy (Brown, 2007a, 2014; Johnson, Brown, Gardiner, Kirkland, & Smithies, 2017; Johnson et al., 2014; Van Hunen & Moyen, 2012). However, numerical models have been produced to account for the transition between a delaminating lithosphere and a subducting lithosphere (Sizova, Gerya, Brown, & Perchuk, 2010). These models reconcile the geological evidence for ultra-high temperature and very rare high-pressure metamorphism during the Archaean, with evidence suggesting the first transition toward modern style tectonics occurring in the late Archaean. Currently, the oldest recorded preservation of high pressure metamorphism occurs within the Barberton granitoid-greenstone terrain, at *ca.* 3.23 Ga, where garnet-albite-bearing mineral assemblages

within supracrustal amphibolites recorded conditions of 12–15 kbars at temperatures of 600–650°C. These conditions coincide with apparent geothermal gradients of 12–15°C km^{-1}, which are comparable to geothermal gradients associated with modern subduction (Van Hunen & Moyen, 2012). Recently, another pre-Neoarchaean high-pressure metamorphic occurrence has been proposed in the Mercara Shear Zone in south-west India (Amaldev et al., 2016; Mansfield, 2016). The Mercara Shear Zone is a proposed suture, formed through the collision of the Coorg Block and the Western Dharwar Craton between *ca.* 1.5–1.2 Ga (Ishwar-Kumar et al., 2016; Santosh et al., 2015). However, studies show that the rocks of the Mercara Shear Zone were subject to metamorphism prior to this event. Rekha, Bhattacharya, and Chatterjee (2014) calculated a U–Th total Pb monazite chemical age of *ca.* 2.5 Ga, while a reconnaissance study from Mansfield (2016) alluded to the potential for high-pressure granulite facies metamorphism during the Mesoarchaean at *ca.* 3.07 Ga. That study inferred peak metamorphic conditions of 11–13 kbars at *ca.* 860 °C, conditions that correlate to burial beneath ~40km of continental crust. Another study by Amaldev et al. (2016) also reported similar conditions at this time, producing peak conditions of 10–12 kbar at 700–900 °C.

The absence of high pressure metamorphism during the earlier stages of the Archaean essentially constitutes the evidence upon which the hypothesis for stagnant lid tectonics is built (Brown, 2006, 2014; Johnson et al., 2014). However, metamorphic evidence for significant crustal thickening within the rocks in this study, combined with potential evidence of subduction within the Barberton granitoid-greenstone terrain (Moyen, Stevens, & Kisters, 2006) better support Archaean tectonic models put forward by Sizova et al. (2010). Whilst there have been geochronological and pressure–temperature (*P–T*) studies undertaken on the Mesoarchaean rocks of the Mercara Shear Zone, the constraints

on *P–T* conditions and metamorphic age are lacking. *P–T* phase equilibria models by Amaldev et al. (2016) are inappropriate because they inferred subsolidus conditions in rocks that are clearly migmatitic. Meanwhile, age constraints from Mansfield (2016) can be improved by application of trace element analysis and in-situ age dating to better link the mineral assemblages with age constraints.

In this study, zircon and monazite U–Pb geochronology are combined with trace element data, providing a link between ages and the equilibrium assemblage of the rock. In addition, a detailed metamorphic study with phase equilibria models and calculated modes constrain the peak conditions, as part of a full pressure–temperature–time *(P–T–t)* evolution of the hypothesized Mesoarchaean high-pressure granulite metamorphic event. This study aims to provide evidence that can be used to improve the current understanding of tectonic processes operating during the Archaean.

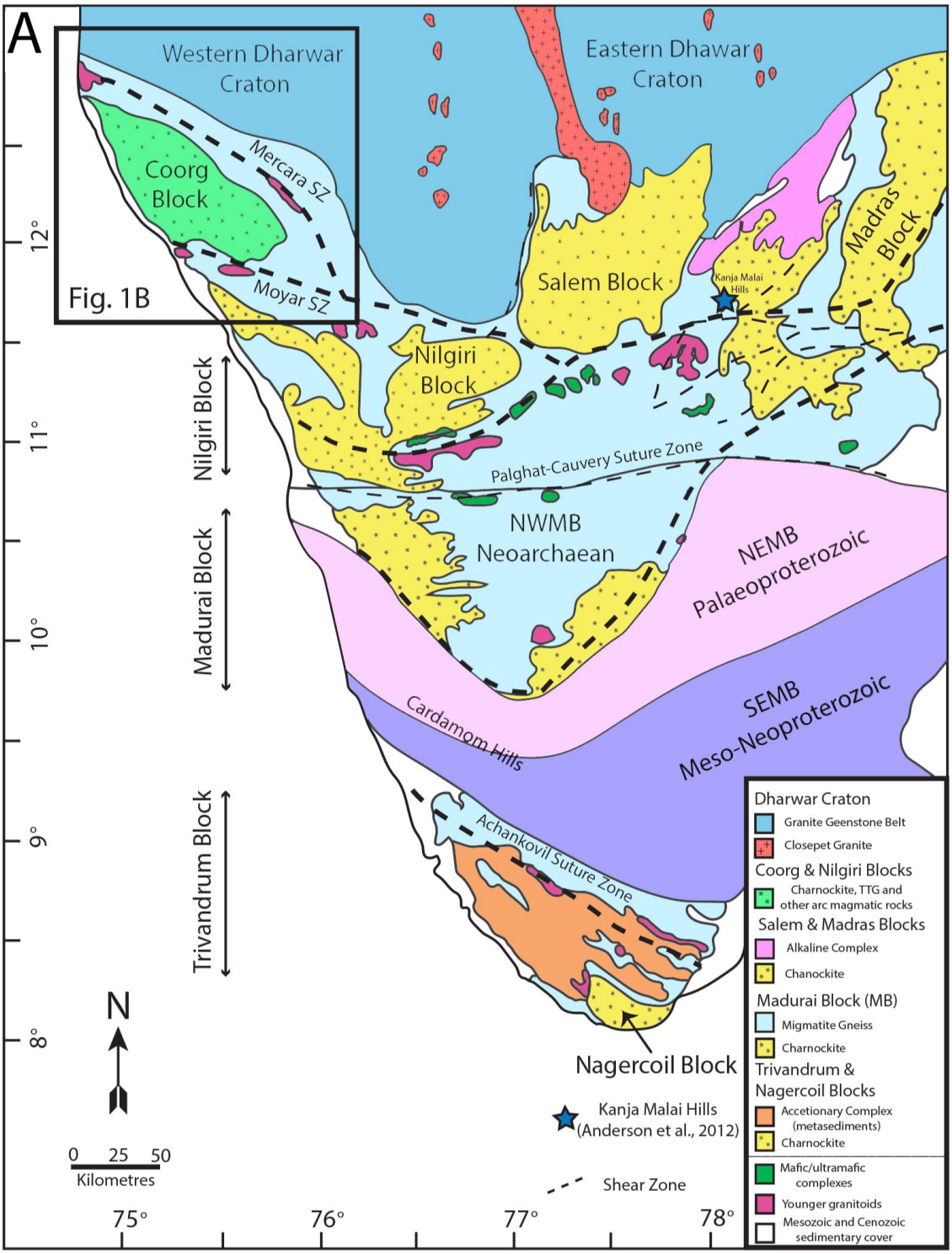
A
Western Dharwar Craton
Eastern Dhawar Craton
Coorg Block
Mercara SZ
Moyar SZ
Fig. 1B
Salem Block
Kanja Malai Hills
Madras Block
Nilgiri Block
Palghat-Cauvery Suture Zone
NWMB
Neoarchaean
NEMB
Palaeoproterozoic
SEMB
Meso-Neoproterozoic
Cardamom Hills
Achankovil Suture Zone
Nagercoil Block
Kanja Malai Hills (Anderson et al., 2012)
Shear Zone
Nilgiri Block
Madurai Block
Trivandrum Block
12°
11°
10°
9°
8°
75°
76°
77°
78°
N
0 25 50
Kilometres
Dharwar Craton
Granite Geenstone Belt
Closepet Granite
Coorg & Nilgiri Blocks
Charnockite, TTG and other arc magmatic rocks
Salem & Madras Blocks
Alkaline Complex
Chanockite
Madurai Block (MB)
Migmatite Gneiss
Charnockite
Trivandrum & Nagercoil Blocks
Accetionary Complex (metasediments)
Charnockite
Mafic/ultramafic complexes
Younger granitoids
Mesozoic and Cenozoic sedimentary cover

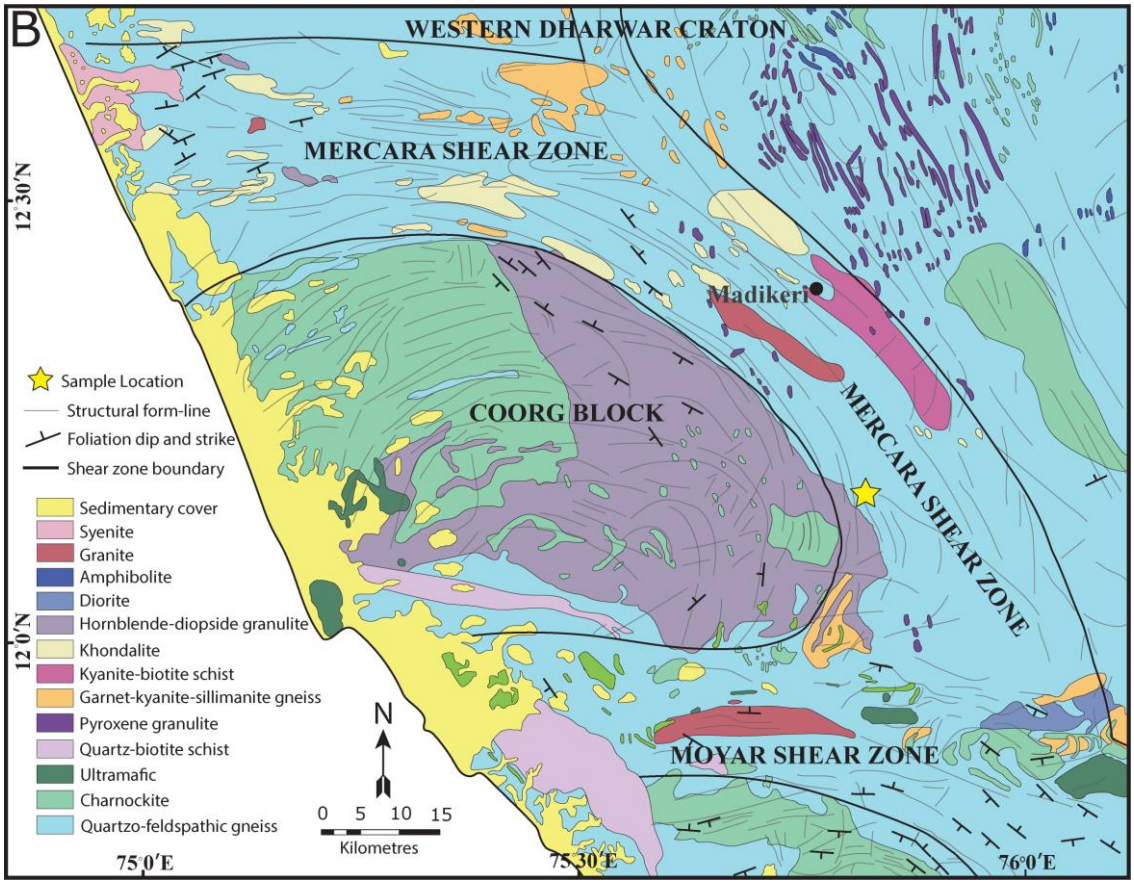

Figure 1: Geological maps of the study area (a) Generalised geological map of the broader geology of central southern India (modified after Santosh et al., 2015). (b) Detailed geological map of the study area (adapted from Ishwar-Kumar et al., 2016).

GEOLOGICAL SETTING

MERCARA SHEAR ZONE

The Mercara Shear Zone is a curvilinear transpressional shear zone that separates the Coorg block from the southern margin of the Western Dharwar Craton. The shear zone extends for a strike-length of over 100 km, along which examples of dextral movement are well documented. The shear zone is marked by a steep gravity gradient that has been interpreted to signify dense mafic/ultramafic underplating of the lower crust (Chetty, Mohanty, & Yellappa, 2012).

Lithologically, the Mercara Shear Zone is dominated by granulite-facies metapelites, largely consisting of mylonitic quartzo-feldspathic and biotite-rich gneisses. Felsic garnet-kyanite-sillimanite-bearing gneisses, Tonalite–Trondhjemite–Granodiorite (TTG) gneisses and mafic granulites also feature, occasionally intruded by Cryogenian-aged suites of syenites and granites (Fig. 1b) (Fig. 1b; Chetty et al., 2012; Ishwar-Kumar et al., 2016; Santosh et al., 2014; Santosh et al., 2015). Rocks of the Mercara Shear Zone have previously been correlated with the Sargur supracrustals of the Western Dharwar Craton (Adiga, 1982; Nair, Vidyadharan, Pawar, Sukumaran, & Murthy, 1976; Nutman, Chadwick, Ramakrishnan, & Viswanatha, 1992), but other authors have proposed these are exotic to the Dharwar Craton (Santosh et al., 2015).

A number of metamorphic ages have been proposed from the Mercara Shear Zone, portraying a complex tectonic history.

In addition to proposed suturing ages of *ca.* 1.2 Ga and 1464 $\pm$ 94 Ma (Ishwar-Kumar et al., 2016; Santosh et al., 2015), Rekha et al. (2014) obtained Th–U total Pb monazite chemical ages of 2.5–2.2 Ga from a range of different lithologies in the west of the Mercara Shear Zone. These ages correlate well with metamorphic ages from the Betsimisaraka Suture Zone of Madagascar, leading authors to interpret the Betsimisaraka Suture Zone as the western extension of the Mercara Shear Zone. More recent metamorphic studies on the Mercara Shear Zone have revealed an older metamorphic event from the Mesoarchaean. Amaldev et al. (2016) recorded metamorphic overgrowths on zircon rims, giving a U–Pb age of *ca*. 3.0 Ga, while Mansfield (2016) obtained U–Pb zircon and monazite geochronology, giving an interpreted metamorphic age of *ca*. 3.07 Ga. These studies also produced thermobarometric constraints on the metamorphic peak of this event in the Mercara Shear Zone. Amaldev et al. (2016) conducted phase equilibria

modelling on mafic granulite, calculating peak conditions of 10–12 kbars at 700–900 ºC. Mansfield (2016) modelled a kyanite-sillimanite-garnet-bearing felsic granulite with near-peak conditions of 11–13 kbar at *ca.* 860 ºC.

WESTERN DHARWAR CRATON

The Dharwar Craton is largely composed of a Mesoarchaean Tonalite–Trondhjemite–Granodiorite (TTG) gneiss complex, commonly referred to as the Peninsular Gneissic Complex (Adiga, 1982; Bhaskar Rao, Sivaraman, Pantulu, Gopalan, & Naqvi, 1992; Hegde & Chavadi, 2009; Ramakrishnan & Nath, 1981). Lying unconformably above this system are two generations of greenstones; the 3.58–3.23 Ga Sargur Group, and the younger (2.9–2.6 Ga) Dharwar Supergroup (Nutman et al., 1992; Nutman, Chadwick, Rao, & Vasudev, 1996; Peucat, Bouhallier, Fanning, & Jayananda, 1995). A later suite of calc-alkaline to potassic granites also occur between 2.61–2.5 Ga (Jayananda, Chardon, Peucat, & Capdevila, 2006). The Western Dharwar Craton gradually increases in metamorphic grade from greenschist facies in the north to upper amphibolite facies in the south. It also exhibits a broad N-S to NNW structural trend, as a result of Neoarchean E–W compression (Chardon, Jayananda, Chetty, & Peucat, 2008).

COORG BLOCK

The origin of the Coorg Block is still uncertain. Santosh et al. (2015) suggested it formed from passive margin sediments developed in Proterozoic continental rifts. It then became its own microcontinent and was sutured onto the Western Dharwar Craton between 1.5–1.2 Ga (Ishwar-Kumar et al., 2016; Santosh et al., 2015). Other authors challenge this model, suggesting that the Coorg Block is the higher grade southern extension of the Western Dharwar Craton (Bhaskar Rao et al., 1992; Devaraju & Janardhan, 2004; Ghosh,

de Wit, & Zartman, 2004; Peucat, Mahabaleswar, & Jayananda, 1993; Rao et al., 2003; Sato, Santosh, Tsunogae, Chetty, & Hirata, 2011).

Lithologically, the Coorg Block is dominated by charnockites and TTG (Tonalite–Trondhjemite–Granodiorite) gneisses, with common occurrences of granite, diorite and metamorphosed felsic volcanic tuffs. Vijaya Kumar et al. (2013) published U–Pb zircon ages $\geq$ 3.3 Ga from a sample in the northern part of the Coorg Block, with the oldest concordant zircons having ages of *ca.* 3.9 Ga. *P–T* modelling of the Coorg granulites recorded near-peak metamorphic conditions of 7–8.6 kbar at 720–760°C, and a *P–T* path suggesting rapid uplift and erosion of a tectonically thickened crust (Srikantappa, Venugopal, Devaraju, & Basavalingu, 1994). More recently, Santosh et al. (2015) used the mineral chemistry of hornblende in Coorg Block charnockite to calculate *P–T* conditions of ~6 kbar at 820–870 °C.

Study area and sample selection

The samples used in this study were taken from an outcrop of anatectic gneiss, located approximately in the centre of the Mercara Shear Zone (Fig. 1b). The outcrop was selected based on a previous study by Amaldev et al., (2016), where old ages were obtained, but the phase equilibria model assumed subsolidus conditions in rocks that were clearly anatectic in character.

The samples selected are interpreted to reflect progressive stages of the metamorphic evolution. Sample Co17-37 is interpreted as the near-peak assemblage, with samples Co17-38–40 representing increasingly intense retrogression toward the most retrogressed sample, Co17-41 (Fig. 3).

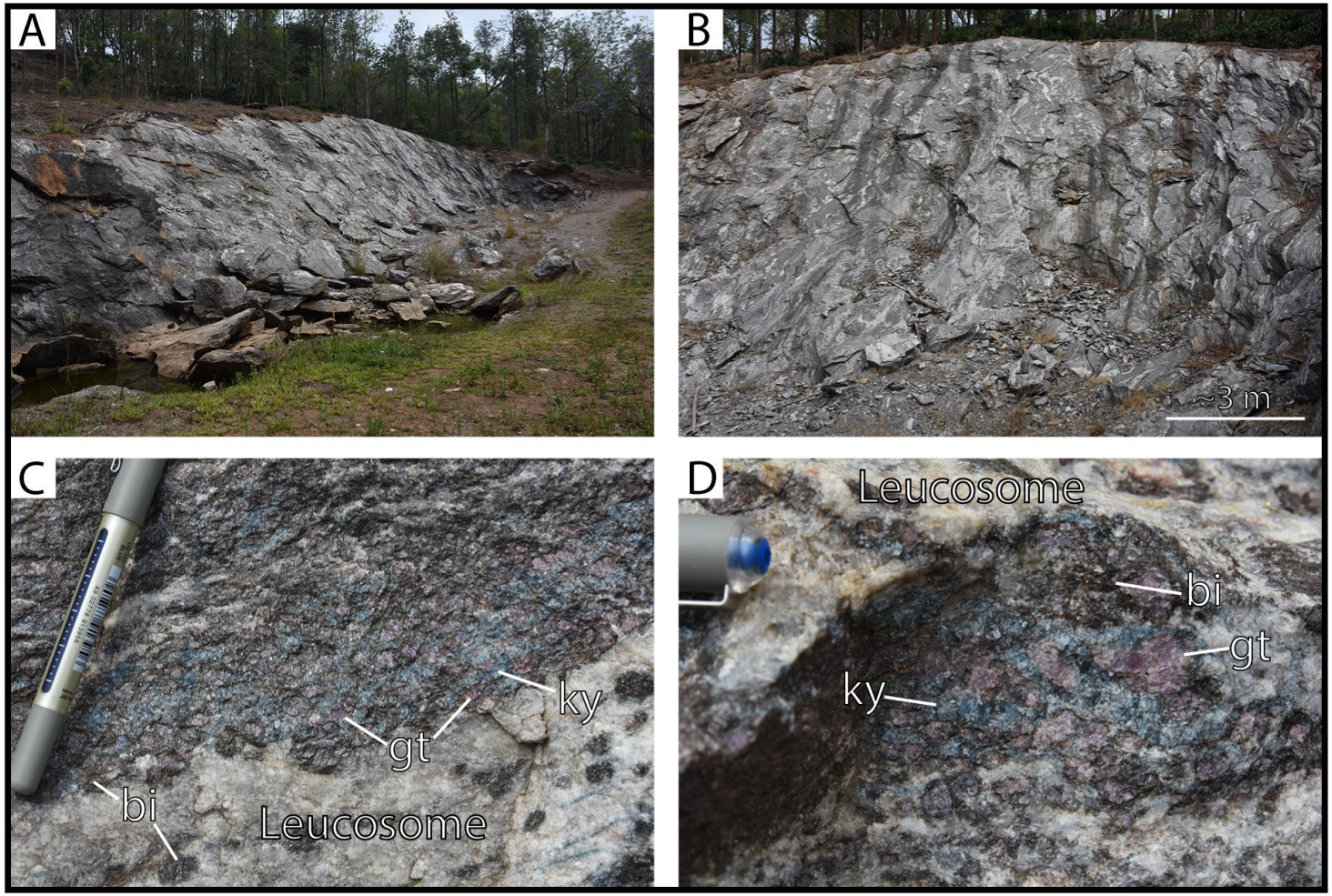

Figure 2: Anatectic garnet–kyanite–biotite gneiss outcrop where the samples in this study were taken. (a, b) Images of the outcrop, showing pale leucosomes percolating through the rock. (c, d) Near-peak garnet–kyanite assemblages in close proximity to leucosomes within the outcrop. Outcrop coordinates are: N12º 20' 26.4" E75º 49' 8.4".

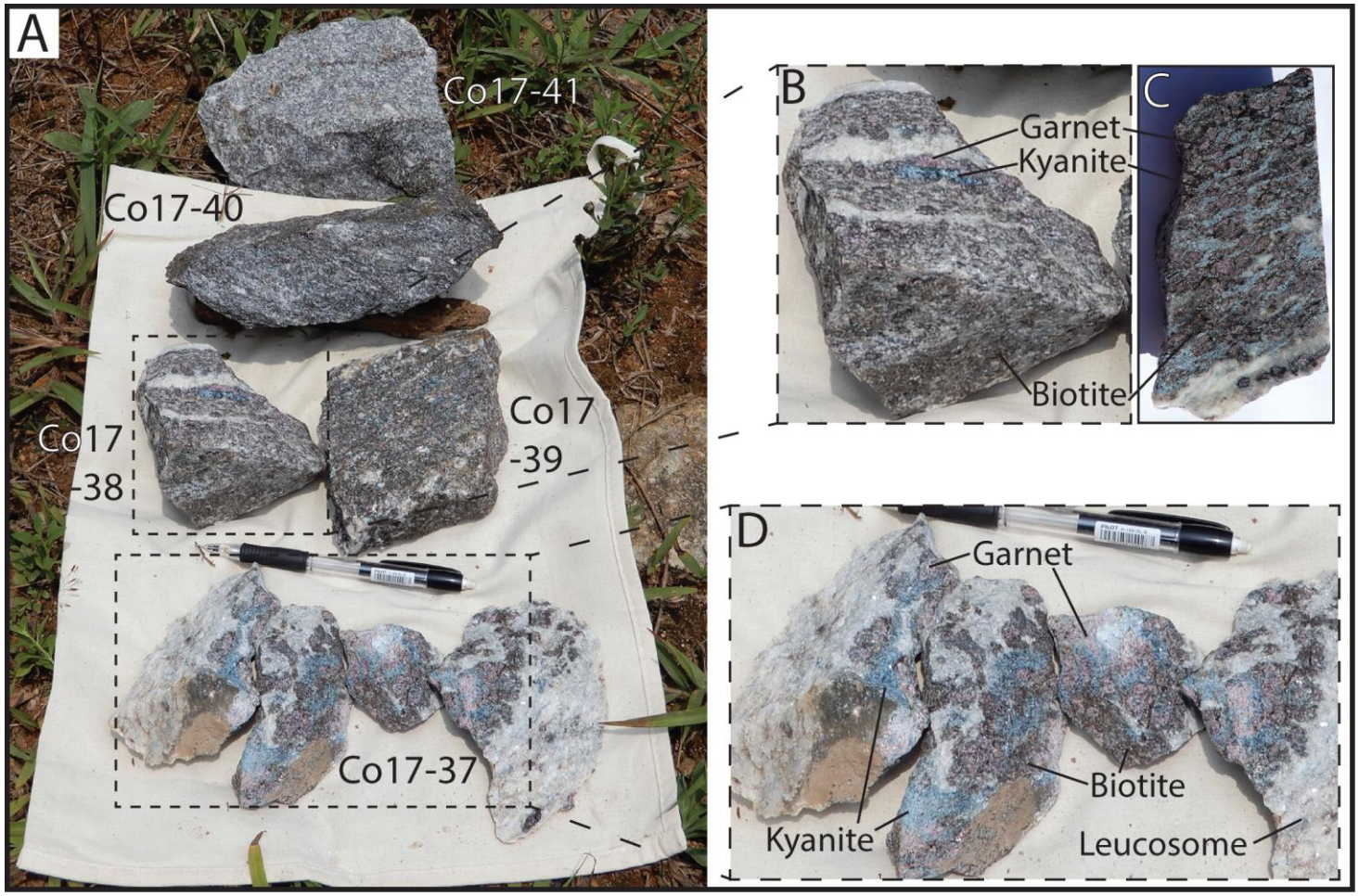

Figure 3: Samples used in the study. (a) All samples collected from the outcrop in Fig. 2. Data for samples Co17-39 and Co17-40 are not presented in this study. (b) close-up image of sample Co17-38 collected in the field. (c) sample Co17-38 with a wet and recently cut surface, highlighting blue kyanite, purple garnet and black biotite. (d) A close-up image of the four rocks that collectively comprise near-peak sample Co17-37

ANALYTICAL METHODS

U–Pb LA–ICP–MS geochronology

Zircon and monazite U–Pb isotopic data were acquired from three samples using Laser Ablation–Inductively Coupled Plasma–Mass Spectrometry (LA–ICP–MS) using a RESOlution LR 193 nm Excimer laser system coupled with an Agilent 7700s ICP–MS at Adelaide Microscopy, University of Adelaide, following the methods of (Payne, Hand, Barovich, & Wade, 2008). All three samples were analysed in-situ so that relationships with the major metamorphic minerals could be maintained. Samples Co17-38 and Co17-41 were further analysed using zircon and monazite grain separates to create larger data sets. Data processing and reduction was performed using the software *Iolite* (Hellstrom, Paton, Woodhead, & Hergt, 2008; Paton, Hellstrom, Paul, Woodhead, & Hergt, 2011). Sample preparation and analytical procedures are provided in Appendix A. Zircon U–Pb age data are presented in Appendix B, while monazite U–Pb age data are presented in Appendix C.

Trace element LA–ICP–MS

Zircon, monazite and garnet were analysed for trace elements using Laser Ablation–Inductively Coupled Plasma–Mass Spectrometry (LA–ICP–MS) using a RESOlution LR 193 nm Excimer laser system coupled with an Agilent 7700s ICP–MS at Adelaide Microscopy, University of Adelaide. Trace element data for zircon and monazite were collected from all three samples, while garnet trace element data were only collected from samples Co17-37 and Co17-38. Data was processed using *Iolite* software. Extended methods are presented in Appendix D. Trace element data for zircon are presented in Appendix E, monazite trace element data are provided in Appendix F, and garnet trace element data are provided in Appendix G.

Whole-rock geochemistry

Whole-rock chemical compositions were determined for twenty-two samples. The data from two samples were used in the calculation of metamorphic phase equilibria diagrams. Geochemical determination was undertaken at Franklin & Marshall College, Lancaster, Pennsylvania. Extended methods and data are presented in Appendix H.

Electron probe micro analyses (EPMA)

Element X-ray maps and mineral chemical composition analyses were undertaken using a CAMECA SX-five electron microprobe at the University of Adelaide. Garnets were mapped at 15 μm resolution using a beam current of 150 nA and accelerating voltage of 15 kV. Spot analyses were undertaken using a beam current of 20 nA and accelerating voltage of 15 kV. Wavelength Dispersive Spectrometers (WDS) were used for the analysis of Si, Ti, Al, Fe, Mn, Mg, Ca, P, Na and K in X-ray maps and spot analyses. Element X-ray maps and spot analysis values for each mineral can be found in Appendix I.

Phase equilibria calculations

Phase equilibria calculations were performed using THERMOCALC v. 3.40 software (Holland & Powell, 2011; Powell & Holland, 1988) in the model chemical system MnNCKFMASHTOaxOam ($MnO–Na_2O–CaO–K_2O–FeO–MgO–Al_2O_3–SiO_2–H_2O–TiO_2–O$), where O is a proxy for Fe_2O_3, using the latest internally consistent thermodynamic data set, ds6 (Holland & Powell, 2011). Activity-composition (*a*-*x*) models used were taken from (Powell, White, Green, Holland, & Diener, 2014; White, Powell, Holland, Johnson, & Green, 2014) . Whole rock major element geochemical compositions were converted from weight-percent to molar oxide percent to use for

modelling. Calculations in THERMOCALC are manually completed by the user, involving many trial and error calculations to determine which phases appear or disappear as a function of pressure, temperature and/or composition. See Appendix J for more detailed methodology.

RESULTS

Petrography

Samples Co17-37, Co17-38 and Co17-41 were all obtained from the same outcrop of garnet–kyanite–biotite gneiss (Figs 2, 3). Overall, leucosome comprised 37% of the outcrop, with the remnants consisting of gt–ky–bi rich pelite. The three samples are interpreted as components of an initial metamorphic assemblage that underwent progressive retrogression. The peak assemblage is interpreted as: garnet + kyanite + rutile + K-feldspar + quartz + melt. Sillimanite and biotite are preserved from the prograde evolution, while plagioclase, and additional generations of biotite, kyanite and quartz are interpreted as retrograde products.

CO17-37

This sample is interpreted to preserve the best representation of the peak assemblage. Kyanite (up to 5 mm) and highly fractured garnet porphyroblasts (up to 15 mm) dominate the largely anhydrous assemblage. Garnet contains inclusions of early quartz, sillimanite and biotite, along with kyanite and rutile (Fig. 4a, b). Coarse-grained kyanite commonly appears in large aggregates within the matrix (Fig. 4b). Interspersed between porphyroblastic garnet and kyanite are domains of finely intergrown quartz and plagioclase. The finely intergrown textures are interpreted as melt crystallisation (Fig.

4b). Biotite and fine-grained kyanite (10–50 μm) consistently occur around the rims and within fractures of garnet (Fig. 4a). Leucosomes are dominated by K-feldspar (~60%) and quartz (~35%). Microperthitic K-feldspar grains are rimmed by fine grained kyanite coronas (Fig. 4c).

CO17-38

Kyanite (up to 3 mm) and fractured garnet porphyroblasts (up to 6 mm) dominate the assemblage. However, biotite and quartz abundance is significantly greater compared to the near-peak sample. Inclusions of quartz, biotite, sillimanite and kyanite occur in garnet (Fig. 4d, e). Biotite prominently pseudomorphs garnet, but also constitutes a large proportion of the matrix (Fig. 4d, e). Garnet and interpreted plagioclase-quartz bearing recrystallised melt domains are commonly separated by biotite, quartz and fine-grained kyanite (Fig. 4e). The abundance of interpreted recrystallised melt is significantly less than in the near-peak sample.

CO17-41

A gneissic fabric is defined by biotite, garnet and kyanite within a quartz dominated matrix (~85%) (Fig. 4f). Kyanite grains (up to 2 mm) exhibit heavily retrogressed textures, warping in response to the orientation of the fabric. Coarse grained biotite (up to 1mm) wraps around garnet and kyanite grains in the foliation (Fig. 4f).

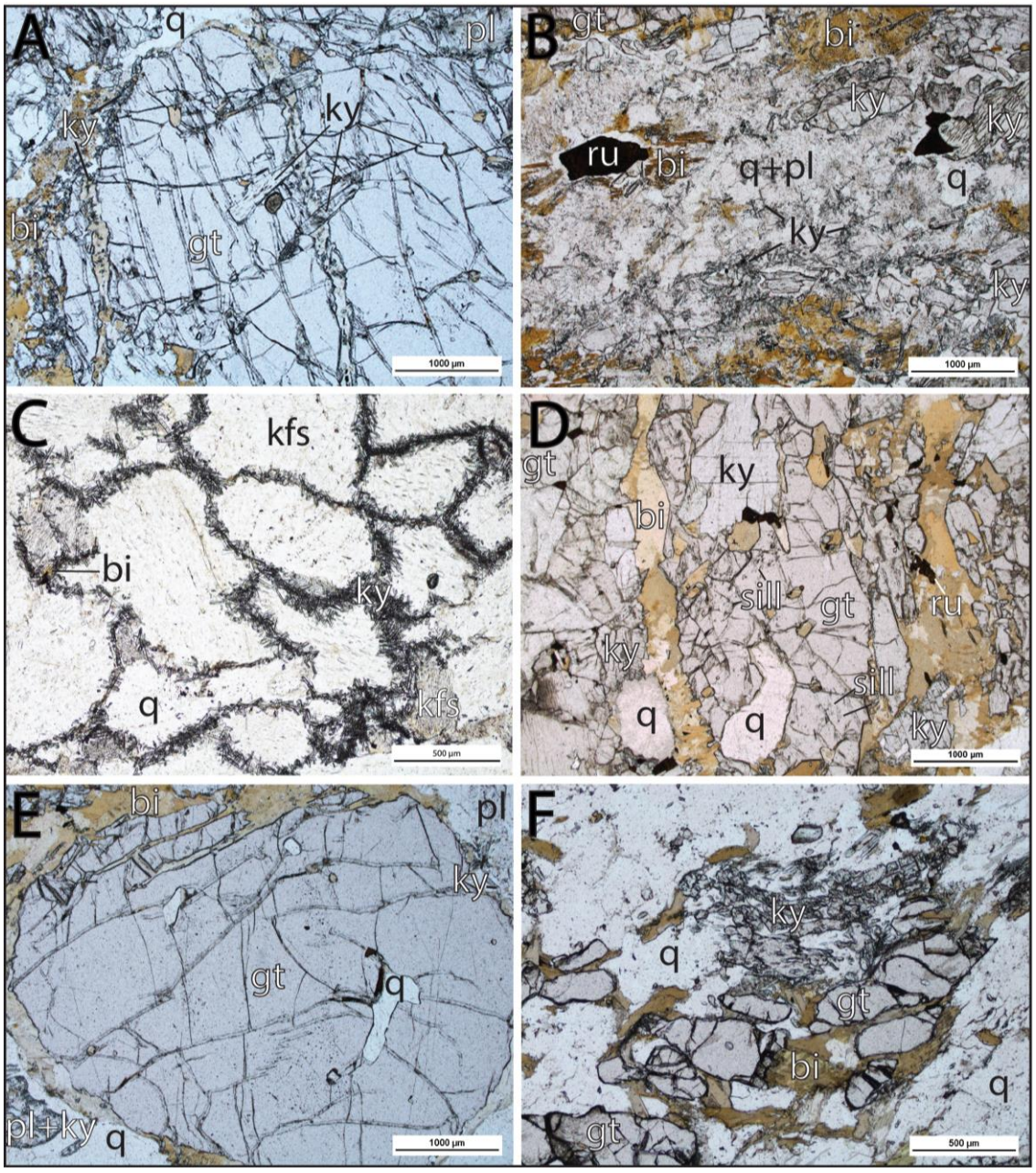

Figure 4: **Photomicrographs of the samples used in this study. (a) Co17-37 showing a fractured garnet porphyroblast with kyanite and biotite inclusions being mantled by biotite and fine grained kyanite. (b) Co17-37 showing fine grained sillimanite needles within garnet, and a domain of finely intertwined quartz and plagioclase captured within the kyanite dominated ground mass. (c) Co17-37 leucosome showing K-feldspar with microperthite textures, rimmed by fine-grained kyanite (d) Co17-38 showing kyanite, rutile and fine sillimanite inclusions within garnet, rimmed by biotite. (e) Co17-38 showing biotite and fine-grained kyanite clearly rimming a large garnet porphyroblast, segregating it from quartz and plagioclase in recrystallised melt. (f) Co17-41 showing garnet, biotite and relict kyanite aligning with the fabric within a largely quartz dominated matrix.**

Abbreviations: gt: garnet, ky: kyanite, sill: sillimanite, bi: biotite, q: quartz, pl: plagioclase, ru: rutile.

Mineral chemistry

Representative analyses of garnet, biotite and plagioclase from samples Co17-37 and Co17-38 are summarised in Table 1. An extended data table containing elemental oxide values is presented in Appendix I. The composition of garnet is similar in both samples, dominated by almandine (42–60%) and pyrope (35–53%). Mg enrichment in the cores and Fe enrichment in the rims and along fractures are observed in both garnets, while Ca and Mn concentrations are comparatively low with little variation. Zonation is more prevalent in sample Co17-38 (Fig. 5a, b, 6a, b). Biotite inclusions in Co17-37 show little difference in x(Mg) when compared to biotite in the matrix. Biotite in Co17-38 shows large differences in x(Mg), with biotite in the matrix being more magnesium rich compared to inclusions (Table 1). The feldspar within domains of recrystallised melt in Co17-38 is plagioclase (69-77% albite, 22-30% anorthite); (Table 1).

Trace element data, acquired through LA–ICP–MS, were also obtained along the traverses shown in Fig. 5. Both samples exhibit similar zoning patterns, though trace element concentrations in sample Co17-38 are significantly less than Co17-37. The heaviest Rare Earth Elements are most enriched in the garnet's core, with concentrations becoming progressively less enriched in lighter REEs. Heavy REEs deplete rapidly from cores to rims, while lighter REEs experience less pronounced changes. Yttrium follows the HREE distribution pattern, depleting from core to rim in both samples (Fig. 6c, d).

Table 1: Representative mineral end-member and compositional data from plagioclase, biotite and garnet in samples Co17-37 and Co17-38. Values listed for end-member compositions in garnet and plagioclase are cation proportions. x(gt): $Fe^{2+}/(Fe^{2+}+Mg)$ and x(Mg): Mg/(Fe+Mg).

	Co17-37		Co17-38	
	Garnet Rim	Garnet Core	Garnet Rim	Garnet Core
x(gt)	0.6098	0.4853	0.6308	0.4455
Almandine	0.5825	0.4695	0.6017	0.4257
Pyrope	0.3727	0.4980	0.3522	0.5298
Grossular	0.0346	0.0262	0.0332	0.0387
Spessartine	0.0102	0.0064	0.0129	0.0059
	Biotite inclusions	Retrograde Biotite	Biotite inclusions	Retrograde Biotite
x(Mg)	0.8355	0.8397	0.9264	0.8174
			Plagioclase (range)	
Albite	-	-	0.6958	0.7698
Anorthite	-	-	0.3035	0.2280
Sanidine	-	-	0.0008	0.0021

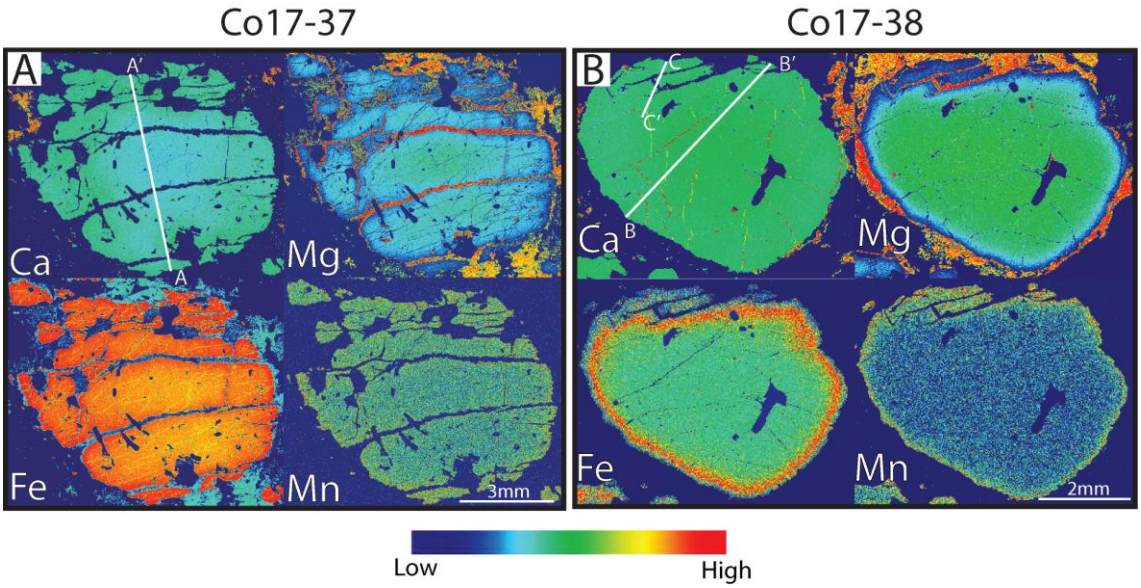

Figure 5: Electron Probe Micro Analyses (EPMA) major element maps for Ca, Mg, Fe and Mn in garnet. Blue represents the low concentration of an element, while red indicates relatively high concentration of that element. The white line traversing garnet grains represents the transect along which values were collected for Fig. 6. Traverse C–C' in Co17-38 is represented in Appendix I. (a) Elemental maps of garnet from near-peak sample Co17-37. (b) Elemental maps of garnet from sample Co17-38.

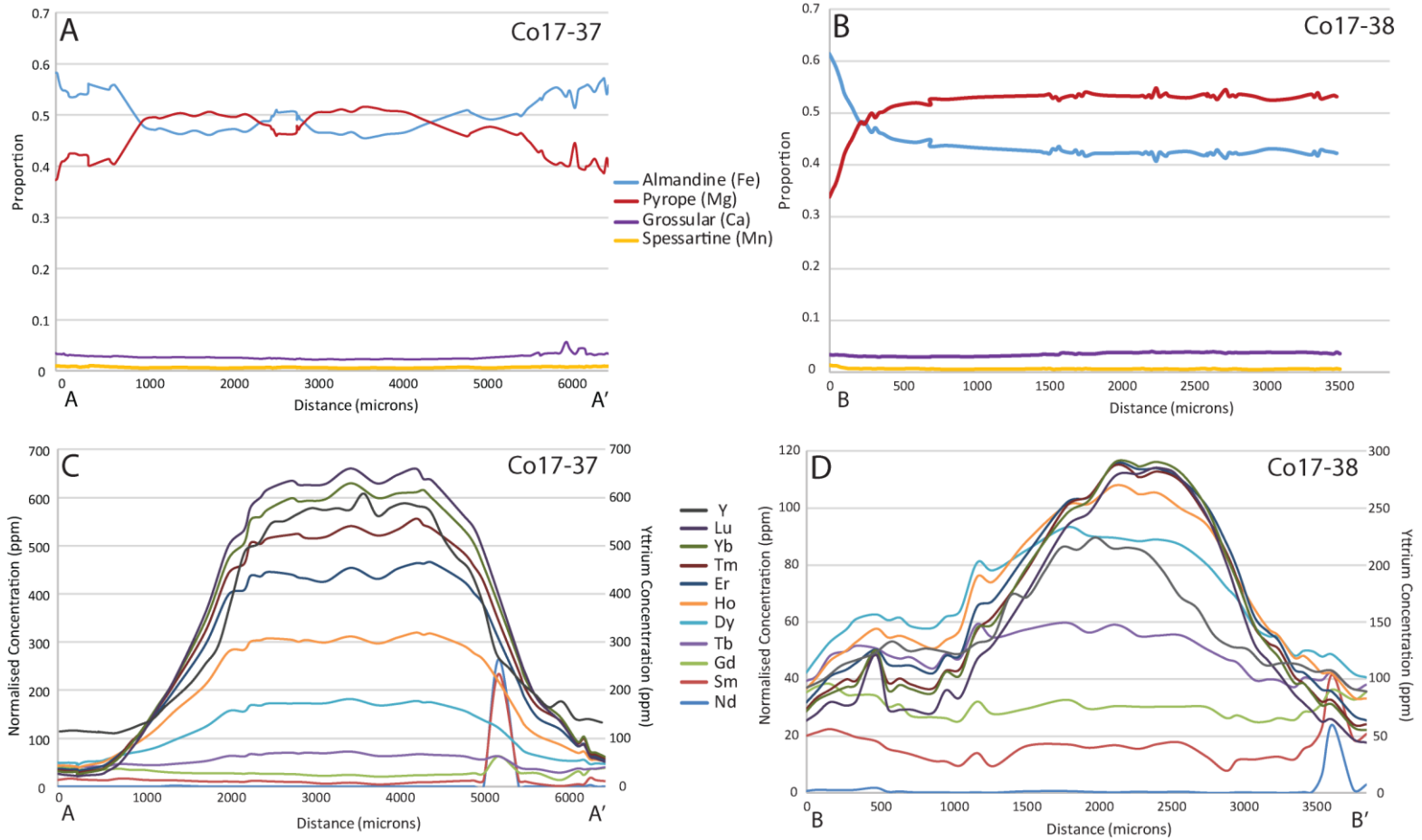

Figure 6: Garnet chemistry along traverses from rim to rim. Traverse orientations with respect to the grain are shown in Fig. 5. (a) Mineral end-member cation proportions from near-peak sample Co17-37, calculated from EPMA data. (b) Mineral end-member cation proportions for sample Co17-38, calculated from EPMA data. Missing values in the second rim are due to poor analyses totals. (c) Trace element data for sample Co17-37, collected from LA-ICP-MS. Normalised REE values are on the left Y-axis, concentrations for yttrium are located on the right. (d) Trace element data for sample Co17-38, collected from LA-ICP-MS. Normalised REE values are on the left Y-axis, concentrations for yttrium are located on the right.

LA–ICP–MS zircon U–Pb geochronology

In-situ zircon U–Pb geochronology was undertaken on samples Co17-37, Co17-38 and Co17-41. Individual analysis values are provided in Appendix B. Zircon was not abundant in thin sections, with only ~20 suitable grains per sample. Grains <40 μm were deemed too small for geochronological analysis using a 29 μm spot. Due to the paucity of suitable in-situ zircon, samples Co17-38 and Co17-41 were supplemented with grain mount analyses (Fig. 7c, e). Co17-37 in-situ geochronology could not be supplemented with a grain mount due to a lack of expendable sample. Zircon geomorphologies are summarised in Table 2, while age data are displayed on Wetherill concordia plots (Fig. 8a–e). Intercept ages have not been presented as they have little meaning due to the largely discordant arrays. Extended descriptions of zircon geomorphologies can be found in Appendix K.

Table 2: The summarised U–Pb zircon and geomorphology results from this study. Data summarised is a combination of in-situ and grain mounted analyses for each sample. Zircon textures described in the table include; Concentric zoning, characteristic of igneous formation (e.g. Corfu, Hanchar, Hoskin, & Kinny, 2003), Fir-tree textures, associated with high-pressure metamorphism (Root, Hacker, Mattinson, & Wooden, 2004) and metamorphic rims grown around detrital cores, formed during partial melting, particularly in the leucosomes of rocks of pelitic/arkosic compositions (Rubatto, Williams, & Buick, 2001; Williams, 2001). For more detailed descriptions, refer to Appendix K.

	Number of grains	Number of analyses	Size	Textures	Aspect ratios	Grain habit	Ages	Relation to mineral phase
Co17-37	10	15	10 µm–120 µm	Zircons largely display metamorphic textures, including fir-tree and metamorphic growth around an inherited core in larger grains.	1–2	Largely anhedral	2505–2170 Ma	No relation to mineral phase could be made based on analyses occurring in a lack of different phases.
Co17-38	119	131	10 µm–250 µm	Approximately a third of zircons display significant metamorphic textures, including fir-tree and metamorphic growth around an inherited core in larger grains.	1–1.5	Largely anhedral	< 3200 Ma	Zircons located out of garnet were predominately younger Zircons in kyanite and biotite return ages of 3156–2777 Ma, while a single analysis in plagioclase returned an age of 2293 ± 39 Ma.
				The remaining zircons exhibited concentric zonation, or weak internal structure associated with igneous formation.	Largely between 2–3	Mostly euhedral to sub-rounded	Largely >3000 Ma, however some were as young as 2500 Ma	Zircons in garnet commonly showed igneous zonation and higher aspect ratios. They were also older, with ages between 3286–3120 Ma.
Co17-41	90	129	10 µm–260 µm	Few zircons display metamorphic textures. However, there are still fir tree textures and metamorphosed rims around inherited cores.	1–2	Largely anhedral	Mostly < 3200 Ma	No relation to mineral phase could be made based on analyses occurring in a lack of different phases.
				Zircons showing concentric zonation dominated this sample.	Largely between 2–3	Mostly euhedral to sub-rounded	Largely >3000 Ma, ranging up to 3800 Ma. Though some were as young as 2600 Ma	

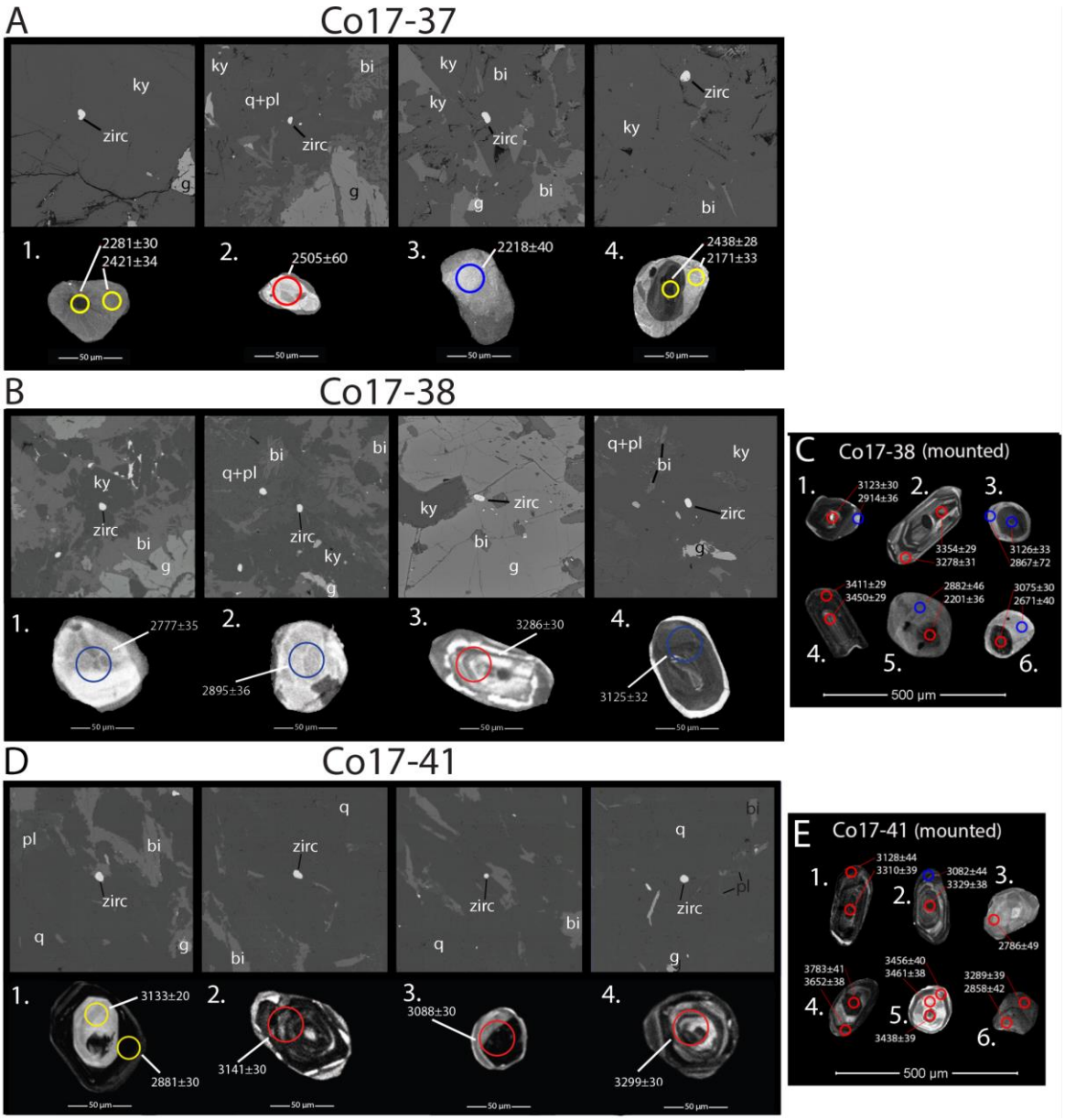

Figure 7: Zircon cathodoluminescence (CL) images coupled with backscattered electron (BSE) images for microstructural context from in-situ analyses. All BSE images are taken at the same distance, so zircons can be used for scale. The rings on CL images indicate where the analyses took place. The corresponding value is the $^{207}Pb/^{206}Pb$ age from that analysis. The colour of the ring refers to the REE values from that analysis (discussed later). Red: HREE-enriched, blue: HREE-depleted and yellow: no trace element data obtained. (a) Sample Co17-37 in-situ zircon CL images coupled with backscatter image showing surrounding phases. (b) Sample Co17-38 in-situ zircon CL images coupled with backscatter image showing surrounding phases. (c) Sample Co17-38 mounted zircon CL images. (d) Sample Co17-41 in-situ zircon CL images coupled with backscatter image showing surrounding phases. (e) Sample Co17-41 mounted zircon CL images.

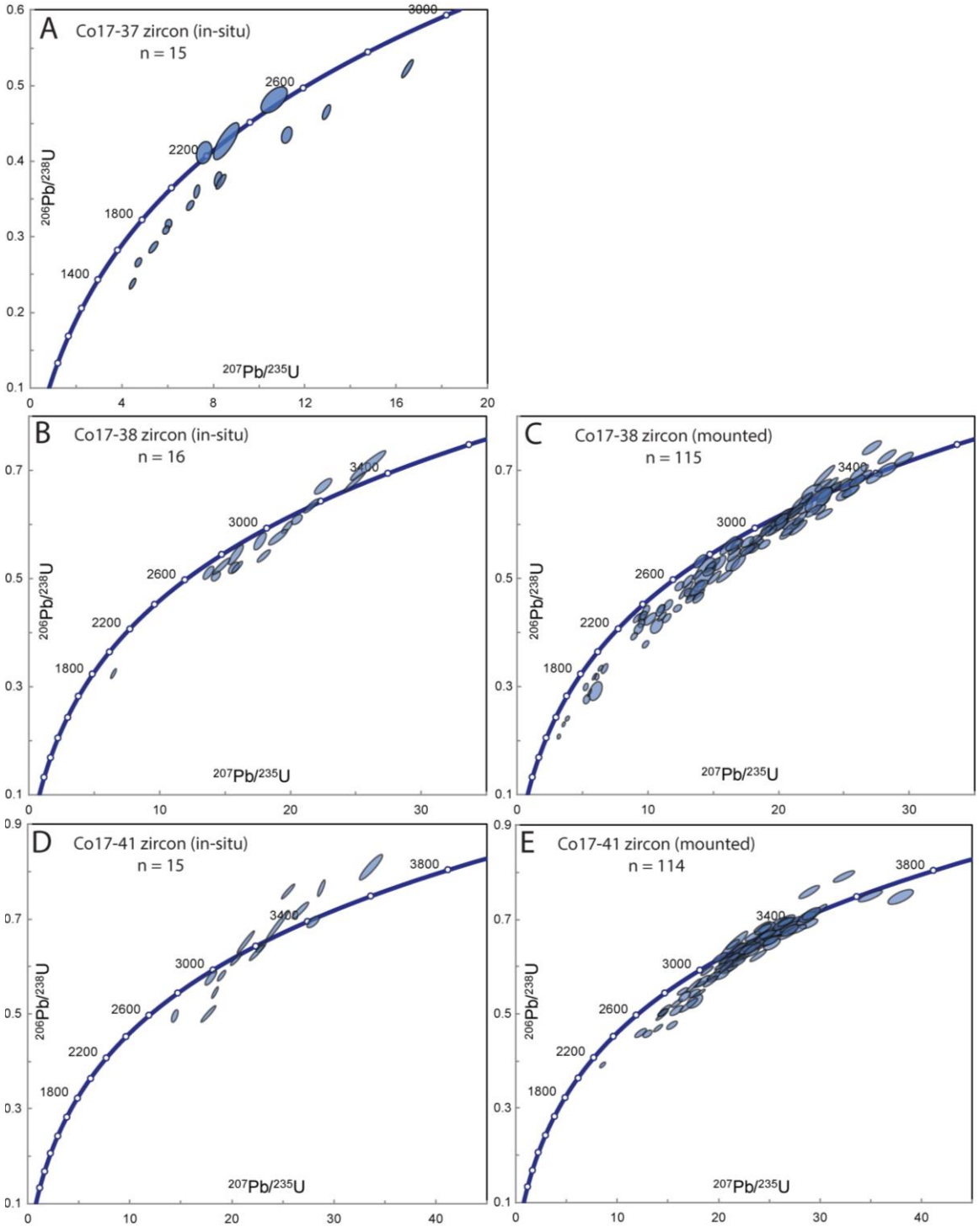

Figure 8: U–Pb Concordia diagrams for zircon analyses with 2σ error ellipses. Intercept values mean very little, due to the largely discordant arrays of data. (a) Near-peak sample Co17-37 in-situ, n = 15. (b) Co17-38 in-situ, n = 16. (c) Co17-38 mounted grains. n = 115. (d) Co17-41 in-situ, n = 15. (e) Co17-41 mounted grains, n = 114.

LA–ICP–MS zircon trace element chemistry

The analysis of trace elements in zircon produced variation both within individual samples and between samples, particularly in the partitioning of heavy Rare Earth Elements (HREEs). The gadolinium/lutetium ratio (Gd/Lu) is a value that relates to the slope of the line between middle and heavy Rare Earth Elements (M-HREE), quantifying the degree of HREE partitioning into zircon during its formation. Gd/Lu values of ~1 or greater indicate zircon is depleted in HREEs, due to competition with another phase. Values << 1 indicate the zircon in enriched in HREEs, implying it formed in the absence of a competing phase. Garnet is commonly a major reservoir for HREEs in medium to high-grade metamorphic rocks (e.g. Hickmott, Shimizu, Spear, & Selverstone, 1987). Its remarkably high abundance in these rocks suggests it could have been the phase competing with zircon for HREEs. To assess this, M-HREE spider plots for garnet are shown in Figs. 9a, 10a for comparison with zircon trends.

The europium (Eu) anomaly is another variable component in the REE chemistry of zircon. A large Eu deficiency (i.e. negative europium anomaly) indicates coeval growth with feldspars (e.g. Rubatto, 2002; Schaltegger et al., 1999). In supra-solidus conditions, melting reactions involving micas form K-feldspar, sequestering all available Eu^{2+}. This results in a negative Eu anomaly in zircons formed in melt.

CO17-37

A flat slope is consistently observed between middle and heavy REEs in zircon, comparable to the distribution observed in the rims of garnet (Fig. 9a). The Eu anomaly is non-existent for four out of five analyses (Fig. 9a, b). However, too few analyses were taken to assess the effect of the in-situ mineral phase on the relationship between trace element concentrations and the ages recorded (Fig. 9b).

CO17-38

A large range of HREE concentrations occur in this sample, with Lu values ranging over three orders of magnitude. A Gd/Lu ratio of 0.3 was used to differentiate the two populations, based on a lack of analyses around this value (Fig. 10c, d). Using this, 48 out of a total 115 zircons analyses are classified as being HREE-depleted. The M–HREE slopes in this population are comparable to the values in the rims and outer core of garnet in this sample (Fig. 10a). These zircons also have a consistently larger negative Eu anomaly compared to the HREE-enriched population (Fig. 10a). The in-situ data indicate that most zircons analysed within garnet are HREE-enriched, implying they formed without the presence of garnet. No relation of Eu concentration to mineral phase could be made (Fig. 10b). Zircons depleted in HREEs generally have ages younger than 3150 Ma, while the HREE-enriched population are largely older than 3000 Ma (Fig. 10b, 10d). The HREE-enriched zircon population comprises a large range of hafnium values (~6000–15000 ppm) compared to the HREE-depleted population (~10000–12000 ppm); (Fig. 10c).

CO17-41

A more consistent trend of M–HREE trend occurs in this sample, as it is dominated by a population of HREE-enriched zircons (Fig. 11a). A Gd/Lu ratio of 0.15 was used to differentiate the two populations, based on the lack of analyses around this value (Fig. 11c, d). Using this, six out of a total 114 zircons were classified as being HREE-depleted. Eu values were highly variable, with a range of positive and negative values in each population (Fig. 11a). In-situ data indicate zircons within biotite and the quartz-dominated matrix of the rock were HREE-enriched, implying they formed in the absence of garnet (Fig. 11b). No relationship between the phase and Eu anomaly could be made, while no

in-situ data were recorded for HREE-depleted zircons (Fig. 11b). Once again, HREE-enriched population of zircons have a broad range of Hf concentrations (~7000–14000 ppm) with respect to the HREE-depleted population (~10000–12000 ppm) (Fig. 11c). The HREE-enriched population also dominates the older proportion of zircons in this sample (Fig. 11d).

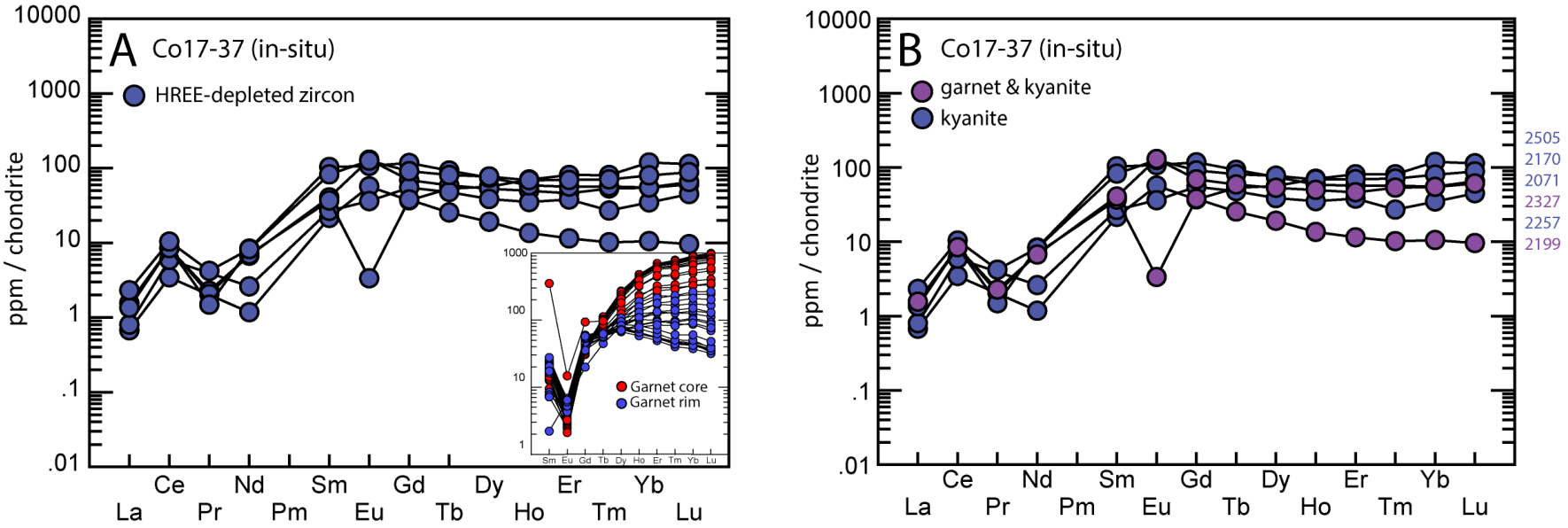

Figure 9: Zircon trace element data for near-peak sample Co17-37. (a) REE spider plot from in-situ zircon analyses. Garnet middle to heavy REE chemistry is inserted for comparison. (b) REE spider plot from in-situ zircon analyses, coloured per the mineral phase the zircon existed. $^{207}Pb/^{206}Pb$ ages to the right of the figure are spatially ordered and coloured to their corresponding analyses.

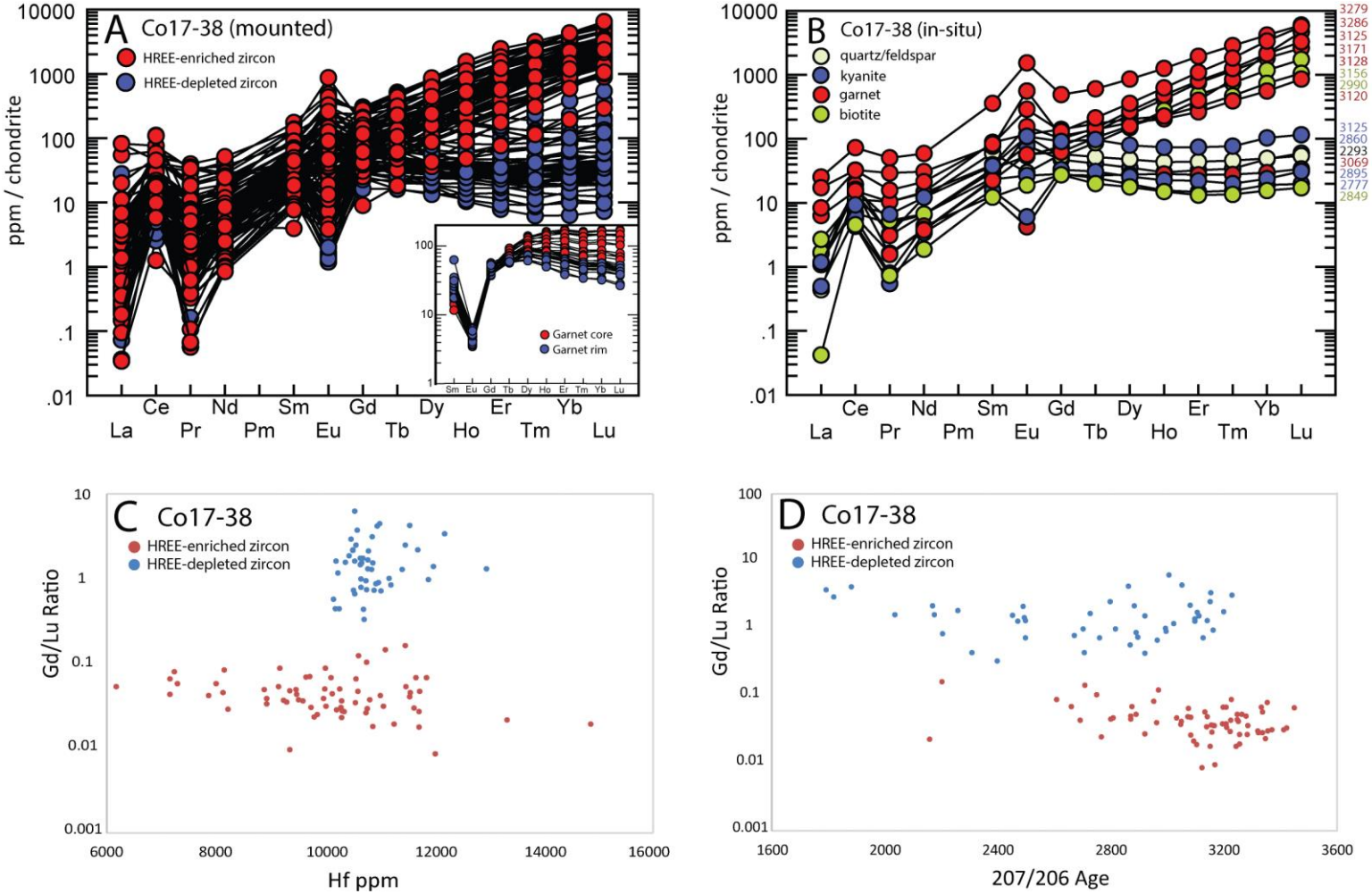

Figure 10: Zircon trace element data for sample Co17-38. A Gd/Lu ratio of 0.3 differentiates the two populations. (a) REE spider plot from mounted zircon grains. Garnet middle to heavy REE chemistry is inserted for comparison. (b) REE spider plot from in-situ zircon analyses, coloured per the mineral phase the zircon existed. $^{207}Pb/^{206}Pb$ ages to the right of the figure are spatially ordered and coloured to their corresponding analyses. (c) Gd/Lu against hafnium concentration in zircon. (d) Gd/Lu against $^{207}Pb/^{206}Pb$ age in zircon.

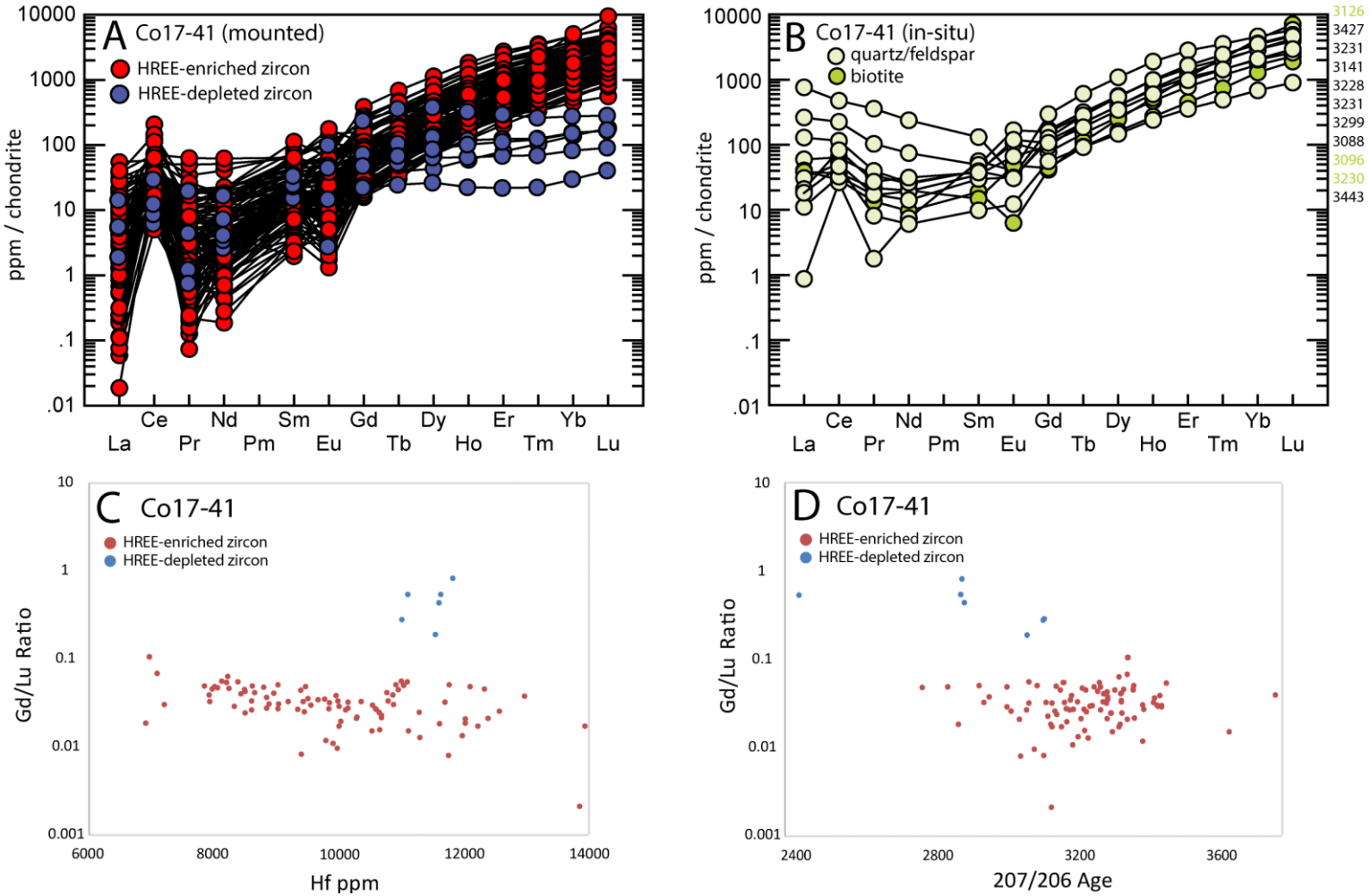

Figure 11: Zircon trace element data for sample Co17-41. A Gd/Lu ratio of 0.15 differentiates the two populations. (a) REE spider plot from mounted zircons. (b) REE spider plot from in-situ zircon analyses, coloured per the mineral phase the zircon existed. $^{207}Pb/^{206}Pb$ ages to the right of the figure are spatially ordered and coloured to their corresponding analyses. (c) Gd/Lu against hafnium concentration in mounted zircons. (d) Gd/Lu against $^{207}Pb/^{206}Pb$ age in mounted zircons.

U–Pb monazite geochronology

In-situ monazite U–Pb geochronology was undertaken on samples Co17-37, Co17-38 and Co17-41. Individual analysis values are provided in Appendix C. Monazite abundance in thin sections are low, with only 10–20 suitable grains per sample. Grains <20 μm were deemed too small for geochronological analysis using a 13 μm spot. Small populations of in-situ analyses are supplemented by grain mounts in Co17-38 and Co17-41. Co17-37 in-situ monazite geochronology could not be supplemented with a grain mount due to a lack of expendable sample. Data are displayed on Wetherill concordia plots with upper and lower intercept ages (Fig. 13a–e).

CO17-37

In-situ monazites range in size from ~10μm to 200μm. The eight analysed grains are almost exclusively found within garnet, with only one occurring in kyanite (Fig. 7a). Multiple analyses are undertaken on each grain. Monazites located along the edges or outside of garnet typically provide younger ages of 3100–2600 Ma. Monazites within garnet porphyroblasts generally yield more ages between 3100–3200 Ma (Fig. 12a).

CO17-38

In-situ monazites range in size from ~10μm to 150μm, while mounted grains are as large as 350μm. Eleven of the fourteen analysed grains are located within garnet, with the rest in biotite (Fig. 12b). Multiple analyses are undertaken on each grain. Monazites located in biotite or at grain boundaries/fractures of garnet typically provide younger ages of 3100–2400 Ma. Monazites within garnet porphyroblasts generally yield ages between 3200–3100 Ma (Fig. 12b).

CO17-41

In-situ monazites range in size from ~10μm to 150μm, while mounted grains are as large as 350 μm. The ten in-situ grains are almost all located in the quartzofeldspathic matrix, excluding one from located in a remnant garnet (Fig. 12c). Multiple analyses are undertaken on most grains. Monazites located in biotite or the quartz-dominated matrix yield ages <3000 Ma, with half of the analyses being <1000 Ma. Larger monazite grains generally provide ages >1000 Ma. The single monazite located in garnet yielded the oldest age in the sample of 3103 $\pm$ 19 Ma (Fig. 12c).

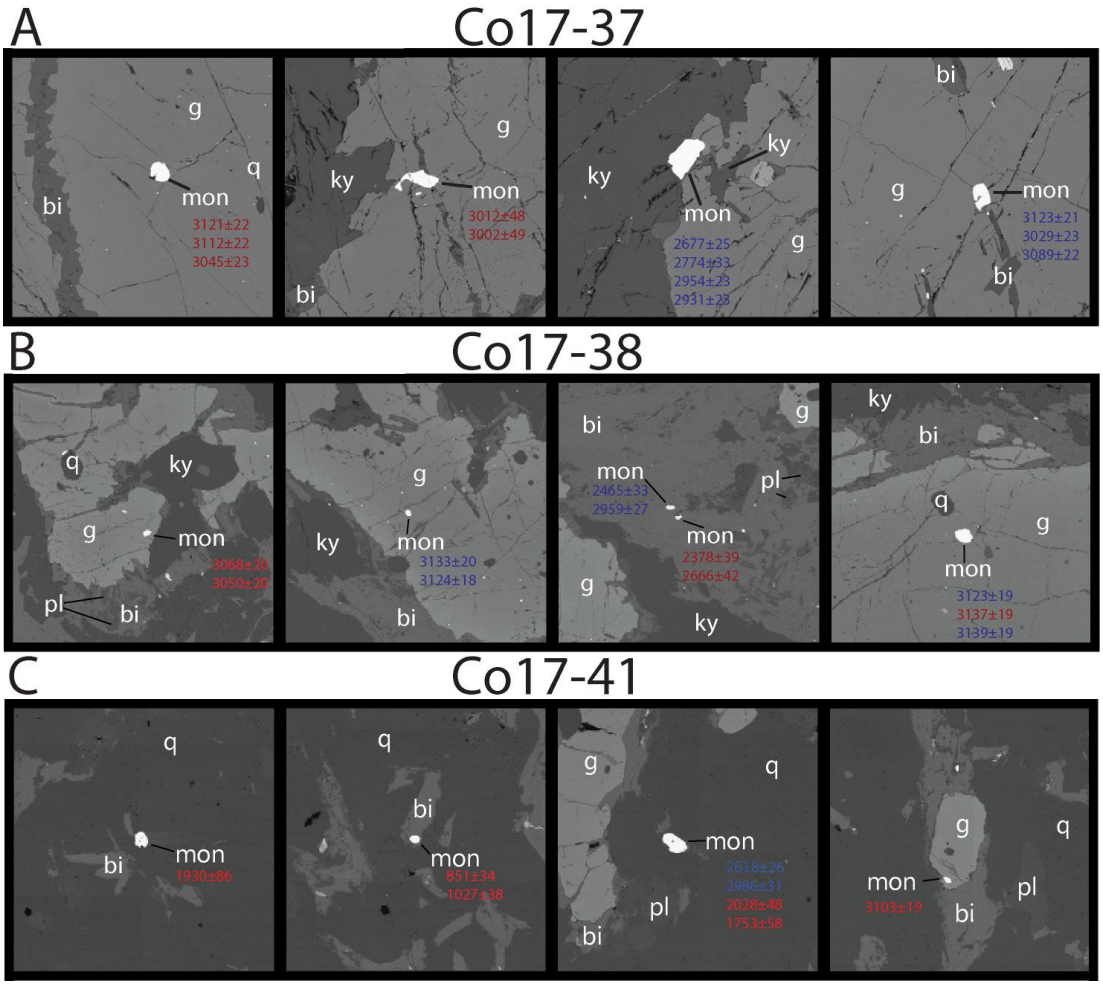

Figure 12: Backscattered electron images showing monazite in context with surrounding mineral phases. Values quoted are $^{207}Pb/^{206}Pb$ ages obtained from the grain. The colour of the text refers to the REE values from the analysis (discussed later). Red: HREE-enriched, blue: HREE-depleted. (a) In-situ monazite grains from near-peak sample Co17-37. (b) In-situ monazite grains from Co17-38. (c) In-situ monazite grains from Co17-41.

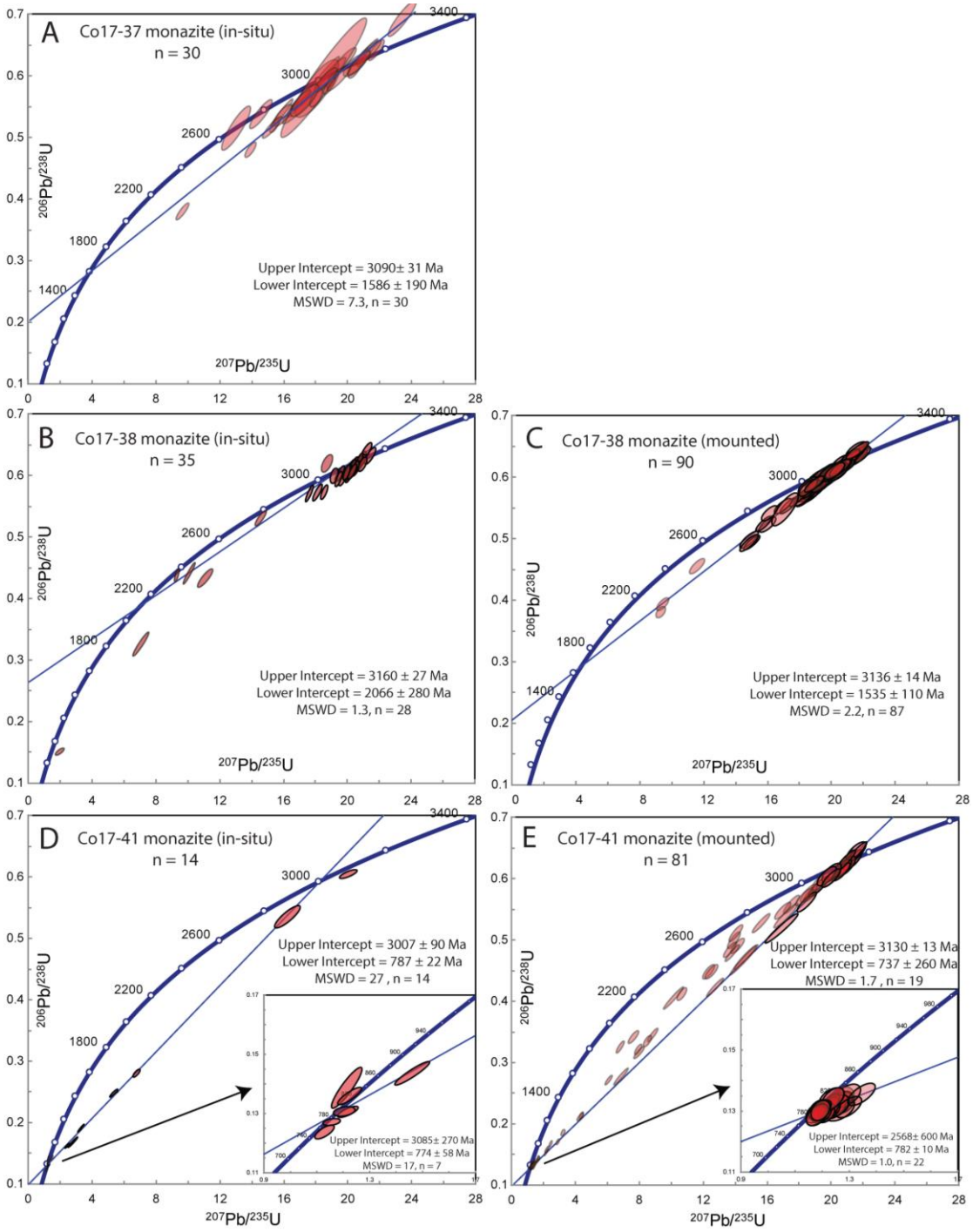

Figure 13: U–Pb Concordia diagrams for monazite analyses with 2σ error ellipses. Ellipses with bold rims were used in the calculation of intercepts. (a) Near-peak sample Co17-37 in-situ. 30 analyses undertaken on 8 individual grains. Upper intercept = 3090 ± 31 Ma, lower intercept = 1586 ± 190 Ma. MSWD = 7.3, n = 30. (b) Co17-38 in-situ, n = 35. Upper intercept = 3160 ± 27 Ma, lower intercept = 2066 ± 280 Ma. MSWD = 1.3, n = 28 (c) Co17-38 mounted grains, n = 90. Upper intercept = 3136 ± 14 Ma, lower intercept = 1535 ± 110 Ma. MSWD = 2.2, n = 87. (d) Co17-41 in-situ, n = 14. Upper intercept = 3007 ± 90 Ma. MSWD = 27, n = 14. Lower intercept = 774 ± 58 Ma. MSWD = 17, n = 7. (e) Co17-41 mounted grains, n = 81. Upper intercept = 3130 ± 13 Ma. MSWD = 1.7, n = 19. Lower intercept = 782 ± 10 Ma. MSWD = 1.0, n = 22.

LA–ICP–MS monazite trace element chemistry

The analysis of trace elements in monazite exposed large variations in the concentrations of HREEs. The Gd/Lu ratio is again used as a value for the slope of the line between middle to HREE, quantifying the level of uptake of HREEs into monazite. However, as monazite REE trends are typically the opposite of zircon, this value must be brought into a different context. High Gd/Lu values in monazite imply relative depletion of HREEs, compared to lower values, which indicate the relative enrichment of HREEs. Unlike zircon, the Gd/Lu ratio in monazite did not provide a clear differentiation between populations. Consequently, a Gd/Lu value of 800 was assigned to differentiate populations across all samples. The Eu anomaly also applies for monazite, with large depletions in Eu corresponding to simultaneous growth with feldspar in melt.

CO17-37

A total of thirty analyses were obtained. Fifteen were classified as HREE-depleted and fifteen were HREE-enriched (Fig. 14b). HREE-enriched monazites exclusively appear in garnet, while HREE-depleted monazites occur in kyanite and garnet (Fig. 14b). HREE-depleted monazites generally possess a larger Eu anomaly in comparison with HREE-enriched population (Fig. 14a). Monazite ages overlap between populations. (Fig. 15b).

CO17-38

A total of ninety grain-mounted analyses were obtained. Fifty-three were classified as HREE-depleted and thirty-seven were HREE-enriched (Fig. 15a). HREE-depleted monazites generally possess larger Eu anomalies, while HREE-enriched monazites show a range of negative anomaly values (Fig. 15a). In-situ analyses indicate HREE-enriched monazites appear exclusively in garnet, while HREE-depleted monazites are recorded in

biotite and garnet (Fig. 15b). Monazite ages are similar between the two populations, resulting in a large overlap (Fig. 15b). Yttrium concentration within monazite is highly variable in 3150 Ma-aged grains, but becomes more consistent as monazite ages young toward *ca.* 3050 Ma. For grains younger than 3050 Ma, yttrium concentration decreases consistently (Fig. 15c). Yttrium also shows a strong inverse relationship with the uptake of HREEs, with HREE-enriched monazites also being enriched in yttrium (Fig. 15d). A large degree of overlap exists between the > 3000 Ma and 3000–2500 Ma monazite populations, while the < 2500 Ma population are distinctly separated with highly depleted yttrium concentrations (Fig. 15d).

CO17-41

A total of eighty-one grain-mounted analyses were obtained. Thirty-two were classified as HREE-depleted and forty-nine were HREE-enriched (Fig. 16a). HREE-depleted monazites possess large negative Eu anomalies, while HREE-enriched monazites show a range of negative anomaly values, many of which are in the range of the HREE-depleted population (Fig. 16a). The in-situ analyses largely represent the HREE-enriched population, analyzing very few HREE-depleted monazites. HREE-enriched monazites were recorded in quartz/feldspar and garnet, while the limited number of analyses of HREE-depleted monazites indicate they exist in the quartz/feldspar matrix (Fig. 16b). Yttrium concentrations within monazite 3150 Ma in age is again highly variable. However, as the monazites become younger, they become consistently enriched in yttrium and HREEs (Fig. 16c, d).

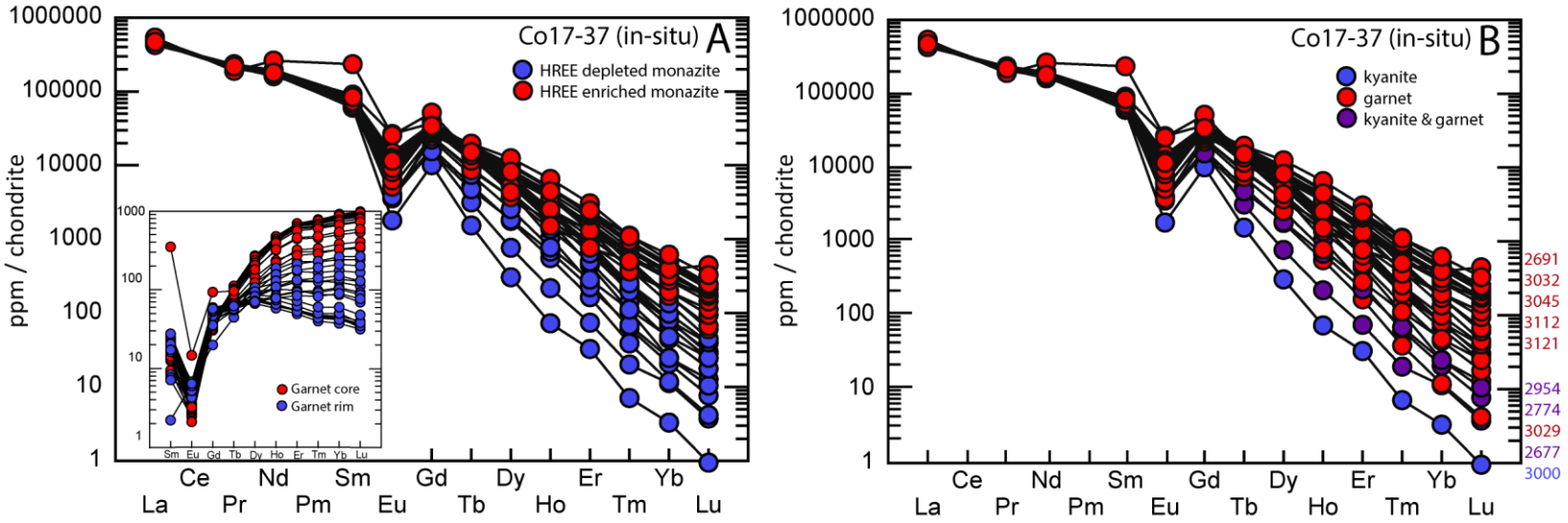

Figure 14: Monazite trace element data for near-peak sample Co17-37. A Gd/Lu ratio of 800 differentiates the two populations. (a) REE spider plot from in-situ monazite analyses. Garnet middle to heavy REE chemistry is inserted for comparison. (b) REE spider plot from in-situ monazite analyses, coloured per the mineral phase the monazite existed. $^{207}Pb/^{206}Pb$ ages to the right of the figure are spatially ordered and coloured to their corresponding analyses. Not all analyses have age values due to the large amount of data. Ages have only been provided for 5 analyses at each end of the spectrum.

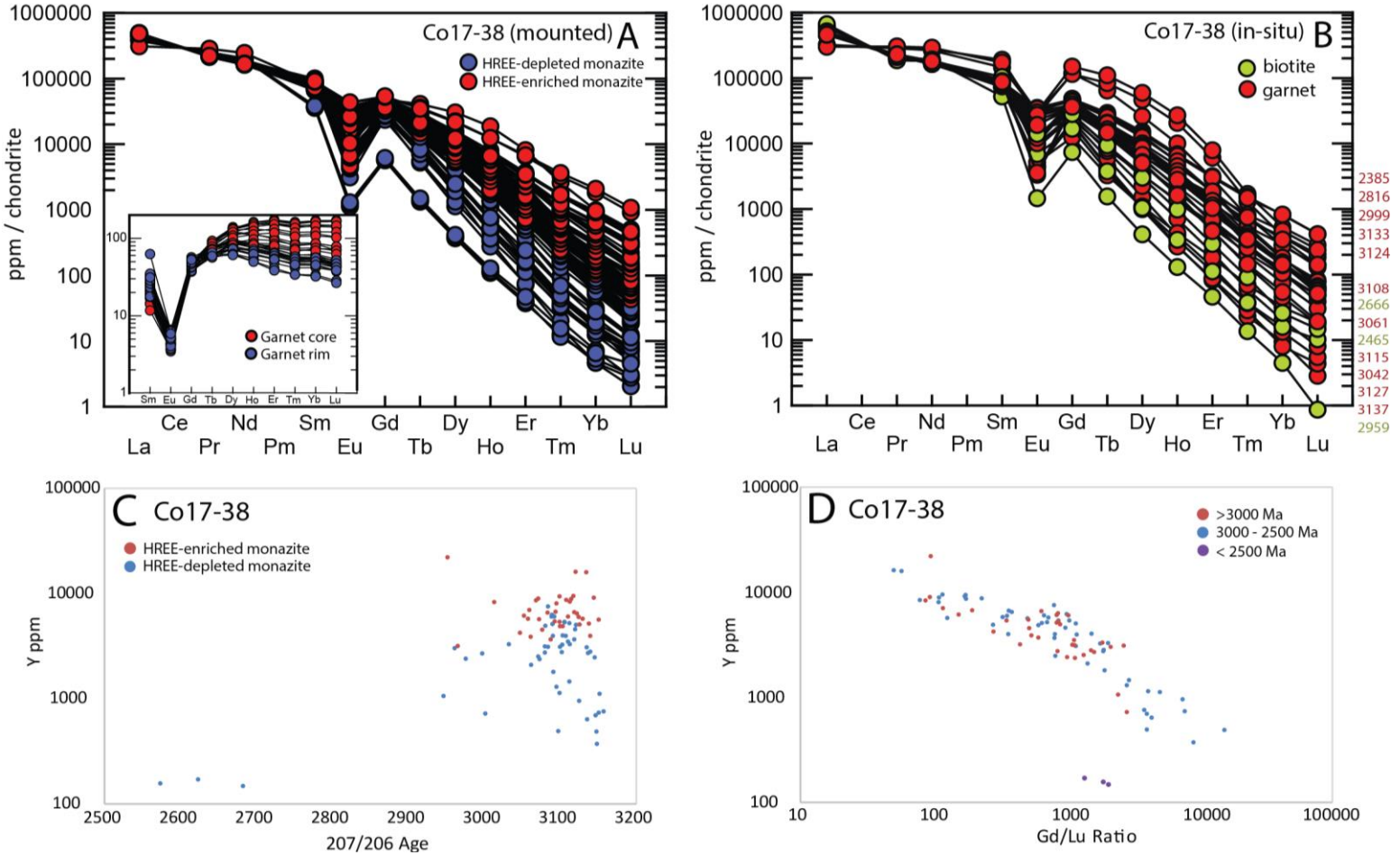

Figure 15: Monazite trace element data for sample Co17-38. A Gd/Lu ratio of 800 differentiates the two populations. (a) REE spider plot from grain mounted monazite analyses. Garnet middle to heavy REE chemistry is inserted for comparison. (b) REE spider plot from in-situ monazite, coloured per the mineral phase the monazite existed. $^{207}Pb/^{206}Pb$ ages to the right of the figure are spatially ordered and coloured to their corresponding analyses. Not all analyses have values due to the large amount of data. Ages have only been provided for analyses at each end of the spectrum. (c) Scatter plot of yttrium concentration versus $^{207}Pb/^{206}Pb$ age. (d) Scatter plot of yttrium concentration versus Gd/Lu.

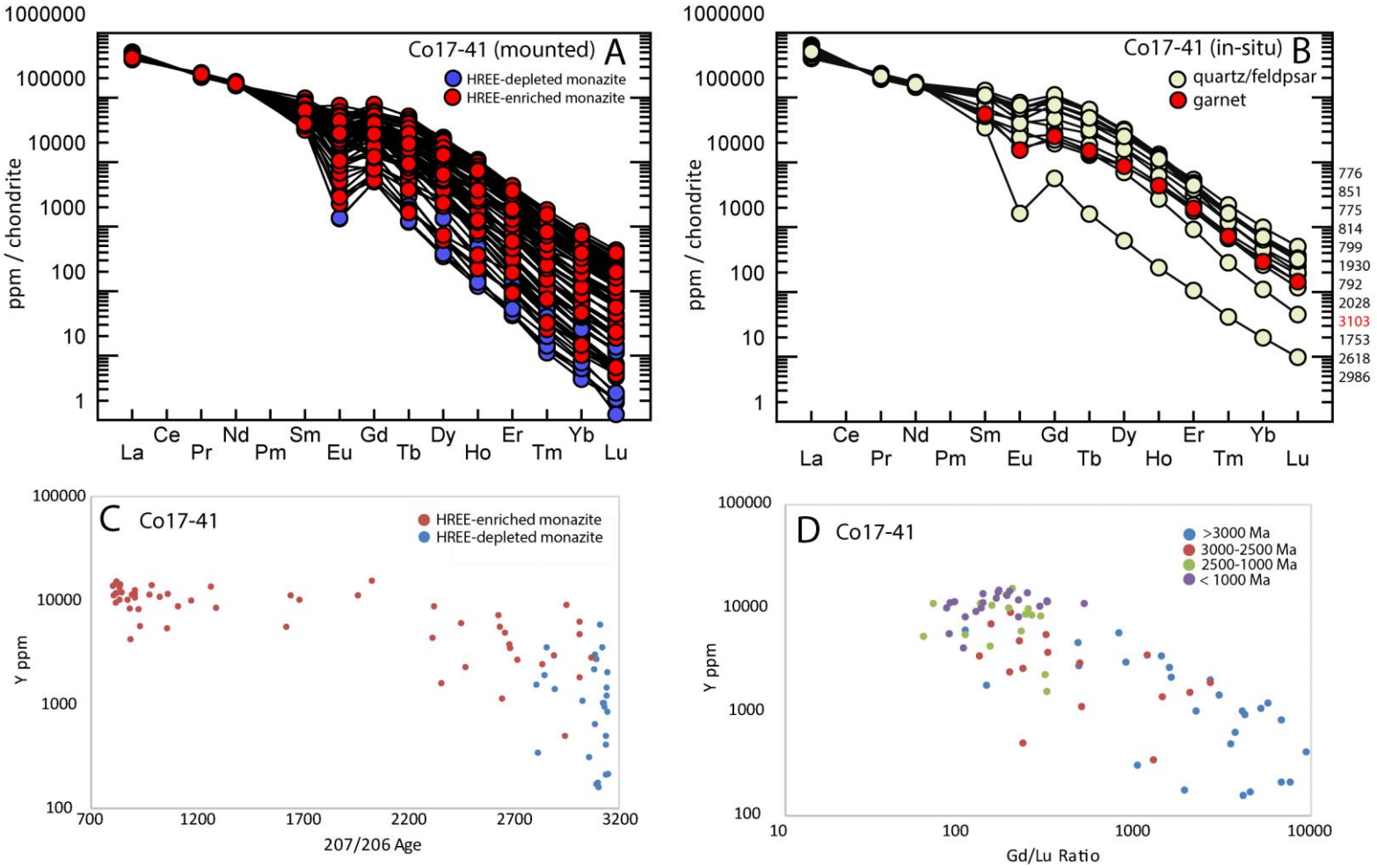

Figure 16: Monazite trace element data for sample Co17-41. A Gd/Lu ratio of 800 differentiates the two populations. (a) REE spider plot from grain mounted monazite analyses. (b) REE spider plot from in-situ monazite, coloured per the mineral phase the monazite existed. $^{207}Pb/^{206}Pb$ ages to the right of the figure are spatially ordered and coloured to their corresponding analyses. (c) Scatter plot of yttrium concentration versus $^{207}Pb/^{206}Pb$ age. (d) Scatter plot of yttrium concentration versus Gd/Lu, coloured to fit within age bins.

Phase equilibria forward modelling

Pressure–Molar oxidation *(P–Mo),* Temperature–Molar water *($T–M_{H2O}$)* and pressure–temperature (*P–T*) pseudosections were calculated for sample Co17-37 and Co17-38 in the MnNCKFMASHTO chemical system. The objective of the phase equilibria modelling was to constrain the peak *P–T* conditions.

The principal uncertainty in phase equilibria modelling relates to the determination of an effective bulk rock composition (Johnson & White, 2011). In supra-solidus rocks, such as the rocks in this study, this relates to the degrees of oxidation and hydration of the rock. To address this, *P–Mo* and *$T–M_{H2O}$* diagrams were used to more accurately constrain the abundances of Fe_2O_3 (oxidation state) and H_2O, as whole rock geochemical analyses are considered unreliable (Kelsey & Hand, 2015). In *P–Mo* sections, the oxidation state along the compositional axis varies from 100% FeO to 66% Fe_2O_3, 33% FeO at M = 0.66. A fixed temperature is required to calculate *P–Mo* sections. A temperature of 860 ^{o}C was used for both samples, based on previous studies (Amaldev et al., 2016; Mansfield, 2016). In *$T–M_{H2O}$* sections, the water content along the compositional axis varies from 0 to 100% H_2O, where 0% is the minimum possible amount of water for the composition of the sample and 100% is the loss on ignition (LOI) value in the geochemical analysis of the sample, normalised to molar-oxide percent values. A fixed pressure is required to calculate *$T–M_{H2O}$* diagrams. A pressure of 12.6 kbars was selected for both samples based on results from previous studies (Amaldev et al., 2016; Mansfield, 2016). *P–Mo* and *$T–M_{H2O}$* diagrams for Co17-37 are presented in Appendix L. All diagrams for Co17-38 are presented in Appendix M.

CO17-37

The calculated *P–Mo* and $T–M_{H2O}$ pseudosections for near-peak sample Co17-37 are shown in Appendix L. The peak assemblage for Co17-37 is interpreted as garnet + kyanite + K-feldspar + rutile + quartz + melt.

The chosen oxidation state corresponds to the composition at M = 0.05 in the $P–M_O$ diagram, based on the occurrence of the peak field at this composition. The chosen amount of H_2O in the sample corresponds to the composition at M = 0.98. The peak field is stable across all H_2O range, but EPMA data supports this degree of hydration, with halogens in biotite, which is the only water-bearing mineral in the assemblage, being virtually zero (Appendix I). This indicates that most of the LOI in the geochemical analysis came from H_2O within biotite.

The peak field in the calculated *P–T* pseudosection (Fig. 17) is poorly constrained, with minimum conditions of 11.6 kbar and 880°C and no upper constrains below 15 kbar and 1000°C. This field is bound by the appearance of biotite down temperature and the transition of kyanite to sillimanite down pressure. Mineral abundances (‘modes’), calculated in TCI, further constrained the metamorphic peak to minimum conditions of 13.1 kbar and ~950°C (Fig. 20). An anti-clockwise *P–T* path is inferred for the sample from petrological observations. Biotite, sillimanite and kyanite inclusions in garnet constrain the prograde evolution, while retrograde kyanite and plagioclase, with the absence of retrograde muscovite constrain the retrograde path. However, the prograde and retrograde conditions are poorly constrained compared to the peak.

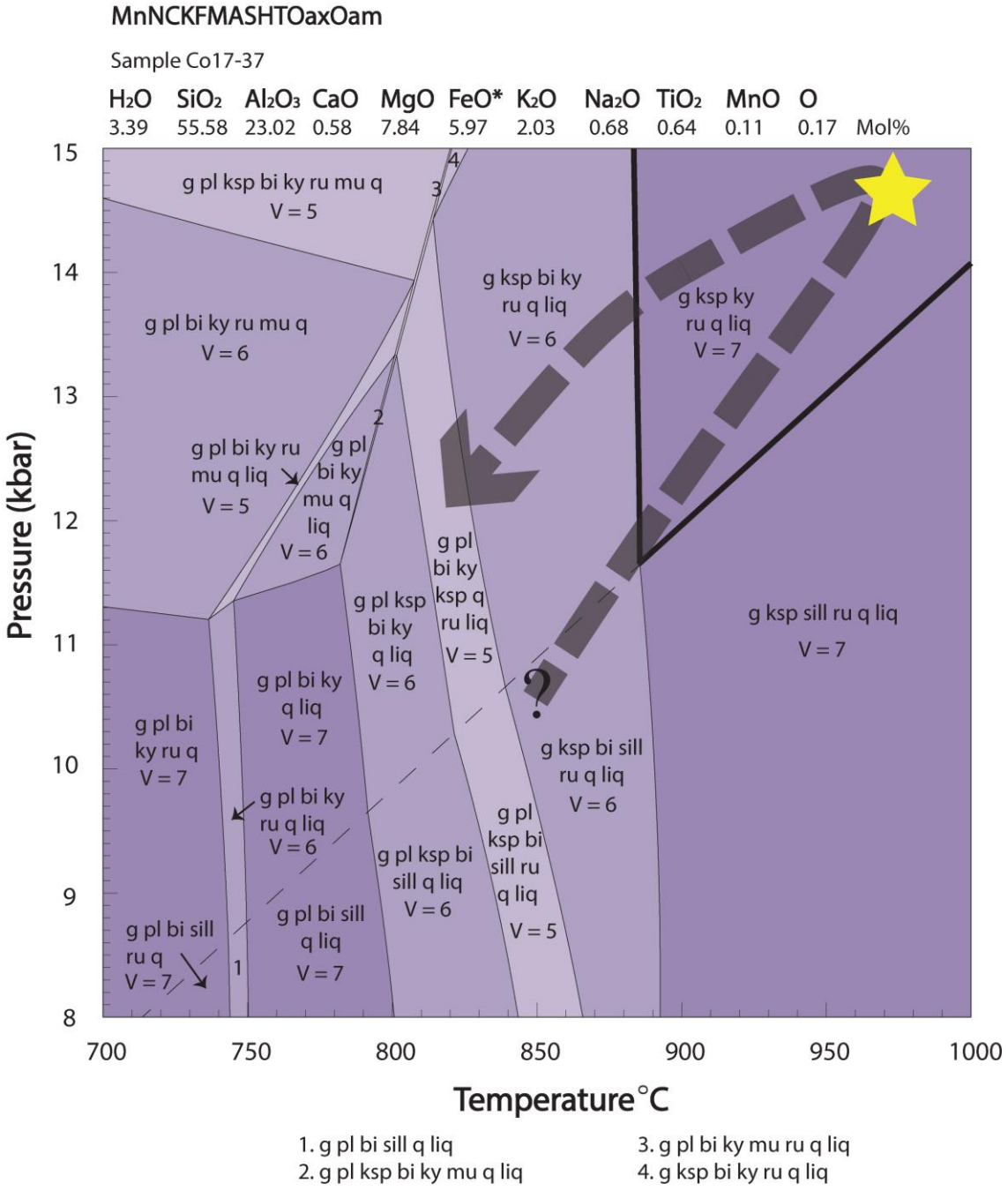

Figure 17: Calculated *P–T* pseudosection for near-peak sample Co17-37. Fields too small to be labelled directly have their assemblages identified either in an adjacent field, or by a number. Progressively darker tones represent increasing variance, V, where V = components – phases + 2 (components = 11). Bold lines highlight the peak field, while the yellow star denotes the further constrained peak (Fig. 19). The large dashed arrow signifies the anti-clockwise *P–T* path interpreted from petrological relationships and the fine-dashed line represents the aluminosilicate phase transition from sillimanite (below) to kyanite (above). The composition in mol% used to calculated the diagram, corresponding to Mo = 0.05 and M_{H2O} = 0.98 (Appendix I), is provided above the diagram. FeO* = FeO + 2 × 'O'.

Abbreviations: g = garnet; pl = plagioclase; ksp = K-feldspar; bi = biotite; ky = kyanite; sill = sillimanite; ru = rutile; mu = muscovite; q = quartz; liq = melt (liquid).

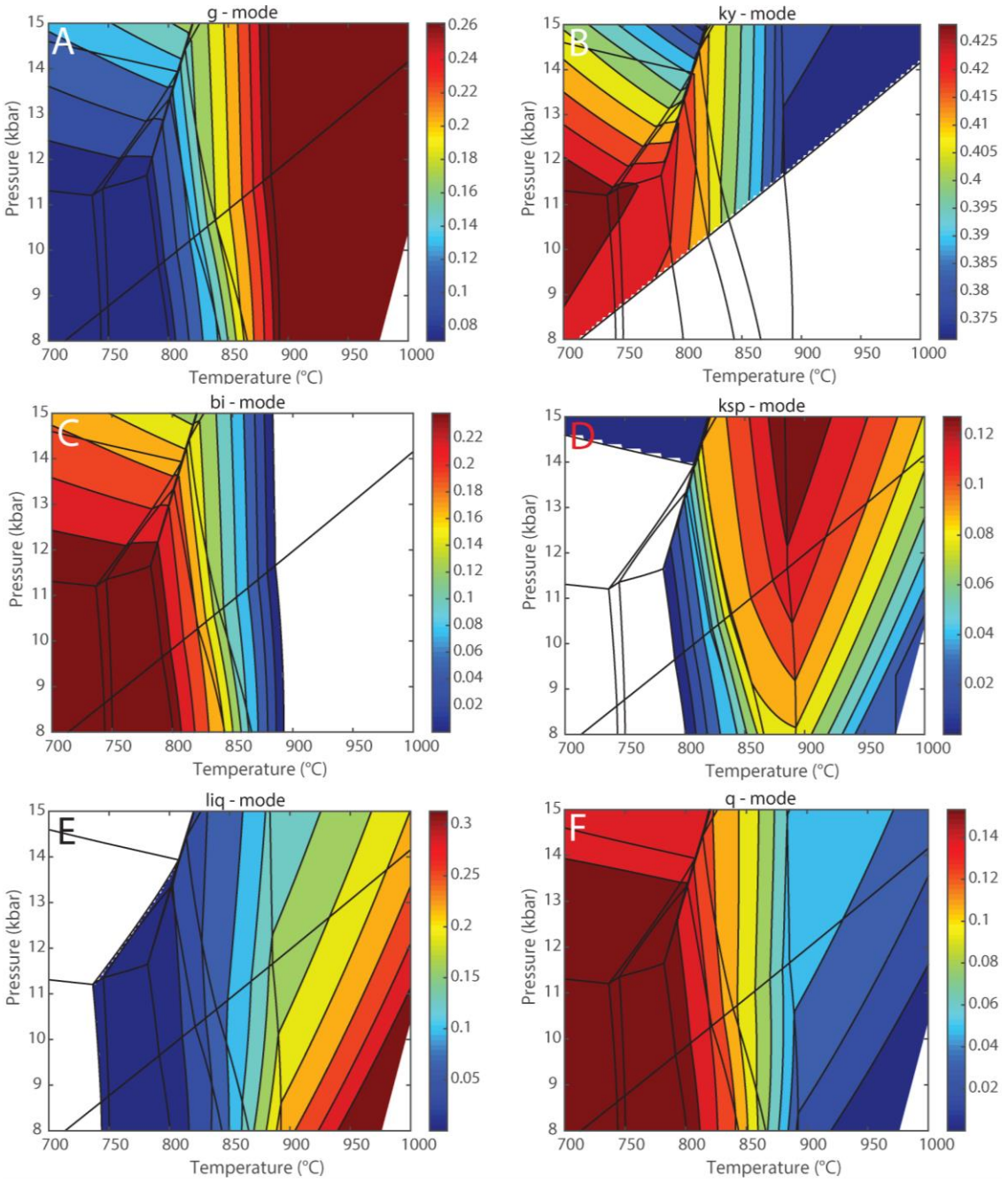

Figure 18: TCI outputs for Co17-37, showing modal proportions of a) garnet, b) kyanite, c) biotite, d) K-feldspar, e) melt (liquid), f) quartz. Modal proportions of sillimanite, biotite, plagioclase and muscovite have not been presented as they did not form a part of the peak assemblage. Rutile is not represented as it forms <1% of the rock's volume.

Table 3: Modal proportions of minerals calculated from the metamorphic peak in near-peak sample Co17-37. Values were calculated using EPMA data, interpreted to best represent mineral chemistries at the metamorphic peak. Methods and assumptions used in the calculations are presented in Appendix N, explaining how the total >100% was achieved. Plagioclase, biotite and sillimanite are not presented as they are interpreted as retrograde products. Rutile is not represented as it constitutes <1% of the rocks volume.

	Garnet	Kyanite	K-feldspar	Quartz	Melt	Total
Co17-37	33.83%	35.57%	9.09%	3.2%	20.07%	101.77%

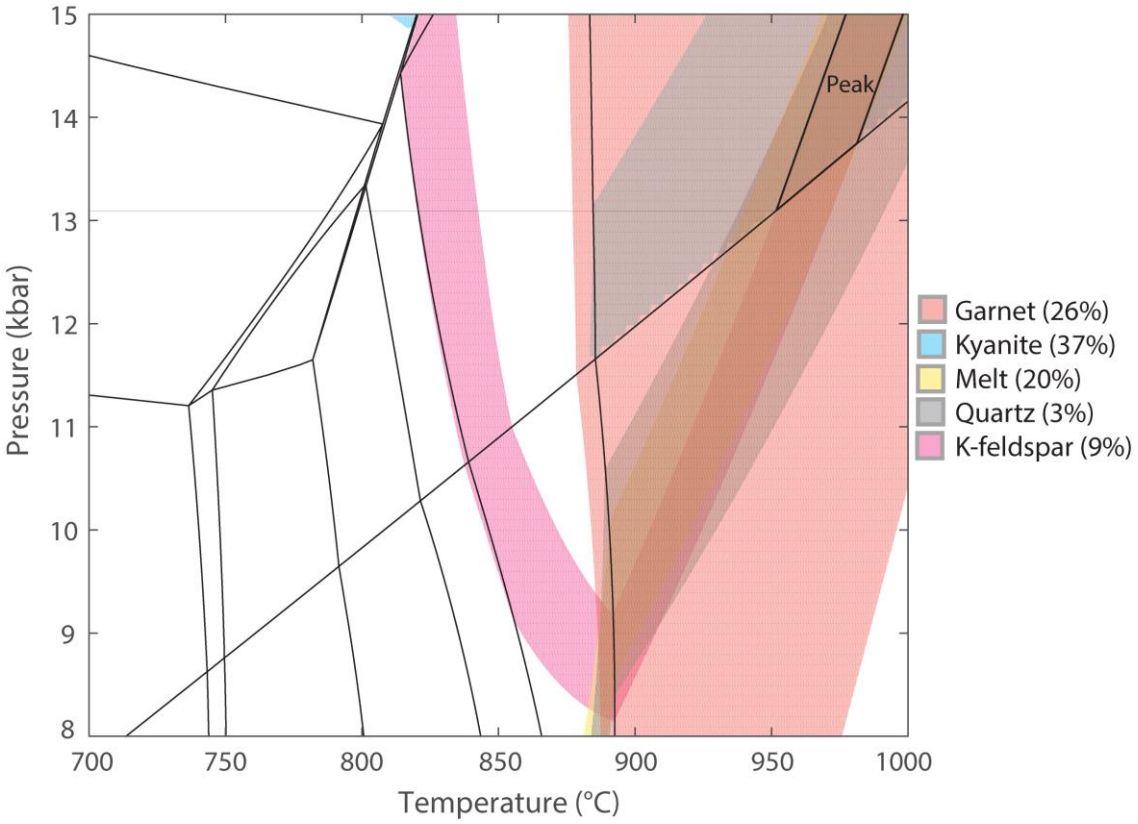

Figure 19: Further constraint of the calculated peak field in sample Co17-37. Compiled TCI output of each mineral in the peak assemblage (Fig. 18), with the shaded area corresponding to the proportion of that mineral calculated in the metamorphic peak (Table 3). Garnet and kyanite modes calculated from EPMA data were not found in TCI output. Therefore, the closest values from TCI were used. The modes represented for each mineral are as follows; garnet: 26%, kyanite: 37%, melt: 20%, quartz: 3%, K-feldspar: 9%. The constrained peak is defined by the box labelled 'peak', where all peak mineral modes overlap. This occurs at minimum *P–T* conditions of 13.1 kbar and ~940 ºC.

DISCUSSION

The aim of this study is to identify the timing of the oldest recorded metamorphic event and constrain the pressure–temperature conditions of the metamorphic peak of that event. The regional implications for the geology of southern India are also discussed from the other metamorphic events determined in this study.

Timing of high-pressure metamorphism

The largely discordant arrays of U–Pb ages, particularly in zircon, describe a complex metamorphic history spanning over 2.5 Ga. Up to three metamorphic events have been identified to have had an influence on these rocks. This is illustrated best in the zircon concordia diagrams, where wide bands of discordant data track down toward an age between 2500–2300 Ma, then curve away from concordia toward a younger age (Fig. 7a–e). This complicates the study, as the observed high-pressure assemblage could potentially be associated with any of the three metamorphic events. Diligence in deciphering the timing of high-pressure metamorphism is crucial in the outcome of this study, as the implications are so heavily reliant on the age of the modelled assemblage.

Zircon and monazite are broadly used in understanding the timing and duration of high-temperature processes within the Earth's crust (e.g. Spear & Pyle, 2002; Taylor, Kirkland, & Clark, 2016). The rocks in this study are high-pressure granulites, reaching conditions above the solidus where partial melting of the rock has occurred. Evidence of partial melting is seen at both the macro-scale, as leucosomes within the outcrop (Fig. 2), and micro-scale as small pockets of interpreted recrystallized melt (Fig. 4b, 4c). This information is important for the interpretation of monazite and zircon U–Pb ages. Monazite is commonly regarded to be responsive to a larger range of conditions, capable

of recording ages from prograde temperatures of ~400–500°C up to peak conditions >1000°C (e.g. Janots et al., 2008; Smith & Barreiro, 1990). Zircon however, is generally considered to be largely unresponsive to metamorphism below the solidus (e.g. Rubatto, Chakraborty, & Dasgupta, 2013; Rubatto et al., 2001). Additionally, the interpretation of lower intercept ages in discordant U–Pb zircon data from metamorphic environments must be done with caution. Many different factors contribute to varying degrees of partial Pb-loss in zircon. Pb diffusion in metamict zircon is considered to be very different to pristine zircon, while leaching and recrystallisation of these zircons also result in varying degrees of Pb-loss (Mezger & Krogstad, 1997). Furthermore, zircon with high U-content (>100 ppm) can suffer damage of the crystal lattice through α-decay, resulting in the instantaneous loss of isotope data (e.g. Chakoumakos, Murakami, Lumpkin, & EWING, 1987), while metamict zircon can easily recrystallize during a later heating event (Geisler and Pidgeon, 2002). Zircon in this study exhibit a variety of textures and are largely U-enriched (>100 ppm), suggesting that some zircon may well have suffered radiogenic crystal damage, enhancing their sensitivity to subsequent thermal events.

INTERPRETATION OF U–PB ZIRCON PETROCHRONOLOGY

The zircon U–Pb concordia data are highly discordant across all samples (Fig. 7a–e). A limited data set was acquired for near-peak sample Co17-37, thus the large suite of geochronology data from the closely associated sample Co17-38 was heavily relied upon to infer the timing of high-pressure metamorphism.

Three lines of evidence are used to identify a population of zircons that grew in metamorphic environments. Firstly, although trace element data from Co17-37 were limited, they consistently showed zircons that were depleted in HREEs. When compared

to garnet REE data in the same sample, a similar middle to heavy REE (M–HREE) trend suggested these two phases were in competition for HREEs (Fig. 9).

The REE zoning profiles in garnet show that as garnet grew, the budget for HREEs remaining in the rock became increasingly depleted, resulting in the formation of HREE-depleted rims (Fig. 6c). This HREE depletion pattern is reflected in the population of metamorphic zircons, indicating they were formed either in the late stages of garnet growth, or after garnet growth all together. The same REE trends were observed in garnet and zircon from sample Co17-38 (Figs. 6d, 10), making this sample suitable for determining the age of the high-pressure metamorphic event. Secondly, HREE-depleted zircon correlated with CL metamorphic growth (blue circles in Fig. 7), while oscillatory zonation, typically associated with magmatic formation, provided M–HREE trends inferring no competition (red circles in Fig. 7). Lastly, a comparatively small range of Hf concentrations for the HREE-depleted population supports the interpretation of a metamorphic zircon population, formed within the rock with Hf concentrations reflecting a homogenized metamorphic fluid. Conversely, the broad range of Hf concentrations recorded in HREE-enriched zircons supports the interpretation of these zircons as detrital (Fig. 10c). The concentration of Hf in zircon is primarily dependent on the source (Patchett, 1983). Therefore, the large range in Hf concentrations in the detrital population suggests input from multiple sources.

Petrologically, kyanite and rutile occur as inclusions within garnet porphyroblasts, indicating that these three minerals grew simultaneously (Fig. 4a, b). These three minerals form the basis of the observed high-pressure assemblage. Therefore, the age of metamorphic zircons formed in equilibrium with this assemblage reflects the timing of high-pressure metamorphism. This is constrained by an upper intercept age of 3164 ± 31

Ma (MSWD = 2.4) that is calculated from the metamorphic zircon population in sample Co17-38 (Fig. 21a).

A schematic diagram, demonstrating the effect of multiple metamorphic events on the distribution of zircon analyses in concordia diagrams is presented in Fig. 23. This is one possible explanation for the observed trends in zircon concordia in this study. To properly interpret this diagram, it must first be understood that the REE chemistry of geochronometers are generally unaltered after formation. This is due to the high compatibility of these elements, allowing them to resist re-equilibration at high temperatures due to their low rates of diffusivity (e.g. Lanzirotti, 1995; Otamendi, Jesús, Douce, & Castro, 2002; Spear & Kohn, 1996). This explains why detrital zircon U–Pb ages can become reset through metamorphism, but still retain igneous REE signatures (Fig. 22a).

In this scenario, most metamorphic zircon grains, or metamorphically grown rims, were formed at *ca.* 3.15 Ga. This is apparent from the proportion of the metamorphic zircon population that lies discordant between 3.2–2.5 Ga (Fig. 21a). Metamorphic zircons younger than 2.5 Ga could have formed in the Mesoarchaean, and then been reset by the later events, or perhaps were formed in the Palaeoproterozoic event. Either way, this implies some influence from a thermal event in the Palaeoproterozoic, even though constraints on the timing of this event are lacking.

INTERPRETATION OF U–PB MONAZITE PETROCHRONOLOGY

The monazite U–Pb concordia data provides more age consistency than zircon, showing little record of the later events recorded in the zircon data. A limited data set was again acquired for near-peak sample Co17-37, with only eight separate grains being analysed.

Therefore, the large suite of geochronology data from sample Co17-38 is relied upon to infer the timing of high-pressure metamorphism.

The two identified monazite populations are interpreted to represent prograde and peak populations respectively, based largely on the HREE and Y depletion patterns observed in garnet as it grew (Fig. 6c, 6d). These patterns in HREE and Y are well documented as characteristic prograde zonation patterns, due to the resistive nature of these highly compatible elements (e.g. Hickmott et al., 1987; Otamendi et al., 2002; Pyle & Spear, 1999; Raimondo et al., 2017; Rubatto, 2002). As mentioned previously, the REE and Y zoning profiles in garnet are a reflection of decreased elemental availability within the rock. The mimicking trends for HREE and Y observed in monazite reflect the reduced element availability, directly linked to the sequestration of HREE and Y in garnet as it grew (Fig. 15c, 15d).

Monazite age populations in samples Co17-37 and Co17-38 are comparable (Figs. 20b, 21b). However, data from Co17-38 are focused upon as the larger population is more reliable for providing accurate ages. U–Pb monazite upper intercept ages of 3142 ± 24 Ma (MSWD = 2.0) and 3139 ± 15 Ma (MSWD = 1.9) were calculated for the prograde and peak populations, respectively (Fig. 21b). These agree with the interpreted age derived from the U–Pb zircon study (Fig. 22a). The large range in monazite HREE chemistry represents a record of the full duration of garnet growth in the assemblage. The prograde monazite population formed during early stages of garnet formation, possibly pre-dating garnet, while the peak population formed in the later stages, potentially post-dating garnet growth. The large overlap in the ages of prograde and peak monazite populations is evidence indicating that the large garnet porphyroblasts observed in the rock were formed entirely during the *ca.* 3.15 Ga event. Therefore, the associated high-

pressure assemblage captured within garnet must have occurred during the *ca*. 3.15 Ga event.

Monazites in Co17-41 recorded the age of the third event, providing a lower intercept age of 782 ± 10 Ma (MSWD = 1.0) (Fig. 22a). Monazites in this sample show a strong link in HREE and Y enrichment with decreasing age (Fig. 16c, 16d). This suggests that garnet was breaking down, liberating HREEs and Y for monazite to sequester. Thus, ruling it out of contention for having any influence on the garnet-dominated peak assemblage.

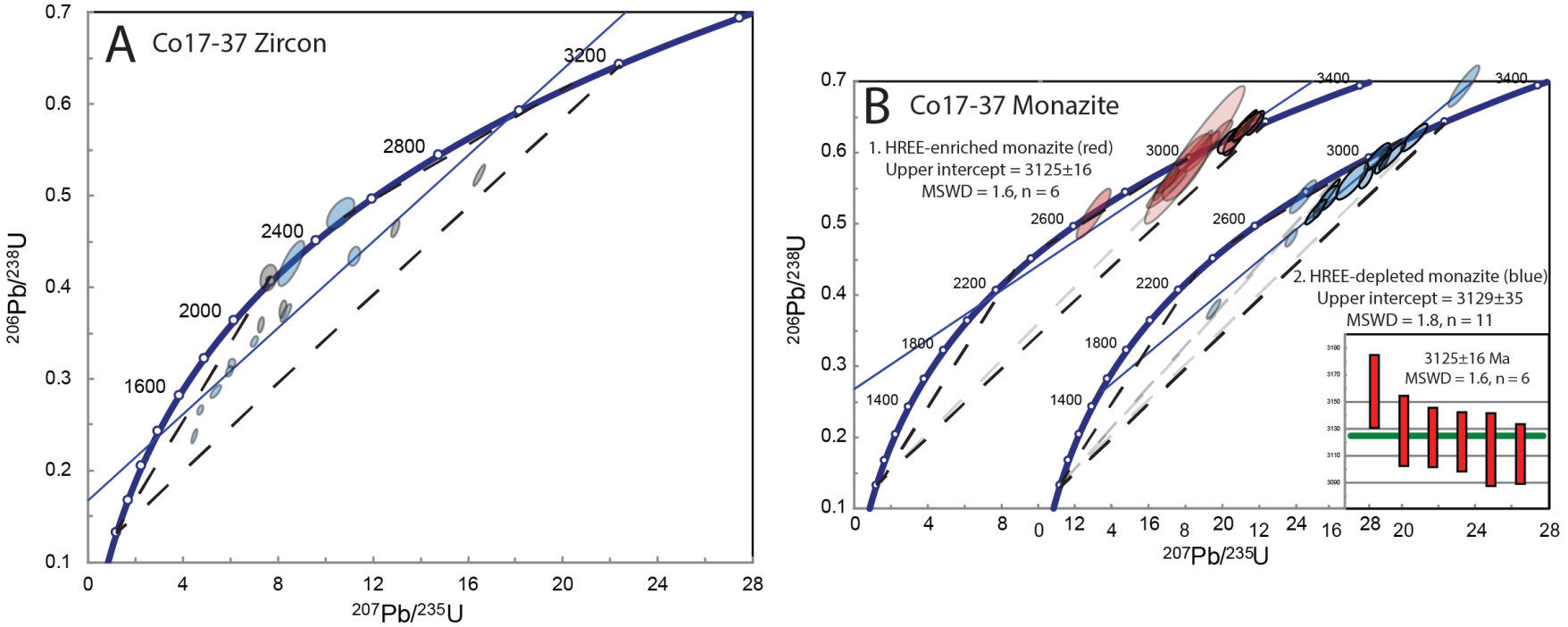

Figure 20: Annotated Concordia diagrams of in-situ analyses from near-peak sample, Co17-37. Opaque dashed lines represent discordant lines between the three identified metamorphic events experienced by this rock. The lines intersect the concordia at 3200–2500 Ma, 2300–800 Ma 3200–800 Ma enclosing virtually all of the data. Transparent dashed lines represent discordant lines that data are observed to follow with partial resetting. Ellipses with bold rims were used in the calculation of intercept ages. (a) Zircon concordia diagram. Blue ellipses represent metamorphic zircons, while grey zircons are unknown as they were not analysed for trace elements. No intercept ages were quoted for due to a lack of data. (b) Monazite concordia plots for HREE-enriched (red) and HREE-depleted (blue) monazites. Concordia are shown side-by-side due to them being largely overlapping populations. Inserted is the ^{207} Pb/^{206}Pb mean-weighted average used to calculate the upper intercept for the HREE-enriched monazites (red).

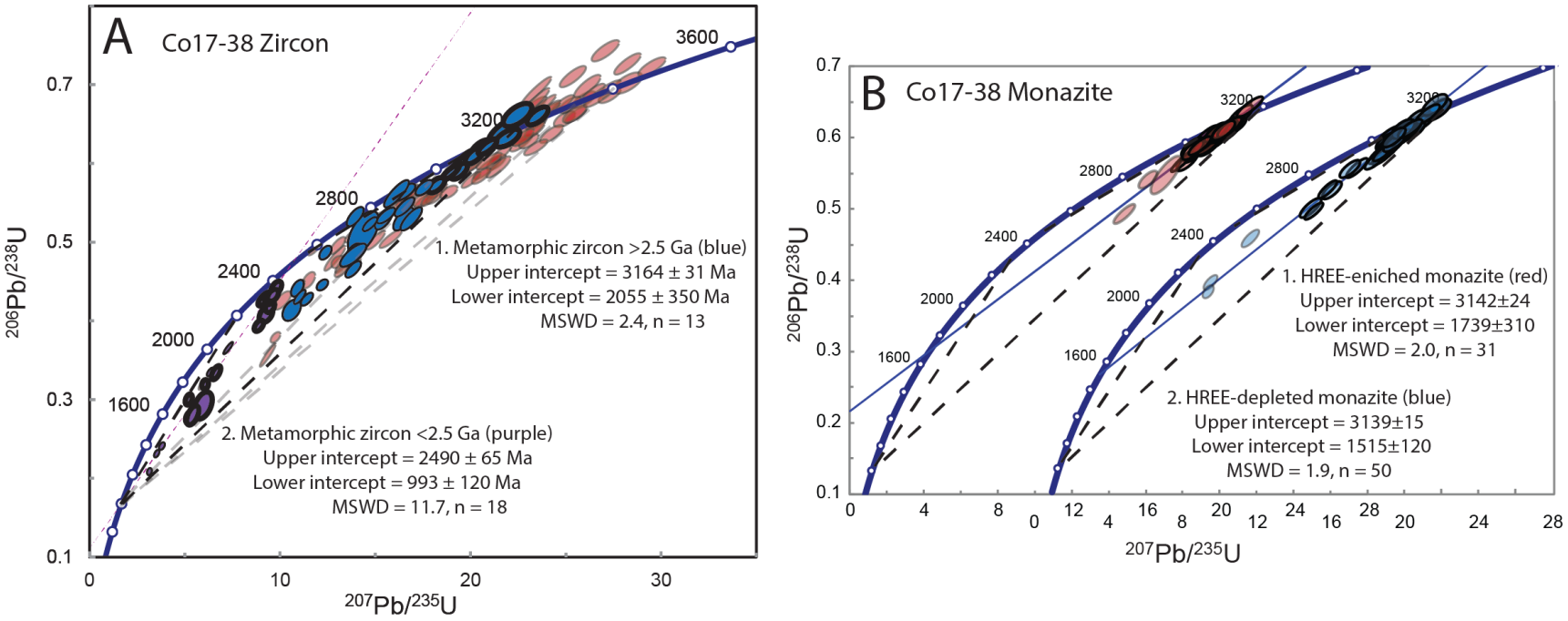

Figure 21: Annotated Concordia diagrams of grain-mounted analyses from sample Co17-38. Opaque dashed lines represent discordant lines between the three identified metamorphic events experienced by this rock. The lines intersect the concordia at 3200–2500 Ma, 2300–800 Ma 3200–800 Ma enclosing virtually all of the metamorphic-related data. Transparent dashed lines represent discordant lines that data are observed to follow with partial resetting. Ellipses with bold rims were used in the calculation of intercepts quoted in the figure. (a) Zircon concordia diagram. Blue ellipses represent metamorphic zircons older than 2.5 Ga, purple ellipses represent metamorphic zircons younger than 2.5 Ga and red ellipses represent detrital zircons. (b) Monazite concordia plots for HREE-enriched (red) and HREE-depleted (blue) monazites. Concordia are shown side-by-side due to them being largely overlapping populations.

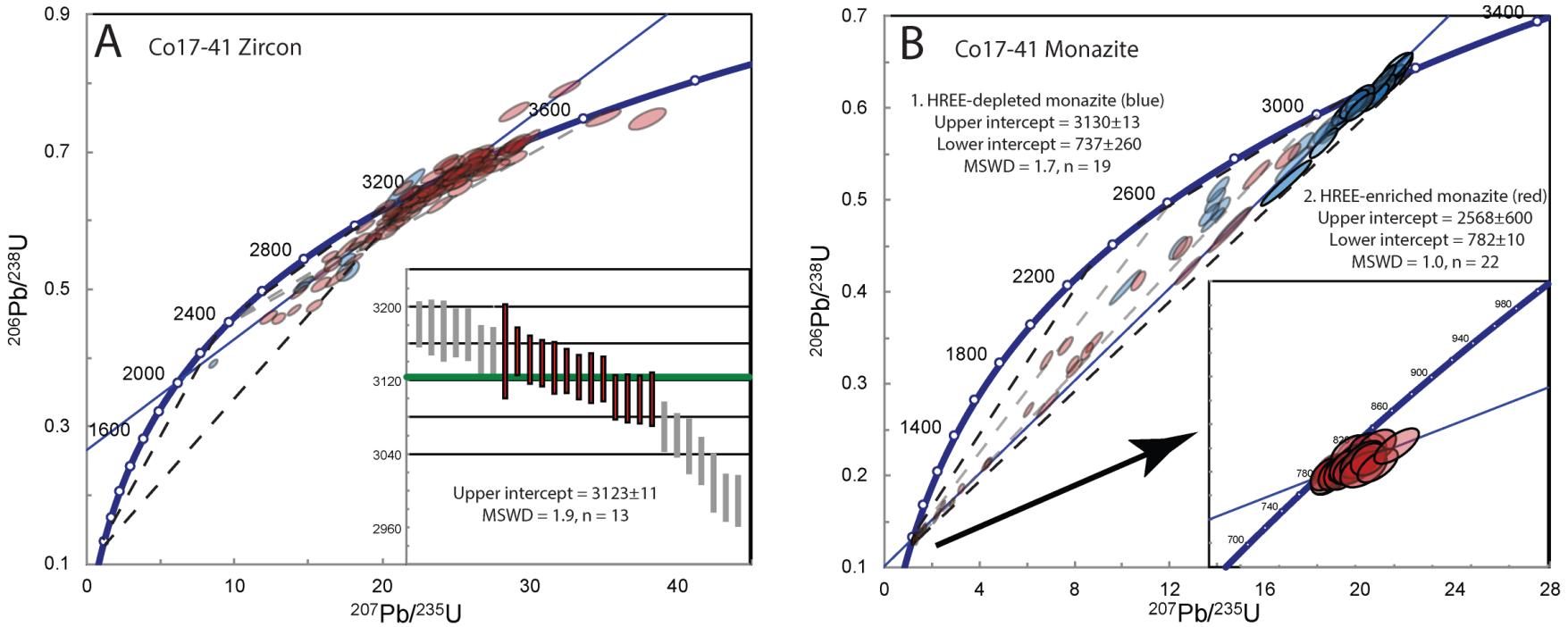

Figure 22: Annotated Concordia diagrams of grain-mounted analyses from sample Co17-41. Opaque dashed lines represent discordant lines between the three identified metamorphic events experienced by this rock. The lines intersect the concordia at 3200–2500 Ma, 2300–800 Ma 3200–800 Ma. Transparent dashed lines represent discordant lines that data are observed to follow with partial resetting. Ellipses with bold rims were used in the calculation of intercepts quoted in the figure. (a) Zircon concordia diagram. Blue ellipses represent metamorphic zircons and red ellipses represent detrital zircons. Inserted is the mean-weighted average used to calculate the upper intercept, where zircons begin becoming discordant. (b) Monazite concordia plots for HREE-enriched (red) and HREE-depleted (blue) monazites. Inserted is an enlarged image of the lower intercept, showing the analyses used in the calculation of the lower intercept age.

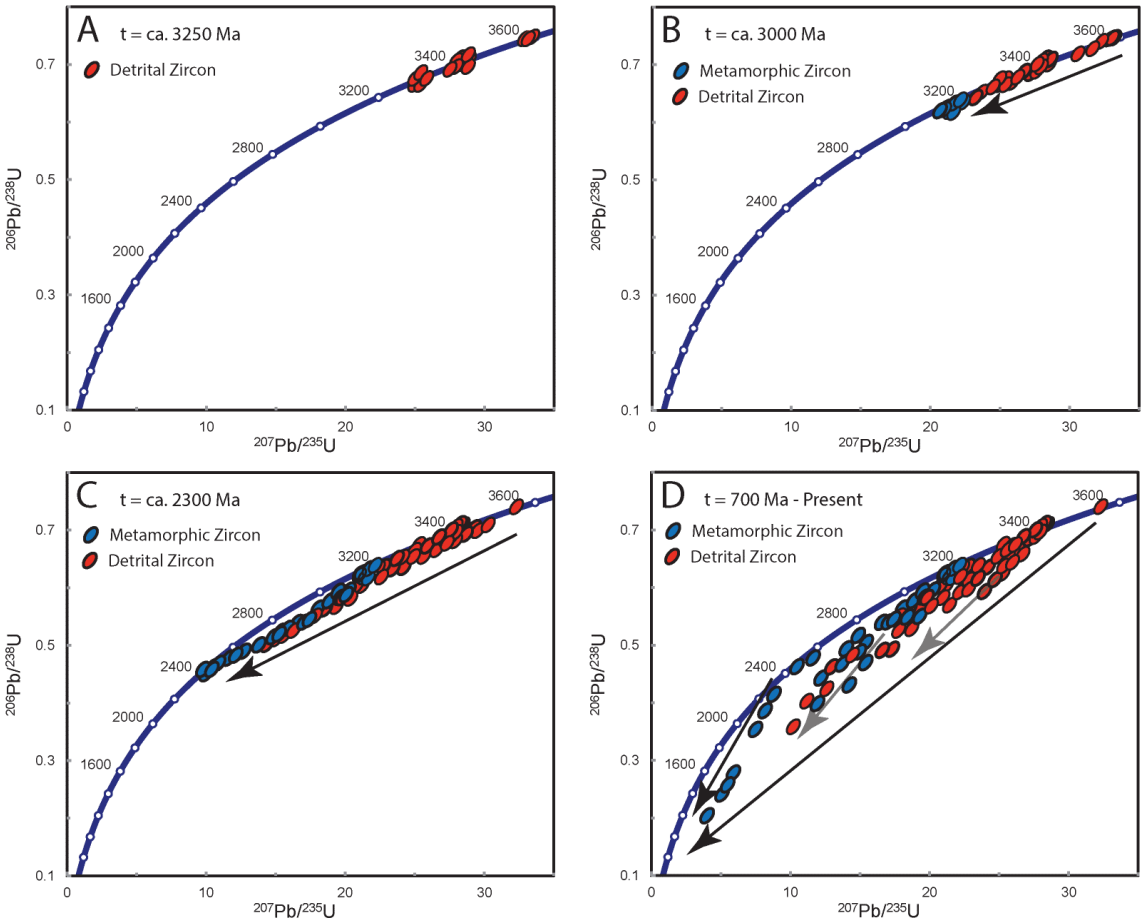

Figure 23: A series of schematic concordia diagram explaining the development of the common trend observed in the zircon concordia in this study (Figs. 20–22). Red ellipses represent detrital zircons, while blue ellipses are zircons formed during metamorphism. (a) showing the representative zircon concordia diagram during the rocks diagenesis. Three zircon populations have been shown to symbolise the input from detrital sources, the ages of these populations are meaningless. (b) zircon concordia after the initial metamorphic event at *ca.* 3150 Ma. The formation of the population of metamorphic zircons has occurred, while detrital zircons have experienced various levels of re-setting, smearing the array toward 3100 Ma. The majority, if not all zircons are believed to have been formed by this point. (c) zircon concordia after the second metamorphic event between 2500–2300 Ma. Both populations have experienced various levels of resetting toward this age. Additional metamorphic zircons may have been formed in this event. (d) zircon concordia after the last metamorphic event at *ca.* 800 Ma, demonstrating how this event has contributed to the largely discordant arrays seen in this study.

Pressure–temperature conditions during the Mesoarchaean event

Phase equilibria modelling of samples Co17-37 and Co17-38 have been undertaken to determine the *P–T* conditions under which the calculated peak assemblage for the rock was formed. The results from Co17-37 are focused upon as this sample more closely reflects the peak assemblage.

DETERMINING THE PEAK ASSEMBLAGE

Sample Co17-37 contains garnet + kyanite + biotite + K-feldspar + plagioclase + quartz + rutile + sillimanite (inclusions in garnet). However, petrological relationships and major element zonation in garnet (Figs. 5, 6) indicate that this mineral association is a combination of peak and retrograde mineral assemblages.

Major element zonation patterns in garnet generally reflect the retrograde progression of the rock, as major elements are relatively incompatible and more sensitive to changing conditions. Mg-enriched cores and Fe-enriched rims in garnet are described as characteristic retrograde zonation patterns. As temperature decreases, Fe is preferentially incorporated into garnet over Mg. Therefore, Mg-rich cores are interpreted as being remnant from compositions as close to the metamorphic peak as preserved, while Fe-rich rims are the product of retrogression down temperature (e.g. Frost, 1962; Kretz, 1964; Saxena, 1968; Saxena & Hollander, 1969; Tracy, Robinson, & Thompson, 1976).

The peak assemblage formed at *ca.* 3.15 Ga is interpreted to be garnet + kyanite + K-feldspar + quartz + rutile + melt. The relationship between K-feldspar in leucosomes, and the peak assemblage was ambiguous from petrography, but large negative Eu anomalies in garnet and monazite, formed at *ca.* 3.15 Ga, confirm it being coeval with the peak assemblage (Figs. 14a, 15a). This also confirms that melt was present in the peak assemblage since melting is required to form leucosomes. Sillimanite, and an early generation of biotite that occur as inclusions within

garnet are interpreted as remnants of the prograde assemblage. Fine-grained plagioclase and secondary kyanite, quartz and biotite are interpreted as retrograde products, formed through a reaction between garnet and melt (Fig. 4b, e). The retrograde reaction is summarised as: garnet + melt → biotite + kyanite + plagioclase + quartz.

CO17-37 P–T CONDITIONS

The region in the peak field that best corresponds to calculated mineral modes provides minimum *P–T* constraints of ~13.1–13.7 kbar, ~950–980◦C. Upper *P–T* constraints have not been made, but for the purpose of providing a *P–T* range, realistic conditions of 15 kbar, 990°C are used. However, peak conditions could exceed this. Nonetheless, the quoted *P–T* range corresponds to apparent thermal gradients of between 72.5◦C/kbar to 66˚C/kbar.

An anti-clockwise *P–T* path is inferred for Co17-37. Inclusions of sillimanite, kyanite and biotite within garnet provide constraints for the prograde path (Fig. 4d). Little can be inferred from this, other than the transition from sillimanite to kyanite up-pressure took place within fields of biotite stability. The retrograde evolution of the rock resulted in an increase in the modes of biotite and kyanite, with a decrease in the abundance of melt. Importantly, the melt recrystallised in the rock as plagioclase, quartz, biotite and kyanite, while little change in the mode of K-feldspar from the peak assemblage appears to have occurred. This information ultimately constrains the field to where retrograde reactions were last recorded (Figs. 17, 19). The anti-clockwise *P–T* path inferred shows that peak conditions are followed by cooling and then decompression (Fig. 17).

Appropriate sample selection and the correct determination of the peak assemblage are crucial for accurately constraining the peak *P–T* conditions. The results from this study, compared to Amaldev et al. (2016) validate the importance of this. Both studies undertook phase equilibria

modelling of rocks from the same outcrop. However, Amaldev et al. (2016) interpreted a sub-solidus peak assemblage of garnet + kyanite + biotite + K-feldspar + plagioclase + rutile + quartz, providing a poorly constrained peak *P–T* range of 5.5–10 kbar, 600–800°C. Furthermore, the sample modelled by Amaldev et al. (2016) largely resembles what has been interpreted in this study as a retrogressed assemblage, influenced by a later event, and their results substantially underestimated the peak *P–T* conditions for the Mesoarchaean event.

Implications for the Proterozoic regional geology

The influence of a Palaeoproterozoic metamorphic event on these high-pressure granulites is ambiguous, provided that only three concordant zircon analyses between 2500–2300 Ma (Fig. 8a), and an array of discordant zircons between *ca.* 2500–1000 Ma (Fig. 22a) constitute the evidence for this event. However, the demonstrated effect of multiple thermal events on a zircon population of various textures supports the influence of a thermal event around this time, while it also accounts for the decoupling between zircon and monazite U–Pb ages.

In addition, ~250 km east in the Salem Block, high-pressure metamorphism has been reported in the Kanja Malai hills at 2490–2470 Ma (Fig. 1a), with kyanite-garnet bearing felsic granulites estimating *P–T* conditions of 14–16 kbar and ~820–860°C (Anderson et al., 2012; Saitoh, Tsunogae, Santosh, Chetty, & Horie, 2011). Currently, the westward extent of the Kanja Malai metamorphism is undefined. The similarities between the assemblages and metamorphic conditions suggest the Kanja Malai tectonothermal event may have had some limited affect in this region. But age constrains in this study are insufficient to confidently link the two events.

The age of the most recent metamorphism was captured by monazite age data. Sample Co17-41 gives a lower intercept age of 782 ± 10 Ma (Fig. 23b). This age corresponds to the ages of syenite magmatism located along the northern margin of the Southern Granulite Terrain (Fig. 1b), believed

to have formed through transcrustal rifting along reactivated paleo-suture zones (Santosh et al., 2014).

Tectonic implications for the Mesoarchaean

The metamorphic conditions recorded in these high-pressure granulites at *ca.* 3.15 Ga are significant, given the rarity of ancient high-pressure metamorphism (Fig. 24b).

Assuming there was no influence from tectonic overpressure (e.g. Gerya, 2015), the constrained peak conditions of ~13.1–15 kbar, 950–990°C corresponds to burial beneath ~45–50 km of continental crust. With a minimum calculated apparent thermal gradient of 72.5°C/kbar, this falls into the eclogite-high pressure granulite (E–HPG) metamorphic field (Fig. 24a); (Brown, 2007a). While there are reports of Archaean high-pressure metamorphism (Anderson et al., 2012; Dziggel, Kokfelt, Kolb, Kisters, & Reifenröther, 2017; Moyen et al., 2006) only one other occurrence of high-pressure metamorphism is currently recorded prior to the Neoarchaean. This occurred in c*a.* 3.23 Ga supracrustal amphibolites of the Barberton Terrane, which recorded conditions of 12–15 kbars at temperatures of 600–650°C, with apparent thermal gradients of 12–15°C/km (Moyen et al., 2006).

These occurrences of high-pressure metamorphism, indicating potential for subduction (Moyen et al., 2006) and orogenesis (this study) in the early Mesoarchaean, are not supported in stagnant lid convection theory conditions (Brown, 2014; Johnson et al., 2014; Reese, Solomatov, & Moresi, 1998). This theory proposes that in the primitive Earth, a largely immobile lithosphere sat on top of a vigorously convecting mantle. 2D geodynamic models suggest that potential mantle temperatures of >1600 ^{o}C occurred during the Mesoarchaean, capable of causing instability and basal delamination of the lower crust (Johnson et al., 2014) .Therefore, it is generally considered

that tectonically thickened crust was not preserved in these conditions. The Archaean metamorphic record largely supports the existence of this regime up until the end of the Neoarchaean, where occurrences of high-pressure metamorphism become more frequent (Brown, 2014). However, numerical models produced by Sizova et al. (2010) suggest that the first transition toward a more modern style tectonic regime occurred as early as 3.2 Ga. This model accommodates the observations of high-pressure metamorphism recorded in the earlier stages of the Archaean (e.g. Dziggel et al., 2017; Moyen et al., 2006) implying that the transition from the stagnant lid regime toward a more modern style of tectonics may have occurred significantly earlier than currently recognised (Brown, 2014). The transition toward modern style tectonics is defined by the simultaneous formation of contrasting styles of metamorphism (Brown, 2006). In the modern Earth, this is recorded as ultra-high pressure (UHP) metamorphism formed in the subducting trench, with granulite–ultra-high temperature (G–UHT) metamorphism in the back-arc in the overriding plate. In the ancient Earth, hotter mantle temperatures are thought to have altered subduction mechanisms. Therefore, the record of eclogite–high-pressure granulite (E–HPG) metamorphism with G–UHT metamorphism is interpreted to represent subduction-to-accretion orogenesis with back-arc extension (Brown, 2006). Thus, marking the onset of the transition toward modern day tectonics. Currently, the oldest preserved evidence of a paired metamorphic belt occurs at *ca.* 2720 Ma (Dziggel et al., 2017). However, further investigation of the Mercara Shear Zone and adjacent terranes could expose a contemporaneous G–UHT metamorphic belt for the E–HPG metamorphism identified in this study. This would constitute strong evidence for an earlier transition toward modern style tectonics.

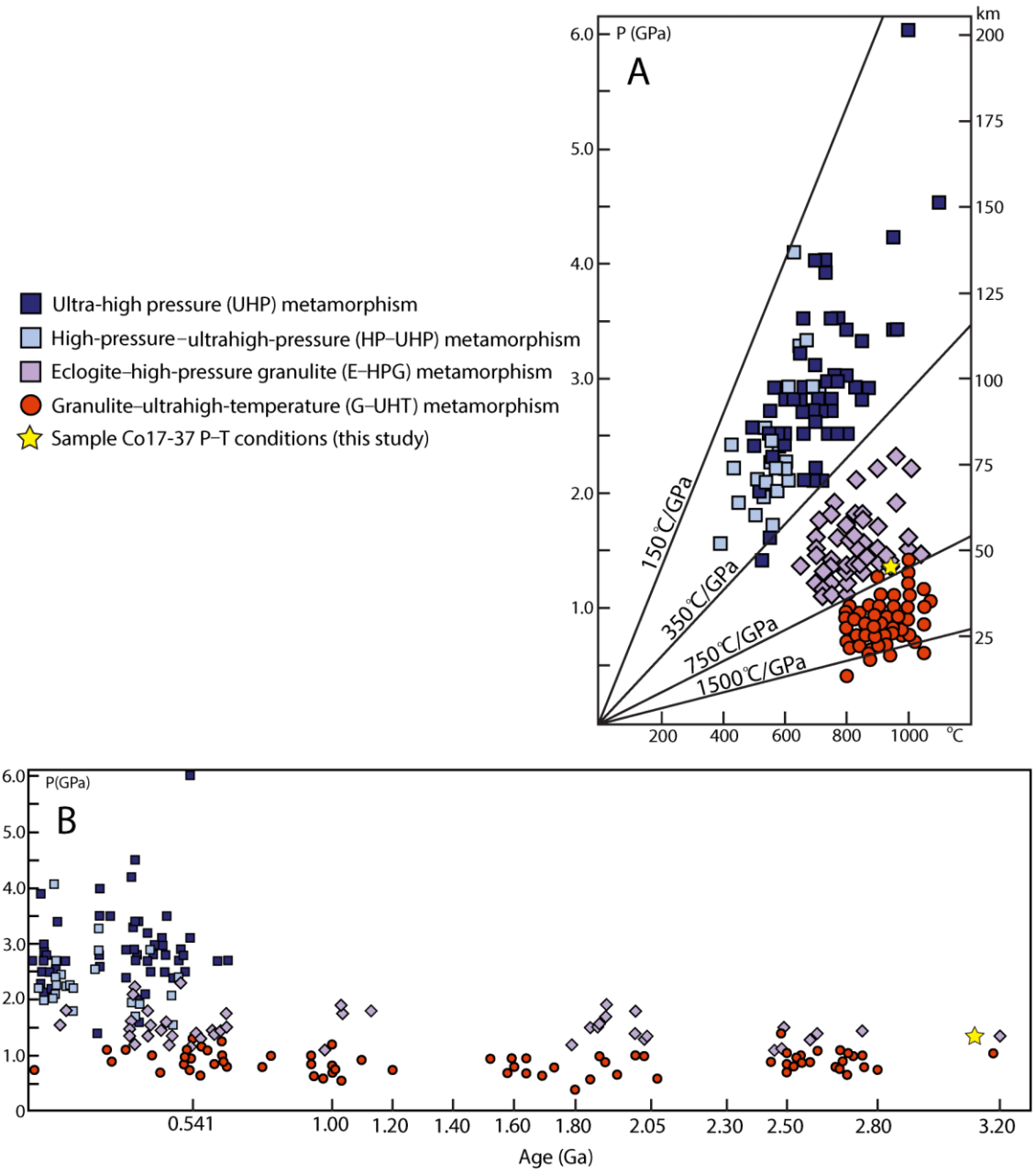

Figure 24: Compiled peak metamorphic conditions plotted by type (annotated from Brown, 2014). Types of metamorphism are: granulite-ultrahigh temperature (G-UHT): orange circles, eclogite–high-pressure granulite (E–HPG): light purple diamonds, high-pressure–ultrahigh-pressure (HP–UHP): light blue squares, ultrahigh-pressure (UHP): pale blue squares. The yellow stars represent the minimum constrained conditions calculated from this study. (A) Apparent thermal gradients of metamorphic belts with corresponding depths of burial beneath continental crust. (B) Peak pressures recorded in metamorphic belts against time.

CONCLUSIONS

This study expands on previous work undertaken on the proposed ancient high-pressure metamorphism in SW India. Integrated U–Pb ages and trace element data from geochronometers provide the essential link between the calculated ages and the observed assemblage, validating the occurrence of high-pressure metamorphism in the Mesoarchaean. In addition, phase equilibria forward modelling, combined with mineral modes calculated from the metamorphic peak improve current constraints on the peak *P–T* conditions of the Mesoarchaean event.

1. Three metamorphic events were reported in this study. Monazite U–Pb intercept ages of 3139 $\pm$ 15 Ma and 782 $\pm$ 10 Ma recorded the ages of the earliest and most recent metamorphic events. The second event is ambiguous, with largely discordant zircon arrays suggesting it may have occurred between 2500–2300 Ma.
2. The peak assemblage in the rock was preserved from the Mesoarchaean event, occurring at minimum conditions of 13.1 kbar at 940°C.
3. Mesoarchaean metamorphic conditions infer burial beneath a minimum of ~45 km of continental crust, with a minimum apparent thermal gradient of 72 ^{o}C/km. Evidence for the preservation of crust in these conditions has not yet been recorded in rocks of this antiquity.

ACKNOWLEDGMENTS

Thank you to my supervisors Prof. Alan Collins and Prof. Martin Hand for their invaluable time and commitment to this project, both in the field and throughout the year. Prof. M. Santosh is thanked for his contribution in funding this project.
Prof. K. Sajeev from the Indian Institute of Science is thanked for his hospitality and his assistance in organising visas and accommodation for field work in India. A huge thank you to post-doc and PhD candidates from the TRaX and CERG groups, for their vital input and advice throughout the course of the year. Brandon Alessio and Morgan Blades are thanked in extension for their assistance in sample preparation, data acquisition and interpretation, while Laura Morrissey, Kiara Bockmann and Naomi Tucker are thanked for their guidance in the use of THERMOCALC and TC-Investigator software. Alec Walsh is thanked for his assistance in the Mawson Laboratories, and Dr. Ben Wade, Dr. Sarah Gilbert and Dr. David Kelsey are thanked for their constant support

and patience during data acquisition at Adelaide Microscopy. Dr. David Kelsey is thanked again for his contributions in data interpretation.

REFERENCES

Adiga, K. (1982). On the high grade schistose rocks equivalent to the Sargur schist complex in Kasaragod taluk, Cannanore district, Kerala. *Records of the Geological Survey of India, 114*(5), 31-36.

Amaldev, T., Santosh, M., Tang, L., Baiju, K., Tsunogae, T., & Satyanarayanan, M. (2016). Mesoarchean convergent margin processes and crustal evolution: Petrologic, geochemical and zircon U–Pb and Lu–Hf data from the Mercara Suture Zone, southern India. *Gondwana Research, 37*, 182-204.

Anderson, J. R., Payne, J. L., Kelsey, D. E., Hand, M., Collins, A. S., & Santosh, M. (2012). High-pressure granulites at the dawn of the Proterozoic. *Geology, 40*(5), 431-434.

Bhaskar Rao, Y., Sivaraman, T., Pantulu, G., Gopalan, K., & Naqvi, S. (1992). Rb− Sr ages of Late Archean metavolcanics and granites Dharwar craton, South India and evidence for Early Proterozoic thermotectonic event (s). *Precambrian research, 59*(1-2), 145-170.

Brown, M. (2006). Duality of thermal regimes is the distinctive characteristic of plate tectonics since the Neoarchean. *Geology, 34*(11), 961-964. doi: 10.1130/G22853A.1

Brown, M. (2007a). Metamorphic conditions in orogenic belts: a record of secular change. *International Geology Review, 49*(3), 193-234.

Brown, M. (2007b). Metamorphism, plate tectonics, and the supercontinent cycle. *Earth Science Frontiers, 14*(1), 1-18.

Brown, M. (2014). The contribution of metamorphic petrology to understanding lithosphere evolution and geodynamics. *Geoscience Frontiers, 5*(4), 553-569.

Chakoumakos, B. C., Murakami, T., Lumpkin, G. R., & EWING, R. (1987). Alpha-decay-induced fracturing in zircon--the transition from the crystalline to the metamict state. *Science, 236*(4808), 1556-1559.

Chardon, D., Jayananda, M., Chetty, T. R., & Peucat, J. J. (2008). Precambrian continental strain and shear zone patterns: South Indian case. *Journal of Geophysical Research: Solid Earth, 113*(B8).

Chetty, T., Mohanty, D., & Yellappa, T. (2012). Mapping of shear zones in the Western Ghats, Southwestern part of Dharwar Craton. *Journal of the Geological Society of India, 79*(2), 151-154.

Corfu, F., Hanchar, J. M., Hoskin, P. W., & Kinny, P. (2003). Atlas of zircon textures. *Reviews in mineralogy and geochemistry, 53*(1), 469-500.

Deer, W. A., Howie, R. A., & Zussman, J. (1992). *An introduction to the rock-forming minerals* (Vol. 2): Longman Scientific & Technical Hong Kong.

Devaraju, J., & Janardhan, A. (2004). Metamorphic History of Staurolite-Kyanite-Garnet-Cordieritebearing Pelites of Mangalore-Mercaka Lineament, South India. *Geological Society of India, 63*(5), 555-561.

Dziggel, A., Kokfelt, T. F., Kolb, J., Kisters, A. F. M., & Reifenröther, R. (2017). Tectonic switches and the exhumation of deep-crustal granulites during Neoarchean terrane accretion in the area around Grædefjord, SW Greenland. *Precambrian Research,*

300(Supplement C), 223-245. doi: https://doi.org/10.1016/j.precamres.2017.07.027

Frost, M. J. (1962). Metamorphic grade and iron-magnesium distribution between co-existing garnet-biotite and garnet-hornblende. *Geological Magazine, 99*(5), 427-438.

Gerya, T. (2015). Tectonic overpressure and underpressure in lithospheric tectonics and metamorphism. *Journal of Metamorphic Geology, 33*(8), 785-800.

Ghosh, J. G., de Wit, M. J., & Zartman, R. (2004). Age and tectonic evolution of Neoproterozoic ductile shear zones in the Southern Granulite Terrain of India, with implications for Gondwana studies. *Tectonics, 23*(3).

Hegde, V., & Chavadi, V. (2009). Geochemistry of late Archaean metagreywackes from the Western Dharwar Craton, South India: implications for provenance and nature of the Late Archaean crust. *Gondwana Research, 15*(2), 178-187.

Hellstrom, J., Paton, C., Woodhead, J., & Hergt, J. (2008). Iolite: software for spatially resolved LA-(quad and MC) ICPMS analysis. *Mineralogical Association of Canada short course series, 40*, 343-348.

Hickmott, D., Shimizu, N., Spear, F., & Selverstone, J. (1987). Trace-element zoning in a metamorphic garnet. *Geology, 15*(6), 573-576.

Holland, T., & Powell, R. (2011). An improved and extended internally consistent thermodynamic dataset for phases of petrological interest, involving a new equation of state for solids. *Journal of Metamorphic Geology, 29*(3), 333-383.

Ishwar-Kumar, C., Santosh, M., Wilde, S., Tsunogae, T., Itaya, T., Windley, B., & Sajeev, K. (2016). Mesoproterozoic suturing of Archean crustal blocks in western peninsular India: Implications for India–Madagascar correlations. *Lithos, 263*, 143-160.

Jackson, S. E., Pearson, N. J., Griffin, W. L., & Belousova, E. A. (2004). The application of laser ablation-inductively coupled plasma-mass spectrometry to in situ U–Pb zircon geochronology. *chemical Geology, 211*(1), 47-69.

Janots, E., Engi, M., Berger, A., Allaz, J., Schwarz, J. O., & Spandler, C. (2008). Prograde metamorphic sequence of REE minerals in pelitic rocks of the Central Alps: implications for allanite–monazite–xenotime phase relations from 250 to 610 C. *Journal of Metamorphic Geology, 26*(5), 509-526.

Jayananda, M., Chardon, D., Peucat, J.-J., & Capdevila, R. (2006). 2.61 Ga potassic granites and crustal reworking in the western Dharwar craton, southern India: tectonic, geochronologic and geochemical constraints. *Precambrian Research, 150*(1), 1-26.

Jochum, K. P., Weis, U., Stoll, B., Kuzmin, D., Yang, Q., Raczek, I., . . . Frick, D. A. (2011). Determination of reference values for NIST SRM 610–617 glasses following ISO guidelines. *Geostandards and Geoanalytical Research, 35*(4), 397-429.

Johnson, T. E., Brown, M., Gardiner, N. J., Kirkland, C. L., & Smithies, R. H. (2017). Earth's first stable continents did not form by subduction. *Nature, 543*(7644), 239-242.

Johnson, T. E., Brown, M., Kaus, B. J., & VanTongeren, J. A. (2014). Delamination and recycling of Archaean crust caused by gravitational instabilities. *Nature Geoscience, 7*(1), 47.

Johnson, T. E., & White, R. (2011). Phase equilibrium constraints on conditions of granulite-facies metamorphism at Scourie, NW Scotland. *Journal of the Geological Society, 168*(1), 147-158.

Kelsey, D. E., & Hand, M. (2015). On ultrahigh temperature crustal metamorphism: phase equilibria, trace element thermometry, bulk composition, heat sources, timescales and tectonic settings. *Geoscience Frontiers, 6*(3), 311-356.

Kretz, R. (1964). Analysis of equilibrium in garnet–biotite–sillimanite gneisses from Quebec. *Journal of Petrology, 5*(1), 1-20.

Lanzirotti, A. (1995). Yttrium zoning in metamorphic garnets. *Geochimica et Cosmochimica Acta, 59*(19), 4105-4110.

Mansfield, W. (2016). Age, provenance and metamorphic conditions of the Mercara Shear Zone, Coorg Block, India. Honours Thesis. *University of Adelaide, (Unpublished)*.

Mezger, K., & Krogstad, E. J. (1997). Interpretation of discordant U-Pb zircon ages: An evaluation. *Journal of Metamorphic Geology, 15*(1), 127-140. doi: 10.1111/j.1525-1314.1997.00008.x

Moyen, J.-F., Stevens, G., & Kisters, A. (2006). Record of mid-Archaean subduction from metamorphism in the Barberton terrain, South Africa. *Nature, 442*(7102), 559.

Nair, M., Vidyadharan, K., Pawar, S., Sukumaran, P., & Murthy, Y. (1976). The structural and stratigraphic relationship of the schistose rocks and associated igneous rocks of the Tellicherry–Manantoddy area, Cannanore district. *Kerala India Mineral, 16*, 89-100.

Nutman, A., Chadwick, B., Ramakrishnan, M., & Viswanatha, M. (1992). SHRIMP U-Pb ages of detrital zircon in Sargur supracrustal rocks in western Karnataka, southern India. *Geological Society of India, 39*(5), 367-374.

Nutman, A., Chadwick, B., Rao, B. K., & Vasudev, V. (1996). SHRIMP U/Pb zircon ages of acid volcanic rocks in the Chitradurga and Sandur groups, and granites adjacent to the Sandur schist belt, Karnataka. *Geological Society of India, 47*(2), 153-164.

Otamendi, J. E., Jesús, D., Douce, A. E. P., & Castro, A. (2002). Rayleigh fractionation of heavy rare earths and yttrium during metamorphic garnet growth. *Geology, 30*(2), 159-162.

Patchett, P. J. (1983). Importance of the Lu-Hf isotopic system in studies of planetary chronology and chemical evolution. *Geochimica et Cosmochimica Acta, 47*(1), 81-91.

Paton, C., Hellstrom, J., Paul, B., Woodhead, J., & Hergt, J. (2011). Iolite: Freeware for the visualisation and processing of mass spectrometric data. *Journal of Analytical Atomic Spectrometry, 26*(12), 2508-2518.

Payne, J. L., Hand, M., Barovich, K., & Wade, B. (2008). Temporal constraints on the timing of high-grade metamorphism in the northern Gawler Craton: implications for assembly of the Australian Proterozoic. *Australian Journal of Earth Sciences, 55*(5), 623-640.

Peucat, J., Bouhallier, H., Fanning, C., & Jayananda, M. (1995). Age of the Holenarsipur greenstone belt, relationships with the surrounding gneisses (Karnataka, South India). *The Journal of Geology, 103*(6), 701-710.

Peucat, J., Mahabaleswar, B., & Jayananda, M. (1993). Age of younger tonalitic magmatism and granulitic metamorphism in the South Indian transition zone (Krishnagiri area); comparison with older Peninsular gneisses from the Gorur–Hassan area. *Journal of Metamorphic Geology, 11*(6), 879-888.

Powell, R., & Holland, T. (1988). An internally consistent dataset with uncertainties and correlations: 3. Applications to geobarometry, worked examples and a computer program. *Journal of metamorphic Geology, 6*(2), 173-204.

Powell, R., White, R., Green, E., Holland, T., & Diener, J. (2014). On parameterizing thermodynamic descriptions of minerals for petrological calculations. *Journal of Metamorphic Geology, 32*(3), 245-260.

Pyle, J. M., & Spear, F. S. (1999). Yttrium zoning in garnet: coupling of major and accessory phases during metamorphic reactions. *Geological Materials Research, 1*(6), 1-49.

Raimondo, T., Payne, J., Wade, B., Lanari, P., Clark, C., & Hand, M. (2017). Trace element mapping by LA-ICP-MS: assessing geochemical mobility in garnet. *Contributions to Mineralogy and Petrology, 172*(4), 17.

Ramakrishnan, M., & Nath, J. S. (1981). *Early Precambrian supracrustals of southern Karnataka* (Vol. 112): Geological Survey of India.

Rao, Y. B., Janardhan, A., Kumar, T. V., Narayana, B., Dayal, A., Taylor, P., & Chetty, T. (2003). Sm-Nd model ages and Rb-Sr isotopic systematics of charnockites and gneisses across the Cauvery shear zone, Southern India: Implications for the Archaean-Neoproterozoic terrane boundary in the Southern Granulite Terrain. *MEMOIRS-GEOLOGICAL SOCIETY OF INDIA*, 297-317.

Reese, C., Solomatov, V., & Moresi, L. N. (1998). Heat transport efficiency for stagnant lid convection with dislocation viscosity: Application to Mars and Venus. *Journal of Geophysical Research: Planets, 103*(E6), 13643-13657.

Rekha, S., Bhattacharya, A., & Chatterjee, N. (2014). Tectonic restoration of the Precambrian crystalline rocks along the west coast of India: Correlation with eastern Madagascar in East Gondwana. *Precambrian Research, 252*, 191-208.

Root, D. B., Hacker, B., Mattinson, J., & Wooden, J. L. (2004). Zircon geochronology and ca. 400 Ma exhumation of Norwegian ultrahigh-pressure rocks: an ion microprobe and chemical abrasion study. *Earth and Planetary Science Letters, 228*(3), 325-341.

Rubatto, D. (2002). Zircon trace element geochemistry: partitioning with garnet and the link between U–Pb ages and metamorphism. *Chemical geology, 184*(1), 123-138.

Rubatto, D., Chakraborty, S., & Dasgupta, S. (2013). Timescales of crustal melting in the Higher Himalayan Crystallines (Sikkim, Eastern Himalaya) inferred from trace element-constrained monazite and zircon chronology. *Contributions to Mineralogy and Petrology, 165*(2), 349-372.

Rubatto, D., Williams, I. S., & Buick, I. S. (2001). Zircon and monazite response to prograde metamorphism in the Reynolds Range, central Australia. *Contributions to Mineralogy and Petrology, 140*(4), 458-468.

Saitoh, Y., Tsunogae, T., Santosh, M., Chetty, T., & Horie, K. (2011). Neoarchean high-pressure metamorphism from the northern margin of the Palghat–Cauvery Suture Zone, southern India: Petrology and zircon SHRIMP geochronology. *Journal of Asian Earth Sciences, 42*(3), 268-285.

Santosh, M., Yang, Q.-Y., Mohan, M. R., Tsunogae, T., Shaji, E., & Satyanarayanan, M. (2014). Cryogenian alkaline magmatism in the Southern Granulite Terrane, India: Petrology, geochemistry, zircon U–Pb ages and Lu–Hf isotopes. *Lithos, 208*, 430-445.

Santosh, M., Yang, Q.-Y., Shaji, E., Tsunogae, T., Mohan, M. R., & Satyanarayanan, M. (2015). An exotic Mesoarchean microcontinent: the Coorg Block, southern India. *Gondwana Research, 27*(1), 165-195.

Sato, K., Santosh, M., Tsunogae, T., Chetty, T., & Hirata, T. (2011). Subduction–accretion–collision history along the Gondwana suture in southern India: a laser ablation ICP-MS study of zircon chronology. *Journal of Asian Earth Sciences, 40*(1), 162-171.

Saxena, S. (1968). Distribution of iron and magnesium between coexisting garnet and clinopyroxene in rocks of varying metamorphic grade. *American Mineralogist, 53*(11-1), 2018-&.

Saxena, S., & Hollander, N. (1969). Distribution of iron and magnesium in coexisting biotite, garnet, and cordierite. *American Journal of Science, 267*(2), 210-216.

Schaltegger, U., Fanning, C., Günther, D., Maurin, J., Schulmann, K., & Gebauer, D. (1999). Growth, annealing and recrystallization of zircon and preservation of monazite in high-grade metamorphism: conventional and in-situ U-Pb isotope, cathodoluminescence and microchemical evidence. *Contributions to Mineralogy and Petrology, 134*(2), 186-201.

Sizova, E., Gerya, T., Brown, M., & Perchuk, L. (2010). Subduction styles in the Precambrian: insight from numerical experiments. *Lithos, 116*(3), 209-229.

Sláma, J., Košler, J., Condon, D. J., Crowley, J. L., Gerdes, A., Hanchar, J. M., . . . Norberg, N. (2008). Plešovice zircon—a new natural reference material for U–Pb and Hf isotopic microanalysis. *Chemical Geology, 249*(1), 1-35.

Smith, H. A., & Barreiro, B. (1990). Monazite U-Pb dating of staurolite grade metamorphism in pelitic schists. *Contributions to Mineralogy and Petrology, 105*(5), 602-615.

Spear, F. S., & Kohn, M. J. (1996). Trace element zoning in garnet as a monitor of crustal melting. *Geology, 24*(12), 1099-1102.

Spear, F. S., & Pyle, J. M. (2002). Apatite, monazite, and xenotime in metamorphic rocks. *Reviews in Mineralogy and Geochemistry, 48*(1), 293-335.

Srikantappa, C., Venugopal, L., Devaraju, J., & Basavalingu, B. (1994). PT conditions of metamorphism and fluid inclusion characteristics of the Coorg granulites, Karnataka. *Geological Society of India, 44*(5), 495-504.

Taylor, R. J., Kirkland, C. L., & Clark, C. (2016). Accessories after the facts: Constraining the timing, duration and conditions of high-temperature metamorphic processes. *Lithos, 264*, 239-257.

Tracy, R. J., Robinson, P., & Thompson, A. B. (1976). Garnet composition and zoning in the determination of temperature and pressure of metamorphism, central Massachusetts. *American Mineralogist, 61*(7-8), 762-775.

Van Hunen, J., & Moyen, J.-F. (2012). Archean subduction: fact or fiction? *Annual Review of Earth and Planetary Sciences, 40*, 195-219.

Vijaya Kumar, T., Bhaskar Rao, Y., Clark, C., Taylor, R., Tomson, J., Sreenivas, B., . . . Vijaya Gopal, B. (2013). *Zircon U-Pb ages and Hf-isotopic compositions of late Archean charnockites from the Biligiri Rangan, Nilgiri Vythiri, and Coorg granulite massifs, the Southern Granulite Terrane, S. India: Constraints on terrane assembly and charnockite precursors.* Paper presented at the Hyderabad, Granulites & Granulites Conference abstract.

White, R., Powell, R., Holland, T., Johnson, T., & Green, E. (2014). New mineral activity–composition relations for thermodynamic calculations in metapelitic systems. *Journal of Metamorphic Geology, 32*(3), 261-286.

Williams, I. (2001). Response of detrital zircon and monazite, and their U–Pb isotopic systems, to regional metamorphism and host-rock partial melting, Cooma Complex, southeastern Australia. *Australian Journal of Earth Sciences, 48*(4), 557-580.

APPENDIX A: EXTENDED GEOCHRONOLOGY METHODS

Mineral Separate Preparation

Zircon and monazite grains were obtained through standard crushing, sieving and panning procedures. Approximately 200 grains were hand-picked from each separate and mounted onto the base of a 2.5 cm-diameter mold. The mold was then filled with epoxy resin, allowed to set, then polished down to expose the centre of each grain.

Prior to LA–ICP–MS analysis, zircon and monazite grains, both in grain mount and in-situ, were imaged using a back-scattered electron (BSE) detector on a FEI Quanta MLA-600 scanning electron microscope (SEM) to locate grains for LA–ICP–MS analysis. Mounted and in-situ zircon grains were then imaged using a Gatan cathodoluminescence (CL) analyser, attached to the FEI Quanta MLA-600 SEM. CL images were used to identify zonation in zircon and potential metamorphic rims to target in LA-ICP-MS analysis. Zircon grains could be distinguished from monazite using a combination of backscatter and CL imagery. Zircon is comparatively dull in backscatter and commonly shows zoning or other characteristic textures in CL images. Monazite is far brighter and more homogeneous in backscatter images due to its greater atomic mass, but appears black and shows no zonation in CL images. E-DAX software on the Quanta MLA-600 SEM was used as a first-pass process for distinguishing the two minerals.

LA–ICP–MS Analysis

LA–ICP–MS analyses took place at the University of Adelaide using a RESOlution LR 193 nm Excimer laser system coupled with an Agilent 7700s ICP–MS for the purpose of acquiring U–Pb isotopic data with trace element data. U–Pb data from monazite and zircon will be focussed on in this appendix, for methods on trace element data acquisition, see Appendix D. Ablation of zircon and monazite was performed in a He-ablation atmosphere with a frequency of 5 Hz. A spot size of 29 μm was used on grain mounted zircons. In-situ zircon analyses involved the use of a 19 μm spot when specific zones were being targeted, and a 29 μm spot for whole grain analyses. Trace element data were not collected in 19 μm spot analyses in zircon to maximize the accuracy of U–Pb isotopic data. For monazite, a 13 μm spot was used for in-situ analyses, while 19 μm spots were used for grain-mounted monazite analyses. The total acquisition time of each zircon analysis was 60 s. This included 30 s of background acquisition followed by 30 s of sample ablation. Each monazite analysis had a total acquisition time of 80 s. This included 30 s of

background measurement, 10 s of the laser firing with the shutter closed to allow for beam stabilisation, and 40 s of sample ablation.
Elemental fractionation and mass bias for zircon grain analyses were corrected using the primary standard GJ (206Pb/238U = 608.5 ± 0.4 Ma); (Jackson, Pearson, Griffin, & Belousova, 2004) Throughout this study, two runs of zircon data were collected. GJ yielded weighted mean averages of 206Pb/238U = 602 ± 10 Ma, 207Pb/235U = 605 ± 15 Ma (n = 28, 2σ errors); and 206Pb/238U = 601 ± 8 Ma, 207Pb/235U = 605 ± 15 Ma (n = 80, 2σ errors), respectively. Data accuracy was monitored using secondary zircon standard Plešovice (206Pb/238U = 337.13 ± 0.37 Ma); (Sláma et al., 2008). Throughout this study, Plešovice yielded average ages of 206Pb/238U = 339 ± 6 Ma, 207Pb/235U = 339 ± 10 Ma (n = 14, 2σ errors); and 206Pb/238U = 339 ± 4.3 Ma, 207Pb/235U = 342 ± 9 Ma (n = 40, 2σ errors), respectively.
Elemental fractionation and mass bias for monazite grain analyses were corrected using the primary standard MAdel (TIMS normalization data: 206Pb/238U = 518.37 ± 0.99 Ma and 207Pb/235U = 513.13 ± 0.19 Ma: updated from Payne et al. (2008) with additional TIMS analyses). Throughout this study, three runs of monazite data were collected. MAdel yielded weighted mean ages of 206Pb/238U = 518 ± 5 Ma and 207Pb/235U = 514 ± 10 Ma (n = 20, 2σ errors); 206Pb/238U = 518 ± 10 Ma and 207Pb/235U = 513 ± 11 Ma (n = 64, 2σ errors); 206Pb/238U = 519 ± 5 Ma and 207Pb/235U = 513.7 ± 10.3 Ma (n = 12, 2σ errors), respectively. Data accuracy was monitored using monazite standard 94-222/Bruna-NW (c. 450 Ma: Payne et al., 2008). As a secondary standard, 94-222 yielded weighted mean ages of 206Pb/238U = 450 ± 4 Ma, 207Pb/235U = 449 ± 9 Ma (n = 10, 2σ errors); 206Pb/238U = 451 ± 9 Ma, 207Pb/235U = 452 ± 10 Ma (n = 32, 2σ errors). Another secondary standard, Ambat, was used in the last monazite run. This yielded a mean weighted age of 206Pb/238U = 450 ± 4 Ma, 207Pb/235U = 527± 5 Ma (n = 6, 2σ errors).

Data Processing and Reduction

U–Pb isotopic data were reduced using Iolite version 3.6 data processing software (Paton et al., 2011). This software uses data from standards to adjust for instrument drift and down-hole fractionation during data acquisition. To do this, background signals must first be processed. Background is collected for the first 30 seconds of every analysis. During background acquisition, signals should be flat. If spikes in baseline signal occur, they must be removed. Following this, a data reduction scheme (DRS) is applied to the data. A polynomial fit is generally the best as it accommodates for instrument drift. However, a number of different schemes should be trialled for the best fit. The application of the DRS corrects analyses for downhole fractionation and instrument drift, making the signals acquired much more consistent and easier to analyse. Next, standard and sample data signals can be bracketed to improve the quality of the analysis. The aim of this process is to select as much of the signal as possible that constitutes a good analysis. A good analysis is one that shows consistency in U and Pb isotope values (i.e. a relatively flat slope). Common things that need to be corrected are; large spikes in

signal, that may reflect ablation of an inclusion, and strong decreases in signal toward the end of an analysis, which generally mean ablation through the grain has occurred. Bi-modal signals are also common in zircon. These may reflect the ablation of two different zones (i.e. a metamorphic rime and an inherited core). In this case, only one signal must be chosen as an average of the two will result in a meaningless age. These corrections must be applied with caution as it is important not to manipulate the data to create the trends you want to see. Finally, data is once again corrected using the DRS used previously, then it can be exported to be put on concordia plots.

APPENDIX B: U–PB GEOCHRONOLOGY ZIRCON ANALYSES

Session 1 - Standards	$^{207}Pb/^{235}U$	2σ	$^{206}Pb/^{238}U$	2σ	Rho	$^{207}Pb/^{235}U$ Age	2σ	$^{206}Pb/^{238}U$ Age	2σ	$^{207}Pb/^{206}U$ Age	2σ
External Standards											
GJ - 1.d	0.841	0.028	0.0989	0.0016	-0.044739	618	16	608.1	9.4	638	81
GJ - 2.d	0.812	0.028	0.0979	0.0016	0.11131	604	16	601.8	9.4	610	75
GJ - 3.d	0.81	0.026	0.0992	0.0016	0.062193	601	14	609.7	9.4	572	80
GJ - 4.d	0.809	0.025	0.097	0.0015	0.036192	601	14	596.9	9	594	76
GJ - 5.d	0.812	0.028	0.0981	0.0016	0.10178	602	16	603.4	9.3	593	80
GJ - 6.d	0.809	0.026	0.0973	0.0017	0.18825	601	14	598.5	9.7	591	75
GJ - 7.d	0.817	0.025	0.0985	0.0014	-0.021256	605	14	605.6	8.4	604	75
GJ - 8.d	0.793	0.029	0.0974	0.0016	0.1597	595	17	598.8	9.5	572	88
GJ - 9.d	0.814	0.026	0.0974	0.0015	0.11677	609	15	599.1	8.9	616	75
GJ - 10.d	0.846	0.029	0.0974	0.0016	0.15176	621	16	599	9.6	686	77
GJ - 11.d	0.815	0.025	0.0978	0.0016	0.1871	606	14	601.2	9.4	620	70
GJ - 12.d	0.799	0.029	0.097	0.0016	0.19744	597	17	596.7	9.2	577	84
GJ - 13.d	0.823	0.028	0.0969	0.0015	0.054622	608	16	596.1	9	620	80
GJ - 14.d	0.803	0.024	0.09937	0.0014	0.13411	601	14	610.7	8.4	574	71
GJ - 15.d	0.82	0.024	0.0971	0.0015	0.087497	608	13	597.4	9	631	68
GJ - 16.d	0.824	0.026	0.0975	0.0015	0.0037915	609	14	599.4	9	637	74
GJ - 17.d	0.817	0.029	0.0981	0.002	0.22864	605	16	603.4	12	596	85
GJ - 18.d	0.818	0.028	0.0972	0.0019	0.024091	608	16	597.9	11	624	85
GJ - 19.d	0.815	0.024	0.098	0.0019	0.11133	603	13	602.5	11	575	75
GJ - 20.d	0.811	0.027	0.0977	0.002	-0.003614	609	16	600.7	12	622	85
GJ - 21.d	0.819	0.026	0.0985	0.0021	0.059424	607	15	605.7	12	604	74
GJ - 22.d	0.809	0.034	0.0995	0.0021	0.084082	604	19	611.3	12	556	98

GJ - 23.d	0.812	0.023	0.0976	0.002	0.2172	606	12	600.9	12	621	66
GJ - 24.d	0.816	0.027	0.0971	0.0021	0.22267	604	15	597.2	12	622	73
GJ - 25.d	0.819	0.026	0.0992	0.0021	0.073706	609	14	609.8	12	579	80
GJ - 26.d	0.829	0.026	0.0972	0.0019	0.1759	615	14	597.7	11	664	73
GJ - 27.d	0.803	0.025	0.0974	0.0019	0.066199	595	14	599	11	546	76
GJ - 28.d	0.812	0.026	0.0977	0.002	0.11684	600	15	600.7	12	576	76

Internal Standards	$^{207}Pb/^{235}U$	2σ	$^{206}Pb/^{238}U$	2σ	Rho	$^{207}Pb/^{235}U$ Age	2σ	$^{206}Pb/^{238}U$ Age	2σ	$^{207}Pb/^{206}U$ Age	2σ
Plesovice - 1.d	0.4	0.012	0.05386	0.00081	0.084931	341.2	8.5	338.2	4.9	377	72
Plesovice - 2.d	0.4	0.012	0.05412	0.00083	0.08887	341.1	9	339.8	5.1	342	74
Plesovice - 3.d	0.3955	0.0099	0.05419	0.00072	0.30932	338.1	7.2	340.2	4.4	332	64
Plesovice - 4.d	0.388	0.012	0.05404	0.00079	0.26245	332.4	8.9	339.3	4.9	296	69
Plesovice - 5.d	0.387	0.013	0.05351	0.00079	0.2591	331.8	9.3	336	4.8	286	74
Plesovice - 6.d	0.397	0.012	0.05335	0.00081	0.079224	340.2	8.6	335.1	4.9	375	77
Plesovice - 7.d	0.404	0.012	0.05427	0.00084	0.033865	343.7	8.9	340.7	5.1	368	74
Plesovice - 8.d	0.397	0.012	0.05345	0.00082	0.078537	339	8.7	335.6	5	365	77
Plesovice - 9.d	0.393	0.014	0.05341	0.0012	-0.068656	336	9.9	335.4	7.2	313	87
Plesovice - 10.d	0.401	0.014	0.05463	0.0011	-0.090514	340	10	342.8	6.8	332	87
Plesovice - 11.d	0.396	0.018	0.05355	0.0011	0.025001	339	13	336.2	6.7	318	99
Plesovice - 12.d	0.407	0.015	0.05493	0.0011	0.053474	345	11	344.7	6.5	326	81
Plesovice - 13.d	0.398	0.016	0.0537	0.0011	0.018942	341	12	337.1	6.7	335	90
Plesovice - 14.d	0.401	0.016	0.05448	0.0011	0.056002	341	12	341.9	6.6	292	92

91500 - 1.d	1.85	0.084	0.1763	0.0038	0.098637	1061	30	1046	21	1067	96
91500 - 2.d	1.909	0.084	0.1793	0.0041	0.37545	1078	30	1063	22	1111	88
91500 - 3.d	1.953	0.07	0.1765	0.0038	0.34527	1096	25	1047	21	1169	76
91500 - 4.d	1.868	0.074	0.1776	0.004	0.16915	1075	27	1053	22	1082	84
91500 - 5.d	1.8	0.084	0.1787	0.0044	0.036277	1041	30	1059	24	1000	100
91500 - 6.d	1.788	0.08	0.1764	0.0045	0.12411	1034	29	1047	24	954	100
91500 - 7.d	1.788	0.08	0.1785	0.0043	0.10034	1044	29	1058	23	977	99

Session 2 - Standards	**$^{207}Pb/^{235}U$**	**2σ**	**$^{206}Pb/^{238}U$**	**2σ**	**Rho**	**$^{207}Pb/^{235}U$ Age**	**2σ**	**$^{206}Pb/^{238}U$ Age**	**2σ**	**$^{207}Pb/^{206}U$ Age**	**2σ**
External Standards											
GJ - 1.d	0.787	0.019	0.0968	0.0011	0.12359	590	11	595.8	6.3	522	58
GJ - 2.d	0.815	0.024	0.0974	0.0012	0.19761	604	14	599.2	7.2	606	65
GJ - 3.d	0.825	0.021	0.09907	0.00097	0.10208	611	12	608.9	5.7	632	55
GJ - 4.d	0.811	0.023	0.0979	0.001	0.28731	602	13	602.1	5.9	586	59
GJ - 5.d	0.837	0.021	0.0976	0.0012	-0.03736	617	12	600.5	6.9	683	67
GJ - 6.d	0.798	0.023	0.0989	0.001	0.20358	596	13	607.9	5.9	553	65
GJ - 7.d	0.829	0.023	0.0971	0.0012	0.15649	614	12	597.4	7	679	60
GJ - 8.d	0.82	0.021	0.09865	0.00091	0.19446	608	12	606.5	5.3	604	49
GJ - 9.d	0.842	0.022	0.0977	0.0012	0.33255	621	12	601.9	7	627	46
GJ - 10.d	0.831	0.021	0.0974	0.001	0.27834	615	11	598.9	5.9	610	54
GJ - 11.d	0.812	0.022	0.0975	0.0012	0.076137	602	13	600	7.1	545	65
GJ - 12.d	0.845	0.023	0.0968	0.0012	0.14331	621	12	596.5	6.7	652	60
GJ - 13.d	0.805	0.028	0.0981	0.0014	0.16675	598	16	603.2	8.4	590	76
GJ - 14.d	0.794	0.026	0.0961	0.0014	0.16242	596	15	591.5	8.4	608	71
GJ - 15.d	0.817	0.026	0.0973	0.0015	0.088751	605	14	598.7	8.8	635	77
GJ - 16.d	0.836	0.023	0.0969	0.0014	0.44586	616	13	596.1	8.3	665	58
GJ - 17.d	0.826	0.028	0.09866	0.0014	0.041403	610	16	606.5	8	608	80
GJ - 18.d	0.822	0.025	0.0981	0.0015	0.16098	608	14	603.3	8.7	627	68
GJ - 19.d	0.818	0.024	0.09828	0.0014	0.15879	608	13	604.3	8.1	631	67
GJ - 20.d	0.795	0.028	0.0973	0.0015	0.41911	592	16	598.6	8.6	590	67
GJ - 21.d	0.788	0.027	0.0979	0.0016	0.18738	592	15	602.2	9.2	534	74

GJ - 22.d	0.805	0.025	0.09908	0.0014	0.069458	599	14	609	8	559	69
GJ - 23.d	0.812	0.023	0.0974	0.0016	0.46201	604	13	599	9.5	599	63
GJ - 24.d	0.824	0.027	0.0984	0.0014	0.25802	609	15	604.9	8.5	615	68
GJ - 25.d	0.797	0.027	0.09745	0.0014	0.27055	596	15	599.4	8.2	574	73
GJ - 26.d	0.818	0.026	0.0987	0.0015	-0.12041	606	15	606.5	8.9	599	74
GJ - 27.d	0.838	0.026	0.0978	0.0014	0.13863	617	14	601.2	8.4	671	69
GJ - 28.d	0.837	0.024	0.09796	0.0014	0.16327	616	13	602.4	8.2	665	67
GJ - 29.d	0.813	0.025	0.0972	0.0015	-0.046272	604	14	597.6	8.8	648	73
GJ - 30.d	0.819	0.026	0.0977	0.0015	0.22984	610	14	601.9	9.3	633	69
GJ - 31.d	0.819	0.024	0.0991	0.0015	-0.016654	608	13	608.9	8.5	610	66
GJ - 32.d	0.814	0.025	0.0972	0.0016	0.3089	603	14	597.8	9.3	630	65
GJ - 33.d	0.792	0.026	0.0969	0.0015	0.12617	593	14	596	8.6	593	73
GJ - 34.d	0.822	0.026	0.0975	0.0015	-0.10108	608	15	599.6	9	626	75
GJ - 35.d	0.802	0.022	0.0978	0.0015	0.15896	597.4	12	601.4	8.8	598	62
GJ - 36.d	0.802	0.025	0.0969	0.0016	0.17132	600	14	596.2	9.5	593	69
GJ - 37.d	0.821	0.027	0.09778	0.0013	0.27606	609	15	601.3	7.9	611	71
GJ - 38.d	0.81	0.022	0.0978	0.0015	0.24648	602	13	601.2	8.9	601	64
GJ - 39.d	0.822	0.025	0.0986	0.0015	0.25117	608	14	606.1	8.9	604	69
GJ - 40.d	0.818	0.029	0.0972	0.0015	0.21782	609	16	597.8	8.6	636	78
GJ - 41.d	0.81	0.024	0.0983	0.0015	0.12355	601	13	604.6	8.8	610	73
GJ - 42.d	0.808	0.025	0.0978	0.0016	0.056146	602	14	601.7	9.1	601	77
GJ - 43.d	0.806	0.025	0.0977	0.0015	-0.15958	599	14	601	8.9	578	75
GJ - 44.d	0.824	0.029	0.0991	0.0015	0.27946	610	16	608.8	8.8	598	73
GJ - 45.d	0.812	0.024	0.0964	0.0016	0.16637	604	14	593	9.1	659	65
GJ - 46.d	0.82	0.027	0.098	0.0016	0.43705	607	15	602.8	9.3	610	67
GJ - 47.d	0.812	0.025	0.0981	0.0016	0.33314	603	14	603.1	9.5	594	70
GJ - 48.d	0.841	0.024	0.0984	0.0016	0.24402	622	13	604.8	9.6	685	62
GJ - 49.d	0.836	0.028	0.0974	0.0014	0.24549	616	15	599.1	8	689	72
GJ - 50.d	0.821	0.032	0.0979	0.0015	0.077585	609	18	602.2	8.8	655	86
GJ - 51.d	0.82	0.029	0.0986	0.0013	0.38866	607	16	606.3	7.8	593	81
GJ - 52.d	0.809	0.027	0.0979	0.0014	0.2688	604	16	601.8	8	608	69

GJ - 53.d	0.803	0.029	0.09668	0.0012	0.21078	597	16	594.9	7	603	81
GJ - 54.d	0.822	0.026	0.0978	0.0013	-0.14641	610	15	601.2	7.5	631	74
GJ - 55.d	0.786	0.031	0.0979	0.0014	0.049761	589	17	602	8.5	550	88
GJ - 56.d	0.817	0.03	0.0964	0.0014	0.1617	605	17	593.2	8.1	637	82
GJ - 57.d	0.82	0.028	0.0981	0.0013	0.1942	607	16	603.3	7.6	624	77
GJ - 58.d	0.811	0.027	0.0978	0.0012	0.099352	604	16	601.7	7.3	611	79
GJ - 59.d	0.816	0.03	0.0979	0.0014	0.072221	604	17	601.8	8	602	76
GJ - 60.d	0.825	0.027	0.098	0.0014	0.14006	610	15	602.8	8.2	603	71
GJ - 61.d	0.82	0.031	0.09771	0.0012	0.019031	606	18	600.9	7	656	82
GJ - 62.d	0.823	0.033	0.0966	0.0013	0.16012	608	18	594.2	7.4	661	85
GJ - 63.d	0.814	0.028	0.0984	0.0013	0.15794	604	16	605.1	7.6	583	78
GJ - 64.d	0.814	0.029	0.0977	0.0014	0.18995	606	16	601	8.4	649	83
GJ - 65.d	0.804	0.029	0.098	0.0014	0.14901	598	17	602.4	8.5	582	87
GJ - 66.d	0.791	0.028	0.09748	0.0012	0.21971	594	16	599.6	7.2	566	78
GJ - 67.d	0.79	0.029	0.0975	0.0014	0.12048	592	16	600.6	8.2	561	81
GJ - 68.d	0.81	0.03	0.09809	0.0012	0.0075255	601	17	603.2	7.2	590	85
GJ - 69.d	0.823	0.029	0.0977	0.0013	0.27267	609	16	600.9	7.9	654	75
GJ - 70.d	0.826	0.03	0.0976	0.0012	-0.029717	610	17	600.3	7.3	651	79
GJ - 71.d	0.81	0.029	0.0977	0.0013	-0.047683	601	16	600.8	7.4	596	81
GJ - 72.d	0.805	0.029	0.0976	0.0014	0.1317	602	15	600.2	8.2	594	75
GJ - 73.d	0.815	0.026	0.0988	0.0014	0.051398	605	15	607.4	8.1	633	72
GJ - 74.d	0.815	0.028	0.0971	0.0015	0.083487	606	16	598.4	8.5	636	79
GJ - 75.d	0.853	0.029	0.0986	0.0014	0.14227	625	16	606.4	8.2	709	76
GJ - 76.d	0.812	0.031	0.0987	0.0014	0.27826	602	17	607	8.1	582	79
GJ - 77.d	0.836	0.029	0.0976	0.0014	0.10631	616	16	600	8.3	684	80
GJ - 78.d	0.793	0.029	0.0974	0.0014	0.42787	591	16	598.8	8.5	588	74
GJ - 79.d	0.811	0.028	0.0989	0.0013	0.15354	602	16	607.9	7.8	566	73
GJ - 80.d	0.811	0.028	0.098	0.0013	0.29169	605	16	602.9	7.8	594	80

Internal Standards	$^{207}Pb/^{235}U$	2σ	$^{206}Pb/^{238}U$	2σ	Rho	$^{207}Pb/^{235}U$ Age	2σ	$^{206}Pb/^{238}U$ Age	2σ	$^{207}Pb/^{206}U$ Age	2σ
Plesovice - 1.d	0.3929	0.0092	0.05359	0.00055	-0.11735	336.2	6.7	336.5	3.4	331	61
Plesovice - 2.d	0.3951	0.0094	0.05376	0.00048	0.2085	337.7	6.8	337.5	2.9	335	57
Plesovice - 3.d	0.3944	0.0088	0.05366	0.00052	-0.065332	337.3	6.4	336.9	3.2	333	56
Plesovice - 4.d	0.394	0.01	0.05369	0.00044	-0.0014652	337.7	7.3	337.1	2.7	325	63
Plesovice - 5.d	0.3886	0.0086	0.05372	0.00049	0.087876	333	6.3	337.3	3	302	52
Plesovice - 6.d	0.3993	0.0087	0.05364	0.00051	0.2543	341.7	6.2	336.8	3.1	379	49
Plesovice - 7.d	0.4007	0.011	0.05381	0.00069	-0.2648	343.7	8.3	337.8	4.2	391	70
Plesovice - 8.d	0.3932	0.011	0.05387	0.00073	0.39001	336.4	7.8	338.2	4.5	309	59
Plesovice - 9.d	0.3956	0.01	0.05443	0.00072	0.2276	339	7.6	341.7	4.4	322	58
Plesovice - 10.d	0.4017	0.011	0.05339	0.00081	0.18956	343.4	8.2	335.3	4.9	400	66
Plesovice - 11.d	0.401	0.013	0.05389	0.0008	0.33658	341.9	9.1	338.3	4.9	352	68
Plesovice - 12.d	0.3967	0.012	0.05386	0.00078	0.094346	339.8	8.6	338.2	4.8	347	69
Plesovice - 13.d	0.3935	0.012	0.05352	0.00072	0.34037	336.5	8.6	336.1	4.4	336	68
Plesovice - 14.d	0.4093	0.012	0.05322	0.00082	0.33831	348	8.5	334.3	5	396	68
Plesovice - 15.d	0.403	0.012	0.05402	0.0007	0.085537	343.3	9	339.2	4.3	359	70
Plesovice - 16.d	0.4047	0.011	0.05419	0.00076	0.31844	344.7	8.1	340.2	4.6	376	59
Plesovice - 17.d	0.3991	0.01	0.05422	0.00071	0.20093	340.8	7.4	340.4	4.4	328	61
Plesovice - 18.d	0.3922	0.01	0.05422	0.00072	-0.044256	336.6	7.6	340.3	4.4	308	62
Plesovice - 19.d	0.4134	0.011	0.05431	0.00075	0.19741	351	8.1	340.9	4.6	443	64
Plesovice - 20.d	0.3916	0.011	0.05421	0.00075	0.12827	335.2	7.8	340.3	4.6	325	64
Plesovice - 21.d	0.3996	0.012	0.05328	0.00078	-0.0082209	341	8.5	334.6	4.8	374	69
Plesovice - 22.d	0.4012	0.011	0.05426	0.00072	0.096687	342.2	8	340.6	4.4	334	67
Plesovice - 23.d	0.391	0.013	0.05389	0.00079	0.1051	335.7	9	338.4	4.8	301	76
Plesovice - 24.d	0.405	0.012	0.05408	0.00083	0.17507	344.8	9	339.5	5.1	380	67
Plesovice - 25.d	0.394	0.014	0.05353	0.00071	0.19707	336.7	9.8	336.2	4.4	336	82
Plesovice - 26.d	0.403	0.015	0.05428	0.0007	0.086162	343.6	11	340.7	4.3	364	85
Plesovice - 27.d	0.389	0.015	0.05422	0.00074	0.33634	332.7	11	340.4	4.5	291	80
Plesovice - 28.d	0.393	0.015	0.05321	0.00072	-0.16341	336.2	11	334.2	4.4	358	88
Plesovice - 29.d	0.385	0.014	0.05443	0.00077	0.29357	330.3	11	341.6	4.7	243	85
Plesovice - 30.d	0.402	0.014	0.05382	0.00068	0.17515	343	9.8	337.9	4.1	381	75

Plesovice - 31.d	0.431	0.018	0.05478	0.00064	0.26245	363	13	343.8	3.9	500	91
Plesovice - 32.d	0.404	0.016	0.05334	0.00085	0.34979	343.9	12	335	5.2	409	86
Plesovice - 33.d	0.397	0.016	0.0538	0.00074	0.35405	342.8	11	337.8	4.5	405	80
Plesovice - 34.d	0.398	0.015	0.05435	0.0007	0.32224	339.7	11	341.2	4.3	313	85
Plesovice - 35.d	0.4	0.014	0.05532	0.00068	0.12229	342.4	9.6	347.1	4.2	295	76
Plesovice - 36.d	0.405	0.014	0.05488	0.00075	0.14866	344.9	10	344.4	4.6	344	81
Plesovice - 37.d	0.409	0.016	0.05459	0.00077	0.18953	347.4	11	342.6	4.7	397	90
Plesovice - 38.d	0.4	0.014	0.05437	0.00068	0.037355	342.3	9.8	341.3	4.1	348	86
Plesovice - 39.d	0.4588	0.014	0.05703	0.00084	0.42423	383.1	9.8	357.5	5.1	545	66
Plesovice - 40.d	0.4068	0.012	0.05428	0.00061	0.032018	346.4	8.5	340.8	3.7	392	70
91500 - 1.d	1.879	0.063	0.1806	0.003	0.26304	1080	21	1070	16	1108	65
91500 - 2.d	1.862	0.064	0.1765	0.0022	0.30019	1071	23	1048	12	1113	59
91500 - 3.d	1.787	0.058	0.1765	0.0032	0.15155	1044	23	1047	17	1037	81
91500 - 4.d	1.816	0.071	0.1793	0.0036	0.26387	1054	26	1063	20	1031	81
91500 - 5.d	1.909	0.066	0.1784	0.0032	0.19978	1084	23	1058	17	1166	74
91500 - 6.d	1.896	0.078	0.1774	0.0034	0.19293	1074	27	1053	19	1119	84
91500 - 7.d	1.814	0.073	0.1776	0.0037	0.20107	1053	28	1053	20	1075	88
91500 - 8.d	1.866	0.079	0.1794	0.0034	0.2578	1071	30	1063	18	1052	90
91500 - 9.d	1.887	0.076	0.1821	0.0038	0.20301	1075	27	1078	21	1064	86
91500 - 10.d	1.785	0.059	0.1768	0.0032	-0.084926	1038	21	1049	18	1007	82
91500 - 11.d	1.844	0.081	0.1814	0.0036	0.060947	1056	29	1076	19	1003	95
91500 - 12.d	1.849	0.078	0.1803	0.0034	0.12697	1058	28	1068	18	1058	91
91500 - 13.d	1.935	0.083	0.1817	0.0034	0.20435	1095	28	1076	19	1118	88
91500 - 14.d	1.854	0.081	0.1792	0.0034	0.071492	1064	30	1062	19	1066	100
91500 - 15.d	1.867	0.085	0.1761	0.0032	0.11752	1072	29	1045	18	1111	93
91500 - 16.d	1.832	0.094	0.1748	0.0035	0.17336	1058	33	1038	19	1118	100
91500 - 17.d	1.808	0.081	0.1754	0.0036	0.055425	1047	29	1042	20	1051	99
91500 - 18.d	1.883	0.088	0.1809	0.0038	0.15643	1080	30	1071	21	1081	98
91500 - 19.d	1.868	0.079	0.1781	0.0034	0.10354	1072	27	1056	19	1067	98
91500 - 20.d	1.921	0.083	0.1797	0.0038	0.19428	1090	28	1065	21	1113	89

Session 1 - Samples	$^{207}Pb/^{235}U$	2σ	$^{206}Pb/^{238}U$	2σ	Rho	$^{207}Pb/^{235}U$ Age	2σ	$^{206}Pb/^{238}U$ Age	2σ	$^{207}Pb/^{206}U$ Age	2σ
Co17-41zc1 - 1.d	22.82	0.41	0.6418	0.0086	0.8172	3218.7	18	3199	34	3231.3	30
Co17-41zc3 - 1.d	21.34	0.69	0.654	0.019	0.96624	3149	32	3239	73	3096	30
Co17-41zc4 - 1.d	20.34	0.42	0.6154	0.01	0.9086	3106	20	3090	40	3126.1	30
Co17-41zc5 - 1.d	27.91	0.5	0.6964	0.01	0.67886	3415	18	3406	39	3427	31
Co17-41zc6 - 1.d	17.69	0.59	0.501	0.014	0.94668	2966	33	2612	62	3230	32
Co17-41zc7 - 1.d	22.41	0.58	0.631	0.014	0.93859	3201	24	3150	56	3227.9	29
Co17-41zc10 - 1.d	18.96	0.34	0.583	0.0093	0.84343	3039	18	2960	38	3087.9	30
Co17-41zc11 - 1.d	24.4	0.92	0.688	0.026	0.97689	3279	36	3363	97	3231	30
Co17-41zc12 - 1.d	25.49	0.51	0.76	0.013	0.9408	3326	19	3643	47	3141.2	30
Co17-41zc13 - 1.d	26.68	0.67	0.72	0.014	0.91424	3368	25	3498	52	3299	30
Co17-41zc14 - 1.d	33.62	0.9	0.812	0.022	0.91082	3595	27	3836	78	3443	31
Co17-40zc2 - 1.d	18.48	0.34	0.5603	0.0082	0.79105	3018	18	2867	34	3119	32
Co17-40zc3 - 1.d	18.45	0.31	0.5527	0.0068	0.65718	3014.2	16	2836	28	3124	29
Co17-40zc5 - 1.d	10.15	0.22	0.3964	0.0065	0.51672	2449	21	2155	29	2700	37
Co17-40zc6 - 1.d	16.19	0.43	0.5145	0.011	0.88044	2889	25	2682	44	3053	32
Co17-40zc7 - 1.d	8.89	0.19	0.3908	0.0067	0.3824	2327	20	2126	31	2511	42
Co17-40zc8 - 1.d	10.52	0.2	0.4083	0.0056	0.63136	2481	17	2207	26	2713	34
Co17-40zc10 - 1.d	2.876	0.093	0.2002	0.0037	0.79739	1374	24	1176	20	1687	45
Co17-40zc11 - 1.d	14.25	0.34	0.4961	0.0084	0.90692	2766	23	2596	36	2883	31
Co17-40zc12 - 1.d	25.3	0.47	0.6838	0.0095	0.89046	3319	18	3358	36	3284.8	29
Co17-40zc14 - 1.d	9.22	0.3	0.3626	0.0079	0.8794	2357	28	1994	37	2702	37
Co17-40zc14 - 1.d	14.07	0.6	0.458	0.016	0.92849	2749	41	2426	73	2983	38
Co17-40zc14 - 2.d	14.31	0.29	0.496	0.0081	0.8067	2769	19	2595	35	2893	31
Co17-40zc15 - 1.d	14.17	0.4	0.493	0.012	0.91258	2769	29	2582	50	2908	35
Co17-40zc17 - 1.d	23.62	0.41	0.6567	0.009	0.72576	3252.1	17	3257	34	3238	30
Co17-21zc2 - 1.d	21.27	0.47	0.6204	0.01	0.55033	3149	21	3110	41	3176	34
Co17-21zc2 - 2.d	21.59	0.44	0.6271	0.01	0.56591	3164	20	3142	40	3184	36
Co17-21zc3 - 1.d	22.62	0.54	0.67	0.013	0.5282	3208	23	3304	50	3144	40
Co17-21zc3 - 2.d	21.36	0.5	0.6312	0.01	0.70851	3152	23	3153	41	3171	33

Co17-21zc4 - 1.d	18.37	0.52	0.5618	0.011	0.93009	3004	28	2872	47	3106	32
Co17-21zc5 - 1.d	20.06	0.4	0.6088	0.009	0.58952	3095	20	3065	36	3112	34
Co17-21zc7 - 1.d	19.64	0.36	0.5929	0.0089	0.84124	3073	18	3001	36	3116	30
Co17-21zc8 - 1.d	22.16	0.41	0.6507	0.0089	0.71817	3190	18	3230	35	3171	29
Co17-21zc9 - 1.d	22.81	0.4	0.6713	0.0095	0.72947	3219.5	18	3313	36	3161	30
Co17-21zc9 - 2.d	20.6	0.38	0.612	0.0099	0.69905	3123	18	3077	40	3144	31
Co17-21zc12 - 1.d	21.22	0.45	0.6232	0.01	0.53946	3149	20	3122	40	3155	34
Co17-21zc14 - 1.d	23.09	0.51	0.6692	0.011	0.8564	3229	21	3306	43	3183	31
Co17-21zc6 - 1.d	20.33	0.17	0.6054	0.01	0.47219	3106.2	8.2	3052	42	3150	22
Co17-21zc6 - 2.d	16.18	0.31	0.507	0.01	0.35107	2886	18	2645	45	3049	35
Co17-21zc10 - 1.d	20.97	0.42	0.625	0.015	0.76455	3135	20	3128	62	3121	28
Co17-21zc11 - 1.d	19.78	0.39	0.595	0.014	0.83407	3077	20	3007	57	3128	25
Co17-21zc11 - 2.d	21.02	0.24	0.6155	0.012	0.60423	3142	11	3093	46	3170	23
Co17-21zc13 - 1.d	20.19	0.28	0.6182	0.011	0.53661	3101	13	3104	47	3099	27
Co17-21zc14 - 2.d	22.6	0.36	0.6448	0.014	0.879	3209	15	3208	53	3203	20
Co17-21zc14 - 3.d	20.06	0.32	0.593	0.012	0.63542	3091	16	2999	49	3161	26
Co17-21zc15 - 1.d	20.97	0.26	0.6128	0.011	0.7186	3135	12	3080	46	3171	23
Co17-21zc15 - 2.d	20.73	0.21	0.5962	0.011	0.46681	3126	10	3016	43	3195	22
Co17-21zc16 - 1.d	20.73	0.21	0.6177	0.011	0.6565	3124.6	9.6	3102	43	3140	21
Co17-21zc16 - 2.d	21.22	0.27	0.6207	0.012	0.34034	3146	12	3111	46	3168	27
Co17-21zc17 - 1.d	21.84	0.38	0.633	0.014	0.81185	3176	17	3161	56	3177	23
Co17-37zc9 - 1.d	7.27	0.11	0.3606	0.007	0.45441	2145	13	1984	33	2281	30
Co17-37zc9 - 2.d	8.19	0.14	0.3769	0.0077	0.39739	2251	15	2062	36	2421	34
Co17-37zc11 - 1.d	12.92	0.15	0.4657	0.0082	0.65895	2675	11	2464	36	2830	22
Co17-37zc11 - 2.d	16.47	0.21	0.5236	0.01	0.88532	2903	13	2713	44	3036	20
Co17-37zc11 - 3.d	7.59	0.27	0.4118	0.012	0.24497	2179	33	2221	53	2105	68
Co17-37zc12 - 1.d	11.2	0.2	0.4355	0.0085	0.34377	2543	17	2329	38	2703	35
Co17-37zc15 - 1.d	8.32	0.18	0.3738	0.008	0.79363	2267	19	2047	38	2438	28
Co17-37zc15 - 1.d	4.46	0.11	0.2387	0.0061	0.76234	1721	20	1379	32	2171	33
Co17-40zc13 - 1.d	21.37	0.26	0.6117	0.012	0.80918	3156	11	3081	46	3198	20
Co17-40zc13 - 2.d	24.48	0.33	0.6484	0.012	0.52512	3289	13	3223	49	3330	25
Co17-40zc1 - 1.d	16.64	0.52	0.522	0.016	0.9088	2900	30	2701	66	3040	23
Co17-40zc1 - 2.d	20.24	0.46	0.607	0.014	0.7645	3102	22	3053	56	3122	27
Co17-40zc4 - 1.d	5.92	0.14	0.3077	0.0075	0.85743	1961	20	1727	37	2225	29
Co17-40zc4 - 2.d	5.756	0.094	0.3034	0.0057	0.41439	1940	14	1708	28	2181	32
Co17-40zc4 - 3.d	5.47	0.17	0.2924	0.0083	0.72264	1895	27	1651	41	2181	39
Co17-41zc2 - 1.d	18.32	0.28	0.5461	0.01	0.87864	3008	15	2808	42	3133	20

Co17-41zc2 - 2.d	14.4	0.26	0.4973	0.011	0.59454	2774	17	2601	46	2881	30
Co17-41zc2 - 3.d	28.72	0.3	0.7664	0.014	0.84399	3442	10	3669	53	3308.8	19
Co17-41zc8 - 1.d	17.91	0.44	0.5774	0.013	0.81509	2982	23	2936	53	2999	27
Session 2 - Samples	**$^{207}Pb/^{235}U$**	**2σ**	**$^{206}Pb/^{238}U$**	**2σ**	**Rho**	**$^{207}Pb/^{235}U$ Age**	**2σ**	**$^{206}Pb/^{238}U$ Age**	**2σ**	**$^{207}Pb/^{206}U$ Age**	**2σ**
Co17-37-zc1 - 1.d	10.86	0.46	0.488	0.014	0.61521	2505	40	2558	61	2509	51
Co17-37-zc2 - 1.d	6.954	0.084	0.3397	0.0035	0.58414	2105	11	1885	17	2323	19
Co17-37-zc3 - 1.d	8.45	0.41	0.421	0.018	0.74263	2284	45	2256	83	2260	61
Co17-37-zc4 - 1.d	5.989	0.098	0.3152	0.0037	0.25337	1973	14	1766	18	2203	30
Co17-37-zc5 - 1.d	4.674	0.085	0.2642	0.0038	0.49635	1761	15	1511	19	2075	28
Co17-37-zc6 - 1.d	5.3	0.17	0.2831	0.0057	0.8172	1870	28	1606	29	2174	34
Co17-37-zc7 - 1.d	1.73	0.17	0.1652	0.0087	0.52461	1003	68	983	48	1070	170
Co17-37-zc14 - 1.d	5.872	0.067	0.3064	0.0032	0.38536	1956.3	9.9	1725	15	2223	24
Co17-38-zc1 - 1.d	14.09	0.21	0.5005	0.005	0.47352	2754	14	2615	22	2865	21
Co17-38-zc2 - 1.d	6.37	0.12	0.3222	0.0059	0.78052	2025	17	1800	29	2298	23
Co17-38-zc3 - 1.d	19.53	0.17	0.5922	0.0053	0.66032	3068	8.4	2998	21	3133	12
Co17-38-zc4 - 1.d	20.33	0.18	0.6066	0.005	0.66527	3106.4	8.7	3056	20	3161	11
Co17-38-zc7 - 1.d	16.26	0.34	0.5343	0.0086	0.85278	2892	20	2758	36	2991	19
Co17-38-zc8 - 1.d	29.7	1.3	0.798	0.03	0.91713	3472	44	3780	110	3305	21
Co17-38-zc11 - 1.d	13.9	0.23	0.5151	0.0069	0.61778	2741	16	2677	29	2779	21
Co17-38-zc12 - 1.d	15.96	0.35	0.547	0.013	0.79792	2877	21	2808	52	2897	22
Co17-38-zc13 - 1.d	15.1	0.42	0.5009	0.0093	0.93831	2816	27	2615	40	2942	19
Co17-38-zc16 - 1.d	17	1.2	0.53	0.027	0.94792	2913	71	2720	120	3076	41
Co17-38-zc15 - 1.d	15.02	0.44	0.5248	0.0093	0.88797	2810	29	2723	39	2849	26
Co17-38-zc18 - 1.d	18.55	0.31	0.5434	0.0073	0.84707	3021	16	2797	31	3124	15
Co17-38-zc19 - 1.d	22.11	0.27	0.6332	0.0066	0.83889	3187	12	3161	26	3169	11
Co17-38-zc20 - 1.d	25.71	0.58	0.684	0.012	0.96369	3339	21	3358	47	3283	10
Co17-38-zc21 - 1.d	23.07	0.37	0.6694	0.0098	0.76262	3228	16	3302	38	3121	15
Sample Co17-38											
Mount-4-zc1 - 1.d	19.17	0.47	0.5978	0.011	0.87183	3050	23	3025	47	3082	31
Mount-4-zc2 - 1.d	9.78	0.21	0.3795	0.0055	0.57163	2415	19	2074	26	2708	33
Mount-4-zc3 - 1.d	23.07	0.42	0.629	0.0075	0.63735	3229.4	18	3145	30	3282.2	29
Mount-4-zc4 - 1.d	15.46	0.38	0.53	0.011	0.65604	2848	24	2740	44	2920	38

Mount-4-zc5 - 1.d	9.38	0.34	0.357	0.012	0.95018	2378	32	1968	56	2751	32
Mount-4-zc6 - 1.d	9.5	0.24	0.4299	0.0072	0.35742	2385	23	2304	33	2452	43
Mount-4-zc6 - 2.d	5.31	0.2	0.2776	0.0068	0.28802	1865	32	1578	35	2175	65
Mount-4-zc7 - 1.d	6.089	0.14	0.3197	0.0049	0.16764	1987	20	1788	24	2168	44
Mount-4-zc7 - 2.d	5.44	0.26	0.2805	0.01	0.53918	1885	41	1592	51	2287	70
Mount-4-zc8 - 1.d	21.36	0.41	0.602	0.0082	0.70606	3154.4	18	3040	32	3223	30
Mount-4-zc9 - 1.d	21.48	0.52	0.596	0.011	0.84892	3159	23	3012	46	3251	30
Mount-4-zc10 - 1.d	11.43	0.26	0.428	0.0066	0.64418	2558	21	2296	30	2797	35
Mount-4-zc11 - 1.d	20.55	0.43	0.6195	0.0088	0.66043	3116	20	3107	35	3126	33
Mount-4-zc11 - 2.d	14.39	0.66	0.513	0.022	0.57917	2769	44	2662	93	2867	72
Mount-4-zc12 - 1.d	24.95	0.46	0.6567	0.0084	0.6059	3306.9	18	3254	33	3336.3	29
Mount-4-zc13 - 1.d	18.22	0.36	0.5728	0.0079	0.60118	3003.5	19	2919	32	3052	31
Mount-4-zc14 - 1.d	20.05	0.41	0.5796	0.0083	0.84173	3093	20	2947	34	3195.3	30
Mount-4-zc15 - 1.d	11.52	0.28	0.4522	0.0084	0.57101	2565	22	2404	37	2692	42
Mount-4-zc15 - 3.d	13.35	0.35	0.4735	0.01	0.86466	2703	25	2498	44	2870	34
Mount-4-zc16 - 1.d	18.33	0.48	0.572	0.012	0.95094	3007	26	2912	49	3072.9	30
Mount-4-zc17 - 1.d	19.97	0.62	0.596	0.012	0.91573	3090	31	3014	49	3152	34
Mount-4-zc18 - 1.d	23.43	0.59	0.679	0.014	0.92871	3242	24	3339	52	3187	30
Mount-4-zc19 - 1.d	18.34	0.37	0.5651	0.0075	0.82289	3010	20	2887	31	3092	31
Mount-4-zc20 - 1.d	20.57	0.4	0.5847	0.0082	0.74878	3118	19	2967	34	3207	30
Mount-4-zc21 - 1.d	10.63	0.39	0.414	0.011	0.42649	2494	33	2231	51	2705	63
Mount-4-zc22 - 2.d	21.79	0.66	0.644	0.013	0.82336	3178	31	3204	50	3161	37
Mount-4-zc23 - 1.d	13.89	0.33	0.4877	0.0091	0.54361	2743	24	2560	39	2888	41
Mount-4-zc24 - 1.d	16.49	0.43	0.53	0.012	0.67436	2904	25	2741	50	2996	36
Mount-4-zc25 - 1.d	10.14	0.37	0.4264	0.0095	0.68717	2448	33	2288	43	2608	48
Mount-4-zc26 - 1.d	3.168	0.1	0.2089	0.0036	0.2675	1447	24	1222	19	1791	59
Mount-4-zc27 - 1.d	13.23	0.28	0.4634	0.0058	0.70007	2699	19	2454	26	2888	32
Mount-4-zc28 - 1.d	16.28	0.33	0.5472	0.0067	0.7525	2894	20	2813	28	2948	32
Mount-4-zc29 - 1.d	15.04	0.4	0.503	0.0098	0.86103	2816	25	2626	42	2967	33
Mount-4-zc30 - 1.d	12.24	0.24	0.4461	0.0056	0.46801	2622.3	18	2378	25	2815	33
Mount-4-zc31 - 1.d	3.549	0.11	0.2318	0.0038	0.53043	1538	23	1343	20	1818	46

Mount-4-zc32 - 1.d	13.86	0.34	0.4719	0.0075	0.88341	2738	23	2491	33	2920	31
Mount-4-zc33 - 1.d	20.23	0.4	0.6108	0.0088	0.66215	3101	19	3072	35	3111	32
Mount-4-zc34 - 1.d	11.04	0.23	0.4452	0.0057	0.62975	2526	20	2374	26	2659	33
Mount-4-zc35 - 1.d	20.66	0.44	0.6164	0.0092	0.87896	3122	21	3099	36	3140.6	30
Mount-4-zc36 - 1.d	20.11	0.4	0.6037	0.0078	0.73834	3096	19	3044	31	3132	30
Mount-4-zc37 - 1.d	3.822	0.12	0.2414	0.0038	0.45179	1598	24	1394	20	1880	53
Mount-4-zc38 - 1.d	17.42	0.35	0.5541	0.0068	0.60506	2959	19	2842	28	3032	31
Mount-4-zc39 - 1.d	18.1	0.35	0.5575	0.0068	0.66941	2994.3	19	2858	29	3082	30
Mount-4-zc40 - 1.d	25.38	0.56	0.7108	0.011	0.82456	3324	22	3465	42	3233	30
Mount-4-zc41 - 1.d	22.48	0.61	0.6619	0.012	0.61772	3206	26	3273	45	3151	39
Mount-4-zc41 - 2.d	21.94	0.53	0.6327	0.0093	0.61076	3181	23	3159	37	3200	34
Mount-4-zc42 - 1.d	24.12	0.48	0.6673	0.0084	0.83739	3272	19	3295	33	3256.3	29
Mount-4-zc43 - 1.d	23.37	0.43	0.6435	0.0083	0.74613	3241.9	18	3202	32	3264.1	29
Mount-4-zc44 - 1.d	26.14	0.57	0.6983	0.012	0.82582	3352	22	3413	45	3322	30
Mount-4-zc45 - 1.d	14.9	0.49	0.5253	0.011	0.86351	2805	32	2720	47	2875	39
Mount-4-zc45 - 2.d	13.96	0.36	0.5328	0.01	0.69501	2746	24	2752	42	2759	40
Mount-4-zc46 - 1.d	25.52	0.46	0.6623	0.0083	0.80338	3328.9	17	3276	32	3355.5	28
Mount-4-zc46 - 2.d	16.13	0.53	0.562	0.014	0.84111	2881	31	2872	56	2895	39
Mount-4-zc47 - 1.d	22.79	0.45	0.6336	0.0091	0.74536	3218.4	19	3163	36	3262	30
Mount-4-zc47 - 2.d	12.4	0.26	0.4871	0.0071	0.50852	2635	19	2558	31	2701	35
Mount-4-zc48 - 1.d	11.82	0.28	0.4923	0.007	0.81696	2590	22	2580	30	2594	33
Mount-4-zc49 - 1.d	23.37	0.52	0.6739	0.0094	0.83312	3241	22	3320	36	3194	30
Mount-4-zc50 - 1.d	9.18	0.26	0.4281	0.007	0.71899	2353	26	2297	32	2398	40
Mount-4-zc50 - 2.d	9.49	0.2	0.4185	0.0061	0.34011	2387	20	2253	28	2497	36
Mount-4-zc51 - 1.d	5.907	0.13	0.3189	0.0049	0.7818	1963	20	1784	24	2157	36
Mount-4-zc53 - 1.d	16.55	0.42	0.5452	0.0099	0.76433	2907	24	2804	41	2993	35
Mount-4-zc54 - 1.d	16.77	0.4	0.5631	0.0094	0.65062	2922	22	2878	39	2951	34
Mount-4-zc54 - 2.d	26.45	0.5	0.6898	0.0097	0.81524	3363.9	19	3381	37	3353.5	29
Mount-4-zc54 - 3.d	27.09	0.59	0.7436	0.011	0.8041	3385	21	3583	40	3278	31
Mount-4-zc55 - 1.d	20.9	0.4	0.6216	0.0081	0.74962	3135.7	19	3116	32	3153.3	30
Mount-4-zc56 - 1.d	23.46	0.65	0.692	0.015	0.94111	3243	27	3389	55	3157	30
Mount-4-zc57 - 1.d	24.84	0.47	0.6761	0.0091	0.8495	3301.2	19	3329	35	3284.3	29

Mount-4-zc58 - 1.d	21.09	0.4	0.6225	0.008	0.7094	3142.1	19	3119	32	3155.2	30
Mount-4-zc59 - 1.d	16.95	0.41	0.5601	0.011	0.88363	2937	22	2865	45	2965	31
Mount-4-zc60 - 1.d	20.99	0.54	0.6035	0.0086	0.80687	3136	25	3043	35	3198	34
Mount-4-zc61 - 1.d	16.53	0.34	0.5548	0.0078	0.81225	2907	20	2844	32	2962.1	30
Mount-4-zc62 - 1.d	9.28	0.29	0.4086	0.0083	0.42184	2361	29	2207	38	2498	53
Mount-4-zc62 - 2.d	13.04	0.33	0.4962	0.0088	0.76393	2687	24	2601	39	2750	35
Mount-4-zc63 - 1.d	20.89	0.59	0.595	0.012	0.8521	3134	29	3006	50	3210	34
Mount-4-zc64 - 1.d	12.9	0.45	0.48	0.013	0.91461	2666	32	2524	56	2765	35
Mount-4-zc65 - 1.d	20.12	0.44	0.6016	0.0088	0.59264	3096	21	3036	35	3141	35
Mount-4-zc66 - 1.d	17.87	0.36	0.5565	0.0081	0.77545	2983	20	2855	34	3075	30
Mount-4-zc66 - 2.d	10.93	0.27	0.4419	0.0086	0.53745	2518	24	2358	38	2671	40
Mount-4-zc67 - 1.d	14.74	0.31	0.5234	0.0073	0.74554	2798	20	2713	31	2862	32
Mount-4-zc68 - 1.d	23.53	0.45	0.6608	0.0093	0.6641	3248.5	19	3273	37	3229	29
Mount-4-zc68 - 2.d	19.4	0.36	0.5905	0.0082	0.61529	3061.2	18	2991	33	3106	31
Mount-4-zc69 - 1.d	24.11	0.51	0.6689	0.0093	0.88105	3272	21	3301	36	3248	30
Mount-4-zc70 - 1.d	25.49	0.52	0.6636	0.0094	0.73411	3326	20	3280	36	3337	30
Mount-4-zc71 - 1.d	5.98	0.39	0.293	0.014	0.42519	1979	59	1653	68	2308	100
Mount-4-zc71 - 2.d	14.58	0.35	0.5135	0.0062	0.44256	2789	24	2671	26	2871	38
Mount-4-zc72 - 1.d	5.23	0.15	0.3005	0.0057	0.37877	1857	24	1693	28	2035	52
Mount-4-zc73 - 1.d	22.03	0.45	0.6487	0.01	0.91913	3184	20	3222	39	3163.4	29
Mount-4-zc74 - 1.d	25.22	0.47	0.6749	0.0085	0.68964	3317.2	18	3324	33	3319	29
Mount-4-zc74 - 2.d	25.97	0.5	0.6815	0.0087	0.70507	3344.6	19	3350	33	3346	30
Mount-4-zc74 - 3.d	28.25	0.57	0.7269	0.011	0.84514	3428	19	3521	39	3369.7	29
Mount-4-zc75 - 1.d	21.35	0.44	0.6294	0.0096	0.8857	3154	20	3146	38	3165	30
Mount-4-zc76 - 1.d	17.58	0.42	0.5533	0.0083	0.82425	2965	23	2838	35	3050	31
Mount-4-zc77 - 1.d	15.83	0.48	0.5048	0.0095	0.87159	2867	30	2634	41	3048	35
Mount-4-zc77 - 2.d	16.53	0.48	0.564	0.0088	0.695	2908	29	2882	36	2921	44
Mount-4-zc78 - 1.d	23.48	0.49	0.655	0.0095	0.68924	3246	20	3247	37	3248	32
Mount-4-zc79 - 1.d	8.91	0.2	0.3943	0.0058	0.53128	2328	21	2142	27	2493	39
Mount-4-zc79 - 2.d	11.05	0.25	0.4308	0.0073	0.77957	2528	21	2308	33	2726	33
Mount-4-zc80 - 1.d	13.77	0.29	0.5084	0.0067	0.79359	2733	20	2650	29	2799	33

Mount-4-zc80 - 2.d	13.04	0.27	0.4753	0.0063	0.3752	2681	20	2506	28	2807	34
Mount-4-zc81 - 1.d	13.86	0.33	0.4659	0.0084	0.70032	2743	24	2469	36	2963	34
Mount-4-zc82 - 1.d	24.26	0.5	0.6378	0.0094	0.77965	3278	20	3180	37	3330	30
Mount-4-zc83 - 1.d	23.44	0.5	0.6209	0.0082	0.81815	3244	21	3113	33	3333	30
Mount-4-zc84 - 1.d	23.81	0.56	0.6742	0.011	0.92459	3263	24	3321	41	3226	30
Mount-4-zc85 - 1.d	6.66	0.2	0.3346	0.0072	0.61069	2064	26	1864	36	2258	44
Mount-4-zc86 - 1.d	26.94	0.79	0.689	0.014	0.89822	3378	28	3375	53	3389	32
Mount-4-zc87 - 1.d	21.25	0.44	0.6229	0.0089	0.93247	3149	20	3121	35	3168.2	29
Mount-4-zc88 - 1.d	19.58	0.49	0.6009	0.011	0.95951	3068	24	3032	46	3102.7	29
Mount-4-zc89 - 1.d	21.04	0.41	0.6248	0.009	0.85731	3139.6	19	3128	36	3147.4	29
Mount-4-zc90 - 1.d	23.51	0.47	0.6583	0.0096	0.80545	3249	20	3260	37	3242.2	30
Mount-4-zc91 - 1.d	23.03	0.84	0.647	0.019	0.71226	3220	36	3209	74	3224	49
Mount-4-zc91 - 2.d	16.9	0.46	0.53	0.012	0.79915	2926	27	2740	49	3022	40
Mount-4-zc92 - 1.d	21.6	0.45	0.6126	0.0098	0.85659	3167	19	3083	38	3208	30
Mount-4-zc93 - 1.d	7.3	0.2	0.3659	0.0062	0.89876	2147	25	2010	29	2286	37
Mount-4-zc94 - 1.d	18.88	0.37	0.5641	0.0067	0.59113	3035.1	19	2883	28	3139	30
Mount-4-zc95 - 1.d	9.82	0.23	0.4421	0.0071	0.48701	2418	21	2359	32	2470	39
Mount-4-zc95 - 2.d	9.65	0.23	0.4329	0.0062	0.42142	2402	22	2318	28	2488	40
Mount-4-zc96 - 1.d	6.358	0.14	0.3356	0.0043	0.67277	2027	18	1865	21	2203	35
Mount-4-zc97 - 1.d	17.58	0.37	0.5696	0.008	0.64789	2966	20	2906	33	3005	33
Mount-4-zc98 - 1.d	28.25	0.63	0.7026	0.011	0.66775	3426	22	3435	43	3422	32
Mount-4-zc99 - 1.d	22.67	0.47	0.6267	0.009	0.82369	3212	20	3136	36	3255	31
Mount-4-zc100 - 1.d	5.51	0.14	0.2895	0.0055	0.8461	1900	22	1638	28	2201	36
Mount-4-zc100 - 2.d	13.86	0.56	0.484	0.012	0.76048	2736	39	2542	53	2882	46
Mount-4-zc101 - 1.d	19.8	0.37	0.6078	0.0078	0.81497	3081.3	18	3061	31	3096.1	30
Mount-4-zc101 - 2.d	19.39	0.36	0.5979	0.0076	0.81699	3060.8	18	3021	30	3096.5	29
Mount-4-zc102 - 1.d	29.53	0.59	0.7233	0.0098	0.79615	3471	19	3508	37	3450.1	29
Mount-4-zc102 - 2.d	27.32	0.49	0.6878	0.0086	0.70551	3394.8	18	3377	33	3410.8	29
Mount-4-zc103 - 1.d	18.97	0.37	0.5889	0.0078	0.83542	3039.7	19	2985	32	3080	30
Mount-4-zc104 - 1.d	20.2	0.4	0.6108	0.0081	0.73652	3103.4	19	3073	32	3123	30
Mount-4-zc104 - 2.d	15.58	0.39	0.5342	0.0082	0.72636	2852	23	2759	35	2914	36

Sample Co17-41											
Mount-4-zc105 - 1.d	16.4	0.43	0.5496	0.0062	0.78142	2901	25	2823	26	2961.1	39
Mount-4-zc106 - 1.d	14.34	0.41	0.4974	0.0074	0.90211	2771	26	2602	32	2889	40
Mount-4-zc106 - 2.d	23.51	0.59	0.6407	0.0082	0.87396	3247.3	24	3191	32	3290.2	38
Mount-4-zc107 - 1.d	26.55	0.67	0.6776	0.0086	0.63968	3366	25	3334	33	3382	39
Mount-4-zc107 - 2.d	26.51	0.74	0.6918	0.0099	0.76331	3366	27	3388	38	3354	41
Mount-4-zc108 - 1.d	21.76	0.57	0.6418	0.009	0.85304	3172	25	3195	35	3166.7	38
Mount-4-zc109 - 1.d	27.18	0.68	0.6829	0.0082	0.79477	3389.2	24	3358	31	3410.8	38
Mount-4-zc110 - 1.d	28.72	0.77	0.7107	0.011	0.83958	3443	26	3459	43	3442	38
Mount-4-zc111 - 1.d	18.08	0.47	0.5642	0.0062	0.89591	2993	25	2883	25	3064	39
Mount-4-zc112 - 1.d	24.26	0.64	0.6618	0.009	0.81274	3279	26	3273	35	3287	39
Mount-4-zc112 - 2.d	25.15	0.67	0.6713	0.01	0.88402	3317	28	3314	38	3323	40
Mount-4-zc113 - 1.d	23.33	0.63	0.667	0.0085	0.80049	3242	27	3294	33	3202	40
Mount-4-zc114 - 1.d	27.37	0.7	0.6931	0.0098	0.87749	3399	25	3393	37	3393	38
Mount-4-zc114 - 2.d	25.82	0.74	0.6814	0.011	0.79931	3340	28	3348	41	3345	41
Mount-4-zc115 - 1.d	28.83	0.73	0.6919	0.0084	0.68473	3447	25	3393	33	3475	38
Mount-4-zc115 - 2.d	25.27	0.66	0.6495	0.0097	0.66197	3318	25	3225	38	3383	40
Mount-4-zc116 - 2.d	18.43	0.58	0.571	0.01	0.79366	3009	31	2910	41	3081	44
Mount-4-zc117 - 1.d	24.22	0.9	0.704	0.022	0.98843	3271	37	3441	82	3177.5	38
Mount-4-zc118 - 1.d	17.63	0.64	0.529	0.012	0.52048	2973	37	2748	48	3130	55
Mount-4-zc119 - 1.d	8.56	0.23	0.3931	0.0054	0.70853	2292	24	2137	25	2439	44
Mount-4-zc120 - 1.d	20.84	0.51	0.5943	0.0062	0.70871	3130.7	24	3007	25	3207	39
Mount-4-zc121 - 1.d	20.66	0.52	0.6113	0.0068	0.81941	3122	24	3075	27	3150.9	39
Mount-4-zc122 - 1.d	18.23	0.54	0.577	0.011	0.93079	3000	28	2938	43	3050	39
Mount-4-zc123 - 1.d	24.79	0.61	0.6618	0.008	0.78967	3299.4	24	3277	31	3318	38
Mount-4-zc124 - 1.d	20.21	0.55	0.5986	0.0093	0.88126	3100	26	3023	37	3164	39
Mount-4-zc125 - 1.d	21.13	0.58	0.5993	0.0071	0.77862	3143	26	3026	29	3224	40
Mount-4-zc128 - 1.d	24.25	0.66	0.6868	0.009	0.87867	3279	27	3370	34	3226	39
Mount-4-zc129 - 1.d	24.12	0.6	0.647	0.0077	0.79354	3273.8	25	3216	30	3310	39
Mount-4-zc129 - 2.d	21.51	1.1	0.649	0.023	0.92987	3152	51	3227	91	3128	44

Mount-4-zc130 - 1.d	24.34	0.7	0.6567	0.0095	0.92079	3280	28	3253	37	3307	38
Mount-4-zc131 - 1.d	25.17	0.63	0.6646	0.0079	0.72396	3314.1	24	3284	31	3329	38
Mount-4-zc131 - 2.d	17.61	0.46	0.5448	0.0074	0.57474	2968	25	2806	31	3082	44
Mount-4-zc132 - 1.d	22.37	0.55	0.6342	0.0074	0.56431	3199.5	24	3168	30	3213	40
Mount-4-zc132 - 2.d	23.11	0.59	0.649	0.0086	0.57143	3231	25	3223	34	3238	38
Mount-4-zc133 - 1.d	24.5	0.61	0.6596	0.0085	0.77498	3289.1	24	3265	33	3308	39
Mount-4-zc134 - 1.d	24.82	0.61	0.6712	0.0077	0.76522	3300.7	24	3310	30	3309.6	37
Mount-4-zc134 - 2.d	22.5	0.57	0.6255	0.0095	0.82161	3206	26	3135	37	3259	40
Mount-4-zc135 - 1.d	12.95	0.34	0.459	0.0068	0.55311	2675	25	2438	31	2858	42
Mount-4-zc135 - 2.d	24.6	0.61	0.67	0.0081	0.69668	3291.7	24	3305	31	3289	39
Mount-4-zc136 - 1.d	26.84	0.7	0.7125	0.01	0.81776	3376	26	3466	40	3327	39
Mount-4-zc137 - 1.d	23.87	0.65	0.6254	0.01	0.90043	3262	27	3130	40	3348	38
Mount-4-zc138 - 1.d	24.94	0.62	0.655	0.0079	0.71879	3306.6	23	3251	31	3346	39
Mount-4-zc139 - 1.d	22.82	0.94	0.65	0.023	0.9847	3211	39	3219	89	3221.4	39
Mount-4-zc140 - 1.d	23.72	0.62	0.6502	0.0082	0.50211	3257	26	3228	32	3282	42
Mount-4-zc141 - 1.d	22.02	0.57	0.6421	0.0091	0.8618	3187	23	3196	36	3184	39
Mount-4-zc141 - 2.d	25.34	0.62	0.6732	0.0077	0.77023	3320.7	24	3317	30	3334	39
Mount-4-zc142 - 1.d	12.27	0.44	0.4601	0.0077	0.76297	2625	34	2439	34	2786	49
Mount-4-zc143 - 1.d	15.36	0.42	0.4773	0.0077	0.71759	2836	26	2514	34	3088	43
Mount-4-zc144 - 1.d	20.91	0.59	0.6162	0.0073	0.69719	3134	28	3094	29	3161	42
Mount-4-zc145 - 1.d	26.2	0.66	0.6756	0.0078	0.77464	3353.2	25	3327	30	3365	38
Mount-4-zc145 - 2.d	25.09	0.63	0.6566	0.0078	0.72042	3311	24	3253	31	3347.9	37
Mount-4-zc146 - 1.d	26.24	0.66	0.6782	0.0083	0.70978	3355	25	3337	32	3366	40
Mount-4-zc146 - 2.d	27.27	0.71	0.6961	0.0094	0.85923	3392	25	3405	36	3380.9	38
Mount-4-zc147 - 1.d	15.87	0.43	0.5238	0.0071	0.82414	2867	26	2714	30	2976	40
Mount-4-zc147 - 2.d	14.73	0.42	0.5119	0.0077	0.85686	2796	27	2667	32	2895	41
Mount-4-zc148 - 1.d	26.63	0.69	0.7009	0.0093	0.69686	3369	25	3423	35	3348	40
Mount-4-zc148 - 2.d	25.96	0.68	0.695	0.0099	0.67619	3344	25	3405	38	3319	40
Mount-4-zc149 - 1.d	21.04	0.54	0.6124	0.0068	0.86582	3139	25	3079	27	3179.4	39
Mount-4-zc149 - 2.d	28.66	0.84	0.769	0.015	0.94934	3439	28	3682	53	3308	38
Mount-4-zc150 - 1.d	26.78	0.7	0.6706	0.0089	0.84599	3374	25	3307	34	3408.9	38

Mount-4-zc150 - 2.d	22.24	0.54	0.6204	0.0063	0.72862	3193.6	24	3111	25	3254.1	38
Mount-4-zc151 - 1.d	37.92	1	0.75	0.013	0.70237	3718	27	3608	49	3783	41
Mount-4-zc151 - 2.d	34.94	0.96	0.7507	0.01	0.80854	3635	27	3609	37	3652	38
Mount-4-zc152 - 1.d	24.78	0.65	0.6836	0.01	0.57239	3298	25	3357	38	3272	41
Mount-4-zc152 - 2.d	24.14	0.6	0.6502	0.0078	0.85807	3274.8	24	3228	30	3308	38
Mount-4-zc152 - 3.d	26.07	0.66	0.6766	0.0085	0.84706	3348	25	3330	33	3364.6	38
Mount-4-zc152 - 4.d	28.91	0.8	0.76	0.012	0.8556	3449	27	3641	43	3341	39
Mount-4-zc153 - 1.d	15.85	0.52	0.5088	0.0086	0.7175	2869	32	2650	37	3038	47
Mount-4-zc154 - 1.d	18.86	0.49	0.5923	0.0076	0.89196	3033	25	2998	31	3060.8	39
Mount-4-zc155 - 1.d	20.16	0.56	0.6211	0.0082	0.78778	3101	26	3113	33	3102	40
Mount-4-zc156 - 1.d	21.93	0.66	0.6321	0.01	0.91059	3178	29	3161	42	3192	40
Mount-4-zc157 - 1.d	26.28	0.78	0.6928	0.011	0.7706	3358	30	3392	43	3349	41
Mount-4-zc158 - 1.d	28.64	0.81	0.704	0.012	0.7847	3441	27	3435	44	3438	39
Mount-4-zc158 - 2.d	29.58	0.86	0.717	0.014	0.92857	3471	29	3483	52	3461	38
Mount-4-zc158 - 3.d	28.73	0.71	0.7072	0.0092	0.50268	3443.7	24	3447	35	3456	40
Mount-4-zc159 - 1.d	21.29	0.53	0.6121	0.0078	0.81897	3152.3	25	3078	31	3211.2	38
Mount-4-zc159 - 2.d	25.05	0.64	0.6767	0.0088	0.88332	3311	24	3331	34	3297.8	38
Mount-4-zc160 - 1.d	24.45	0.79	0.667	0.013	0.93084	3292	33	3291	51	3298	39
Mount-4-zc160 - 2.d	17.02	0.72	0.52	0.012	0.90086	2929	40	2706	50	3088	46
Mount-4-zc161 - 1.d	26.9	0.7	0.686	0.0094	0.85782	3379	26	3366	36	3385	39
Mount-4-zc162 - 1.d	18.04	0.51	0.5454	0.007	0.90618	2990	27	2805	29	3129	38
Mount-4-zc163 - 1.d	14.01	0.38	0.4719	0.0063	0.83662	2752	27	2496	29	2947	41
Mount-4-zc164 - 1.d	19.38	0.46	0.5766	0.006	0.52615	3060.8	23	2934	24	3149	39
Mount-4-zc164 - 2.d	22.25	0.82	0.635	0.011	0.84953	3188	36	3168	45	3204	45
Mount-4-zc165 - 1.d	21.36	0.54	0.6487	0.0083	0.84797	3154	25	3226	31	3110.8	39
Mount-4-zc166 - 1.d	27.73	0.74	0.6809	0.0083	0.70724	3410	26	3347	32	3448	40
Mount-4-zc166 - 2.d	20.25	0.61	0.5853	0.0082	0.59544	3100	29	2969	33	3188	45
Mount-4-zc167 - 1.d	29.12	0.73	0.7137	0.011	0.6923	3458	26	3471	40	3461	39
Mount-4-zc167 - 2.d	32.31	0.83	0.7923	0.01	0.84339	3559	25	3760	37	3452.4	38
Mount-4-zc168 - 1.d	20.24	0.5	0.6041	0.0073	0.86535	3102.1	24	3049	30	3136.5	39
Mount-4-zc169 - 1.d	20.67	0.53	0.6147	0.0066	0.81232	3124	24	3088	27	3152	39

Mount-4-zc169 - 2.d	17.53	0.6	0.561	0.012	0.93899	2960	33	2868	48	3026	41
Mount-4-zc170 - 1.d	23.05	0.58	0.6488	0.0085	0.8595	3228	25	3223	33	3241.6	39
Mount-4-zc170 - 2.d	21.63	0.64	0.6104	0.01	0.90528	3174	32	3070	41	3244	41
Mount-4-zc171 - 1.d	14.44	0.41	0.5043	0.0062	0.75339	2778	26	2632	27	2898	42
Mount-4-zc172 - 1.d	21.73	0.6	0.6245	0.0084	0.86145	3170	27	3127	33	3195	39
Mount-4-zc172 - 2.d	19.55	0.53	0.5822	0.008	0.76979	3070	26	2957	33	3153	40
Mount-4-zc172 - 3.d	21.93	0.55	0.6116	0.0071	0.79717	3181.3	24	3076	28	3249.7	38
Mount-4-zc173 - 1.d	21.32	0.57	0.6187	0.0085	0.83395	3152	26	3104	34	3186.8	39
Mount-4-zc173 - 2.d	23.23	0.57	0.6317	0.007	0.71095	3235.9	24	3156	28	3296	39
Mount-4-zc174 - 1.d	21.32	0.58	0.6322	0.0099	0.91068	3152	27	3157	39	3149	39
Mount-4-zc175 - 1.d	16.63	0.45	0.5382	0.0085	0.63556	2913	26	2775	36	3025	44
Mount-4-zc175 - 2.d	24.33	0.67	0.6818	0.0091	0.80672	3283	26	3350	35	3243	40
Mount-4-zc176 - 1.d	23.06	0.62	0.6447	0.0076	0.65978	3228	26	3207	30	3235	41
Mount-4-zc176 - 2.d	14.55	0.38	0.5046	0.0065	0.74418	2785	24	2633	28	2906	41
Mount-4-zc177 - 1.d	15.31	0.44	0.4931	0.007	0.88344	2835	27	2583	30	3023	41
Mount-4-zc178 - 1.d	26.57	0.66	0.6974	0.0078	0.77952	3368.2	24	3413	30	3341.3	38
Mount-4-zc178 - 2.d	20.7	0.58	0.6024	0.011	0.8991	3123	27	3038	42	3176	40
Mount-4-zc179 - 1.d	24.46	0.6	0.663	0.0082	0.83007	3286.3	24	3278	32	3301.9	38
Mount-4-zc179 - 2.d	22.81	0.68	0.6387	0.0086	0.67256	3219	28	3187	35	3248	41
Mount-4-zc179 - 3.d	24.82	0.62	0.6698	0.0074	0.71384	3300.4	24	3305	29	3308	37
Mount-4-zc180 - 1.d	19.17	0.56	0.5707	0.0091	0.85508	3049	29	2910	38	3141	41
Mount-4-zc180 - 2.d	23.31	0.67	0.6408	0.0099	0.86178	3240	29	3195	40	3267	40
Mount-4-zc181 - 1.d	26.94	0.68	0.6786	0.0093	0.68658	3381	25	3342	37	3408	40

APPENDIX C: U–PB GEOCHRONOLOGY MONAZITE ANALYSES

	$^{207}Pb/^{235}U$	2σ	$^{206}Pb/^{238}U$	2σ	Rho	$^{207}Pb/^{235}U$ Age	2σ	$^{206}Pb/^{238}U$ Age	2σ	$^{207}Pb/^{206}U$ Age	2σ
Session 1 - Standards											
External Standards											
MAdel - 1	0.653	0.018	0.08392	0.00092	0.28914	510	11	520.1	5.3	487	44
MAdel - 2	0.6632	0.017	0.08377	0.00076	0.37026	516.3	10	518.5	4.5	506	40
MAdel - 3	0.649	0.017	0.08325	0.00084	0.23556	507.6	11	515.5	5	494	43
MAdel - 4	0.647	0.016	0.08338	0.00096	0.17609	507.1	9.9	516.2	5.7	478	40
MAdel - 5	0.6495	0.016	0.08386	0.00087	0.34462	508	10	519.1	5.1	452	41
MAdel - 6	0.669	0.018	0.08434	0.00087	0.18922	520.5	11	521.9	5.2	503	45
MAdel - 7	0.6701	0.017	0.08347	0.0009	0.37914	521.4	10	516.8	5.4	531	39
MAdel - 8	0.664	0.018	0.08392	0.00095	0.24156	517.8	11	519.4	5.7	483	43
MAdel - 9	0.657	0.017	0.084	0.00076	0.37402	512.6	11	519.9	4.5	484	40
MAdel - 10	0.6562	0.017	0.08399	0.00082	0.32579	512	10	519.9	4.9	462	36
MAdel - 11	0.678	0.02	0.083	0.0011	0.78945	525.4	12	514.2	6.5	538	42
MAdel - 12	0.6611	0.016	0.08376	0.00078	0.26699	515.8	10	518.5	4.6	492	36
MAdel - 13	0.6521	0.017	0.08353	0.00085	0.26191	510.3	10	517.1	5.1	484	43
MAdel - 14	0.6617	0.017	0.08375	0.00083	0.32333	515.4	10	518.5	5	480	38
MAdel - 15	0.6551	0.016	0.08383	0.00074	0.46086	511.5	9.7	518.9	4.4	485	34
MAdel - 16	0.6584	0.016	0.08344	0.00079	0.41456	513.5	9.6	516.6	4.7	506	36
MAdel - 17	0.6551	0.017	0.08335	0.00073	0.23955	512.2	10	516.1	4.3	487	38
MAdel - 18	0.6665	0.016	0.08451	0.00079	0.36139	519.1	9.6	522.9	4.7	496	36
MAdel - 19	0.6548	0.016	0.08373	0.00082	0.43435	511.2	9.6	518.3	4.9	488	32
MAdel - 20	0.647	0.016	0.08338	0.00082	0.21957	506.4	10	516.2	4.9	480	38
MAdel - 21	0.654	0.019	0.08378	0.0016	0.31728	511.4	11	518.6	9.7	474	44
MAdel - 22	0.6565	0.019	0.08277	0.0016	0.30484	512.2	12	512.6	9.2	503	47
MAdel - 23	0.6598	0.019	0.08381	0.0015	0.19451	514.9	11	518.8	9.2	481	45

MAdel - 24	0.6614	0.019	0.08367	0.0016	0.33633	515.9	11	518	9.6	502	45
MAdel - 25	0.6642	0.019	0.08397	0.0016	0.37314	516.9	12	519.8	9.3	494	45
MAdel - 26	0.6574	0.019	0.08366	0.0016	0.47107	512.8	11	517.9	9.7	491	42
MAdel - 27	0.6607	0.019	0.08413	0.0015	0.28711	516.3	12	520.7	9.2	475	46
MAdel - 28	0.6611	0.019	0.08439	0.0016	0.25353	515	12	522.2	9.4	469	47
MAdel - 29	0.6655	0.019	0.08521	0.0016	0.33654	517.7	12	527.1	9.4	468	45
MAdel - 30	0.6548	0.019	0.08323	0.0016	0.38601	511.1	12	515.4	9.4	486	47
MAdel - 31	0.6494	0.019	0.08286	0.0016	0.50284	508.6	12	513.2	9.4	481	44
MAdel - 32	0.627	0.018	0.08206	0.0016	0.36775	494	11	508.4	9.4	430	44
MAdel - 33	0.6603	0.018	0.08385	0.0016	0.11932	515.3	12	519	9.5	507	46
MAdel - 34	0.6573	0.019	0.08391	0.0015	0.15199	513.4	12	519.4	9.2	487	46
MAdel - 35	0.6593	0.019	0.08353	0.0015	0.30314	513.9	12	517.1	9.1	510	44
MAdel - 36	0.662	0.02	0.08396	0.0016	0.31806	516.1	12	519.7	9.5	507	49
MAdel - 37	0.6613	0.019	0.08338	0.0015	0.28737	515.9	11	516.3	9.2	517	42
MAdel - 38	0.671	0.019	0.08536	0.0016	0.2982	521.1	11	528	9.6	508	43
MAdel - 39	0.6485	0.019	0.08321	0.0015	0.36015	507.2	12	515.2	9.1	480	47
MAdel - 40	0.6529	0.019	0.08316	0.0016	0.50087	510	12	514.9	9.3	502	42
MAdel - 41	0.6738	0.019	0.08476	0.0016	0.40735	522.9	11	524.4	9.4	507	40
MAdel - 42	0.6445	0.018	0.08366	0.0016	0.28083	505.5	11	517.9	9.4	449	43
MAdel - 43	0.652	0.019	0.08302	0.0016	0.4499	509.4	11	514.1	9.3	491	44
MAdel - 44	0.669	0.02	0.08359	0.0016	0.37481	519.6	12	517.5	9.5	546	48
MAdel - 45	0.6505	0.016	0.08382	0.0018	0.33074	509.3	10	518.9	11	464	34
MAdel - 46	0.6572	0.017	0.08408	0.0018	0.36915	512.7	10	520.4	10	488	35
MAdel - 47	0.658	0.017	0.08419	0.0018	0.32833	513.1	10	521	11	463	35
MAdel - 48	0.658	0.018	0.08347	0.0017	0.32108	513.3	11	516.8	10	506	40
MAdel - 49	0.6591	0.017	0.08347	0.0018	0.28296	513.8	10	516.8	10	500	38
MAdel - 50	0.6577	0.016	0.08366	0.0017	0.40357	513.1	10	517.9	10	488	33
MAdel - 51	0.6558	0.016	0.08377	0.0018	0.28394	511.9	10	518.6	10	495	35
MAdel - 52	0.6593	0.017	0.08392	0.0018	0.2785	514.7	10	519.4	10	489	36
MAdel - 53	0.6586	0.017	0.08344	0.0017	0.31168	513.5	11	516.6	10	507	35
MAdel - 54	0.6535	0.017	0.08335	0.0017	0.46768	510.4	11	516	10	494	37

MAdel - 55	0.648	0.017	0.08294	0.0017	0.25867	506.8	11	513.6	10	487	41
MAdel - 56	0.6491	0.017	0.08235	0.0017	0.38397	507.6	11	510.1	10	499	35
MAdel - 57	0.6633	0.017	0.08365	0.0017	0.28	516.4	10	517.9	10	494	36
MAdel - 58	0.6571	0.017	0.08355	0.0017	0.37335	512.7	10	517.3	10	485	35
MAdel - 59	0.6456	0.017	0.08243	0.0017	0.47977	505.5	11	510.6	10	493	35
MAdel - 60	0.6612	0.017	0.08475	0.0018	0.19305	515.2	10	524.4	10	479	36
MAdel - 61	0.663	0.018	0.08541	0.0018	0.30953	516.3	11	528.3	11	463	39
MAdel - 62	0.67	0.019	0.08471	0.0018	0.34402	520.5	11	524.1	11	505	41
MAdel - 63	0.667	0.018	0.08431	0.0017	0.32234	518.4	11	521.8	10	499	39
MAdel - 64	0.6532	0.017	0.08328	0.0017	0.38585	510.9	11	515.7	10	486	35
Internal Standards											
AMBAT - 1	0.664	0.016	0.08425	0.00086	0.31944	516.9	9.9	521.4	5.1	497	35
AMBAT - 2	0.6631	0.017	0.08492	0.0011	0.49484	516.2	10	525.4	6.3	477	37
AMBAT - 3	0.6623	0.016	0.08438	0.00075	0.49735	515.8	9.9	522.2	4.5	493	33
AMBAT - 4	0.6653	0.016	0.08389	0.00091	0.32939	517.7	9.7	519.3	5.4	520	38
AMBAT - 5	0.6569	0.017	0.08425	0.00089	0.5266	512.4	10	521.4	5.3	460	40
AMBAT - 6	0.6609	0.017	0.08287	0.00091	0.52737	515.7	10	513.9	5.6	505	37
AMBAT - 7	0.6439	0.016	0.08269	0.0009	0.55734	504.5	10	512.1	5.4	492	34
AMBAT - 8	0.651	0.016	0.08298	0.00081	0.57509	508.8	10	513.9	4.8	479	35
AMBAT - 9	0.6535	0.016	0.08363	0.00082	0.30832	510.4	9.9	517.8	4.9	491	35
AMBAT - 10	0.6491	0.016	0.08355	0.00084	0.34091	507.7	9.9	517.3	5	477	38
AMBAT - 11	0.6621	0.018	0.08316	0.0016	0.37849	515.7	11	514.9	9.3	509	44
AMBAT - 12	0.6695	0.019	0.08386	0.0016	0.58266	520.2	12	519.1	9.6	525	43
AMBAT - 13	0.6496	0.018	0.08238	0.0016	0.53305	508	11	510.3	9.3	482	40
AMBAT - 14	0.6793	0.019	0.08568	0.0017	0.61659	526.8	12	529.9	10	487	40
AMBAT - 15	0.6559	0.018	0.08319	0.0016	0.56235	511.9	11	515.1	9.4	506	41
AMBAT - 16	0.677	0.022	0.0862	0.0022	0.83232	524.2	14	533	13	492	40
AMBAT - 17	0.6628	0.019	0.08351	0.0016	0.3678	516.1	11	517	9.6	531	43
AMBAT - 18	0.669	0.023	0.08527	0.0016	0.36863	519.5	13	527.5	9.7	509	54
AMBAT - 19	0.887	0.049	0.08701	0.0017	0.64341	640	26	537.8	10	1011	95

AMBAT - 20	0.6705	0.02	0.08546	0.0016	0.44904	520.7	12	528.6	9.8	485	46
AMBAT - 21	0.6626	0.019	0.0836	0.0016	0.48887	516	11	517.6	9.5	497	44
AMBAT - 22	0.661	0.019	0.08425	0.0016	0.36805	515	12	521.4	9.5	480	45
AMBAT - 23	0.6653	0.017	0.08402	0.0018	0.48982	517.6	10	520	11	497	33
AMBAT - 24	0.6628	0.017	0.08426	0.0017	0.46692	516.1	10	521.5	10	482	34
AMBAT - 25	0.6492	0.017	0.08406	0.0017	0.60331	507.7	10	520.3	10	460	35
AMBAT - 26	0.6582	0.017	0.08346	0.0018	0.28863	514	10	516.7	10	510	36
AMBAT - 27	0.6542	0.017	0.08284	0.0017	0.65883	510.8	11	513.1	10	521	32
AMBAT - 28	0.639	0.016	0.08338	0.0017	0.32787	502.2	9.8	516.2	10	451	38
AMBAT - 29	0.6494	0.017	0.08341	0.0017	0.2223	507.8	11	516.4	10	474	39
AMBAT - 30	0.6507	0.016	0.08346	0.0018	0.37824	508.7	10	516.7	10	472	36
AMBAT - 31	0.6462	0.017	0.08278	0.0017	0.49504	506.7	10	512.7	10	486	34
AMBAT - 32	0.6399	0.017	0.08261	0.0017	0.23489	502	10	511.6	10	445	38
222 - 1	0.5526	0.014	0.07244	0.00083	0.2631	446.5	9.1	450.8	5	440	39
222 - 2	0.5571	0.013	0.07293	0.00067	0.1617	450	8.7	453.8	4	428	34
222 - 3	0.5688	0.014	0.07206	0.00067	0.38924	457.1	9	448.5	4	495	35
222 - 4	0.553	0.013	0.07253	0.00069	0.43323	446.8	8.8	451.3	4.1	427	34
222 - 5	0.5585	0.014	0.07206	0.00064	0.50516	450.4	9.2	448.6	3.9	445	35
222 - 6	0.5509	0.013	0.0717	0.00071	0.28055	445.4	8.8	446.4	4.3	417	33
222 - 7	0.5614	0.014	0.07224	0.0007	0.15491	452.9	9	449.6	4.2	453	40
222 - 8	0.5572	0.014	0.07315	0.00072	0.1419	449.5	9.3	455.1	4.3	431	44
222 - 9	0.5518	0.013	0.07223	0.00075	0.34043	446.1	8.5	449.6	4.5	428	36
222 - 10	0.5487	0.014	0.07138	0.00061	0.21972	444.5	9.1	444.5	3.7	450	38
222 - 11	0.5592	0.016	0.07283	0.0014	0.2809	450.8	10	453.2	8.3	408	46
222 - 12	0.5638	0.016	0.07208	0.0014	0.55173	453.8	10	448.7	8.2	479	42
222 - 13	0.5698	0.016	0.07255	0.0014	0.37381	458.4	10	451.5	8.1	487	43
222 - 14	0.5275	0.015	0.06832	0.0014	0.64076	429.9	10	426	8.3	441	44
222 - 15	0.5503	0.017	0.07157	0.0014	0.32471	444.9	11	445.6	8.1	436	48
222 - 16	0.5685	0.017	0.07266	0.0014	0.32657	456.8	11	452.2	8.3	479	47
222 - 17	0.559	0.016	0.07199	0.0013	0.35679	452	10	448.1	8.1	475	42

222 - 18	0.5616	0.016	0.07286	0.0014	0.27218	452.4	10	453.4	8.3	455	47
222 - 19	0.5725	0.016	0.07339	0.0014	0.28855	459.4	10	456.6	8.3	477	42
222 - 20	0.5641	0.016	0.07262	0.0014	0.2863	453.9	10	451.9	8.4	480	48
222 - 21	0.5613	0.016	0.07345	0.0014	0.42598	452.1	11	456.9	8.5	422	44
222 - 22	0.5636	0.016	0.07328	0.0014	0.36421	453.7	10	456.4	8.3	440	46
222 - 23	0.5602	0.014	0.07299	0.0015	0.33987	451.5	9.2	454.1	9	443	37
222 - 24	0.5591	0.014	0.07235	0.0015	0.3866	450.8	9.4	450.3	9	457	38
222 - 25	0.5642	0.016	0.07264	0.0015	0.53446	454	10	452	9	459	35
222 - 26	0.5631	0.014	0.0733	0.0015	0.36919	453.4	9.1	456	9.1	456	34
222 - 27	0.56	0.015	0.07302	0.0016	0.36401	452	9.8	454.3	9.4	434	37
222 - 28	0.5569	0.015	0.07299	0.0015	0.20941	449.3	9.7	454.1	9.1	424	38
222 - 29	0.5492	0.015	0.07258	0.0015	0.34682	444.2	9.6	451.7	8.9	410	35
222 - 30	0.5569	0.014	0.07141	0.0015	0.27384	449.3	9.4	444.7	8.9	481	36
222 - 31	0.5652	0.015	0.07277	0.0016	0.4303	455.5	9.4	452.8	9.3	469	37
222 - 32	0.5542	0.014	0.07179	0.0015	0.5255	447.5	9.3	446.9	9.3	460	32

Session 2 - Standards	**$^{207}Pb/^{235}U$**	**2σ**	**$^{206}Pb/^{238}U$**	**2σ**	**Rho**	**$^{207}Pb/^{235}U$ Age**	**2σ**	**$^{206}Pb/^{238}U$ Age**	**2σ**	**$^{207}Pb/^{206}U$ Age**	**2σ**
MADEL - 2	0.654	0.013	0.0832	0.0015	0.15715	510.5	8.1	515.2	8.8	507	50
MADEL - 3	0.661	0.013	0.0849	0.0016	0.30896	514.6	7.8	525.1	9.3	453	48
MADEL - 4	0.663	0.013	0.0836	0.0016	0.37047	516.1	7.7	517.8	9.2	510	43
MADEL - 5	0.648	0.012	0.08395	0.0015	0.2836	506.8	7.2	519.6	8.9	489	46
MADEL - 6	0.655	0.013	0.08328	0.0014	0.21659	511.2	8.1	515.7	8.4	481	47
MADEL - 7	0.664	0.012	0.0842	0.0016	0.49169	517.6	7	520.9	9.5	476	43
MADEL - 8	0.653	0.013	0.08378	0.0014	0.35569	510.1	7.9	518.6	8.5	487	47
MADEL - 9	0.655	0.012	0.08442	0.0015	0.19101	510.8	7.6	522.4	8.7	459	46
MADEL - 10	0.659	0.014	0.0833	0.0016	0.31865	513.4	8.8	515.7	9.3	517	49
MADEL - 11	0.647	0.013	0.08263	0.0014	0.33468	508.9	7.9	511.8	8.6	481	48
MADEL - 12	0.659	0.013	0.08386	0.0015	0.3976	514.5	7.9	519.1	8.9	480	43
MADEL - 13	0.666	0.014	0.08365	0.0015	0.35571	517.4	8.8	517.8	8.8	500	51

MADEL - 14	0.655	0.012	0.08495	0.0015	0.40481	511	7.6	525.5	8.8	451	46
MADEL - 15	0.66	0.015	0.08338	0.0015	0.36922	515	9.2	516.2	9	502	53
MADEL - 16	0.662	0.013	0.08336	0.0014	0.35448	516.3	7.8	516.1	8.5	507	48
Ambat - 1	0.393	0.021	0.05131	0.0011	0.30235	335	15	322.5	6.8	440	110
Ambat - 2	0.406	0.02	0.05089	0.0011	0.35609	351	15	320.8	7.2	520	110
Ambat - 3	0.379	0.018	0.04938	0.0011	0.15002	328	12	310.7	7	442	100
Ambat - 4	0.355	0.016	0.0496	0.0012	0.12843	307	12	312	7.1	290	100
Ambat - 5	0.38	0.017	0.0506	0.0012	0.16948	327	12	318.4	7.6	363	100
Ambat - 6	0.382	0.019	0.05003	0.001	-0.1511	328	14	314.7	6.4	360	120
Ambat - 7	0.39	0.022	0.0513	0.0013	0.12991	336	15	322.5	7.7	450	120
Ambat - 8	0.428	0.021	0.04999	0.0012	0.22078	362	15	314.4	7.5	660	110
222 - 1	0.561	0.011	0.07316	0.0012	0.17569	452	7.2	455.2	7.5	444	51
222 - 2	0.551	0.012	0.0732	0.0014	0.45175	445.1	8	455.3	8.4	367	48
222 - 3	0.565	0.012	0.0727	0.0012	0.34702	454.6	7.7	452.4	7.4	439	51
222 - 4	0.552	0.011	0.0713	0.0014	0.48099	446.7	7.5	444	8.6	482	46
222 - 5	0.5625	0.0096	0.07209	0.0013	0.17015	454.5	6.6	448.7	7.6	483	46
222 - 6	0.573	0.012	0.07284	0.0013	0.40676	459.5	7.8	453.9	7.4	481	46
222 - 7	0.568	0.012	0.07222	0.0014	0.14353	457.4	8.1	449.5	8.1	510	56
222 - 8	0.577	0.013	0.07274	0.0013	0.37591	461.9	8.4	452.6	7.5	518	50
Session 3 - Standards	**$^{207}Pb/^{235}U$**	**2σ**	**$^{206}Pb/^{238}U$**	**2σ**	**Rho**	**$^{207}Pb/^{235}U$ Age**	**2σ**	**$^{206}Pb/^{238}U$ Age**	**2σ**	**$^{207}Pb/^{206}U$ Age**	**2σ**
MAdel - 1	0.645	0.021	0.08304	0.0021	0.48901	505.9	12	514.2	12	471	40
MAdel - 2	0.671	0.021	0.08519	0.0022	0.56395	521.1	13	527	13	504	39
MAdel - 3	0.658	0.02	0.0837	0.0021	0.27851	513.1	12	518.1	12	485	40
MAdel - 4	0.6548	0.02	0.08309	0.0021	0.19964	512.1	12	514.5	12	497	43
MAdel - 5	0.6533	0.02	0.08339	0.0021	0.35849	510.2	12	516.3	12	476	40
MAdel - 6	0.648	0.02	0.08305	0.0021	0.40056	506.6	13	514.3	13	468	47
MAdel - 7	0.672	0.021	0.0857	0.0021	0.41788	521.6	13	530	13	482	44
MAdel - 8	0.67	0.021	0.0837	0.0021	0.4937	520.2	13	518.1	13	527	41

MAdel - 9	0.661	0.021	0.08355	0.0021	0.48037	515.2	13	517.2	12	506	38
MAdel - 10	0.649	0.021	0.08343	0.0021	0.44468	507.2	13	516.5	12	475	45
MAdel - 11	0.6568	0.02	0.08305	0.0021	0.50817	512.4	13	514.3	12	488	41
MAdel - 12	0.657	0.022	0.08465	0.0022	0.38992	512.4	13	523.8	13	478	49
Ambat - 1	0.682	0.022	0.08487	0.0022	0.50604	527.7	14	525.1	13	544	43
Ambat - 2	0.673	0.021	0.08559	0.0022	0.53887	522.4	13	529.4	13	497	41
Ambat - 3	0.679	0.024	0.08521	0.0022	0.43568	526.6	14	527.1	13	545	54
Ambat - 4	0.674	0.023	0.08518	0.0022	0.54627	522.3	14	526.9	13	507	46
Ambat - 5	0.677	0.022	0.08532	0.0022	0.45116	524.5	13	527.7	13	501	46
Ambat - 6	0.677	0.023	0.08479	0.0022	0.41986	524.5	14	525.4	13	515	50

Session 1 - Samples	**$^{207}Pb/^{235}U$**	**2σ**	**$^{206}Pb/^{238}U$**	**2σ**	**Rho**	**$^{207}Pb/^{235}U$ Age**	**2σ**	**$^{206}Pb/^{238}U$ Age**	**2σ**	**$^{207}Pb/^{206}U$ Age**	**2σ**
Co17-21 mon7 - 1	1.165	0.029	0.1311	0.0013	0.38164	784.1	13	794.2	7.3	761	33
Co17-21 mon7 - 2	1.197	0.029	0.13159	0.0012	0.38974	798.8	13	796.9	6.6	798	33
Co17-21 mon2 - 1	1.319	0.067	0.1305	0.0022	0.9209	849	27	791	12	1024	75
Co17-21 mon3 - 1	1.189	0.029	0.13214	0.0012	0.28692	795.2	13	800	6.8	793	33
Co17-21 mon4 - 1	1.242	0.034	0.1381	0.0016	0.729	820.4	15	833.8	9.2	791	34
Co17-21 mon9 - 1	1.003	0.024	0.1153	0.0013	0.25856	705	12	703.2	7.7	704	37
Co17-21 mon11 - 1	13.11	0.38	0.4483	0.0071	0.90004	2686	27	2387	32	2914	24
Co17-21 mon12 - 1	1.592	0.093	0.1514	0.0048	0.87162	965	34	908	27	1132	55
Co17-21 mon13 - 1	1.176	0.029	0.133	0.0013	0.42675	788.9	13	804.9	7.6	745	32
Co17-21 mon13 - 2	1.36	0.078	0.1431	0.0037	0.96014	865	31	861	21	893	62
Co17-21 mon14 - 1	1.238	0.051	0.134	0.0035	0.8978	817	22	811	20	864	65
Co17-21 mon15 - 1	17.73	0.41	0.5848	0.006	0.64443	2974.6	22	2968	24	2995	22
Co17-41 mon1 - 2	2.77	0.25	0.1692	0.0069	0.97419	1343	67	1007	38	1930	86
Co17-41 mon2 - 1	1.217	0.032	0.1307	0.0015	0.7525	807.8	14	791.9	8.4	851	34
Co17-41 mon2 - 2	1.46	0.054	0.1437	0.0032	0.93304	912	21	865	18	1027	38
Co17-41 mon3 - 2	5.35	0.21	0.2488	0.0052	0.934	1874	35	1432	27	2415	35

Co17-41 mon4 - 1	1.212	0.047	0.1388	0.0056	0.90633	804	20	837	31	776	45
Co17-41 mon5 - 1	6.76	0.18	0.2815	0.0052	0.7967	2081	23	1599	26	2618	26
Co17-41 mon5 - 2	16.2	0.64	0.536	0.015	0.85604	2894	41	2764	64	2986	31
Co17-41 mon5 - 3	3.28	0.17	0.1917	0.0053	0.97313	1475	40	1130	28	2028	48
Co17-41 mon5 - 4	2.43	0.12	0.163	0.003	0.93759	1245	38	973	17	1753	58
Co17-41 mon8 - 1	1.128	0.03	0.1239	0.0019	0.71922	766.4	14	753	11	792	31
Co17-41 mon11 - 1	1.1558	0.027	0.12724	0.001	0.36139	779.8	13	772.7	6	799	31
Co17-41 mon12 - 1	20.02	0.45	0.6062	0.0055	0.77643	3091.9	22	3054	22	3102.8	19
Co17-41 mon7 - 1	1.224	0.037	0.136	0.0024	0.85437	811	17	822	13	775	32
Co17-41 mon10 - 1	1.203	0.033	0.1308	0.0013	0.3441	801.4	15	792.4	7.1	814	39
Co17-40 mon1 - 1	1.197	0.034	0.1329	0.0021	0.88542	799	16	804	12	782	39
Co17-40 mon2 - 1	1.166	0.031	0.1311	0.0022	0.35589	784.4	14	794	13	793	45
Co17-40 mon3 - 1	1.184	0.032	0.1304	0.0013	0.57407	792.4	15	789.9	7.3	787	33
Co17-40 mon3 - 2	1.152	0.029	0.1266	0.0012	0.40857	777.9	13	768.5	7	798	33
Co17-40 mon4 - 1	1.152	0.028	0.12696	0.0012	0.36327	778	13	770.5	6.6	796	32
Co17-40 mon5 - 1	1.165	0.028	0.12869	0.0011	0.45326	784.1	13	780.4	6.2	793	31
Co17-40 mon6 - 1	1.165	0.029	0.1288	0.0012	0.3882	783.7	14	782	7.1	784	32
Co17-40 mon7 - 1	1.389	0.039	0.1309	0.0016	0.35761	884	17	793.2	9.2	1114	41
Co17-40 mon8 - 1	1.182	0.031	0.1301	0.002	0.31151	791.9	14	788	11	809	47
Co17-40 mon11 - 1	1.193	0.029	0.12981	0.0012	0.33902	797.1	13	786.7	6.7	818	33
Co17-40 mon12 - 1	1.147	0.027	0.12619	0.0011	0.088916	775.7	13	766.1	6.4	779	34
Co17-40 mon13 - 1	1.161	0.032	0.1289	0.0019	0.33961	782	15	781.3	11	800	43
Co17-40 mon14 - 1	1.16	0.028	0.12914	0.0012	0.43177	781.6	13	782.9	6.8	768	32
Co17-40 mon15 - 1	1.009	0.028	0.116	0.002	0.62374	708	14	708	12	706	43
Co17-38 monmount1 - 1	20.34	0.53	0.6084	0.011	0.66836	3108.5	25	3063	45	3136.2	26
Co17-38 monmount1 - 2	19.73	0.53	0.6011	0.011	0.8095	3078.5	26	3034	45	3106.9	26
Co17-38 monmount1 - 3	19.79	0.53	0.5974	0.011	0.80904	3080.6	26	3019	45	3125.4	25
Co17-38 monmount1 - 4	19.1	0.5	0.5896	0.011	0.73158	3046.8	25	2987	44	3087.1	25
Co17-38 monmount1 - 5	18.98	0.5	0.5925	0.011	0.67185	3040.2	25	2999	44	3070.6	26
Co17-38 monmount1 - 6	19.18	0.51	0.5885	0.011	0.78462	3050.3	26	2983	44	3092.2	26
Co17-38 monmount2 - 1	20.01	0.52	0.6069	0.011	0.74193	3091.6	25	3057	45	3114.4	26
Co17-38 monmount2 - 2	20.19	0.52	0.6114	0.011	0.79585	3100	25	3075	45	3118.3	25
Co17-38 monmount3 - 1	19.8	0.51	0.6091	0.011	0.74854	3082.2	26	3066	45	3094.7	26
Co17-38 monmount3 - 2	20.25	0.53	0.6134	0.011	0.75526	3103	25	3083	45	3112.6	25
Co17-38 monmount3 - 3	19.11	0.52	0.595	0.012	0.89473	3047	27	3009	48	3067.9	25
Co17-38 monmount3 - 4	19.72	0.51	0.6054	0.011	0.77712	3077.5	25	3054	45	3099	25
Co17-38 monmount3 - 5	19.75	0.51	0.6001	0.011	0.80549	3079.1	25	3030	45	3107.8	25

Co17-38 monmount4 - 1	9.279	0.25	0.3817	0.0074	0.53446	2365.3	24	2084	35	2623	30
Co17-38 monmount4 - 2	11.58	0.39	0.4566	0.0099	0.78147	2570	30	2424	44	2682	32
Co17-38 monmount4 - 3	9.43	0.3	0.3951	0.0087	0.70982	2383	29	2146	40	2573	33
Co17-38 monmount5 - 1	20.25	4.4	0.6125	0.14	0.79098	3103.2	110	3080	350	3125.4	28
Co17-38 monmount5 - 2	20.3	0.53	0.611	0.011	0.85535	3108	26	3074	45	3124	25
Co17-38 monmount5 - 3	19.98	0.52	0.6071	0.011	0.83062	3091	24	3058	45	3112.4	26
Co17-38 monmount5 - 4	20.06	0.52	0.6093	0.011	0.82464	3093.8	25	3069	45	3109.9	25
Co17-38 monmount6 - 1	18.93	0.49	0.5897	0.011	0.81824	3037.9	25	2988	44	3070.7	26
Co17-38 monmount6 - 2	17.06	0.67	0.5485	0.022	0.79594	2937.4	32	2818	71	3012.6	27
Co17-38 monmount6 - 3	19.16	0.57	0.5936	0.012	0.87529	3049	31	3003	49	3072.1	31
Co17-38 monmount7 - 1	10.24	18	0.4572	0.73	0.76922	2458	300	2427	1.20E+03	2482	31
Co17-38 monmount8 - 1	19.73	0.52	0.5978	0.011	0.70335	3077.9	26	3021	45	3102.8	26
Co17-38 monmount8 - 2	18.35	0.48	0.5672	0.011	0.82507	3007.6	25	2896	44	3079.4	26
Co17-38 monmount8 - 3	18.69	0.51	0.58	0.011	0.86562	3026.4	26	2948	45	3076.3	26
Co17-38 monmount9 - 1	19.68	0.51	0.5984	0.011	0.76407	3075.6	25	3023	44	3103	25
Co17-38 monmount9 - 2	19.39	0.51	0.5917	0.011	0.77821	3061	25	2996	45	3088.3	25
Co17-38 monmount9 - 3	19.36	0.5	0.5933	0.011	0.63958	3059.6	25	3002	45	3088.8	25
Co17-38 monmount9 - 4	19.34	0.51	0.598	0.011	0.7535	3059.5	26	3021	45	3083.6	26
Co17-38 monmount9 - 5	19.21	0.5	0.5894	0.011	0.7826	3051.9	25	2987	44	3083.3	26
Co17-38 monmount9 - 6	19.1	0.5	0.5873	0.011	0.82785	3047.1	24	2978	44	3080.3	25
Co17-38 monmount9 - 7	19.97	0.53	0.6064	0.012	0.81085	3089.4	26	3058	46	3105.3	25
Co17-38 monmount9 - 8	19.82	0.52	0.6004	0.011	0.75527	3082.2	25	3031	45	3102.4	26
Co17-38 monmount9 - 9	19.315	0.49	0.5897	0.011	0.73441	3057.5	25	2988	44	3091.8	25
Co17-38 monmount9 - 10	20.01	0.53	0.6035	0.011	0.75789	3094.2	25	3043	45	3120.4	26
Co17-38 monmount10 - 1	19.62	0.51	0.5958	0.011	0.81197	3072.7	25	3012	45	3105.2	26
Co17-38 monmount10 - 2	18.77	0.5	0.5736	0.011	0.81873	3029.4	26	2922	44	3089.1	27
Co17-38 monmount11 - 1	19.39	0.52	0.5904	0.011	0.81718	3060.6	26	2991	45	3093.8	25
Co17-38 monmount11 - 2	19.69	0.52	0.5984	0.011	0.74345	3077.8	25	3023	44	3094.7	26
Co17-38 monmount12 - 1	18.24	0.48	0.5688	0.011	0.77091	3004	26	2905	42	3060.8	26
Co17-38 monmount12 - 2	19.37	0.5	0.5886	0.011	0.75169	3059.8	25	2986	43	3098.8	26
Co17-38 monmount12 - 3	19.05	0.53	0.5915	0.011	0.87629	3044	27	2995	46	3072.8	26

Co17-38 monmount13 - 1	20.28	0.53	0.6041	0.011	0.85006	3104.3	25	3046	45	3129.1	26
Co17-38 monmount14 - 2	21.53	0.56	0.6344	0.012	0.65832	3163.3	26	3167	46	3146.1	26
Co17-38 monmount14 - 3	21.28	0.56	0.632	0.012	0.8148	3151.1	25	3157	47	3135.4	25
Co17-38 monmount15 - 1	20.61	0.53	0.6185	0.011	0.70789	3120.1	25	3104	45	3122	26
Co17-38 monmount16 - 1	21.56	0.56	0.6351	0.012	0.8162	3163.7	25	3169	47	3148.4	25
Co17-38 monmount17 - 1	18.56	0.5	0.5747	0.011	0.83121	3018.6	26	2927	44	3079.7	26
Co17-38 monmount17 - 2	14.81	0.47	0.4938	0.011	0.85481	2802	29	2587	46	2965	27
Co17-38 monmount17 - 3	15.02	0.41	0.495	0.0099	0.84614	2817.3	25	2591	43	2975.6	26
Co17-38 monmount18 - 1	20.63	0.53	0.6245	0.011	0.68921	3121	25	3127	45	3112.1	26
Co17-38 monmount18 - 2	20.84	0.54	0.6198	0.011	0.76949	3131.6	24	3109	44	3139.3	25
Co17-38 monmount18 - 3	20.12	0.53	0.6138	0.011	0.81188	3098.8	25	3085	45	3098.8	25
Co17-38 monmount19 - 1	19.84	0.51	0.6103	0.011	0.61784	3083.5	25	3071	45	3090.3	26
Co17-38 monmount20 - 1	21.16	0.55	0.6311	0.011	0.78786	3145.8	25	3154	45	3145.3	25
Co17-38 monmount21 - 1	19.07	0.5	0.587	0.011	0.75255	3045.1	25	2977	43	3099.8	25
Co17-38 monmount21 - 2	18.8	0.49	0.5791	0.011	0.85276	3031.3	25	2945	45	3089.3	25
Co17-38 monmount22 - 1	16.93	0.45	0.5538	0.01	0.76666	2930.4	26	2840	43	2996.8	26
Co17-38 monmount22 - 2	15.76	0.42	0.5257	0.01	0.8445	2861.9	26	2723	43	2960.6	26
Co17-38 monmount22 - 3	17.32	0.46	0.5558	0.011	0.85737	2952.4	25	2849	44	3032.2	26
Co17-38 monmount23 - 1	19.24	0.5	0.5879	0.011	0.70913	3053.8	25	2981	44	3101.7	26
Co17-38 monmount23 - 2	18.91	0.49	0.579	0.011	0.74817	3036.8	25	2944	44	3110.3	26
Co17-38 monmount24 - 1	20.84	0.54	0.6184	0.011	0.76758	3132.6	24	3103	45	3150.5	26
Co17-38 monmount25 - 1	18.73	0.52	0.5969	0.012	0.81626	3027	27	3017	49	3045.1	28
Co17-38 monmount25 - 2	20.5	0.53	0.6157	0.012	0.78805	3115.6	25	3092	47	3134.1	25
Co17-38 monmount26 - 1	16.11	0.42	0.5428	0.01	0.71593	2883.1	25	2795	42	2951.4	26
Co17-38 monmount27 - 1	20.19	0.52	0.6117	0.011	0.7215	3100.8	25	3076	46	3119.8	25
Co17-38 monmount27 - 2	20.4	0.54	0.609	0.011	0.76724	3111.2	26	3066	45	3144.1	26
Co17-38 monmount27 - 3	19.97	0.52	0.6061	0.011	0.81196	3089.6	25	3054	45	3119.7	25
Co17-38 monmount28 - 1	21.28	0.55	0.6329	0.012	0.77906	3151.7	26	3161	47	3147.6	26
Co17-38 monmount30 - 1	20.18	0.53	0.6117	0.012	0.84017	3099.7	26	3076	47	3117.2	25
Co17-38 monmount31 - 1	19.72	0.52	0.6067	0.011	0.70488	3078.4	26	3056	46	3097.4	26
Co17-38 monmount31 - 2	15.99	0.43	0.5238	0.0099	0.73991	2875.3	26	2715	42	3000.9	26

Co17-38 monmount31 - 3	14.84	0.47	0.4998	0.011	0.80508	2804	28	2613	47	2946	26
Co17-38 monmount32 - 1	19.33	0.52	0.5931	0.011	0.8315	3057.7	26	3001	45	3099.4	26
Co17-38 monmount32 - 2	18.99	0.5	0.5786	0.011	0.82826	3040.8	25	2945	44	3111.8	26
Co17-38 monmount32 - 3	19.12	0.53	0.6014	0.011	0.79327	3047	26	3035	45	3061.7	26
Co17-38 monmount33 - 1	20.73	0.54	0.6173	0.011	0.73524	3126.6	26	3101	46	3150.2	26
Co17-38 monmount33 - 2	20.21	0.53	0.6105	0.011	0.77546	3100.9	25	3072	45	3118	25
Co17-38 monmount33 - 3	19.07	0.5	0.5902	0.011	0.70319	3045.1	25	2992	46	3083.9	26
Co17-38 monmount34 - 1	19.61	5.2	0.617	0.18	0.89045	3071	130	3095	490	3063	37
Co17-38 monmount35 - 1	18.02	0.53	0.5687	0.013	0.92971	2989	28	2901	51	3052.3	26
Co17-38 monmount36 - 1	18.51	0.48	0.5875	0.011	0.73589	3016.5	25	2981	46	3046.9	26
Co17-38 monmount36 - 2	18.52	0.48	0.584	0.011	0.7123	3016.7	25	2964	44	3059.1	26
Co17-38 monmount37 - 1	21.59	0.57	0.6443	0.012	0.86301	3165	26	3205	48	3139.4	25
Co17-38 monmount37 - 2	19.55	0.55	0.6015	0.012	0.86344	3071	26	3038	48	3090.6	26
Co17-38 monmount38 - 1	21.7	0.57	0.6376	0.012	0.68323	3169.8	25	3179	46	3156.7	26
Co17-38 monmount39 - 1	21.55	0.56	0.644	0.012	0.67312	3163.3	25	3204	46	3134.8	26
Co17-38 monmount39 - 2	21.1	0.54	0.6321	0.012	0.76349	3142.8	25	3158	46	3137.3	26
Co17-38 monmount40 - 1	19.26	0.51	0.6047	0.011	0.85203	3055.5	26	3048	46	3057.5	26
Co17-38 monmount41 - 1	21.61	0.56	0.6408	0.012	0.66384	3167.8	25	3192	48	3151.6	26
Co17-38 monmount41 - 2	20.52	0.55	0.6186	0.012	0.72952	3115.6	26	3104	47	3124.9	26
Co17-41 monmount1 - 1	1.223	0.033	0.132	0.0031	0.72247	810.7	15	799	17	845	34
Co17-41 monmount2 - 1	7.914	0.2	0.3221	0.0071	0.77318	2220.6	22	1800	34	2636	21
Co17-41 monmount2 - 2	1.54	0.055	0.1402	0.0031	0.62553	947	21	845.8	17	1173	45
Co17-41 monmount3 - 1	1.189	0.032	0.1304	0.0028	0.36427	795.1	15	790.3	16	816	36
Co17-41 monmount3 - 2	1.276	0.034	0.1327	0.0028	0.3481	835.6	15	803.4	16	932	39
Co17-41 monmount3 - 3	1.273	0.036	0.1347	0.0028	0.19762	834.4	16	814.7	16	886	41
Co17-41 monmount4 - 1	1.293	0.039	0.1353	0.003	0.48366	842	17	817.7	17	907	41
Co17-41 monmount5 - 1	19.73	0.49	0.6055	0.013	0.72948	3080	23	3051	51	3091	19
Co17-41 monmount7 - 1	21.31	0.49	0.6322	0.013	0.75057	3152.6	22	3158	51	3147.3	18
Co17-41 monmount7 - 2	21.54	0.52	0.6449	0.013	0.7328	3162.6	23	3208	52	3138.7	18
Co17-41 monmount8 - 1	10.11	0.52	0.406	0.015	0.97153	2428	48	2192	67	2645	33
Co17-41 monmount8 - 2	16.95	0.42	0.5487	0.011	0.84591	2933	24	2822	48	3013.2	18

Co17-41 monmount9 - 1	14.02	0.36	0.5124	0.011	0.86986	2750	25	2666	46	2816	20
Co17-41 monmount10 - 1	20.94	0.5	0.6235	0.013	0.82001	3135.2	23	3123	51	3144.2	17
Co17-41 monmount12 - 1	20.69	0.52	0.6191	0.013	0.87681	3123	24	3106	53	3134.6	18
Co17-41 monmount13 - 1	14.52	0.73	0.469	0.02	0.97923	2774	47	2474	88	3014	20
Co17-41 monmount14 - 1	20.66	0.48	0.6182	0.013	0.76707	3122.6	23	3102	52	3141.8	17
Co17-41 monmount14 - 2	20.58	0.48	0.6127	0.012	0.79677	3118.8	22	3080	50	3143.4	17
Co17-41 monmount16 - 1	1.193	0.029	0.1303	0.0027	0.32712	798.1	13	790.2	16	804	33
Co17-41 monmount17 - 1	6.83	0.37	0.2785	0.011	0.95974	2082	48	1582	53	2630	35
Co17-41 monmount18 - 1	4.349	0.11	0.2146	0.0047	0.70727	1704	22	1253	25	2323	24
Co17-41 monmount19 - 1	1.208	0.031	0.1298	0.0028	0.27232	804	14	786.5	16	837	33
Co17-41 monmount19 - 2	1.267	0.036	0.1333	0.0028	0.40367	830	16	806.4	16	907	38
Co17-41 monmount21 - 1	12.72	0.43	0.4241	0.012	0.96096	2661	34	2278	54	2950	24
Co17-41 monmount22 - 1	20.69	0.48	0.618	0.012	0.75194	3123.7	22	3102	50	3142.7	17
Co17-41 monmount23 - 1	14.6	0.59	0.473	0.016	0.9654	2788	38	2492	69	3012	21
Co17-41 monmount23 - 2	1.66	0.055	0.1441	0.0034	0.301	993	21	868	19	1293	55
Co17-41 monmount24 - 1	19.99	0.48	0.602	0.012	0.83824	3090.1	23	3037	50	3119.9	17
Co17-41 monmount24 - 2	18.46	0.48	0.5634	0.013	0.88037	3013	25	2880	54	3109.7	18
Co17-41 monmount25 - 1	8.494	0.21	0.3361	0.0071	0.70639	2284	23	1867	34	2685	21
Co17-41 monmount25 - 2	6.05	0.18	0.2724	0.0064	0.88618	1980	26	1552	33	2453	23
Co17-41 monmount25 - 3	1.342	0.043	0.1355	0.003	0.69577	863	18	819.3	17	986	42
Co17-41 monmount26 - 1	1.259	0.034	0.1321	0.0028	0.38006	831.4	15	799.8	16	909	35
Co17-41 monmount26 - 2	1.196	0.03	0.1305	0.0026	0.55689	798.6	14	790.7	15	820	29
Co17-41 monmount26 - 3	1.177	0.03	0.12865	0.0026	0.48305	789.5	14	780.1	15	816	30
Co17-41 monmount28 - 1	17.16	0.61	0.541	0.016	0.94767	2943	34	2784	66	3058	21
Co17-41 monmount29 - 1	18.31	0.44	0.5715	0.012	0.86245	3007.8	24	2913	50	3067.4	17
Co17-41 monmount29 - 2	1.237	0.034	0.134	0.0031	0.52865	817	15	810.8	17	822	35
Co17-41 monmount30 - 1	12.51	0.32	0.449	0.0098	0.80276	2643	24	2390	44	2837	20
Co17-41 monmount33 - 1	2.86	0.08	0.1713	0.0038	0.67401	1373	20	1019	21	1964	29
Co17-41 monmount34 - 1	21.17	0.49	0.632	0.013	0.74315	3146.1	23	3157	50	3137.3	17
Co17-41 monmount34 - 2	20.08	0.47	0.6047	0.012	0.81319	3095	23	3048	50	3123.4	17
Co17-41 monmount35 - 1	20.87	0.52	0.6302	0.015	0.92261	3132	24	3153	57	3125.6	18

Co17-41 monmount35 - 2	21.52	0.56	0.6431	0.015	0.93633	3161	25	3204	62	3130.4	17
Co17-41 monmount36 - 1	1.181	0.033	0.1289	0.0029	0.47478	791.5	15	781.6	16	806	36
Co17-41 monmount37 - 1	18.57	0.43	0.5774	0.012	0.80705	3019.6	22	2938	48	3081.6	17
Co17-41 monmount38 - 1	1.434	0.065	0.1358	0.0036	0.619	901	27	821	20	1113	69
Co17-41 monmount38 - 2	1.264	0.045	0.1306	0.0031	0.48915	829	20	791	18	924	54
Co17-41 monmount39 - 1	12.33	0.31	0.4488	0.0096	0.78847	2629	24	2389	43	2810	20
Co17-41 monmount39 - 2	10.656	0.25	0.4129	0.0084	0.73687	2494.1	22	2228	38	2719.7	18
Co17-41 monmount40 - 1	14.11	0.34	0.4916	0.01	0.81751	2757.5	23	2577	45	2894	18
Co17-41 monmount41 - 1	2.419	0.083	0.1685	0.0041	0.79434	1246	25	1004	23	1686	33
Co17-41 monmount41 - 2	8.81	0.28	0.3456	0.0092	0.90826	2319	28	1913	44	2681	23
Co17-41 monmount42 - 1	13.9	0.34	0.5008	0.011	0.83267	2745.9	23	2617	46	2847.9	18
Co17-41 monmount42 - 2	13.64	0.33	0.4854	0.01	0.84278	2724.2	23	2553	44	2858	18
Co17-41 monmount43 - 1	17.51	0.42	0.5594	0.012	0.87425	2962.2	23	2864	49	3028.2	17
Co17-41 monmount43 - 2	13.79	0.37	0.4795	0.011	0.94005	2734	26	2524	50	2891.1	18
Co17-41 monmount44 - 1	6.8	0.2	0.326	0.008	0.86538	2084	26	1822	38	2360	24
Co17-41 monmount44 - 2	7.61	0.25	0.3423	0.0083	0.83295	2185	30	1898	40	2474	30
Co17-41 monmount45 - 1	1.654	0.075	0.1433	0.0035	0.85627	992	29	863	20	1267	59
Co17-41 monmount46 - 1	1.371	0.069	0.134	0.0037	0.57478	874	29	811	21	1059	82
Co17-41 monmount47 - 1	1.25	0.039	0.1317	0.0031	0.45737	823	18	798	18	882	55
Co17-41 monmount47 - 2	1.259	0.041	0.1327	0.0032	0.56913	829	18	803	18	907	48
Co17-41 monmount49 - 1	19.32	0.45	0.5966	0.012	0.80052	3057.5	23	3016	48	3084	17
Co17-41 monmount50 - 1	1.432	0.057	0.1394	0.0033	0.7927	903	24	841	19	1064	53
Co17-41 monmount51 - 1	20.9	0.49	0.622	0.013	0.73784	3133.4	23	3120	52	3138.4	17
Co17-41 monmount52 - 1	19.2	0.54	0.5887	0.014	0.88382	3052	27	2983	56	3104	20
Co17-41 monmount53 - 1	18.84	0.48	0.5791	0.013	0.87415	3034	24	2944	55	3092	18
Co17-41 monmount54 - 1	15.6	0.45	0.529	0.013	0.94057	2855	28	2741	55	2944	19
Co17-41 monmount55 - 1	19.99	0.49	0.6108	0.013	0.68609	3090.1	24	3073	54	3101	21
Co17-41 monmount56 - 1	1.234	0.038	0.1342	0.0029	0.47578	816	17	812	17	834	47
Co17-41 monmount56 - 2	1.344	0.055	0.1301	0.0032	0.54542	863	24	788	18	1026	67
Co17-41 monmount57 - 1	1.225	0.033	0.1311	0.0029	0.32514	811.3	15	794.1	16	872	36
Co17-41 monmount57 - 2	1.297	0.039	0.1314	0.0029	0.61571	844	17	795.7	16	978	37

Co17-41 monmount57 - 3	1.239	0.038	0.1309	0.0028	0.42346	818	17	793.1	16	894	42
Co17-41 monmount58 - 1	1.195	0.031	0.1296	0.0028	0.36678	797.7	14	785.7	16	836	36
Co17-41 monmount58 - 2	4.27	0.16	0.2126	0.0057	0.83775	1686	31	1243	30	2316	35
Co17-41 monmount59 - 1	2.163	0.094	0.1547	0.0047	0.92173	1167	30	927	26	1646	40
Co17-41 monmount59 - 2	1.177	0.031	0.1296	0.0028	0.47269	789.4	15	785.5	16	818	38
Co17-41 monmount60 - 1	16.87	0.85	0.52	0.02	0.96479	2921	49	2699	83	3084	30
Co17-41 monmount61 - 2	7.96	0.26	0.3174	0.008	0.89172	2227	30	1777	39	2661	23
Co17-41 monmount62 - 1	2.209	0.09	0.1598	0.0042	0.81635	1182	28	956	23	1625	43
Co17-41 monmount63 - 1	3.206	0.1	0.1871	0.0042	0.56815	1462	27	1106	23	2029	40

Session 2 - Samples	**$^{207}Pb/^{235}U$**	**2σ**	**$^{206}Pb/^{238}U$**	**2σ**	**Rho**	**$^{207}Pb/^{235}U$ Age**	**2σ**	**$^{206}Pb/^{238}U$ Age**	**2σ**	**$^{207}Pb/^{206}U$ Age**	**2σ**
Co17-38mon1 - 1	18.52	0.19	0.5741	0.0099	0.74812	3018	9.3	2924	41	3068	20
Co17-38mon1 - 2	18.1	0.23	0.574	0.011	0.85105	2996	12	2923	43	3049.9	20
Co17-38mon3 - 1	20.76	0.26	0.6228	0.011	0.65163	3129	12	3120	44	3137	23
Co17-38mon3 - 2	20.83	0.28	0.6255	0.012	0.78041	3129	13	3131	46	3127	21
Co17-38mon4 - 1	9.31	0.12	0.4393	0.0085	0.76891	2369	12	2347	38	2385	23
Co17-38mon4 - 2	14.57	0.29	0.5323	0.0099	0.86447	2789	20	2750	41	2816	25
Co17-38mon4 - 3	17.6	0.21	0.5722	0.011	0.8887	2969	12	2916	43	2998.6	19
Co17-38mon5 - 1	19.49	0.24	0.604	0.011	0.83198	3065	12	3045	45	3087	20
Co17-38mon5 - 2	21.15	0.3	0.6395	0.013	0.81905	3146	14	3185	50	3118	22
Co17-38mon5 - 3	20.67	0.39	0.6201	0.013	0.82796	3122	18	3109	52	3135	23
Co17-38mon6 - 1	20.58	0.19	0.6203	0.01	0.72998	3118.6	9.2	3110	40	3133	20
Co17-38mon6 - 2	20.19	0.22	0.6074	0.011	0.84816	3100.9	11	3059	43	3123.7	18
Co17-38mon7 - 1	1.95	0.23	0.1519	0.0048	0.76923	1087	76	912	27	1440	180
Co17-38mon9 - 1	20.36	0.24	0.6168	0.012	0.80859	3109	12	3096	47	3115	20
Co17-38mon9 - 2	20.2	0.25	0.6141	0.011	0.7726	3100	12	3085	45	3104	21
Co17-38mon9 - 3	19.72	0.22	0.5981	0.011	0.79563	3077	11	3021	42	3108	20
Co17-38mon10 - 1	11.06	0.4	0.434	0.012	0.86079	2518	35	2322	56	2666	42
Co17-38mon10 - 2	7.02	0.41	0.327	0.016	0.94997	2095	53	1815	77	2378	39
Co17-38mon11 - 1	10.07	0.3	0.442	0.014	0.95482	2434	30	2356	65	2465	33
Co17-38mon11 - 3	18.69	0.28	0.6212	0.012	0.60152	3024	15	3113	48	2959	27

Co17-38mon13 - 1	20.71	0.21	0.6244	0.011	0.81564	3124.4	9.8	3127	42	3122.6	19
Co17-38mon13 - 2	20.13	0.23	0.6033	0.011	0.8343	3096.7	11	3042	43	3136.6	19
Co17-38mon13 - 3	20.54	0.24	0.6131	0.01	0.79965	3118	12	3085	40	3135.5	19
Co17-38mon14 - 1	20.35	0.23	0.6121	0.011	0.88394	3109	11	3077	44	3124.7	19
Co17-38mon14 - 2	20.26	0.21	0.6139	0.011	0.83175	3106.8	10	3088	43	3116.4	19
Co17-38mon15 - 1	20	0.2	0.6053	0.01	0.73767	3090.6	9.9	3051	42	3112	21
Co17-38mon15 - 2	20.08	0.23	0.6055	0.01	0.80211	3097	11	3051	42	3128	20
Co17-38mon15 - 3	20.02	0.21	0.6061	0.0099	0.76408	3091.7	10	3054	40	3113.7	20
Co17-38mon16 - 1	21.41	0.27	0.6337	0.011	0.7915	3156	12	3163	44	3144	21
Co17-38mon16 - 2	20.43	0.22	0.6119	0.011	0.7638	3113.2	11	3077	43	3129.3	20
Co17-38mon16 - 3	20.29	0.22	0.6078	0.01	0.7935	3105.9	11	3063	42	3133.8	20
Co17-38mon16 - 4	20.92	0.22	0.6198	0.01	0.64593	3135.2	10	3108	40	3142	21
Co17-38mon18 - 1	19.95	0.18	0.6064	0.0099	0.68909	3088.3	8.8	3055	40	3107.6	20
Co17-38mon18 - 2	19.16	0.19	0.6007	0.01	0.4215	3050.7	9.5	3032	41	3061	21
Co17-38mon18 - 3	19.43	0.2	0.596	0.01	0.74478	3062.5	10	3013	41	3095	20
Co17-37mon1 - 1	20.4	0.23	0.6131	0.01	0.68632	3109.7	11	3082	42	3114	21
Co17-37mon1 - 3	20.85	0.23	0.63	0.011	0.7963	3134.2	10	3149	42	3127.7	19
Co17-37mon4 - 1	16.55	0.19	0.5465	0.0098	0.80541	2908	11	2810	41	2977	21
Co17-37mon4 - 2	15.4	0.16	0.5202	0.0087	0.71146	2840.7	9.5	2699	37	2948	20
Co17-37mon4 - 3	13.91	0.2	0.4818	0.0089	0.78938	2744	14	2534	39	2902	21
Co17-37mon6 - 1	19	0.21	0.593	0.01	0.76696	3041.3	10	3001	41	3072	21
Co17-37mon6 - 2	18.86	0.21	0.5854	0.01	0.74721	3033.8	11	2970	41	3085.3	20
Co17-37mon6 - 3	18.03	0.24	0.5669	0.01	0.67802	2990	13	2894	43	3056	23
Co17-37mon6 - 4	22.86	0.6	0.677	0.022	0.95198	3218	26	3329	85	3145	22

Session 3 - Samples	**$^{207}Pb/^{235}U$**	**2σ**	**$^{206}Pb/^{238}U$**	**2σ**	**Rho**	**$^{207}Pb/^{235}U$ Age**	**2σ**	**$^{206}Pb/^{238}U$ Age**	**2σ**	**$^{207}Pb/^{206}U$ Age**	**2σ**
Co17-37mon1r - 1	20.43	0.58	0.6188	0.015	0.73354	3111.6	28	3105	61	3120.7	22
Co17-37mon1r - 2	19.79	0.6	0.6267	0.017	0.88165	3080	29	3135	66	3045	23
Co17-37mon1r - 3	21.06	0.65	0.6389	0.018	0.97861	3140	29	3183	69	3111.7	22
Co17-37mon1c - 1	21.29	0.63	0.6387	0.016	0.88955	3151	29	3183	64	3124	22
Co17-37mon7 - 1	18.89	0.78	0.603	0.023	0.92738	3034	71	3038	120	3032	29

Co17-37mon7 - 2	18.22	1	0.593	0.032	0.97718	2998	59	2996	120	3008	24
Co17-37mon2c - 1	16.96	0.87	0.5501	0.022	0.93143	2932	61	2825	97	3002	49
Co17-37mon2r - 1	18.05	1.1	0.5805	0.038	0.81733	2992	54	2950	150	3012	48
Co17-37mon2r - 2	18.47	2.2	0.598	0.079	0.95848	3012	150	3020	330	3014	96
Co17-37mon3c - 1	25.4	1.9	0.758	0.054	0.97247	3310	97	3620	210	3137	30
Co17-37mon3r - 1	12.99	0.75	0.516	0.029	0.88325	2673	70	2676	140	2691	55
Co17-37mon5c - 1	15.86	0.58	0.54	0.019	0.96766	2864	35	2774	98	2910	35
Co17-37mon6r - 1	20.67	0.6	0.6227	0.016	0.87881	3122.3	28	3120	63	3122.7	21
Co17-37mon6r - 2	18.62	0.57	0.5951	0.016	0.87594	3025	29	3009	65	3028.6	23
Co17-37mon6r - 3	19.44	0.59	0.5969	0.016	0.9205	3063	29	3016	62	3088.4	22
Co17-37mon4 r - 1	9.64	0.32	0.3813	0.011	0.88279	2399	30	2081	50	2677	25
Co17-37mon4 r - 2	14.55	0.59	0.539	0.019	0.88335	2795	43	2788	83	2774	33
Co17-37mon4 r - 3	15.93	0.47	0.5373	0.014	0.77829	2872	28	2774	59	2954	23
Co17-37mon4c - 1	15.24	0.48	0.5175	0.014	0.90781	2829	30	2691	60	2931	23
Co17-37mon4c - 2	17.02	0.5	0.5614	0.014	0.89094	2935.1	28	2872	59	2975	23
Co17-37mon4c - 3	-	-	-	-	-	-	-	-	-	-	-
Co17-37mon8c - 1	17.27	0.72	0.5612	0.021	0.82054	2948	42	2871	83	3000	28

APPENDIX D: EXTENDED TRACE ELEMENT LA–ICP–MS METHODS

LA–ICP–MS analyses took place at the University of Adelaide using a RESOlution LR 193 nm Excimer laser system coupled with an Agilent 7700s ICP–MS for the purpose of acquiring trace element data with U–Pb isotopic data. Ablation of zircon, monazite and garnet was performed in a He-ablation atmosphere with a frequency of 5 Hz. Trace element data were acquired in large zircons where a 29 μm could be used. For monazite and garnet, trace element data were acquired for all analyses. A 13 μm spot was used for in-situ analyses, while 19 μm spots were used for grain-mounted monazites. A 51 μm spot was used for all garnet analyses. These took place in-situ, along transect on garnet porphyroblasts from sample Co17-37 and Co17-38 (Fig. 5). Analyses were selectively placed to avoid fractures and inclusions in garnet. Spacing between analyses decreased near fractures and grain boundaries, to acquire high resolution in areas where zonation might be expected. The total acquisition time for each zircon, monazite and garnet analysis was 80 s. This included 30 s of background measurement, 10 s of the laser firing with the shutter closed to allow for beam stabilisation, and 40 s of sample ablation.
Elemental fractionation and mass bias for all trace element analyses were corrected using the external standard NIST SRM610 (P = 413 ± 46 ppm, La = 440 ± 10 ppm, Lu = 439 ± 8 ppm) (Jochum et al., 2011).

Trace element data were reduced using Iolite version 3.6 data processing software (Paton et al., 2011), with similar methods to U–Pb data (see “data processing and reduction” in Appendix A). The signals selected for U–Pb in zircon and monazite data were also used for trace elements, to retain consistency between chemistry and age acquired. In order to process trace element data for minerals in iolite, an in internal element standard must be selected. This standard is an element that is generally consistent within the mineral being processed. Zircon trace element data were processed to internal standard element value of Zr = 43.14%. Monazite trace element data were processed to internal standard element value of Ce = 20%. Garnet trace element chemistry were processed using 22% Al, based on EPMA data (Appendix I). Garnet signals were bracketed accordingly, avoiding signals reflecting inclusions or fractures and culling data that did not reflect general garnet chemistry

APPENDIX E: ZIRCON TRACE ELEMENT ANALYSES (NOT NORMALISED VALUES)

Session 1 - Standards	La	Ce	Pr	Nd	Sm	Eu	Gd	Tb	Dy	Ho	Er	Tm	Yb	Lu	Hf
NIST - 1.d	449	439	421	422	446	452	435	433	417	440	418	410	435	424	424
NIST - 2.d	447	440	422	425	439	453	435	436	421	441	418	414	438	429	424
NIST - 3.d	446	437	421	420	440	450	435	434	417	441	415	412	436	425	423
NIST - 4.d	450	442	422	423	442	453	436	435	419	440	419	412	436	427	424
NIST - 5.d	447	439	422	423	442	451	436	434	419	440	418	411	436	426	424
NIST - 6.d	449	439	422	423	443	453	434	435	419	441	418	412	437	428	424
NIST - 7.d	461	449	432	430	450	462	448	446	428	452	425	422	447	436	434
NIST - 8.d	456	447	428	431	451	457	444	442	425	448	425	418	443	433	431
NIST - 9.d	455	446	428	429	451	461	440	440	427	444	425	418	443	433	431
NIST - 10.d	456	446	427	423	452	458	440	441	425	450	424	420	441	434	432
NIST - 11.d	456	447	430	431	451	462	445	443	426	452	426	419	445	434	431
NIST - 12.d	459	449	431	431	450	463	450	445	427	449	426	421	448	436	434
NIST - 13.d	457	450	430	433	450	462	443	442	424	447	424	417	442	434	431
NIST - 14.d	459	450	429	432	451	461	442	443	428	448	425	418	446	436	432
NIST - 15.d	457	452	431	432	450	460	442	443	427	448	423	419	445	434	430
NIST - 16.d	457	446	430	429	449	459	445	442	427	447	426	421	444	435	431
NIST - 17.d	458	447	430	432	454	462	443	443	429	451	428	421	445	435	431
NIST - 18.d	457	447	428	430	454	461	444	444	426	447	422	419	445	435	430
NIST - 19.d	453	448	430	428	449	460	443	440	425	446	425	418	444	432	432
NIST - 20.d	459	450	433	428	452	461	447	446	427	452	428	419	447	435	431
NIST - 21.d	458	449	432	435	450	462	445	445	429	449	428	421	449	437	434
NIST - 22.d	457	447	430	435	449	460	441	444	429	452	427	421	445	437	434
NIST - 23.d	456	448	429	430	450	460	446	443	427	449	425	422	444	434	432
NIST - 24.d	457	447	430	432	454	464	444	442	427	449	428	421	444	436	433
NIST - 25.d	446	439	421	420	440	451	437	434	419	438	416	409	435	425	421
NIST - 26.d	450	437	420	419	440	451	436	435	419	440	418	410	436	426	422

NIST - 27.d	447	441	425	420	443	451	437	434	418	440	417	411	437	427	425
NIST - 28.d	449	443	422	427	447	453	435	435	419	441	420	413	437	427	422
NIST - 29.d	448	439	421	424	447	452	436	434	419	440	418	413	435	426	424
NIST - 30.d	448	441	423	426	443	453	436	435	418	442	418	412	436	429	426
NIST - 31.d	447	440	420	422	441	452	434	434	417	442	418	410	436	424	425
NIST - 32.d	449	440	422	423	445	451	439	434	420	439	417	414	437	427	422
NIST - 33.d	448	437	422	424	441	453	434	436	417	439	417	412	436	426	424
NIST - 34.d	448	439	421	419	439	451	434	433	419	441	417	411	437	426	421
NIST - 35.d	448	436	422	424	439	453	435	434	418	440	417	411	435	426	423
NIST - 36.d	448	442	422	424	442	452	434	435	420	441	420	415	438	428	426
NIST - 37.d	449	439	423	421	443	452	438	434	418	440	418	411	436	427	424
NIST - 38.d	447	439	421	423	441	452	435	434	419	442	416	412	436	426	424
NIST - 39.d	448	442	424	427	446	454	439	436	421	442	420	412	437	428	425
NIST - 40.d	449	436	420	421	439	451	431	433	417	438	417	410	436	424	422

Session 2 - Standards	La	Ce	Pr	Nd	Sm	Eu	Gd	Tb	Dy	Ho	Er	Tm	Yb	Lu	Hf
NIST610 - 1.d	459	451	432	433	453	464	444	446	428	451	428	421	448	437	433
NIST610 - 2.d	457	446	427	428	450	458	445	441	426	447	424	417	443	432	431
NIST610 - 3.d	454	448	430	433	454	461	444	443	428	450	426	422	445	439	433
NIST610 - 4.d	457	447	431	429	448	461	442	444	427	448	426	420	445	435	433
NIST610 - 5.d	458	447	431	432	453	461	444	443	427	451	427	420	445	435	432
NIST610 - 6.d	457	447	428	432	448	462	442	444	426	448	425	418	446	434	429
NIST610 - 7.d	458	451	433	429	454	464	443	444	428	448	427	420	445	435	433
NIST610 - 8.d	456	447	428	432	449	459	447	442	427	449	425	420	445	434	433

Session 1 - Samples	La	Ce	Pr	Nd	Sm	Eu	Gd	Tb	Dy	Ho	Er	Tm	Yb	Lu	Hf
Co17-41zc1 - 1.d	179.8	289.7	34.0	110.9	20.0	2.0	35.0	11.8	142	55	246	52	495	100	10601
Co17-41zc3 - 1.d	14.1	39.1	3.2	11.7	6.1	6.1	15.8	5.6	68	27	129	30	288	58	12049
Co17-41zc4 - 1.d	9.5	17.6	1.3	4.5	2.9	0.4	8.5	4.1	63	29	182	54	711	180	18153
Co17-41zc5 - 1.d	0.2	16.1	0.2	3.5	8.5	2.3	60.4	22.6	274	107	464	90	780	147	9520
Co17-41zc6 - 1.d	9.1	22.3	2.0	9.3	2.3	2.8	9.0	3.5	41	15	74	19	219	48	11609

Co17-41zc7 - 1.d	2.6	19.8	1.6	9.0	5.3	3.9	19.5	8.2	100	41	208	50	502	107	12398
Co17-41zc10 - 1.d	7.3	31.2	1.6	6.6	4.5	1.8	23.9	8.1	101	39	179	37	344	66	10941
Co17-41zc11 - 1.d	61.9	137.6	9.8	34.8	7.5	9.7	32.4	10.5	139	56	276	61	609	124	10750
Co17-41zc12 - 1.d	30.5	70.2	3.8	12.2	6.0	1.8	26.2	10.5	138	55	273	62	591	117	10680
Co17-41zc13 - 1.d	4.9	50.3	2.6	14.6	5.7	6.9	21.9	6.9	87	34	162	36	354	74	9142
Co17-41zc14 - 1.d	4.3	28.5	0.8	2.8	1.5	0.7	11.4	3.4	37	14	59	12	116	23	9424
Co17-40zc2 - 1.d	0.0	11.8	0.1	1.4	4.9	1.0	25.0	6.0	52	16	70	14	131	27	11349
Co17-40zc3 - 1.d	-	8.4	0.0	0.3	0.9	0.4	7.9	4.1	57	20	81	17	151	30	11069
Co17-40zc5 - 1.d	0.1	4.9	0.1	2.5	4.8	1.9	13.2	2.0	11	2	5	1	7	1	11140
Co17-40zc6 - 1.d	0.9	40.8	0.5	4.3	4.0	5.5	16.6	5.5	58	22	105	25	282	62	10350
Co17-40zc7 - 1.d	-	4.2	0.1	2.3	2.8	0.3	6.7	1.3	7	1	3	0	3	0	10755
Co17-40zc8 - 1.d	0.2	18.0	0.2	1.2	1.9	1.7	13.0	3.7	42	17	85	23	259	62	11329
Co17-40zc10 - 1.d	0.5	5.4	0.3	3.4	12.6	2.1	29.6	5.2	31	5	12	2	10	1	12473
Co17-40zc11 - 1.d	7.9	30.6	1.6	11.2	13.5	6.3	54.5	17.4	196	73	321	67	600	118	10719
Co17-40zc12 - 1.d	0.8	19.7	0.7	5.6	7.9	4.1	56.3	23.8	299	120	528	105	921	177	9740
Co17-40zc14 - 1.d	1.3	8.7	0.9	5.0	3.8	3.3	9.9	2.8	23	7	31	7	77	19	8013
Co17-40zc14 - 2.d	0.1	3.6	0.1	0.9	2.4	0.5	12.0	2.7	20	6	26	6	65	14	11509
Co17-40zc15 - 1.d	1.3	10.5	0.7	4.2	4.2	1.9	10.7	1.7	13	3	15	4	43	12	11280
Co17-40zc17 - 1.d	1.6	42.7	0.6	4.7	4.2	2.1	23.9	7.4	93	38	183	42	415	88	8863
Co17-21zc2 - 1.d	0.0	1.1	0.0	0.2	1.1	1.0	19.9	11.4	157	56	206	34	231	38	12199
Co17-21zc2 - 2.d	0.0	1.5	0.0	0.0	1.6	1.2	23.3	12.4	178	60	220	35	238	37	12152
Co17-21zc3 - 1.d	0.0	1.2	0.0	0.3	1.4	1.1	22.9	12.7	176	60	220	35	238	40	12079
Co17-21zc3 - 2.d	-	1.0	0.0	0.2	1.3	0.9	16.9	9.6	141	52	210	40	336	60	12089
Co17-21zc4 - 1.d	0.3	2.1	0.2	1.5	2.3	1.0	13.0	6.7	94	35	158	36	373	76	12095
Co17-21zc5 - 1.d	0.0	1.3	0.0	0.2	1.5	1.2	19.3	10.7	166	63	259	50	423	74	12094
Co17-21zc7 - 1.d	1.1	7.0	1.2	7.6	8.3	4.3	30.3	12.0	134	42	157	30	262	50	12159
Co17-21zc8 - 1.d	0.0	1.5	0.0	0.1	0.9	0.8	16.6	9.1	133	47	181	35	291	53	12079
Co17-21zc9 - 1.d	-	1.2	-	0.0	0.8	0.6	11.7	7.4	115	47	223	53	539	113	11999
Co17-21zc9 - 2.d	0.0	1.3	0.1	0.4	1.2	0.7	11.3	7.2	103	37	156	34	344	75	12119
Co17-21zc12 - 1.d	0.0	1.2	0.0	0.0	1.7	1.1	17.0	9.7	151	60	260	52	450	78	12259
Co17-21zc14 - 1.d	0.0	0.3	0.0	0.0	0.0	0.1	3.9	2.6	41	16	63	12	97	17	12349

Co17-38 zircon

Mount-4-zc1 - 1.d	0.48	10.63	0.60	4.80	6.70	5.59	23.64	6.90	78	30	140	30	292	62	9344
Mount-4-zc2 - 1.d	0.15	4.19	0.16	1.79	5.49	2.14	15.81	3.05	19	6	26	6	65	14	11099
Mount-4-zc3 - 1.d	0.32	15.22	0.31	2.74	3.50	2.12	12.79	4.21	50	20	102	23	253	59	11717
Mount-4-zc4 - 1.d	-	3.16	0.06	1.16	2.73	0.10	5.88	0.86	6	1	3	0	3	0	10661
Mount-4-zc5 - 1.d	23.90	103.88	17.07	99.39	63.67	239.69	99.57	17.20	128	35	151	34	379	83	14150
Mount-4-zc6 - 1.d	0.00	3.68	0.10	2.14	3.23	0.56	7.39	1.09	7	1	3	1	3	1	10367
Mount-4-zc6 - 2.d	0.05	4.18	0.06	2.81	9.32	2.11	15.88	2.36	13	3	8	1	9	1	10193
Mount-4-zc7 - 1.d	0.05	2.57	0.05	1.95	10.91	1.00	20.02	2.69	15	2	6	1	7	1	10500
Mount-4-zc7 - 2.d	3.76	18.12	4.61	73.34	455.56	93.01	1656.58	320.96	1967	366	808	86	469	56	10433
Mount-4-zc8 - 1.d	0.98	15.31	0.75	5.52	9.97	6.33	21.05	5.87	57	20	100	27	343	88	11624
Mount-4-zc9 - 1.d	1.16	12.61	0.83	4.75	6.89	10.16	19.50	5.38	56	21	99	24	259	58	11006
Mount-4-zc10 - 1.d	0.06	2.61	0.09	2.02	4.57	0.53	14.84	1.93	10	2	4	1	5	1	11465
Mount-4-zc11 - 1.d	0.15	4.04	0.23	3.33	5.25	2.93	11.75	1.78	11	2	7	1	11	2	11021
Mount-4-zc11 - 2.d	0.00	3.50	0.04	1.76	3.97	0.36	6.73	1.24	10	2	4	1	7	1	10147
Mount-4-zc12 - 1.d	0.95	14.79	0.69	4.12	3.92	6.97	13.53	4.12	50	21	109	26	269	60	10210
Mount-4-zc13 - 1.d	0.00	2.76	0.05	1.69	3.31	0.12	8.89	1.07	5	1	2	0	2	0	10996
Mount-4-zc14 - 1.d	2.45	85.93	2.45	16.91	24.68	27.09	53.84	13.72	140	49	234	54	556	119	8564
Mount-4-zc15 - 1.d	0.06	7.04	0.01	0.57	2.36	0.55	23.64	8.63	111	45	205	40	359	68	9470
Mount-4-zc15 - 3.d	0.14	3.83	0.00	0.47	2.11	0.40	18.46	5.75	72	27	121	25	245	46	10267
Mount-4-zc16 - 1.d	0.93	15.51	0.94	7.66	10.68	9.28	27.09	6.97	68	25	125	29	308	69	9468
Mount-4-zc17 - 1.d	0.88	6.01	0.27	2.21	2.83	5.23	8.52	2.28	22	8	47	14	201	60	11712
Mount-4-zc18 - 1.d	6.21	38.14	3.95	21.57	16.48	30.89	38.65	10.46	111	39	180	40	402	82	11310
Mount-4-zc19 - 1.d	0.71	13.44	0.67	3.68	5.54	7.25	15.19	4.59	56	23	130	34	389	88	13334
Mount-4-zc20 - 1.d	2.21	29.09	1.78	11.39	12.67	18.29	34.34	9.65	104	38	171	35	327	64	10109
Mount-4-zc21 - 1.d	0.00	2.48	0.05	2.09	3.62	0.46	5.26	1.35	9	2	7	1	11	1	10183
Mount-4-zc22 - 2.d	0.06	3.52	0.10	1.52	2.02	0.98	4.64	0.82	5	1	3	0	3	1	10742
Mount-4-zc23 - 1.d	0.00	3.57	0.09	1.21	2.45	0.53	6.47	1.13	8	2	5	1	6	1	10923
Mount-4-zc24 - 1.d	0.04	3.85	0.10	1.57	2.81	0.54	6.52	1.19	7	1	4	1	5	1	10977
Mount-4-zc25 - 1.d	0.41	11.20	0.35	3.95	6.92	8.90	17.26	4.07	38	12	54	12	115	24	9163
Mount-4-zc26 - 1.d	-	3.64	0.12	1.79	5.26	0.34	9.39	1.52	7	1	3	0	2	0	10581

Mount-4-zc27 - 1.d	0.27	6.87	0.25	2.48	3.61	2.62	21.33	7.16	86	32	141	29	266	50	11480
Mount-4-zc28 - 1.d	*828.29*	*1225.18*	*101.81*	*517.68*	*70.75*	*9.02*	*35.03*	*7.80*	*94*	*39*	*207*	*47*	*473*	*99*	*12191*
Mount-4-zc29 - 1.d	2.67	22.93	2.88	19.76	26.75	27.78	47.45	10.77	92	25	107	24	232	48	10612
Mount-4-zc30 - 1.d	2.64	11.82	1.47	8.89	10.35	14.75	31.58	7.63	47	9	23	3	25	4	11893
Mount-4-zc31 - 1.d	0.05	4.99	0.11	3.59	12.03	1.24	19.24	2.75	15	2	6	1	6	1	10466
Mount-4-zc32 - 1.d	0.55	7.49	0.45	3.78	6.28	5.66	19.50	5.35	60	23	119	30	355	89	10312
Mount-4-zc33 - 1.d	0.00	3.90	0.11	2.21	2.76	0.08	7.99	1.35	10	2	5	1	5	1	10871
Mount-4-zc34 - 1.d	0.60	7.02	0.40	2.88	4.37	5.18	14.06	4.24	44	14	59	12	120	25	9641
Mount-4-zc35 - 1.d	6.59	25.37	3.18	17.08	13.11	21.22	56.25	11.72	73	14	35	5	33	5	12956
Mount-4-zc36 - 1.d	0.11	24.69	0.39	5.35	10.11	4.69	60.91	18.36	211	77	348	71	671	131	7996
Mount-4-zc37 - 1.d	0.04	4.38	0.07	3.30	12.20	0.66	22.14	3.28	15	2	5	1	5	1	10952
Mount-4-zc38 - 1.d	0.00	15.08	0.03	0.50	1.52	0.29	14.20	4.83	58	22	97	20	186	38	10600
Mount-4-zc39 - 1.d	0.73	14.55	0.52	4.52	4.92	8.40	15.91	5.09	60	25	127	30	339	75	10742
Mount-4-zc40 - 1.d	4.73	36.07	2.23	13.05	6.51	5.92	21.14	8.42	128	62	360	90	894	179	9924
Mount-4-zc41 - 1.d	0.00	2.76	0.06	1.17	1.78	0.07	4.92	0.60	4	1	2	0	2	0	10562
Mount-4-zc41 - 2.d	0.00	3.64	0.09	2.61	2.90	0.09	8.37	1.26	8	2	4	1	4	1	10681
Mount-4-zc42 - 1.d	0.81	12.18	0.47	2.81	3.45	5.09	12.70	5.02	67	28	148	36	379	82	11254
Mount-4-zc43 - 1.d	0.32	67.40	0.74	10.46	13.70	2.74	56.08	17.00	192	72	339	72	687	132	6169
Mount-4-zc44 - 1.d	0.02	8.01	0.09	1.41	2.11	2.04	16.57	6.44	83	34	163	34	339	72	8214
Mount-4-zc45 - 1.d	1.36	14.12	0.98	6.99	8.33	11.32	31.06	8.58	95	34	151	31	286	56	9715
Mount-4-zc45 - 2.d	0.09	3.38	0.12	1.71	2.48	3.45	5.78	0.96	6	1	4	1	6	1	10890
Mount-4-zc46 - 1.d	0.29	66.21	0.20	2.59	3.99	4.23	21.67	7.18	84	33	167	39	409	90	10285
Mount-4-zc46 - 2.d	0.05	3.42	0.09	1.40	1.90	0.99	5.18	0.75	5	1	3	1	4	1	10752
Mount-4-zc47 - 1.d	*367.55*	*862.80*	*96.63*	*448.66*	*110.44*	*3.28*	*49.52*	*8.25*	*79*	*30*	*139*	*29*	*271*	*53*	*9603*
Mount-4-zc47 - 2.d	-	3.24	0.04	1.09	1.78	0.12	3.33	0.61	3	1	2	0	2	0	10657
Mount-4-zc48 - 1.d	151.85	193.27	13.29	63.85	20.19	19.52	32.10	8.42	97	38	179	40	422	91	9983
Mount-4-zc49 - 1.d	12.94	38.31	3.36	13.46	5.37	4.50	24.75	8.39	105	41	197	41	395	80	8925
Mount-4-zc50 - 1.d	0.20	4.21	0.13	2.21	4.26	0.86	8.28	1.59	12	3	10	2	17	3	10709
Mount-4-zc50 - 2.d	0.00	3.43	0.11	3.35	4.78	0.89	10.68	1.84	11	2	6	1	7	1	10778
Mount-4-zc51 - 1.d	0.01	7.13	0.01	0.45	1.31	0.26	6.32	2.13	28	12	63	15	154	34	10295
Mount-4-zc53 - 1.d	0.07	3.74	0.17	2.86	2.93	0.99	7.42	1.36	9	2	5	1	6	1	11170

Mount-4-zc54 - 1.d	0.45	8.09	0.25	1.67	4.66	3.12	15.17	4.09	42	14	57	12	111	23	8145
Mount-4-zc54 - 2.d	0.00	12.92	0.14	2.09	3.90	2.35	24.37	7.23	75	26	113	22	197	38	7234
Mount-4-zc54 - 3.d	1.02	8.08	0.68	5.02	4.50	4.83	10.94	2.38	24	9	41	10	120	27	9986
Mount-4-zc55 - 1.d	0.00	2.50	0.08	2.09	9.97	0.74	59.71	12.72	66	10	22	3	16	2	12190
Mount-4-zc56 - 1.d	0.55	13.53	0.59	4.33	4.18	7.32	15.01	4.73	57	23	118	28	296	64	10766
Mount-4-zc57 - 1.d	1.26	20.05	1.09	7.30	7.71	18.84	18.58	5.68	68	26	131	31	304	64	10300
Mount-4-zc58 - 1.d	0.08	27.63	0.07	1.33	4.81	1.48	41.41	16.20	218	88	404	81	733	138	9513
Mount-4-zc59 - 1.d	28.13	62.12	4.83	22.26	16.91	17.43	35.20	9.44	109	41	211	49	481	91	10574
Mount-4-zc60 - 1.d	0.85	5.82	0.48	4.07	6.09	5.66	13.98	3.07	25	8	37	10	110	26	11662
Mount-4-zc61 - 1.d	1.69	10.42	1.06	6.14	7.07	17.95	16.79	4.59	44	15	74	19	225	52	11546
Mount-4-zc62 - 1.d	0.24	4.94	0.25	3.40	4.57	2.64	7.75	1.42	11	2	7	1	8	1	10521
Mount-4-zc62 - 2.d	0.05	4.50	0.12	2.47	2.80	0.40	6.11	1.21	9	3	13	3	33	7	10754
Mount-4-zc63 - 1.d	0.85	13.05	0.35	2.38	2.67	2.78	10.25	2.92	33	12	62	15	162	37	10545
Mount-4-zc64 - 1.d	0.04	11.03	0.01	0.48	1.45	0.77	5.18	1.79	23	9	47	11	115	26	9857
Mount-4-zc65 - 1.d	-	7.80	0.00	0.86	2.11	0.52	16.41	5.31	67	25	110	23	212	42	8882
Mount-4-zc66 - 1.d	4.75	30.89	3.76	23.99	20.53	50.21	33.30	8.16	78	26	125	29	303	64	10562
Mount-4-zc66 - 2.d	0.09	4.02	0.14	2.86	3.76	2.07	7.30	1.27	8	2	5	1	7	1	10649
Mount-4-zc67 - 1.d	0.00	2.76	0.07	2.09	7.11	0.23	17.41	2.40	10	1	4	1	3	1	11549
Mount-4-zc68 - 1.d	0.00	3.12	0.16	3.24	6.87	0.22	15.44	2.04	9	2	4	1	4	1	10863
Mount-4-zc68 - 2.d	0.18	4.50	0.30	3.74	6.89	3.16	14.58	1.87	10	2	5	1	6	1	10638
Mount-4-zc69 - 1.d	0.20	21.64	0.40	4.49	7.32	3.87	34.34	12.72	149	55	240	46	418	81	9142
Mount-4-zc70 - 1.d	0.05	9.87	0.28	4.97	7.40	2.43	50.21	17.36	202	75	325	64	567	109	7285
Mount-4-zc71 - 1.d	-	2.02	0.00	1.17	1.36	1.41	10.18	2.30	16	3	11	2	14	3	10247
Mount-4-zc71 - 2.d	0.24	13.93	0.17	1.92	6.49	2.81	43.14	15.72	199	76	340	66	578	118	8121
Mount-4-zc72 - 1.d	0.13	2.86	0.07	1.74	5.07	0.65	9.96	1.37	7	1	4	1	4	1	10542
Mount-4-zc73 - 1.d	2.64	19.97	1.17	8.35	10.75	10.61	32.61	10.91	130	50	245	54	528	112	9594
Mount-4-zc74 - 1.d	0.00	13.89	0.04	1.12	2.43	0.65	15.98	5.50	72	28	140	31	315	66	9743
Mount-4-zc74 - 2.d	1.10	17.96	0.66	3.21	3.83	6.01	13.18	4.78	63	26	136	32	329	71	9798
Mount-4-zc74 - 3.d	1.47	18.14	1.03	7.23	4.61	8.70	10.84	3.37	40	16	83	20	200	43	10012
Mount-4-zc75 - 1.d	1.14	10.20	0.83	6.13	7.71	9.30	28.13	9.16	116	45	211	45	455	96	9235
Mount-4-zc76 - 1.d	0.14	12.80	0.18	2.42	3.26	1.82	11.61	3.55	41	14	67	15	161	35	7858

Mount-4-zc77 - 1.d	0.91	6.61	0.72	5.14	5.94	12.51	16.46	4.88	55	21	96	22	233	55	10807
Mount-4-zc77 - 2.d	0.02	3.02	0.11	1.14	2.69	0.39	6.54	1.24	7	2	6	1	11	2	10697
Mount-4-zc78 - 1.d	0.59	14.93	0.39	3.14	4.14	3.93	19.17	5.64	64	24	112	25	256	54	10124
Mount-4-zc79 - 1.d	0.06	3.42	0.12	2.23	7.39	0.59	9.27	1.44	8	1	4	1	4	1	10637
Mount-4-zc79 - 2.d	0.00	4.04	0.13	3.18	4.38	0.16	10.28	1.84	11	2	6	1	5	1	10783
Mount-4-zc80 - 1.d	0.23	13.03	0.32	2.71	4.92	3.43	16.39	4.24	47	17	86	20	209	45	11560
Mount-4-zc80 - 2.d	-	9.90	-	0.64	2.24	0.58	10.35	2.74	28	10	47	11	117	28	11729
Mount-4-zc81 - 1.d	0.07	3.55	0.03	1.83	4.76	2.07	18.17	3.80	23	5	13	2	19	3	10533
Mount-4-zc82 - 1.d	0.17	29.58	0.26	2.90	4.52	0.63	18.17	6.04	74	29	137	29	276	54	9458
Mount-4-zc83 - 1.d	2.57	26.64	2.16	14.55	21.05	25.11	49.01	14.18	144	51	234	51	478	90	11848
Mount-4-zc84 - 1.d	1.57	37.48	1.83	12.89	18.33	14.17	48.83	12.94	123	39	170	36	338	69	10005
Mount-4-zc85 - 1.d	0.08	3.92	0.18	2.78	6.26	1.68	9.59	1.43	7	1	3	1	4	1	10438
Mount-4-zc86 - 1.d	*828.29*	*2829.98*	*389.99*	*1915.42*	*276.10*	*8.80*	*105.26*	*9.21*	*75*	*28*	*133*	*30*	*321*	*71*	*8966*
Mount-4-zc87 - 1.d	19.33	27.61	1.74	11.39	6.78	2.36	12.53	3.95	61	30	202	59	730	164	9353
Mount-4-zc88 - 1.d	0.74	11.37	0.49	3.95	7.58	15.00	23.81	8.52	113	47	254	64	714	156	14859
Mount-4-zc89 - 1.d	24.68	60.74	5.40	36.07	21.40	23.47	45.21	12.20	118	44	223	55	569	129	12062
Mount-4-zc90 - 1.d	0.00	10.75	0.01	0.39	1.17	0.22	7.87	3.13	40	17	93	23	246	55	10875
Mount-4-zc91 - 1.d	0.00	0.77	0.03	0.53	1.60	1.44	12.23	4.06	51	20	88	18	173	35	7156
Mount-4-zc91 - 2.d	0.00	3.19	0.10	2.23	2.85	0.18	7.13	1.19	8	2	4	1	4	1	10224
Mount-4-zc92 - 1.d	0.32	24.71	0.28	2.81	5.47	3.31	26.92	8.94	115	46	216	45	435	86	9964
Mount-4-zc93 - 1.d	*6022.34*	*13804.80*	*1691.09*	*7316.54*	*966.34*	*53.84*	*274.37*	*20.19*	*121*	*37*	*173*	*38*	*385*	*80*	*8971*
Mount-4-zc94 - 1.d	0.48	19.15	0.42	2.93	5.09	6.97	9.97	3.04	28	10	49	12	141	36	9287
Mount-4-zc95 - 1.d	-	5.06	0.12	3.54	5.69	0.36	11.34	1.80	10	2	6	1	7	1	10844
Mount-4-zc95 - 2.d	0.00	4.50	0.13	2.95	4.87	0.16	11.16	1.62	10	2	5	1	5	1	10787
Mount-4-zc96 - 1.d	0.12	9.39	0.28	6.64	21.71	1.68	32.10	4.42	22	4	10	2	19	5	11201
Mount-4-zc97 - 1.d	0.00	2.78	0.07	1.78	4.69	0.22	9.21	0.93	5	1	1	0	1	0	10540
Mount-4-zc98 - 1.d	0.03	7.28	0.06	0.57	1.33	0.42	8.42	2.69	35	14	67	15	149	32	8923
Mount-4-zc99 - 1.d	0.00	35.55	0.06	1.16	2.90	1.09	17.00	5.37	69	28	141	33	356	79	10343
Mount-4-zc100 - 1.d	0.18	3.11	0.06	1.57	4.31	0.48	12.36	2.26	14	3	13	3	39	9	11463
Mount-4-zc100 - 2.d	0.00	3.00	0.11	2.38	3.54	1.12	8.89	1.48	8	2	4	0	3	1	10500
Mount-4-zc101 - 1.d	0.01	1.55	0.02	0.98	4.52	0.64	36.25	9.06	57	10	25	3	21	3	11984

Mount-4-zc101 - 2.d	0.21	3.76	0.29	2.31	5.19	4.66	26.30	6.26	39	7	17	2	17	3	11408
Mount-4-zc102 - 1.d	0.69	20.41	0.90	9.11	15.00	7.87	62.29	19.19	212	77	333	66	592	118	7158
Mount-4-zc102 - 2.d	19.50	46.59	3.19	12.08	5.00	1.62	29.51	11.67	157	63	301	62	589	118	11063
Mount-4-zc103 - 1.d	0.00	4.94	0.03	1.07	4.24	0.39	13.96	1.95	10	2	5	1	5	1	11693
Mount-4-zc104 - 1.d	1.61	3.55	0.23	1.98	0.60	2.73	1.85	0.68	11	5	29	8	100	27	12015
Mount-4-zc104 - 2.d	0.08	2.76	0.08	2.02	4.40	1.05	15.19	2.11	12	2	5	1	6	1	11027
Co17-41 zircon															
Mount-4-zc105 - 1.d	0.03	21.40	0.00	0.49	3.06	0.84	22.30	8.53	108	42	198	42	400	84	10367
Mount-4-zc106 - 1.d	0.65	3.95	0.10	0.20	0.39	0.81	4.63	2.26	33	12	59	13	145	31	11620
Mount-4-zc106 - 2.d	1.12	43.50	0.71	3.57	3.58	1.91	17.00	6.08	74	31	154	34	360	77	9846
Mount-4-zc107 - 1.d	0.04	20.36	0.28	5.78	8.96	3.27	44.40	14.54	176	69	316	64	598	117	8062
Mount-4-zc107 - 2.d	0.00	18.17	0.22	4.09	6.93	2.53	36.40	12.11	151	58	261	53	486	97	8250
Mount-4-zc108 - 1.d	0.22	8.11	0.18	1.67	2.78	1.04	19.60	7.19	92	38	193	45	462	100	8502
Mount-4-zc109 - 1.d	0.00	14.68	0.00	0.68	1.92	0.14	16.40	5.97	85	37	181	39	375	74	10158
Mount-4-zc110 - 1.d	0.00	9.17	0.02	1.24	2.70	0.64	19.50	6.97	87	35	164	34	322	66	8847
Mount-4-zc111 - 1.d	0.03	8.35	0.00	0.13	0.36	0.28	4.98	2.15	30	15	90	25	306	77	11761
Mount-4-zc112 - 1.d	0.49	6.19	0.59	3.13	2.54	0.79	9.10	2.39	27	9	43	9	96	20	11107
Mount-4-zc112 - 2.d	0.02	3.08	0.05	0.49	0.53	0.24	3.63	1.61	22	9	48	11	129	29	11118
Mount-4-zc113 - 1.d	4.59	23.70	0.71	2.32	2.59	1.07	23.40	8.60	120	49	242	54	532	108	10600
Mount-4-zc114 - 1.d	1.40	4.46	0.28	0.83	0.00	0.06	0.16	0.15	2	1	9	3	40	12	8782
Mount-4-zc114 - 2.d	0.00	5.61	0.10	1.81	2.34	1.40	10.60	3.63	48	19	100	25	290	70	6912
Mount-4-zc115 - 1.d	2.68	20.50	1.62	10.00	7.78	3.13	35.20	12.02	140	51	228	46	414	80	8210
Mount-4-zc115 - 2.d	2.67	21.80	1.90	9.20	5.16	2.38	15.90	4.53	58	22	99	21	195	38	9032
Mount-4-zc116 - 2.d	2.60	7.98	0.64	2.63	1.11	0.69	4.72	2.05	24	10	46	10	98	22	9349
Mount-4-zc117 - 1.d	84.60	154.00	9.80	23.50	4.00	2.09	23.60	10.24	150	64	317	72	687	134	11870
Mount-4-zc118 - 1.d	2.18	10.80	1.29	9.20	9.40	8.50	33.10	9.40	80	16	49	8	77	14	17030
Mount-4-zc119 - 1.d	1.26	5.29	0.44	1.93	3.52	0.85	10.10	1.99	16	4	11	2	14	2	11110
Mount-4-zc120 - 1.d	2.66	21.90	0.84	5.48	4.15	1.49	19.70	7.09	88	35	162	34	318	62	10874
Mount-4-zc121 - 1.d	2.52	10.30	0.76	4.10	1.10	0.29	4.16	1.89	34	20	164	58	864	242	13860
Mount-4-zc122 - 1.d	101.00	97.90	3.35	6.80	1.00	0.49	2.71	1.79	36	22	169	60	818	206	17390
Mount-4-zc123 - 1.d	0.32	27.60	0.10	1.23	2.63	0.94	16.30	5.53	73	30	152	36	367	81	9452

Mount-4-zc124 - 1.d	1.44	17.70	1.11	6.50	2.95	3.99	13.30	4.60	57	21	88	18	165	33	11041
Mount-4-zc125 - 1.d	0.44	6.39	0.23	1.33	1.55	0.80	9.39	2.85	34	14	66	16	161	35	10798
Mount-4-zc128 - 1.d	9.60	15.00	0.75	1.90	0.30	0.59	3.54	1.55	20	9	48	12	144	33	11980
Mount-4-zc129 - 1.d	0.37	28.20	0.07	1.05	2.36	0.32	16.50	5.20	67	27	127	28	268	53	9962
Mount-4-zc129 - 2.d	3.38	18.10	1.86	7.80	5.10	5.76	9.80	2.54	22	6	19	3	26	4	11017
Mount-4-zc130 - 1.d	1.03	14.37	0.17	2.01	4.69	0.50	33.00	12.39	169	69	328	71	654	126	11710
Mount-4-zc131 - 1.d	0.00	25.06	0.08	1.68	3.77	0.61	19.00	6.80	81	31	140	29	264	52	8497
Mount-4-zc131 - 2.d	0.32	5.69	0.25	2.33	2.33	0.86	7.00	1.47	11	3	13	3	24	5	11558
Mount-4-zc132 - 1.d	0.67	31.32	0.19	1.48	1.92	1.24	15.90	5.13	65	26	130	30	323	72	9033
Mount-4-zc132 - 2.d	1.01	24.13	0.30	2.95	3.90	1.69	20.50	6.34	68	25	116	25	253	53	8805
Mount-4-zc133 - 1.d	0.06	44.20	0.19	3.42	6.44	2.06	31.30	10.23	117	44	201	44	430	90	8505
Mount-4-zc134 - 1.d	1.49	68.70	1.16	8.60	6.60	4.08	33.40	10.84	133	52	251	55	553	117	9507
Mount-4-zc134 - 2.d	1.94	17.71	0.83	5.87	3.84	1.99	10.60	4.20	49	20	95	22	212	44	10550
Mount-4-zc135 - 1.d	0.16	9.99	0.14	1.66	3.30	0.53	17.10	5.95	72	27	118	24	220	43	8616
Mount-4-zc135 - 2.d	0.00	19.00	0.05	1.41	3.32	0.24	22.20	8.07	96	37	166	33	295	56	9478
Mount-4-zc136 - 1.d	366.00	1250.00	163.00	740.00	103.00	3.99	53.40	9.94	96	33	148	32	305	63	7985
Mount-4-zc137 - 1.d	0.13	9.30	0.09	0.60	0.99	0.21	7.30	2.82	35	14	64	14	133	26	9677
Mount-4-zc138 - 1.d	0.46	23.78	0.35	3.21	2.80	1.01	16.00	5.34	67	26	116	26	237	48	8969
Mount-4-zc139 - 1.d	118.40	83.40	1.96	5.30	6.10	0.93	43.50	16.50	206	91	450	100	967	199	7360
Mount-4-zc140 - 1.d	0.00	17.30	0.03	1.12	2.75	0.14	15.20	5.50	67	26	117	24	221	43	9400
Mount-4-zc141 - 1.d	4.32	45.20	3.25	19.10	10.90	6.28	46.00	13.52	155	58	261	53	513	103	8390
Mount-4-zc141 - 2.d	360.00	1490.00	224.00	950.00	117.00	2.53	46.00	6.54	62	25	123	27	276	57	10286
Mount-4-zc142 - 1.d	0.01	6.49	0.05	0.99	3.02	1.08	21.10	6.92	87	33	149	30	275	54	8019
Mount-4-zc143 - 1.d	0.00	14.70	0.00	0.56	1.16	0.54	9.10	2.85	39	15	73	16	166	35	10155
Mount-4-zc144 - 1.d	0.00	12.53	0.00	0.56	1.59	0.16	9.01	3.35	46	19	93	21	206	42	10114
Mount-4-zc145 - 1.d	0.00	13.69	0.26	4.62	9.80	1.52	55.00	17.83	210	74	319	62	532	100	7096
Mount-4-zc145 - 2.d	0.00	11.63	0.06	1.06	2.71	0.35	16.90	6.52	82	31	138	28	255	50	8662
Mount-4-zc146 - 1.d	0.05	126.70	0.53	10.13	12.00	5.26	51.70	12.74	126	41	167	33	298	60	6970
Mount-4-zc146 - 2.d	8.80	88.80	1.97	10.60	5.47	1.76	34.30	12.14	151	57	253	52	481	94	10955
Mount-4-zc147 - 1.d	7.31	31.60	4.74	24.00	9.60	10.20	21.70	5.36	56	20	97	24	286	71	12980
Mount-4-zc147 - 2.d	0.00	3.76	0.07	1.61	2.33	0.16	4.55	0.92	7	1	4	1	5	1	11640

Mount-4-zc148 - 1.d	0.00	5.28	0.02	0.95	1.47	0.45	10.97	3.56	46	19	88	20	190	41	8613
Mount-4-zc148 - 2.d	0.00	12.26	0.00	0.31	0.82	0.10	5.42	2.14	28	12	58	13	129	27	10652
Mount-4-zc149 - 1.d	0.51	8.81	0.25	1.05	1.22	0.48	13.80	5.59	81	38	198	47	466	98	13950
Mount-4-zc149 - 2.d	22.50	77.60	6.43	25.70	6.84	5.43	21.20	6.93	84	33	161	36	348	70	10263
Mount-4-zc150 - 1.d	2.04	13.50	0.29	0.90	0.53	0.44	3.60	1.51	20	9	52	13	149	38	9796
Mount-4-zc150 - 2.d	0.08	12.07	0.02	0.09	0.59	0.29	6.23	2.53	37	17	91	24	269	60	11302
Mount-4-zc151 - 1.d	0.31	21.50	0.49	7.20	9.10	0.48	51.90	17.02	215	88	407	86	809	160	8437
Mount-4-zc151 - 2.d	0.93	5.36	0.31	1.41	0.63	0.29	3.25	1.13	18	7	39	10	107	26	10533
Mount-4-zc152 - 1.d	0.71	18.11	0.40	3.84	4.03	1.21	22.70	7.95	93	35	156	31	285	57	7850
Mount-4-zc152 - 2.d	1.97	44.90	0.94	5.52	4.55	0.64	21.60	7.78	98	40	196	43	424	86	9734
Mount-4-zc152 - 3.d	0.47	22.36	0.33	2.30	1.34	0.87	8.87	3.26	42	18	94	23	237	52	10285
Mount-4-zc152 - 4.d	0.24	21.92	0.16	1.06	1.70	0.35	7.20	3.42	46	19	95	23	238	52	10014
Mount-4-zc153 - 1.d	0.00	10.30	0.07	1.43	2.56	1.02	18.00	5.99	72	28	142	35	370	85	8610
Mount-4-zc154 - 1.d	1.57	21.08	1.07	6.63	4.19	3.62	17.10	6.79	86	37	189	46	474	101	12030
Mount-4-zc155 - 1.d	3.81	21.90	1.59	6.20	1.27	2.23	3.52	1.30	17	9	58	15	178	45	9980
Mount-4-zc156 - 1.d	0.82	30.90	0.18	1.95	2.54	1.39	18.90	6.54	81	33	163	37	389	84	8854
Mount-4-zc157 - 1.d	9.00	43.80	5.98	29.00	9.80	6.28	18.00	5.39	67	27	141	36	400	90	11290
Mount-4-zc158 - 1.d	0.00	6.77	0.00	0.57	1.57	0.43	12.30	4.33	57	22	109	23	220	46	7936
Mount-4-zc158 - 2.d	13.00	35.60	2.51	8.20	3.29	1.42	14.60	5.32	68	28	135	30	287	62	8335
Mount-4-zc158 - 3.d	0.00	8.15	0.03	0.76	1.55	0.53	12.70	4.47	56	21	103	21	201	40	7933
Mount-4-zc159 - 1.d	0.38	9.41	0.08	0.46	1.01	0.12	4.54	1.80	28	14	79	20	218	51	9910
Mount-4-zc159 - 2.d	*550.00*	*1500.00*	*191.00*	*640.00*	*58.00*	*2.66*	*25.40*	*4.60*	*52*	*22*	*114*	*27*	*266*	*56*	*10288*
Mount-4-zc160 - 1.d	1.13	13.38	0.78	4.04	3.05	1.08	11.90	4.16	48	18	80	18	175	36	10780
Mount-4-zc160 - 2.d	0.98	10.61	0.47	2.90	1.91	0.65	9.10	2.52	27	10	47	10	100	20	11010
Mount-4-zc161 - 1.d	2.33	10.52	0.84	4.62	1.71	0.83	7.28	2.85	38	16	77	18	188	41	10300
Mount-4-zc162 - 1.d	0.00	7.07	0.02	0.33	0.49	0.18	3.76	1.82	26	12	75	21	228	56	9404
Mount-4-zc163 - 1.d	2.35	11.13	1.01	5.88	4.77	2.49	16.60	5.09	46	15	66	16	176	41	11770
Mount-4-zc164 - 1.d	0.00	10.12	0.00	0.21	0.54	0.08	4.01	1.49	21	9	45	11	122	27	12030
Mount-4-zc164 - 2.d	0.00	16.52	0.01	0.41	0.91	0.16	6.90	2.42	32	12	61	13	116	24	9780
Mount-4-zc165 - 1.d	1.77	20.85	1.01	5.70	6.26	3.07	20.70	6.53	72	26	121	27	255	50	10920
Mount-4-zc166 - 1.d	0.00	7.18	0.02	0.65	1.38	0.42	9.15	3.20	39	16	74	17	170	37	8893

Mount-4-zc166 - 2.d	1.26	14.02	0.65	3.30	1.94	1.47	9.90	3.45	43	17	83	18	179	37	9434
Mount-4-zc167 - 1.d	0.00	12.39	0.05	1.47	2.25	0.91	11.17	3.76	47	19	91	20	204	46	7213
Mount-4-zc167 - 2.d	1.09	21.90	0.25	1.88	2.27	0.83	10.90	3.92	48	19	91	21	209	45	9560
Mount-4-zc168 - 1.d	0.06	12.05	0.05	0.58	2.98	0.50	28.80	10.96	142	58	274	58	550	108	9200
Mount-4-zc169 - 1.d	0.29	5.18	0.11	1.00	1.73	0.38	9.30	4.54	69	31	153	35	339	66	12230
Mount-4-zc169 - 2.d	5.21	20.00	1.80	8.10	2.68	2.72	13.30	3.59	29	10	49	12	149	34	12110
Mount-4-zc170 - 1.d	*1010.00*	*1580.00*	*149.00*	*600.00*	*97.00*	*4.78*	*37.20*	*7.06*	*81*	*34*	*181*	*43*	*417*	*79*	*9404*
Mount-4-zc170 - 2.d	0.79	5.74	0.13	1.60	1.27	0.18	9.60	4.57	74	34	169	40	383	76	10660
Mount-4-zc171 - 1.d	0.45	4.98	0.12	1.22	5.52	2.83	48.10	13.46	96	18	49	7	47	7	11832
Mount-4-zc172 - 1.d	1.06	39.10	0.32	1.65	1.44	0.68	8.44	2.79	35	14	76	20	219	53	10039
Mount-4-zc172 - 2.d	0.20	35.40	0.16	0.97	0.90	0.68	7.80	2.65	30	12	58	13	140	30	9861
Mount-4-zc172 - 3.d	0.45	12.64	0.33	1.93	1.40	1.38	4.49	1.49	18	7	34	8	91	22	12580
Mount-4-zc173 - 1.d	0.12	41.90	0.46	6.60	10.70	2.24	57.30	17.57	205	77	350	72	658	128	8132
Mount-4-zc173 - 2.d	0.00	25.64	0.01	1.02	1.98	0.29	15.70	5.45	68	27	134	29	288	58	9992
Mount-4-zc174 - 1.d	40.00	96.00	5.30	29.40	14.90	9.20	45.00	14.86	159	56	245	52	487	95	10381
Mount-4-zc175 - 1.d	4.88	27.30	1.28	4.33	3.16	1.55	11.60	4.56	58	22	105	24	237	49	10006
Mount-4-zc175 - 2.d	2.44	32.50	0.52	2.10	2.09	1.26	18.40	6.50	85	36	176	40	407	83	10596
Mount-4-zc176 - 1.d	0.00	15.55	0.04	0.33	1.95	0.32	16.80	7.35	102	42	213	48	480	97	10690
Mount-4-zc176 - 2.d	1.32	7.60	0.42	3.39	3.76	2.58	14.90	3.92	34	7	21	3	26	4	11609
Mount-4-zc177 - 1.d	52.00	101.00	8.20	33.00	4.80	1.70	6.80	2.28	29	15	119	42	569	142	13696
Mount-4-zc178 - 1.d	0.98	76.70	0.81	10.03	17.20	3.78	79.20	25.62	288	104	454	90	812	154	8230
Mount-4-zc178 - 2.d	2.82	16.20	1.75	10.60	6.80	5.00	14.90	3.09	29	10	56	15	176	41	12340
Mount-4-zc179 - 1.d	*530.00*	*1520.00*	*241.00*	*990.00*	*134.00*	*7.20*	*81.00*	*17.50*	*192*	*71*	*313*	*64*	*576*	*111*	*8067*
Mount-4-zc179 - 2.d	1.74	23.70	1.31	7.40	7.20	2.59	30.00	11.00	132	51	227	45	412	81	7982
Mount-4-zc179 - 3.d	6.60	24.90	1.92	8.20	2.46	3.14	9.30	2.17	29	12	68	18	216	54	12400
Mount-4-zc180 - 1.d	1.07	20.60	0.50	2.82	3.30	0.81	18.80	7.18	98	41	202	46	477	102	10688
Mount-4-zc180 - 2.d	0.00	16.20	0.00	0.67	2.81	0.37	20.50	8.63	108	45	213	45	425	84	10886
Mount-4-zc181 - 1.d	0.00	23.78	0.08	1.39	2.83	0.93	16.00	5.48	70	28	133	30	297	64	9042

Session 2 - Samples	La	Ce	Pr	Nd	Sm	Eu	Gd	Tb	Dy	Ho	Er	Tm	Yb	Lu	Hf
Co17-37-zc1 - 1.d	0.16	2.11	0.00	0.55	3.30	3.30	7.60	1.99	14	4	13	2	20	3	11310

Co17-37-zc2 - 1.d	0.37	5.15	0.22	3.14	6.20	7.53	14.20	2.20	13	3	8	1	9	2	10698
Co17-37-zc3 - 1.d	0.19	3.62	0.00	1.22	4.10	2.10	11.30	1.79	10	2	6	1	6	1	10110
Co17-37-zc4 - 1.d	0.00	5.19	0.20	3.26	5.63	0.19	7.80	0.95	5	1	2	0	2	0	10861
Co17-37-zc5 - 1.d	0.32	5.20	0.14	3.90	15.80	6.21	24.10	3.47	19	3	9	1	9	2	10750
Co17-37-zc6 - 1.d	0.55	6.36	0.40	3.84	12.60	7.30	18.70	3.03	20	4	12	2	14	2	10870
Co17-37-zc7 - 1.d	26.00	26.00	0.00	0.00	0.00	6.00	43.00	0.00	0	0	0	0	0	0	24600
Co17-37-zc10 - 1.d	-	-	-	-	-	-	-	-	-	-	-	-	-	-	-
Co17-37-zc13 - 1.d	-	-	-	-	-	-	-	-	-	-	-	-	-	-	-
Co17-37-zc14 - 1.d	10.70	45.10	4.30	27.60	36.90	70.00	58.00	7.60	42	8	22	3	22	3	11045
Co17-38-zc1 - 1.d	0.39	4.26	0.45	3.07	4.70	4.56	9.73	1.54	9	2	5	1	8	2	11005
Co17-38-zc2 - 1.d	0.10	8.79	0.31	5.69	9.20	1.72	11.90	1.95	12	2	7	1	8	1	11291
Co17-38-zc3 - 1.d	0.26	11.74	0.29	3.08	5.17	3.13	15.80	4.83	61	24	124	30	312	66	11681
Co17-38-zc4 - 1.d	0.40	9.96	0.50	3.13	3.74	6.31	10.90	3.26	38	16	81	19	201	44	10571
Co17-38-zc5 - 1.d	-	-	-	-	-	-	-	-	-	-	-	-	-	-	-
Co17-38-zc6 - 1.d	-	-	-	-	-	-	-	-	-	-	-	-	-	-	-
Co17-38-zc7 - 1.d	0.00	3.49	0.08	2.02	1.97	0.25	5.65	1.00	7	2	5	1	5	1	11358
Co17-38-zc8 - 1.d	6.00	44.50	4.80	27.60	55.00	89.00	101.00	22.60	218	71	322	73	710	152	12790
Co17-38-zc9 - 1.d	-	-	-	-	-	-	-	-	-	-	-	-	-	-	-
Co17-38-zc11 - 1.d	0.12	3.71	0.16	1.80	3.57	1.55	5.83	0.92	5	1	2	0	3	1	10481
Co17-38-zc12 - 1.d	0.00	2.64	0.05	1.59	2.42	0.35	6.79	1.16	7	1	4	1	4	1	10893
Co17-38-zc13 - 1.d	0.64	6.95	0.99	6.88	13.50	6.83	28.90	6.46	52	13	53	12	125	27	12550
Co17-38-zc16 - 1.d	4.09	20.00	2.78	14.40	11.70	32.50	22.70	5.24	46	12	44	10	95	22	10630
Co17-38-zc15 - 1.d	0.01	2.78	0.07	0.88	1.88	1.10	5.64	0.75	5	1	2	0	3	0	10707
Co17-38-zc17 - 1.d	-	-	-	-	-	-	-	-	-	-	-	-	-	-	-
Co17-38-zc18 - 1.d	0.26	9.70	0.15	1.75	3.43	3.31	12.80	3.91	41	13	66	22	367	119	12170
Co17-38-zc19 - 1.d	1.50	9.47	0.99	6.65	6.04	9.00	20.70	5.49	69	27	133	32	362	84	10080
Co17-38-zc20 - 1.d	1.98	19.75	1.50	10.00	12.70	16.80	26.70	7.96	91	35	181	47	573	145	11090
Co17-38-zc21 - 1.d	0.28	5.70	0.63	5.70	5.80	6.36	18.70	3.64	20	4	12	2	18	3	11090
Co17-37-zc1 - 1.d	0.16	2.11	0	0.55	3.3	3.3	7.6	1.99	14.3	3.98	13.4	2.06	20.2	2.88	11310
Co17-37-zc2 - 1.d	0.37	5.15	0.216	3.14	6.2	7.53	14.2	2.2	13.47	2.82	7.65	1.36	9.3	1.541	10698
Co17-37-zc3 - 1.d	0.19	3.62	0	1.22	4.1	2.1	11.3	1.79	9.8	1.99	6.3	0.69	5.9	1.14	10110

Co17-37-zc4 - 1.d	0	5.19	0.195	3.26	5.63	0.194	7.8	0.951	4.85	0.767	1.9	0.259	1.79	0.244	10861
Co17-37-zc5 - 1.d	0.32	5.2	0.141	3.9	15.8	6.21	24.1	3.47	18.9	3.32	9.37	1.45	9.37	1.66	10750
Co17-37-zc6 - 1.d	0.55	6.36	0.4	3.84	12.6	7.3	18.7	3.03	19.6	3.9	11.5	1.8	13.6	2.24	10870
Co17-37-zc7 - 1.d	26	26	0	0	0	6	43	0	0	0	0	0	0	0	24600
Co17-37-zc10 - 1.d	-	-	-	-	-	-	-	-	-	-	-	-	-	-	-
Co17-37-zc13 - 1.d	-	-	-	-	-	-	-	-	-	-	-	-	-	-	-
Co17-37-zc14 - 1.d	10.7	45.1	4.3	27.6	36.9	70	58	7.6	41.7	8.4	21.6	3.33	22.2	3.25	11045
Co17-38-zc1 - 1.d	0.389	4.26	0.451	3.07	4.7	4.56	9.73	1.54	9.02	1.7	5.35	0.877	8.22	1.52	11005
Co17-38-zc2 - 1.d	0.104	8.79	0.312	5.69	9.2	1.72	11.9	1.95	12.16	2.46	7.27	1.17	8.42	1.38	11291
Co17-38-zc3 - 1.d	0.257	11.74	0.294	3.08	5.17	3.13	15.8	4.83	60.8	23.61	124.3	29.71	311.6	66.38	11681
Co17-38-zc4 - 1.d	0.401	9.96	0.503	3.13	3.74	6.31	10.9	3.26	38	15.79	80.5	19.1	201.1	44.1	10571
Co17-38-zc5 - 1.d	-	-	-	-	-	-	-	-	-	-	-	-	-	-	-
Co17-38-zc6 - 1.d	-	-	-	-	-	-	-	-	-	-	-	-	-	-	-
Co17-38-zc7 - 1.d	0	3.49	0.076	2.02	1.97	0.245	5.65	0.999	7.07	1.6	4.55	0.708	5.05	0.863	11358
Co17-38-zc8 - 1.d	6	44.5	4.8	27.6	55	89	101	22.6	218	71.4	321.8	73	710	152.4	12790
Co17-38-zc9 - 1.d	-	-	-	-	-	-	-	-	-	-	-	-	-	-	-
Co17-38-zc11 - 1.d	0.118	3.71	0.156	1.8	3.57	1.55	5.83	0.917	5.01	0.887	2.46	0.395	3.25	0.502	10481
Co17-38-zc12 - 1.d	0	2.64	0.052	1.59	2.42	0.351	6.79	1.156	6.55	1.28	3.68	0.509	4.06	0.79	10893
Co17-38-zc13 - 1.d	0.64	6.95	0.99	6.88	13.5	6.83	28.9	6.46	51.7	12.81	52.7	11.96	125.3	26.9	12550
Co17-38-zc16 - 1.d	4.09	20	2.78	14.4	11.7	32.5	22.7	5.24	45.5	11.6	43.7	10	95	21.8	10630
Co17-38-zc15 - 1.d	0.01	2.78	0.07	0.88	1.88	1.1	5.64	0.747	4.51	0.852	2.19	0.346	2.65	0.437	10707
Co17-38-zc17 - 1.d	-	-	-	-	-	-	-	-	-	-	-	-	-	-	-
Co17-38-zc18 - 1.d	0.26	9.7	0.149	1.75	3.43	3.31	12.8	3.91	40.5	12.9	66.3	21.72	367	119.3	12170
Co17-38-zc19 - 1.d	1.5	9.47	0.99	6.65	6.04	9	20.7	5.49	68.9	27.33	132.7	31.98	362.4	83.5	10080
Co17-38-zc20 - 1.d	1.98	19.75	1.5	10	12.7	16.8	26.7	7.96	91.1	35.38	181.2	46.6	573	144.8	11090
Co17-38-zc21 - 1.d	0.28	5.7	0.63	5.7	5.8	6.36	18.7	3.64	20.2	4.17	12.29	1.96	17.6	2.95	11090

APPENDIX F: MONAZITE TRACE ELEMENT ANALYSES (NOT NORMALISED VALUES)

Session 1 - Standards	Y	La	Pr	Nd	Sm	Eu	Gd	Tb	Dy	Ho	Er	Tm	Yb	Lu
NIST610 - 1	2.01E+05	2.04E+05	1.92E+05	1.92E+05	2.01E+05	2.06E+05	1.98E+05	1.98E+05	1.90E+05	2.00E+05	1.90E+05	187400	1.98E+05	1.94E+05
NIST610 - 2	2.01E+05	2.04E+05	1.92E+05	1.91E+05	2.01E+05	2.06E+05	1.98E+05	1.98E+05	1.91E+05	2.01E+05	1.90E+05	1.88E+05	1.98E+05	1.94E+05
NIST610 - 3	2.01E+05	2.05E+05	192770	1.93E+05	2.04E+05	2.06E+05	2.00E+05	1.98E+05	1.91E+05	2.01E+05	1.90E+05	1.88E+05	2.00E+05	1.94E+05
NIST610 - 4	2.01E+05	2.04E+05	1.92E+05	1.94E+05	2.01E+05	2.06E+05	1.97E+05	197630	1.91E+05	2.01E+05	1.90E+05	1.87E+05	1.99E+05	194110
NIST610 - 5	2.00E+05	2.04E+05	1.91E+05	1.92E+05	2.00E+05	2.06E+05	1.96E+05	197740	1.91E+05	2.00E+05	1.90E+05	1.87E+05	1.99E+05	1.94E+05
NIST610 - 6	2.02E+05	2.05E+05	1.92E+05	1.91E+05	2.01E+05	2.06E+05	1.98E+05	1.98E+05	1.91E+05	2.01E+05	1.90E+05	1.88E+05	1.98E+05	1.94E+05
NIST610 - 7	2.01E+05	2.03E+05	1.92E+05	1.94E+05	2.02E+05	2.06E+05	2.00E+05	1.98E+05	1.91E+05	2.01E+05	1.90E+05	1.88E+05	1.99E+05	1.94E+05
NIST610 - 8	2.01E+05	2.04E+05	1.92E+05	1.91E+05	2.03E+05	2.05E+05	1.98E+05	1.98E+05	1.91E+05	2.00E+05	1.90E+05	1.88E+05	1.98E+05	1.94E+05
NIST610 - 9	2.01E+05	2.04E+05	1.91E+05	1.92E+05	1.99E+05	2.06E+05	1.97E+05	1.98E+05	1.91E+05	2.00E+05	1.90E+05	1.87E+05	1.98E+05	1.94E+05
NIST610 - 10	2.01E+05	2.04E+05	1.92E+05	1.92E+05	2.02E+05	2.06E+05	1.99E+05	1.98E+05	190590	2.01E+05	1.90E+05	1.88E+05	2.00E+05	1.94E+05
NIST610 - 11	2.01E+05	2.03E+05	1.92E+05	1.94E+05	2.02E+05	2.06E+05	1.98E+05	1.98E+05	1.91E+05	2.01E+05	1.90E+05	1.87E+05	1.99E+05	1.95E+05
NIST610 - 12	2.01E+05	2.05E+05	1.92E+05	1.93E+05	2.02E+05	206130	1.97E+05	1.98E+05	190770	2.01E+05	1.91E+05	1.87E+05	1.99E+05	1.94E+05
NIST610 - 13	2.01E+05	2.03E+05	1.91E+05	1.92E+05	2.00E+05	2.06E+05	1.99E+05	1.97E+05	1.90E+05	2.01E+05	189520	1.87E+05	1.99E+05	1.94E+05
NIST610 - 14	2.01E+05	2.04E+05	1.93E+05	1.92E+05	2.03E+05	2.07E+05	1.98E+05	1.98E+05	1.91E+05	2.00E+05	1.91E+05	1.89E+05	1.99E+05	1.95E+05
NIST610 - 15	2.01E+05	2.05E+05	1.91E+05	1.92E+05	2.02E+05	2.06E+05	1.98E+05	1.98E+05	1.91E+05	1.99E+05	1.90E+05	1.87E+05	1.99E+05	1.94E+05
NIST610 - 16	2.01E+05	204450	1.92E+05	1.93E+05	2.02E+05	2.05E+05	1.98E+05	1.98E+05	1.91E+05	2.00E+05	1.90E+05	1.88E+05	1.99E+05	1.94E+05
NIST610 - 17	2.01E+05	2.04E+05	1.93E+05	1.92E+05	2.00E+05	2.06E+05	1.98E+05	1.98E+05	1.90E+05	2.00E+05	1.90E+05	1.87E+05	1.99E+05	1.93E+05
NIST610 - 18	2.01E+05	2.04E+05	1.91E+05	1.93E+05	2.02E+05	2.06E+05	2.01E+05	1.98E+05	1.91E+05	2.01E+05	1.90E+05	1.88E+05	1.99E+05	1.95E+05

NIST610 - 19	2.01E+05	2.04E+05	1.92E+05	1.91E+05	2.02E+05	2.06E+05	1.98E+05	1.98E+05	1.91E+05	2.01E+05	1.91E+05	1.88E+05	1.99E+05	1.95E+05
NIST610 - 20	2.01E+05	2.04E+05	1.91E+05	1.93E+05	2.02E+05	2.05E+05	1.97E+05	1.98E+05	1.90E+05	2.00E+05	1.90E+05	1.87E+05	1.99E+05	1.93E+05
NIST610 - 21	2.01E+05	2.03E+05	1.92E+05	1.94E+05	2.01E+05	2.06E+05	1.99E+05	1.97E+05	1.92E+05	2.00E+05	1.90E+05	1.88E+05	1.99E+05	1.95E+05
NIST610 - 22	2.01E+05	2.04E+05	1.93E+05	1.92E+05	2.01E+05	2.06E+05	1.98E+05	1.98E+05	1.90E+05	2.01E+05	1.90E+05	1.88E+05	1.98E+05	1.95E+05
NIST610 - 23	2.00E+05	2.03E+05	191490	1.93E+05	2.01E+05	2.05E+05	1.98E+05	1.98E+05	1.90E+05	2.00E+05	1.90E+05	1.87E+05	1.99E+05	1.95E+05
NIST610 - 24	2.00E+05	2.05E+05	1.92E+05	1.91E+05	2.02E+05	2.06E+05	1.98E+05	1.98E+05	1.91E+05	2.00E+05	1.90E+05	1.88E+05	1.98E+05	1.94E+05
NIST610 - 25	2.03E+05	2.04E+05	1.92E+05	1.93E+05	2.02E+05	2.07E+05	1.98E+05	1.97E+05	1.91E+05	2.01E+05	1.91E+05	1.87E+05	1.99E+05	1.94E+05
NIST610 - 26	2.01E+05	2.04E+05	1.92E+05	1.91E+05	2.00E+05	2.06E+05	1.98E+05	1.98E+05	1.91E+05	2.00E+05	1.90E+05	1.89E+05	2.00E+05	1.94E+05
NIST610 - 27	2.01E+05	2.05E+05	1.92E+05	1.93E+05	2.02E+05	2.07E+05	2.00E+05	1.98E+05	1.91E+05	2.01E+05	1.91E+05	1.88E+05	1.99E+05	1.96E+05
NIST610 - 28	2.01E+05	2.03E+05	1.92E+05	1.93E+05	2.02E+05	2.06E+05	1.98E+05	1.98E+05	1.91E+05	2.00E+05	1.90E+05	1.88E+05	1.98E+05	1.94E+05
NIST610 - 29	2.02E+05	2.04E+05	1.92E+05	1.93E+05	2.02E+05	2.05E+05	1.98E+05	1.98E+05	1.90E+05	2.01E+05	1.90E+05	1.87E+05	1.99E+05	1.94E+05
NIST610 - 30	2.02E+05	2.04E+05	1.92E+05	1.93E+05	2.00E+05	2.06E+05	1.99E+05	1.98E+05	1.91E+05	2.00E+05	1.91E+05	1.88E+05	1.98E+05	1.94E+05
NIST610 - 31	2.01E+05	2.04E+05	192730	1.93E+05	2.01E+05	2.06E+05	1.98E+05	1.98E+05	1.90E+05	2.01E+05	1.90E+05	1.88E+05	1.99E+05	1.94E+05
NIST610 - 32	2.00E+05	2.05E+05	1.91E+05	1.92E+05	2.02E+05	2.05E+05	1.97E+05	1.97E+05	1.91E+05	2.00E+05	1.89E+05	1.86E+05	1.98E+05	1.93E+05
Session 2 - Standards	Y	La	Pr	Nd	Sm	Eu	Gd	Tb	Dy	Ho	Er	Tm	Yb	Lu
NIST610 - 1	2.02E+05	2.04E+05	1.92E+05	1.93E+05	2.02E+05	2.06E+05	1.99E+05	1.98E+05	1.92E+05	2.01E+05	1.90E+05	1.88E+05	1.99E+05	1.95E+05
NIST610 - 2	2.00E+05	2.04E+05	1.92E+05	1.92E+05	2.01E+05	2.06E+05	1.97E+05	1.98E+05	1.90E+05	2.00E+05	1.90E+05	1.87E+05	1.98E+05	1.94E+05
NIST610 - 3	2.01E+05	2.05E+05	1.92E+05	1.92E+05	2.02E+05	2.06E+05	1.99E+05	1.98E+05	1.91E+05	2.00E+05	1.90E+05	1.88E+05	1.99E+05	1.94E+05
NIST610 - 4	2.01E+05	2.04E+05	1.92E+05	1.93E+05	2.01E+05	2.06E+05	1.99E+05	1.98E+05	1.90E+05	2.01E+05	1.91E+05	1.88E+05	1.99E+05	1.94E+05
NIST610 - 5	2.00E+05	2.04E+05	1.92E+05	1.93E+05	2.02E+05	2.06E+05	1.99E+05	1.98E+05	1.91E+05	2.00E+05	1.91E+05	1.88E+05	1.99E+05	1.95E+05

NIST610 - 6	2.00E+05	2.04E+05	1.92E+05	1.92E+05	2.01E+05	2.06E+05	1.97E+05	1.97E+05	1.90E+05	2.00E+05	1.90E+05	1.87E+05	1.98E+05	1.94E+05
NIST610 - 7	2.01E+05	2.04E+05	1.92E+05	1.93E+05	2.01E+05	2.06E+05	1.98E+05	1.98E+05	1.91E+05	2.01E+05	1.91E+05	1.88E+05	1.99E+05	1.94E+05
NIST610 - 8	2.02E+05	2.04E+05	1.92E+05	1.92E+05	2.01E+05	2.06E+05	1.98E+05	1.98E+05	1.90E+05	2.00E+05	1.89E+05	1.87E+05	1.98E+05	1.94E+05
Session 3 - Standards	Y	La	Pr	Nd	Sm	Eu	Gd	Tb	Dy	Ho	Er	Tm	Yb	Lu
MAdel - 1	6920	63510	29190	1.27E+05	36360	4.04	16130	989	2081	122	111.5	5.81	19.2	1.31
MAdel - 2	6790	62540	29110	1.26E+05	35720	4.33	15830	950	2043	120.1	107.6	5.77	18.9	1.14
MAdel - 3	7130	63020	29130	1.26E+05	36180	4.42	16300	992	2157	127.1	116.6	6.17	19.4	1.28
MAdel - 4	7180	61950	29180	1.28E+05	36790	4.15	16420	1003	2157	125.4	117	6.21	19.8	1.29
MAdel - 5	7140	62450	29020	1.27E+05	36730	3.91	16240	984	2122	125.8	115.5	6.35	19.78	1.29
MAdel - 6	6740	62220	28590	1.25E+05	35320	4.2	15470	941	2025	117.9	109.1	5.74	17	1.11
MAdel - 7	6950	62140	28890	1.26E+05	35860	4.11	16020	973	2085	121	114.8	5.83	17.8	1.16
MAdel - 8	7050	61940	28770	1.27E+05	36040	4.45	16290	985	2116	123.7	112.4	6.34	20	1.14
MAdel - 9	6780	62880	28790	1.25E+05	35450	4.29	15820	956	2033	119.3	110	6.04	16.3	1.16
MAdel - 10	6650	62270	28740	1.25E+05	35040	4.29	15660	941	2002	116.5	106.9	5.8	17.9	0.93
MAdel - 11	6990	63050	29300	1.28E+05	36070	4.37	16260	987	2126	124	115.6	5.96	19.4	1.24
MAdel - 12	7060	63360	29050	1.28E+05	35710	3.79	16180	974	2120	121.5	112.2	6.05	18.8	1.16
Session 1 - Samples	Y	La	Pr	Nd	Sm	Eu	Gd	Tb	Dy	Ho	Er	Tm	Yb	Lu
Co17-21 mon7 - 1	15960	9.24E+04	25530	1.17E+05	28090	5608	23290	2459	8352	812.1	936.8	59.77	202.1	15.45
Co17-21 mon7 - 2	15790	9.27E+04	25180	1.15E+05	27940	5478	22590	2393	8161	789.4	925	57.9	204.8	15.65

Co17-21 mon8 - 1	10890	8.62E+04	25230	1.13E+05	28440	5570	21690	2306	7600	656	762	55.2	239.8	21
Co17-21 mon10 - 1	14820	9.44E+04	25080	1.15E+05	27220	5380	23430	2359	8110	778	899	60.4	228	18.4
Co17-21 mon1 - 1	-	-	-	-	-	-	-	-	-	-	-	-	-	-
Co17-21 mon2 - 1	14670	9.83E+04	24320	1.07E+05	20410	3143	15930	1832	6838	683.5	752	41.2	122.5	8.23
Co17-21 mon3 - 1	14920	92450	25320	1.13E+05	24820	4725	19250	2029	7241	741.7	969.6	70	260	20.73
Co17-21 mon4 - 1	15800	9.37E+04	25580	1.18E+05	28640	5465	23700	2410	8168	793.9	932	62.2	213.4	15.87
Co17-21 mon5 - 1	-	-	-	-	-	-	-	-	-	-	-	-	-	-
Co17-21 mon9 - 1	15720	9.35E+04	25530	1.17E+05	28070	5450	22870	2362	8234	799.3	965	65.6	236.5	19.33
Co17-21 mon11 - 1	30650	9.40E+04	25170	1.14E+05	27360	4505	25030	2961	11940	1367	1719	106.2	317	23.86
Co17-21 mon12 - 1	14190	9.30E+04	24980	1.12E+05	23920	4460	19010	2058	7200	700	825	54	193.4	14.5
Co17-21 mon13 - 1	13470	9.15E+04	25370	1.15E+05	26210	4814	20800	2116	7141	693.7	833.8	56.3	193.8	15.2
Co17-21 mon13 - 2	14430	9.38E+04	25220	1.15E+05	26940	5313	21870	2266	7563	732.5	897.8	61.6	224.2	16.82
Co17-21 mon14 - 1	10320	8.31E+04	23760	1.05E+05	23130	4190	1.64E+04	1690	5950	562	653	45.1	203	16
Co17-21 mon15 - 1	32920	9.73E+04	25400	1.14E+05	27020	5132	25290	3091	12610	1433	1911	119.1	363.6	27.16
Co17-41 mon1 - 1	6280	1.03E+05	22120	7.98E+04	7490	1800	3970	483	2240	241	292	16.94	54.9	3.59
Co17-41 mon1 - 2	10850	1.05E+05	20770	7.44E+04	9050	2603	7300	1042	4184	426	517	30.3	80.1	6.28
Co17-41 mon2 - 1	16800	1.52E+05	18470	67260	18370	3086	19400	2250	7630	703	784	43.6	122.3	9.24
Co17-41 mon2 - 2	14850	1.41E+05	18210	67490	15680	2539	16210	1941	6650	625	699	39.1	112.3	8.1
Co17-41 mon3 - 1	2420	8.09E+04	12810	3.40E+04	6420	1990	3080	382	1100	103	99	0.43	0	0
Co17-41 mon3 - 2	11620	1.37E+05	19290	7.00E+04	14950	3870	13060	1487	5168	513.7	647	38.5	120.3	8.6

Co17-41 mon4 - 1	14800	1.21E+05	20010	75390	15940	3696	13250	1552	6127	687	896	56.1	168.5	12.77
Co17-41 mon5 - 1	3650	9.96E+04	21460	7.72E+04	7410	969	4560	525	1768	153.5	152.8	7.19	18.6	1.14
Co17-41 mon5 - 2	321	9.47E+04	21810	7.91E+04	5230	94.3	1156	59.6	156.6	13.4	17.4	1.05	3.34	0.25
Co17-41 mon5 - 3	6370	1.01E+05	21670	77320	7820	1399	5560	699	2631	268.4	334.8	20.22	62.5	4.74
Co17-41 mon5 - 4	8720	1.11E+05	20520	75140	10820	2319	9700	1181	4020	353	360	17.37	44.1	2.96
Co17-41 mon8 - 1	15180	1.30E+05	19650	7.35E+04	18750	3888	20800	2344	7442	631.6	637.1	30.21	76.1	5.12
Co17-41 mon11 - 1	18410	1.24E+05	19910	73470	16050	3910	18890	2307	8155	750.8	797.5	41.18	108.7	7.59
Co17-41 mon12 - 1	5880	1.16E+05	19940	69890	8450	893	5154	564	2214	247	321	18.3	49.9	3.67
Co17-41 mon7 - 1	16290	1.22E+05	20240	77450	19580	4840	22480	2439	7780	689	753	42.1	122.5	8.44
Co17-41 mon10 - 1	14770	1.20E+05	20180	74820	16660	4409	15790	1812	6388	634.5	732	41.74	119.1	8.05
Co17-40 mon1 - 1	16430	1.38E+05	19430	8.09E+04	27740	5104	37360	3861	9520	673	589	26.45	63.5	4.07
Co17-40 mon2 - 1	15890	1.35E+05	19110	79780	25260	5608	33830	3499	9240	679	610.4	28.6	72.4	4.71
Co17-40 mon3 - 1	14600	1.30E+05	19730	80060	23530	5297	25990	2862	8429	671.3	617.7	27.73	64.7	4.05
Co17-40 mon3 - 2	17010	1.40E+05	19290	79580	26680	4908	36140	3712	9606	713	655.9	31.42	82.1	5.7
Co17-40 mon4 - 1	17720	1.36E+05	19410	80680	27110	5269	37350	3981	10290	753.4	666.5	31.7	79.8	5.27
Co17-40 mon5 - 1	19200	1.37E+05	19220	8.22E+04	29200	5188	40200	4164	10720	809	746	37.26	95.7	6.52
Co17-40 mon6 - 1	15570	1.37E+05	19510	81600	30650	5730	40210	3970	9760	666.6	554.4	24.54	57.7	3.79
Co17-40 mon7 - 1	13120	1.38E+05	19460	79790	25570	4888	33840	3345	8160	545.1	439.5	19.51	45.7	2.6
Co17-40 mon8 - 1	14660	1.43E+05	18890	78400	29810	6136	36730	3635	9170	646.3	557.8	25.43	67.2	4.81
Co17-40 mon9 - 1	10680	1.31E+05	18370	7.51E+04	23090	5030	28450	2790	6810	467	378	17.7	48	2.61

Co17-40 mon10 - 1	12550	1.30E+05	18080	7.38E+04	2.33E+04	7000	2.92E+04	3080	8010	560	480	22.9	51.9	3.37
Co17-40 mon11 - 1	14150	1.36E+05	19490	79760	26080	6438	31020	3338	9190	639	498	19.3	41.9	2.4
Co17-40 mon12 - 1	10180	1.38E+05	19060	78130	24180	4588	30420	2848	6556	423.2	330.6	14.23	33.2	2.13
Co17-40 mon13 - 1	16680	1.37E+05	19100	78550	25060	5650	35620	3796	9630	699	636	30.11	77.9	5.49
Co17-40 mon14 - 1	16380	1.51E+05	18440	76780	25490	5081	32910	3549	9280	699	672	32.7	86.1	6.11
Co17-40 mon15 - 1	16720	1.36E+05	19140	8.07E+04	26830	7610	36010	3890	9840	715	686	33.8	89.8	5.58
Co17-38 monmount1 – 1	2735	1.15E+05	20390	76180	13030	640.7	9050	724.4	1630	108.8	91.8	4.13	10.72	0.597
Co17-38 monmount1 – 2	3947	1.14E+05	20510	76990	13450	1142	9950	890.5	2281	172	153.7	7.11	16.8	1.04
Co17-38 monmount1 – 3	5100	1.15E+05	20770	78140	13730	1522	9980	925.3	2634	225.5	235.3	11.59	30.6	1.9
Co17-38 monmount1 – 4	3687	1.15E+05	20690	77270	13300	873	9300	801.3	2038	158.3	164.6	9.22	27.7	1.88
Co17-38 monmount1 – 5	2530	1.13E+05	20850	77860	12770	580	7499	573.6	1464	111.7	107.5	4.98	12.37	0.695
Co17-38 monmount1 – 6	5463	1.16E+05	20810	77630	13720	1154	10030	957	2826	247.8	261.9	14.03	37	2.41
Co17-38 monmount2 – 1	8900	1.11E+05	21100	79330	12690	1457	9040	944	3540	404	571	41.5	136	10.2
Co17-38 monmount2 – 2	6660	1.15E+05	20820	78650	12840	1445	9140	949	3250	317	342	17.6	51.4	3.1
Co17-38 monmount3 – 1	8060	1.12E+05	21090	78770	10530	1128	6875	742.1	2889	331.3	458.2	31.34	108.6	7.84

Co17-38 monmount3 – 2	8380	1.14E+05	20980	78560	11230	1528	7490	791	3085	374.1	576	43.4	162.7	11.77
Co17-38 monmount3 – 3	8670	1.10E+05	21190	78690	10090	921	6602	730	2951	336.7	422	25	70.6	4.67
Co17-38 monmount3 – 4	9430	1.11E+05	21100	78660	10160	893	6723	775.1	3182	362.6	458.5	26.7	76.5	4.79
Co17-38 monmount3 – 5	8740	1.10E+05	21330	78740	10860	866	7429	832.6	3235	347.1	407	22.4	61.8	4
Co17-38 monmount4 – 1	170.6	88860	23780	9.51E+04	5861	75.4	1263	55.58	105.2	7.26	7.84	0.396	1.11	0.115
Co17-38 monmount4 – 2	148.3	9.21E+04	23950	9.21E+04	5448	65.2	1162	49.58	93.6	6.19	6.24	0.324	0.8	0.07
Co17-38 monmount4 – 3	156.3	9.09E+04	23810	91830	5584	71.1	1187	51.83	96.7	6.59	6.75	0.295	0.91	0.078
Co17-38 monmount5 – 1	3258	1.12E+05	20790	7.93E+04	13660	1298	9810	931	2630	189.3	141.1	4.81	9.7	0.604
Co17-38 monmount5 – 2	5970	1.13E+05	20930	78150	13560	1235	9870	973	3150	292	312	16.8	47	3.44
Co17-38 monmount5 – 3	3290	1.12E+05	21130	80150	13580	1367	9700	922	2620	193	143	4.96	10.49	0.587
Co17-38 monmount5 – 4	6040	1.14E+05	21050	78880	13820	1487	10280	1072	3532	313	288	12.4	28.5	1.88
Co17-38 monmount6 – 1	8950	1.15E+05	20700	78540	12760	1468	8770	913.1	3455	400	590	44.1	155	11.6
Co17-38 monmount6 – 2	8330	1.15E+05	21070	7.92E+04	12810	1443	8210	831	3120	366	565	43.9	158	11.7

Co17-38 monmount6 – 3	5.70E+03	1.10E+05	21550	8.35E+04	12620	1200	7470	682	2360	262	377	27.5	98	7.3
Co17-38 monmount7 – 1	8660	6.61E+04	28870	1.29E+05	19200	824	12880	1589	5820	581	507	21.19	51.7	4.13
Co17-38 monmount8 – 1	4874	1.16E+05	20520	78460	12540	842	8461	758.6	2440	235.5	265.3	13.24	32.5	1.71
Co17-38 monmount8 – 2	2752	113300	20980	79990	12470	887	7540	584	1588	135.4	139.6	7.11	17.73	1.097
Co17-38 monmount8 – 3	4530	1.13E+05	20690	79230	13090	1208	8750	765	2357	223.9	255	13.42	35.4	2.07
Co17-38 monmount9 – 1	4011	1.13E+05	20770	78280	13390	1971	9750	971	2949	231.6	185.1	6.61	13.06	0.786
Co17-38 monmount9 – 2	6065	1.15E+05	20610	76820	13060	2203	9710	1050	3513	318.1	302.2	12.22	24.9	1.43
Co17-38 monmount9 – 3	6177	1.13E+05	20790	78650	13560	2200	10240	1092	3667	333.7	309.1	11.97	23.7	1.27
Co17-38 monmount9 – 4	7556	1.15E+05	20810	77900	13680	2086	10440	1139	3942	385.1	388.1	16	31.3	1.61
Co17-38 monmount9 – 5	6600	113840	20720	77520	13730	2092	10140	1078	3676	337.4	337.8	14.46	32.8	1.95
Co17-38 monmount9 – 6	4935	1.13E+05	20890	78080	13610	2004	9920	1017	3172	274.3	252.7	10.69	24.5	1.38
Co17-38 monmount9 – 7	5358	1.15E+05	21160	78730	13620	2171	9890	1029	3296	290	263.7	10.11	20.9	1.171
Co17-38 monmount9 – 8	3258	1.13E+05	20730	77660	13260	1947	9480	937	2619	194.4	151.3	5.29	11.49	0.656

Co17-38 monmount9 – 9	6040	1.14E+05	20880	78580	13590	2186	10280	1085	3589	321.9	302	12.19	23.9	1.24
Co17-38 monmount9 – 10	5030	1.15E+05	20840	77640	13210	1734	9720	956	2969	263.4	242.7	9.41	19.64	1.032
Co17-38 monmount10 – 1	5400	1.11E+05	20870	77070	11490	869	8600	904	2752	211.4	186.3	8.25	20.6	1.23
Co17-38 monmount10 – 2	6298	113400	20840	77000	11830	867	9610	1041	3130	241.2	206.9	9.21	22.44	1.38
Co17-38 monmount11 – 1	6750	1.14E+05	20850	77800	13190	1811	8870	844	2896	313.6	411	26.6	83.4	5.63
Co17-38 monmount11 – 2	1303	1.10E+05	21180	79460	12040	863	6560	453	1051	78.1	61.9	2.33	5.01	0.288
Co17-38 monmount12 – 1	3879	1.13E+05	21270	78840	13540	1447	9202	885	2625	214.4	207.4	10.39	29.2	2.1
Co17-38 monmount12 – 2	5370	1.13E+05	20900	79060	13540	1430	9520	923	2902	269	305	17.4	49.7	3.34
Co17-38 monmount12 – 3	2370	1.10E+05	21110	79030	12170	892	6790	564	1600	132	121	5.28	12	0.732
Co17-38 monmount13 – 1	5760	1.12E+05	21020	79790	13530	1480	9630	950	3080	282	270	11.3	26.7	1.64
Co17-38 monmount14 – 2	696.6	1.09E+05	21320	82000	13100	320.8	6438	322.5	524.9	29.17	23.16	1.094	2.67	0.199
Co17-38 monmount14 - 3	637	1.09E+05	21270	79780	12690	313.9	6148	297.6	475.9	26.09	20.36	0.833	2.12	0.175
Co17-38 monmount15 – 1	6480	1.09E+05	21310	82140	14340	488	10660	974	2850	248.8	280	16.41	51.3	3.41

Co17-38 monmount16 – 1	372.6	9.54E+04	22750	89230	14230	181.1	5208	195.6	287	15.59	12.36	0.523	1.22	0.072
Co17-38 monmount17 – 1	3150	1.12E+05	20940	79650	12770	1158	7459	612.6	1802	161	158.9	6.56	13.69	0.838
Co17-38 monmount17 – 2	3190	1.11E+05	21360	80950	13050	820	7470	553	1637	155	185	10.72	32.9	2.08
Co17-38 monmount17 – 3	2410	1.13E+05	21320	79500	12350	989	6580	481	1356	123.7	127	5.92	15.2	0.81
Co17-38 monmount18 - 1 – 1	1457	1.12E+05	20980	79040	12540	715.9	7484	512.8	1116	75.8	64.3	2.54	5.43	0.315
Co17-38 monmount18 – 1	2813	1.13E+05	20790	77450	13030	946.3	8390	679	1808	142.5	131.2	5.11	9.92	0.547
Co17-38 monmount18 – 2	1139	1.14E+05	21060	78850	12590	690	7559	510.7	1030	63.96	48.4	1.78	3.89	0.228
Co17-38 monmount19 – 1	3970	1.11E+05	20950	79770	13130	704	9600	858	2330	181.5	169	7.8	20.8	1.46
Co17-38 monmount20 – 1	2480	1.11E+05	20800	79290	13460	732	8470	601	1461	113.8	121.9	6.31	19.8	1.28
Co17-38 monmount21 – 1	3123	1.13E+05	21140	80350	13570	1380	9700	849	2304	179.2	158.5	6.7	14.85	1.05
Co17-38 monmount21 – 2	5140	1.12E+05	20810	79870	14100	1141	10270	934	2898	259.6	255.1	10.5	26	1.51
Co17-38 monmount22 – 1	2695	1.13E+05	20790	79420	13260	672	8530	653	1658	130.3	118.7	4.97	10.77	0.658
Co17-38 monmount22 – 2	3020	1.13E+05	20890	79710	13640	670	9050	713	1848	145.7	130.2	5.17	10.33	0.523

Co17-38 monmount22 – 3	3299	1.15E+05	20970	79710	13670	673.9	9357	762.5	1976	160.6	148	5.84	12.46	0.626
Co17-38 monmount23 – 1	2787	1.12E+05	21390	81960	13160	1034	8330	721.7	1980	158.3	133.5	5.04	11.67	0.679
Co17-38 monmount23 – 2	3504	1.12E+05	21250	81450	13050	1194	8770	791.9	2325	194	174.9	7.24	15.61	0.954
Co17-38 monmount24 – 1	738	1.03E+05	21980	85560	15280	334.9	7650	366	578	30.81	23.08	0.964	2.12	0.123
Co17-38 monmount25 – 1	1617	1.10E+05	21400	8.66E+04	14240	1275	7950	582	1292	86.9	68.2	2.92	6.52	0.502
Co17-38 monmount25 – 2	15950	1.16E+05	20630	77210	13620	2485	10760	1345	5659	703	1074	82.7	311.4	23.23
Co17-38 monmount26 – 1	22060	73430	27030	1.15E+05	12830	603	9840	1531	7750	1058	1346	66.3	167.4	12.85
Co17-38 monmount27 – 1	16170	115600	21030	77860	13970	2517	11040	1298	5496	701	1122	92.7	355.9	27.32
Co17-38 monmount27 – 2	9120	1.14E+05	20940	78370	13540	1935	10330	1108	3877	403	510	32.1	106	7.5
Co17-38 monmount27 – 3	4580	1.14E+05	20930	77740	13510	2007	9940	988	2991	245.1	218.9	9.06	20.2	1.259
Co17-38 monmount28 – 1	487	1.11E+05	21080	78040	12880	432.9	6410	309	432	18.71	11.93	0.412	0.79	0.052
Co17-38 monmount30 – 1	9490	1.16E+05	20890	78010	13240	2207	9850	1088	4060	452	613	42.5	144	10.5
Co17-38 monmount31 – 1	493	1.06E+05	21690	82580	11980	247.4	4820	207.7	338	20.5	18.6	0.889	2.38	0.149

Co17-38 monmount3 1 – 2	724	1.07E+05	21880	8.28E+04	12440	265.6	5510	264	487	30	27.2	1.262	3.24	0.241
Co17-38 monmount3 1 – 3	1063	1.07E+05	21820	8.30E+04	12490	277.4	5681	311.2	632	43	39.8	1.78	4.78	0.289
Co17-38 monmount3 2 – 1	4890	1.14E+05	21150	78930	12430	1778	8530	805	2455	230	269	17.1	55.5	3.79
Co17-38 monmount3 2 – 2	5261	1.15E+05	20800	78030	13020	1665	9590	965	2939	243.4	226.9	9.81	23.5	1.37
Co17-38 monmount3 2 – 3	2094	1.11E+05	21430	79250	10900	1215	6640	546	1415	106.5	93.1	4.14	9.62	0.574
Co17-38 monmount3 3 – 1	5640	1.15E+05	20950	77690	13840	509.2	9860	907	2768	255.8	279	14.51	37	2.41
Co17-38 monmount3 3 – 2	3669	1.14E+05	21080	8.07E+04	13880	559.8	9070	745.6	2023	173.1	178.7	8.97	23.4	1.39
Co17-38 monmount3 3 – 3	3109	1.15E+05	21040	80550	14150	1422	10280	939	2496	174.8	132.5	4.5	9.03	0.473
Co17-38 monmount3 4 – 1	5.60E+03	1.10E+05	21630	8.43E+04	11450	970	6630	630	2190	251	368	27.6	97	6.8
Co17-38 monmount3 5 – 1	6140	1.13E+05	21300	8.09E+04	13300	913	8800	796	2590	274	375	27.1	97	7.1
Co17-38 monmount3 6 – 1	4230	1.14E+05	21100	78780	11280	723	7436	697.3	2210	210.4	249	15	48.1	3.26
Co17-38 monmount3 6 – 2	7020	1.16E+05	20710	78260	11630	904	8000	828	2970	320	444	31.7	113.2	8.44
Co17-38 monmount3 7 – 1	3980	1.11E+05	21010	80750	13580	361	8460	647	1849	180.5	219.4	12.93	39.1	2.89

Co17-38 monmount37 – 2	1800	1.10E+05	21170	8.04E+04	13090	847	7790	555.7	1337	97.8	81	3.37	8.7	0.5
Co17-38 monmount38 – 1	758	1.05E+05	21300	79570	13380	486.8	6368	311.9	512.2	30.49	26.16	1.139	2.9	0.206
Co17-38 monmount39 – 1	3078	1.07E+05	21800	84330	14310	277	9100	651.1	1569	115.5	110.4	5.56	15.53	0.962
Co17-38 monmount39 – 2	5173	1.06E+05	21810	8.42E+04	14880	271.8	10600	884	2365	187.9	194.3	10.18	27.6	1.84
Co17-38 monmount40 – 1	5770	1.17E+05	20230	75600	10570	390.7	7210	693	2267	218	252.8	13.9	39.9	2.71
Co17-38 monmount41 – 1	1117	1.05E+05	21470	81260	13890	326.6	7511	423.2	759	42.44	32.77	1.29	2.46	0.186
Co17-38 monmount41 - 2	958	1.08E+05	21210	80190	13720	310.3	7446	407.9	702.1	38.47	28.48	1.339	2.81	0.124
Co17-41 monmount1 – 1	12090	1.13E+05	20660	74830	11590	3017	9620	1216	4602	461.8	531	29.41	80.3	5.59
Co17-41 monmount2 – 1	5610	1.06E+05	21300	79110	8550	1518	5090	619	2262	219.5	239	11.66	30.3	2.06
Co17-41 monmount2 – 2	10070	1.03E+05	21400	77430	8450	2860	6617	957	3789	376.4	407.3	21.09	52.4	3.38
Co17-41 monmount3 – 1	14910	1.06E+05	21440	79260	11050	4365	12040	1705	6120	589	665	37.34	106.6	7.87
Co17-41 monmount3 – 2	5730	9.26E+04	22320	80410	5611	1512	2820	428	1866	213	287.6	18.34	54.9	4.09
Co17-41 monmount3 – 3	4220	9.31E+04	22390	81840	5560	1302	2420	338	1400	156.3	215.2	13.54	41.9	2.89

Co17-41 monmount4 – 1	12680	1.14E+05	20520	73730	9950	2696	7710	1032	4357	476.5	572.4	31.25	88	5.97
Co17-41 monmount5 – 1	2726	1.10E+05	20390	7.22E+04	9400	1064	6010	579	1605	112.6	89.4	3.62	8.49	0.483
Co17-41 monmount7 – 1	213.7	1.07E+05	20770	76780	9780	485	2928	111.8	168.8	8.97	7.18	0.316	0.94	0.048
Co17-41 monmount7 – 2	213	1.10E+05	21160	77010	9790	478.5	2881	110.7	163	8.94	6.93	0.368	0.88	0.053
Co17-41 monmount8 – 1	1150	9.47E+04	22120	80150	5480	294	1860	162	527	47.9	51.7	2.75	7.3	0.475
Co17-41 monmount8 – 2	6270	1.13E+05	20210	72050	9080	1627	5630	583.4	2180	257.3	382	27.87	91	6.63
Co17-41 monmount9 – 1	346	9.77E+04	21680	7.95E+04	6466	131.5	1320	68.5	169	13.9	15.5	0.648	1.72	0.13
Co17-41 monmount10 – 1	851	1.13E+05	20370	73530	11130	976	6480	395.1	694.1	35.44	25.77	0.99	2.45	0.119
Co17-41 monmount12 – 1	1370	1.13E+05	20250	73880	11230	1157	6409	402	816	53.3	47	2.33	5.64	0.334
Co17-41 monmount13 – 1	1830	1.00E+05	21400	7.67E+04	6210	512	1607	139	586	70.9	98	6.41	19.6	1.43
Co17-41 monmount14 – 1	1224	1.16E+05	20030	71310	11290	1206	6861	459.6	858	45.4	31.1	1.176	2.39	0.15
Co17-41 monmount14 – 2	2050	1.17E+05	20210	72330	11730	1418	7950	621.1	1331	77.1	57.7	2.38	5.63	0.373
Co17-41 monmount16 – 1	13960	1.05E+05	21240	77150	9410	2326	8610	1255	5200	554	662	37.97	110.1	8.02

Co17-41 monmount17 – 1	7200	1.05E+05	21390	7.62E+04	7430	1931	4669	632.5	2585	273.6	337.3	20.25	57.4	3.9
Co17-41 monmount18 – 1	8880	1.05E+05	21320	7.67E+04	8980	2475	7200	979	3506	338	378.8	20.4	55.4	3.82
Co17-41 monmount19 – 1	14380	1.02E+05	21610	78870	10040	3029	10650	1473	5523	551.7	651.8	37.53	111.3	8.07
Co17-41 monmount19 – 2	11200	1.01E+05	21730	79080	7730	2761	6193	907	3798	420.2	552.5	34.11	104.6	7.54
Co17-41 monmount21 – 1	9140	1.10E+05	20990	7.45E+04	9480	2059	7300	952	3460	346.5	406.4	22.81	66.4	4.71
Co17-41 monmount22 – 1	1458	1.11E+05	20510	74660	11590	1006	6710	456	945	55.5	42	1.85	4.85	0.281
Co17-41 monmount23 – 1	4740	1.10E+05	20610	76130	10840	1336	6430	623	2040	187	197	9.88	26.6	1.71
Co17-41 monmount23 – 2	8580	1.05E+05	21210	7.65E+04	8510	1902	6800	912	3470	337	358	18.26	46.9	2.95
Co17-41 monmount24 – 1	3538	1.12E+05	20630	75280	11290	848	7840	736.1	1999	143	113.4	4.89	10.47	0.7
Co17-41 monmount24 – 2	5890	1.13E+05	20250	7.53E+04	12440	1315	9620	967	2927	237.4	218	9.81	23.1	1.49
Co17-41 monmount25 – 1	3481	9.86E+04	21100	76090	6175	609	2495	303.5	1298	140.8	177.4	10.43	31.4	2.42
Co17-41 monmount25 – 2	6050	1.03E+05	21020	76570	7830	1427	5160	669	2512	244.3	265.8	14.24	40.3	2.9
Co17-41 monmount25 – 3	14110	1.11E+05	20730	75490	11380	3443	11190	1519	5828	561	602.6	31.13	85.6	5.81

Co17-41 monmount26 – 1	10620	1.16E+05	20110	72380	11820	2062	9840	1216	4356	414.6	457	24.6	66.4	4.31
Co17-41 monmount26 – 2	11870	1.20E+05	20160	72680	12980	2509	11480	1410	4950	466	504.2	26.3	70.2	4.6
Co17-41 monmount26 – 3	11720	1.18E+05	20090	72470	12870	2460	11300	1386	4890	459.2	504.6	26.46	69.9	4.51
Co17-41 monmount28 – 1	312	9.86E+04	21550	7.61E+04	5640	166	1370	65.5	156	12.6	15.4	0.82	2.46	0.166
Co17-41 monmount29 – 1	2849	1.12E+05	20340	73430	10380	1009	5710	459.1	1305	111.5	121.4	6.74	21	1.5
Co17-41 monmount29 – 2	15210	1.16E+05	20610	75370	12130	3511	12010	1538	5640	584.7	705.7	41.03	123.4	8.98
Co17-41 monmount30 – 1	2460	1.04E+05	21470	76770	8240	563	3130	262	943	100.1	130.3	8.25	26.8	2.05
Co17-41 monmount33 – 1	11220	1.07E+05	21100	7.72E+04	9650	2508	5593	722	3287	414.6	592	39.07	125.7	9.92
Co17-41 monmount34 – 1	414	1.10E+05	20420	74670	10990	711	4715	218.9	336	16.66	13.17	0.602	1.41	0.063
Co17-41 monmount34 – 2	1034	1.12E+05	20770	7.48E+04	11710	992	6020	359.8	714	43.5	33.9	1.45	3.33	0.186
Co17-41 monmount35 – 1	1040	1.10E+05	20680	73420	10600	977	5180	334	694	43	36.9	1.85	4.34	0.293
Co17-41 monmount35 – 2	960	1.10E+05	20560	75600	11240	970	5680	351	680	37.6	27.2	1.13	2.95	0.169
Co17-41 monmount36 – 1	11270	1.19E+05	19650	7.28E+04	14930	2898	16110	1917	5670	449.3	438.5	21.35	58.6	3.93

Co17-41 monmount367 – 1	2170	1.13E+05	20190	72770	11420	1451	6910	512.5	1212	90.3	84.9	3.98	9.23	0.539
Co17-41 monmount368 – 1	8760	1.11E+05	20970	7.53E+04	11240	2170	7680	948	3465	338.9	382.1	20.62	55.8	3.73
Co17-41 monmount368 – 2	8280	1.12E+05	20290	7.45E+04	10520	2228	6660	840.6	3167	316.3	359.6	19.71	55.9	3.87
Co17-41 monmount369 – 1	1560	1.09E+05	20480	75980	11640	893	5650	352	834	64.4	58.1	2.69	6.7	0.345
Co17-41 monmount369 – 2	2684	1.13E+05	20390	73930	11690	1589	7202	534.6	1291	103.2	131.9	10.98	45.8	3.97
Co17-41 monmount40 – 1	1410	1.09E+05	20680	76380	10970	889	5740	369	811	54.6	50.5	2.42	6.86	0.506
Co17-41 monmount41 – 1	10130	1.06E+05	21000	7.68E+04	9660	2347	7940	1066	3963	395.5	457.8	26.13	73	5.26
Co17-41 monmount41 – 2	3770	1.04E+05	21080	74660	6820	1058	3970	462	1604	151.6	164	8.63	24	1.58
Co17-41 monmount42 – 1	1922	1.12E+05	20490	74040	11290	1029	6690	502	1198	75.1	52.6	2.13	4.47	0.314
Co17-41 monmount42 – 2	3550	1.14E+05	20230	72970	10970	1231	7310	651	1826	133.9	110.6	4.7	11.2	0.78
Co17-41 monmount43 – 1	1093	1.13E+05	20800	74220	11490	1190	6910	461.3	851	45.4	32.7	1.33	3.28	0.166
Co17-41 monmount43 – 2	2980	1.08E+05	21070	74790	9740	1105	5620	483	1431	123.5	131	7.02	19.6	1.46
Co17-41 monmount44 – 1	1608	9.74E+04	21670	7.70E+04	5684	393	1851	181.7	665	66	75.4	3.88	10.54	0.741

Co17-41 monmount44 – 2	2300	1.00E+05	21360	7.70E+04	6270	573	2730	290	1007	96.4	102.1	5.68	14.7	1.12
Co17-41 monmount45 – 1	13720	1.13E+05	20610	75240	11550	3426	10750	1334	5235	559.3	678	37.48	100.9	7.36
Co17-41 monmount46 – 1	5380	9.78E+04	21860	7.71E+04	6040	1619	2471	352.7	1633	205.6	308.4	21.09	66.3	5.01
Co17-41 monmount47 – 1	8330	9.73E+04	22130	7.78E+04	6550	1159	4491	649	2837	327.8	426.8	25.24	74.7	5.27
Co17-41 monmount47 – 2	11670	1.01E+05	21550	7.69E+04	9880	2528	8130	1034	4212	486.3	702	46.14	143.7	10.93
Co17-41 monmount49 – 1	647	1.11E+05	20500	74830	11240	727	5509	288.8	488	27.25	22.09	1.02	2.76	0.186
Co17-41 monmount50 – 1	11610	1.03E+05	21290	77630	10330	2108	10610	1396	4950	451.1	473.9	24.25	63.2	4.21
Co17-41 monmount51 – 1	500	1.06E+05	21290	77270	9800	550	4200	205	340	20.1	16.9	0.833	1.91	0.151
Co17-41 monmount52 – 1	159.5	1.00E+05	21740	75430	5117	77.1	1020	43.85	87.3	6.72	7.37	0.36	1.07	0.031
Co17-41 monmount53 – 1	171.8	9.97E+04	21530	79850	7870	191.5	1947	77.8	121.3	7	7.04	0.281	0.73	0.054
Co17-41 monmount54 – 1	503	91540	22910	81310	4798	167	1077	61.6	186	20.4	31.9	1.91	7.8	0.59
Co17-41 monmount55 – 1	177	1.01E+05	21540	74030	5091	78.9	1025	45.4	95.9	7.73	8.78	0.506	1.31	0.067
Co17-41 monmount56 – 1	13400	1.15E+05	20740	7.54E+04	10860	3211	9360	1247	5007	546	657	35.76	93.4	6.36

Co17-41 monmount5 6 – 2	10870	9.82E+04	21660	7.70E+04	6760	1478	5010	777	3640	418.7	491	26.42	66.3	4.12
Co17-41 monmount5 7 – 1	10160	9.29E+04	22340	79930	5919	2923	3620	592	3019	392	523	31.04	87.2	5.41
Co17-41 monmount5 7 – 2	11430	1.04E+05	21660	77680	7920	2479	5470	824	3860	452	558	30.15	81.7	5.07
Co17-41 monmount5 7 – 3	11480	9.34E+04	22130	8.01E+04	6290	2689	3991	668	3402	432.6	572	32.14	91.6	5.69
Co17-41 monmount5 8 – 1	10220	9.80E+04	21990	8.04E+04	7310	3073	5313	811	3491	372.4	441.5	24.7	71.9	5.02
Co17-41 monmount5 8 – 2	4370	9.50E+04	22320	7.97E+04	5760	1106	2650	353.8	1539	163.2	202.4	11.06	31.4	2.23
Co17-41 monmount5 9 – 1	11310	1.13E+05	20740	7.44E+04	10090	2385	6970	923	3950	433.8	541	32.3	92.4	6.69
Co17-41 monmount5 9 – 2	9490	1.13E+05	20330	7.46E+04	10120	1916	6320	717	3056	361.6	470	29.3	84.6	6.4
Co17-41 monmount6 0 – 1	3030	1.11E+05	20080	7.42E+04	11050	1600	6820	572	1480	118	124	5.8	16.2	0.97
Co17-41 monmount6 1 – 2	4890	1.09E+05	20630	7.64E+04	11030	1561	5565	514	1815	187.9	233.5	14.18	42.5	3.2
Co17-41 monmount6 2 – 1	5620	9.65E+04	21180	7.53E+04	5880	1371	2788	411.2	1840	211.5	270.2	15.97	47.8	3.27
Co17-41 monmount6 3 – 1	15640	1.19E+05	20330	7.57E+04	12370	2840	12560	1590	5940	616	712	38.7	108.9	7.95
Session 1 - Samples	Y	La	Pr	Nd	Sm	Eu	Gd	Tb	Dy	Ho	Er	Tm	Yb	Lu
Co17-38mon1 - 1	3680	1.11E+05	20340	7.66E+04	12050	646	7460	593	1691	157	199	13.7	49	3.29

Co17-38mon1 - 2	4270	1.12E+05	20830	7.65E+04	12210	765	7740	638	1930	184	249	17	64.2	4.62
Co17-38mon2 - 1	-	-	-	-	-	-	-	-	-	-	-	-	-	-
Co17-38mon2 - 2	-	-	-	-	-	-	-	-	-	-	-	-	-	-
Co17-38mon3 - 1	368	1.08E+05	20830	7.88E+04	11130	255.1	4210	167.7	273	15.6	13.68	0.587	1.6	0.072
Co17-38mon3 - 2	348	1.08E+05	21290	8.14E+04	11120	245.6	4080	161.9	251.9	15.09	14.42	0.72	1.36	0.111
Co17-38mon4 - 1	6970	7.64E+04	26930	1.28E+05	29050	1540	24100	2396	6600	565	482	19.6	46.4	3.55
Co17-38mon4 - 2	15650	7.35E+04	27180	1.23E+05	22220	1689	23630	3122	11770	1168	1004	33.1	66	5.18
Co17-38mon4 - 3	19010	7.10E+04	28830	1.36E+05	26330	1758	30700	4105	15090	1521	1308	43.3	89.5	7.12
Co17-38mon5 - 1	2990	1.10E+05	20740	7.94E+04	12170	694	6850	513	1450	125	143	8.6	28.9	2.09
Co17-38mon5 - 2	561	1.10E+05	20950	8.14E+04	11470	265	4550	222	387	22.3	21.7	0.93	2.26	0.139
Co17-38mon5 - 3	255.1	1.11E+05	21190	8.27E+04	11340	231.8	3813	140.1	193.2	10.95	10.2	0.52	1.69	0.091
Co17-38mon6 - 1	8920	1.14E+05	20350	7.64E+04	13100	1747	9890	1098	3869	388	524	39.5	138	10.5
Co17-38mon6 - 2	8170	1.14E+05	20720	78670	13310	2032	9670	1034	3600	367	505	37.6	140	10.5
Co17-38mon7 - 1	2690	1.43E+05	19070	1.28E+05	2.56E+04	1057	8020	477	1290	118.7	165	13.61	48.3	4.22
Co17-38mon8 - 1	-	-	-	-	-	-	-	-	-	-	-	-	-	-
Co17-38mon8 - 2	-	-	-	-	-	-	-	-	-	-	-	-	-	-
Co17-38mon9 - 1	814	1.10E+05	20770	7.76E+04	11270	507	5248	285.8	569	39.9	35.7	1.51	3.43	0.203
Co17-38mon9 - 2	1570	1.11E+05	20350	7.95E+04	11370	568	5650	352	849	73.7	86.4	5.41	16.7	1.21
Co17-38mon9 - 3	3940	1.10E+05	20470	7.60E+04	11330	817	6180	504	1617	180	279	20.9	78.8	6.03
Co17-38mon10 - 1	583	1.38E+05	18730	8.79E+04	11260	299	2560	122.1	278	24.3	29.9	1.77	5.4	0.47

Co17-38mon10 - 2	1780	1.42E+05	18940	8.74E+04	14220	920	4770	314	830	77	99	6.5	20.9	1.94
Co17-38mon11 - 1	430	1.57E+05	17680	8.46E+04	15860	401	3440	141	264	19.2	18.5	0.95	2.7	0.26
Co17-38mon11 - 2	12060	1.62E+05	17320	8.50E+04	4.19E+04	7030	2.70E+04	2230	6290	546	699	42.7	153	13.7
Co17-38mon11 - 3	174.8	1.22E+05	19760	8.96E+04	7990	84.5	1516	58.1	104.4	7.36	7.58	0.348	0.76	0.022
Co17-38mon13 - 1	3730	1.11E+05	21070	7.83E+04	11390	1495	7620	712	2140	184.3	175.9	7.34	18.2	0.98
Co17-38mon13 - 2	6540	1.12E+05	20760	7.68E+04	12250	1803	9390	1011	3333	300.1	290.8	12.74	29.3	1.98
Co17-38mon13 - 3	6160	1.13E+05	20980	7.82E+04	12760	1969	9000	944	3168	303.5	304.4	13.89	30.8	1.69
Co17-38mon14 - 1	3930	1.09E+05	20780	7.73E+04	12300	1528	8020	774	2312	200.8	198.9	9.27	23.8	1.5
Co17-38mon14 - 2	2248	1.11E+05	20760	7.74E+04	11620	1317	7280	602	1540	118.9	100.8	5	12.6	0.77
Co17-38mon15 - 1	5240	1.16E+05	21360	7.85E+04	12610	1736	7960	774	2554	256	308	19.1	58	3.59
Co17-38mon15 - 2	4062	1.12E+05	21150	7.86E+04	12510	1732	8140	748	2351	215.3	221.3	10.74	25.6	1.6
Co17-38mon15 - 3	3400	1.13E+05	21050	7.77E+04	12360	1578	7610	679	1981	179.1	185.6	9.77	26.1	1.59
Co17-38mon16 - 1	2467	1.10E+05	21270	8.06E+04	13390	192.4	7420	491.6	1217	104.6	112.5	6.52	17.9	1.22
Co17-38mon16 - 2	3610	1.10E+05	21110	8.05E+04	13430	585	8590	699	1944	171.6	177.7	8.7	23.8	1.46
Co17-38mon16 - 3	3829	1.14E+05	20900	7.97E+04	13710	707	8930	762.3	2181	187.6	188.2	9.33	23.6	1.42
Co17-38mon16 - 4	3419	1.10E+05	21030	8.04E+04	13360	207.4	8140	619	1698	158.2	170.6	8.83	24.2	1.3
Co17-38mon18 - 1	1720	1.08E+05	21790	8.07E+04	12590	1119	7230	563	1321	94.9	78	3.44	7.7	0.447
Co17-38mon18 - 2	1044	1.09E+05	21880	8.50E+04	12740	809	5800	351.3	763	55.3	48.4	2.31	4.4	0.374
Co17-38mon18 - 3	1667	1.09E+05	21690	8.40E+04	13340	1114	7470	552	1277	91.8	75.9	3.68	9.2	0.488
Co17-37mon1 - 1	3980	1.04E+05	22080	8.16E+04	9790	595	5560	512	1744	197.4	250	15.86	47.1	3.64

Co17-37mon1 - 2	4401	1.05E+05	22050	7.97E+04	9970	650	5960	555	1934	212.6	274.4	17.39	57.3	4.35
Co17-37mon1 - 3	5670	1.09E+05	21400	7.92E+04	10890	736	7160	692	2480	271.7	348	22.04	71.4	5.35
Co17-37mon2 - 1	-	-	-	-	-	-	-	-	-	-	-	-	-	-
Co17-37mon2 - 2	-	-	-	-	-	-	-	-	-	-	-	-	-	-
Co17-37mon4 - 1	4820	1.13E+05	20240	7.51E+04	12130	858	7000	621	2072	214.5	253	13.4	29.6	1.53
Co17-37mon4 - 2	4631	1.13E+05	20170	7.66E+04	12700	855	7500	652	2081	207.6	214.7	10.19	23	1.14
Co17-37mon4 - 3	2853	1.09E+05	20430	7.56E+04	12170	741	6940	520.6	1382	124.2	127.4	6.44	16.7	1.02
Co17-37mon6 - 1	2090	1.07E+05	20970	7.89E+04	12560	571	7260	549	1364	98	73.7	2.76	4.21	0.323
Co17-37mon6 - 2	3360	1.10E+05	20570	7.72E+04	12980	676	8150	662	1798	143.8	133.5	5.58	13.1	0.76
Co17-37mon6 - 3	690	1.09E+05	21180	7.87E+04	9530	227	3550	201	449	31.4	27.1	0.99	2.01	0.106
Co17-37mon6 - 4	3460	1.10E+05	20920	7.86E+04	13240	782	8450	701	1989	172	168.9	8.16	19.7	1.22
Session 3 - Samples	Y	La	Pr	Nd	Sm	Eu	Gd	Tb	Dy	Ho	Er	Tm	Yb	Lu
Co17-37mon1r - 1	5980	1.05E+05	21430	8.08E+04	10960	726	7280	709	2610	282.8	378	22.72	74.4	5.8
Co17-37mon1r - 2	7970	1.01E+05	22190	9.16E+04	13480	533	6570	733	3172	370.2	505.1	28.47	87.2	6.37
Co17-37mon1r - 3	6120	1.04E+05	21740	8.59E+04	11230	604	6610	647	2490	280	387	24.3	78.8	6.03
Co17-37mon1c - 1	5030	1.05E+05	21530	8.36E+04	10580	672.5	6710	617	2211	238.7	316	19.16	62.1	4.46
Co17-37mon7 - 1	5890	1.11E+05	20690	8.37E+04	12830	670	7000	565	2080	252	405	28	105	8.31
Co17-37mon7 - 2	3560	1.14E+05	20540	8.42E+04	13890	1540	7640	577	1629	143.5	177	10.67	33.7	2.4
Co17-37mon2c - 1	3510	1.18E+05	20240	7.84E+04	12160	363.2	6454	442.5	1323	139.6	211.7	14.06	48.6	4.21
Co17-37mon2r - 1	2450	1.12E+05	20590	8.17E+04	10910	297	5070	321	940	98	143	9.3	33.3	2.85

Co17-37mon2r - 2	3540	1.20E+05	20040	7.63E+04	12510	468	6340	432	1348	143.3	215	14.62	53.7	4.68
Co17-37mon3c - 1	3.70E+04	8.51E+04	18910	8.34E+04	1.15E+04	707	3550	411	3.70E+03	1170	4.60E+03	1000	9.60E+03	1640
Co17-37mon3r - 1	2400	1.27E+05	18030	1.22E+05	3.58E+04	1480	1.06E+04	510	1100	86	127	12.9	67	11.3
Co17-37mon5c - 1	1120	1.05E+05	20510	8.01E+04	10600	220	4590	278	650	44	47	2.84	8.1	0.63
Co17-37mon6r - 1	2700	1.08E+05	20550	8.13E+04	12630	398.4	7520	563	1477	108.9	106.5	5.01	13.6	0.99
Co17-37mon6r - 2	1330	1.10E+05	20570	8.06E+04	11310	425	7110	484	1090	59.6	42.8	1.59	3.53	0.194
Co17-37mon6r - 3	2870	1.09E+05	20660	8.16E+04	12230	639	7070	534	1531	128.1	125	4.95	11.1	0.62
Co17-37mon4 r - 1	279.5	1.05E+05	20810	8.06E+04	10350	213.6	3254	117.5	194.1	12.29	12.25	0.513	1.91	0.095
Co17-37mon4 r - 2	800	1.07E+05	19450	7.92E+04	9710	235	3180	177	468	38.4	37.1	1.75	4.2	0.265
Co17-37mon4 r - 3	1730	1.05E+05	20610	8.03E+04	10190	207	5070	337	935	77.4	82.3	3.6	7.6	0.45
Co17-37mon4c - 1	3168	1.11E+05	20360	8.00E+04	12450	738	7830	571	1615	138.1	145.7	6.32	13.69	0.715
Co17-37mon4c - 2	5100	1.09E+05	20180	7.87E+04	11790	862	7230	645	2251	222.4	259.3	12.11	29	1.7
Co17-37mon4c - 3	-	-	-	-	-	-	-	-	-	-	-	-	-	-
Co17-37mon8c - 1	97.1	1.06E+05	20970	8.19E+04	9190	103.9	2066	57.3	77.6	4.11	5.41	0.18	0.56	0.024

APPENDIX G: GARNET TRACE ELEMENT ANALYSES

Standards	La	Ce	Pr	Nd	Sm	Eu	Gd	Tb	Dy	Ho	Er	Tm	Yb	Lu	Y
NIST - 1	253.3	257.4	252.7	241.8	242.6	252.7	260.2	250.4	248.5	240.3	251.1	239.8	235.6	250.5	244.4
NIST - 2	250.1	254.1	248.7	240.3	239.1	251	256	246.2	245.9	236.3	249.2	236.2	233.4	247.5	241.3
NIST - 3	253.3	258.1	253	242.9	241.8	253	260.1	250.2	249.4	240.3	252.8	240.5	236.2	250.5	244.3
NIST - 4	250.6	254	249.9	238.3	241.2	252.3	255.9	247.9	247.4	238.6	251.2	237.5	234.2	248.5	243
NIST - 5	250.8	253.9	249.9	239.4	240.8	251.5	257.3	246.7	246.9	238.8	250.6	237.8	233.9	247	243
NIST - 6	251.7	254.8	249.4	239.8	240.6	252.2	257.7	248.6	249	238.7	252.6	238.4	235.9	248.8	243.8
NIST - 7	251.9	254.3	250.2	239.4	240.4	252.2	256.9	246.5	246.4	237.4	250.2	237.2	233.9	248.2	242.9
NIST - 8	251.3	254.8	249.3	240.3	240.4	251.2	256.8	247	247.4	237.4	250.9	236.5	234.5	248.1	242.4
NIST - 9	250.5	254.9	249.3	239	240.1	251.5	256	246.9	245.3	238	248.1	236.4	233.8	246.7	241.3
NIST - 10	252.6	256.4	252	240.4	241.4	253.4	258.5	248.6	248.5	240	251.5	239.2	236.7	249	244.2
NIST - 11	252.9	256.9	252.5	240.9	241.9	252.8	257.1	250.8	248.1	239.1	251	239.3	234.2	249.7	242.8
NIST - 12	250.3	253.6	249.8	239.2	239.8	250.1	256.4	247.6	246.2	238.1	250.3	235.9	233.5	247.2	241.7
NIST - 13	251.5	257.4	250.9	241.6	241.5	253.8	260.5	249.5	248.8	240.2	252.4	239.4	235.8	251	245.5
NIST - 14	251.8	255	249.8	241.8	241.4	251.2	257.1	248.2	248.5	238.1	251.5	238.5	234.5	249.6	243.3

Samples	La	Ce	Pr	Nd	Sm	Eu	Gd	Tb	Dy	Ho	Er	Tm	Yb	Lu	Y
Co17-37 garnet - 1	106.1	0.026	0.041	0.0034	0.071	3.2	0.385	12.2	2.569	18.93	3.7	9.23	1.222	7.96	1.02
Co17-37 garnet - 2	108.4	0.048	0.054	0.0071	0.064	3.6	0.398	12.34	2.515	18.81	3.74	9.16	1.187	7.57	0.94
Co17-37 garnet - 3	106.1	0.019	0.02	0.0016	0.132	3.88	0.338	11.74	2.518	18.91	3.67	8.88	1.15	7.45	0.898
Co17-37 garnet - 4	105.1	0.046	0.083	0.0086	0.136	3.69	0.361	11.54	2.374	18.48	3.534	9	1.127	7.6	0.84
Co17-37 garnet - 5	102.1	0.021	0.036	0.0056	0.058	3.53	0.327	10.6	2.344	17.08	3.31	8.21	1.025	6.4	0.808
Co17-37 garnet - 6	108.9	0.0079	0.0167	0.0013	0.067	3.32	0.338	10.88	2.38	19.62	3.73	8.88	1.123	7.15	0.891
Co17-37 garnet - 7	120.4	0.52	1.03	0.073	0.35	3.1	0.277	10.9	2.437	20.24	4.22	10.38	1.287	8.56	0.974
Co17-37 garnet - 8	133.8	0.081	0.131	0.0156	0.12	3.08	0.26	10.76	2.49	21.85	4.7	11.97	1.551	10.27	1.226
Co17-37 garnet - 9	163.5	0.0043	0.005	0.0044	0.044	3.86	0.302	11.36	2.715	24.42	5.8	16.46	2.222	14.76	1.774
Co17-37 garnet - 10	189.8	1.51E-06	7.76E-07	0.0006	0.058	3.8	0.282	10.62	2.69	26.44	7	21.96	3.27	21.35	2.85
Co17-37 garnet - 11	218.8	0.066	0.19	0.02	0.195	3.27	0.309	10.62	2.603	28.23	8.37	28.47	4.23	29.95	4.23

Co17-37 garnet - 12	258.3	0.015	0.051	0.0051	0.08	3.06	0.238	9.63	2.588	31.3	10.38	38.2	5.79	41.3	6.18
Co17-37 garnet - 13	301.5	1.9	3.1	0.26	1.4	3.04	0.232	8.84	2.74	37.02	13.38	50.4	7.76	55.4	8.56
Co17-37 garnet - 14	406.3	0.0021	0.0037	-2.7E-06	0.076	2.49	0.203	8.41	3.07	47.4	18.07	73.7	11.64	85.7	13.78
Co17-37 garnet - 15	513	0.0014	0.0068	-2.7E-06	0.076	2.47	0.211	8.46	3.68	59.6	23.78	99.1	15.9	117	18.97
Co17-37 garnet - 16	530.5	7.74E-07	2.85E-07	-2.2E-06	0.06	2.31	0.161	8.17	3.63	59.38	24.16	101.6	16.63	125.2	20.24
Co17-37 garnet - 17	576.6	7.47E-07	2.53E-07	-2.3E-06	0.086	2.74	0.187	8.52	3.92	64.3	25.59	109	18.19	137.2	22.04
Co17-37 garnet - 18	582	6.61E-07	2.02E-07	-2.2E-06	0.097	2.76	0.2	8.15	3.83	64	25.86	108.7	18.13	138.9	22.84
Co17-37 garnet - 19	598	5.95E-07	1.58E-07	-2.2E-06	0.101	2.58	0.213	8.16	3.99	65.7	26.17	111	18.55	142.7	23.47
Co17-37 garnet - 20	611	5.50E-07	1.14E-07	-2.2E-06	0.087	2.24	0.158	7.93	4.08	65.7	25.94	109.7	18.82	148.4	24.14
Co17-37 garnet - 21	606.8	4.45E-07	6.40E-08	-2.1E-06	0.08	2.27	0.163	7.74	3.98	65.9	25.58	108.1	18.87	146.7	23.82
Co17-37 garnet - 22	611	3.85E-07	2.05E-08	-2.1E-06	0.08	2.07	0.167	7.31	4.08	65.8	25.89	107.6	18.56	147.1	23.81
Co17-37 garnet - 23	608	0.0037	0.016	0.0011	0.051	1.44	0.155	6.83	4.02	65.9	25.45	106.1	18.66	148	23.9
Co17-37 garnet - 24	644	0.0014	0.006	-2.2E-06	0.094	1.93	0.165	7.42	4.21	69.2	26.51	113.1	19.46	156.1	25.11
Co17-37 garnet - 25	594	2.12E-07	-1.28E-07	0.0063	0.026	1.11	0.143	6.31	3.69	64.3	25.28	107.4	18.76	148.6	23.93
Co17-37 garnet - 26	612	0.0072	0.044	0.0078	0.032	1.46	0.153	6.65	3.72	65.4	26.3	112.6	19.19	150.9	24.6
Co17-37 garnet - 27	622	0.003	0.017	0.0024	0.073	2.04	0.123	7.18	3.89	67.7	27.19	115.5	20.01	151.5	25.1
Co17-37 garnet - 28	616	-5.40E-09	-2.65E-07	0.0005	0.04	2.2	0.177	7.13	3.89	66.4	26.8	115.3	19.53	152.6	24.26
Co17-37 garnet - 29	605	-6.91E-08	-3.04E-07	-1.8E-06	0.059	2.19	0.165	7.44	3.83	66.6	27	115.9	19.28	148.6	24.17
Co17-37 garnet - 30	544	-1.46E-07	-3.76E-07	-1.9E-06	0.056	2.79	0.175	7.81	3.67	60.4	24.98	106.6	17.54	133	21.5
Co17-37 garnet - 31	501	0.0021	0.0111	0.0027	0.112	2.91	0.184	8.51	3.37	56.2	23.55	100	16.45	125	20.4

Co17-37 garnet - 32	470.6	-5.67E-07	0.0029	-1.6E-06	0.072	3.21	0.189	8.26	3.26	52.4	22.36	93.8	15.29	113.5	18.58
Co17-37 garnet - 33	395.8	98	179	22.6	188	54	0.86	19.3	3.64	46.2	18.47	76.1	12.33	93.1	15.08
Co17-37 garnet - 34	284	0.017	0.055	0.0034	0.06	3.08	0.264	9	2.329	31.74	12.64	53.5	8.61	65.3	10.36
Co17-37 garnet - 35	248.8	0.022	0.07	0.004	0.079	2.51	0.25	8.55	2.132	27.44	10.78	45.6	7.37	55.9	9
Co17-37 garnet - 36	214.5	0.031	0.052	0.0037	0.04	1.29	0.304	8.38	2.081	24.28	8.95	35.39	5.92	44.9	6.8
Co17-37 garnet - 37	188.6	0.175	0.35	0.031	0.092	0.34	0.364	4.11	1.676	20.87	7.42	29.6	4.92	35.96	5.15
Co17-37 garnet - 38	161.1	0.04	0.05	0.0022	0.039	1.18	0.35	9.61	2.179	20.47	5.98	21	3.26	23.24	3.281
Co17-37 garnet - 39	173.6	0.0112	0.0134	0.0015	-4.6E-06	1.1	0.305	7.33	2.08	21.22	6.2	22.15	3.598	25.75	3.31
Co17-37 garnet - 40	134.6	2	2.4	0.23	2.3	4.25	0.373	10.98	2.136	17.83	4.83	15.96	2.488	18.24	2.372
Co17-37 garnet - 41	134.3	0.038	0.073	0.0034	0.09	3.15	0.35	11.17	2.153	18.37	4.76	15.55	2.375	17.47	2.214
Co17-37 garnet - 42	126.5	0.0173	0.051	0.003	0.044	2.66	0.374	11.84	2.333	18	4.47	14.05	2.108	15.38	1.959
Co17-38 garnetA - 1	90.1	-1.3E-06	-1.1E-06	0.0034	0.518	4.64	0.382	10.79	2.284	16.11	3.109	7.93	1.06	7.11	0.968
Co17-38 garnetA - 2	98.5	-1.4E-06	0.002	0.0086	0.79	4.91	0.373	11.41	2.391	18.01	3.45	8.91	1.205	8.06	1.062
Co17-38 garnetA - 3	111.8	0.0033	0.0065	0.0084	0.74	5.18	0.322	11.69	2.799	20.22	3.95	10.21	1.307	8.65	1.215
Co17-38 garnetA - 4	118.2	-1.8E-06	-1.4E-06	0.0098	0.7	4.82	0.294	10.55	2.89	21.87	4.25	10.79	1.436	9.22	1.168
Co17-38 garnetA - 5	124.6	0.029	0.072	0.0142	0.82	4.52	0.255	10.51	3	23.28	4.51	11.4	1.423	9.46	1.236
Co17-38 garnetA - 6	136.2	0.35	0.8	0.1	1.3	4.21	0.282	10.43	2.949	23.88	4.9	12.55	1.743	12.43	1.852
Co17-38 garnetA - 7	126.7	0.0008	0.016	0.0036	0.306	3.57	0.224	9.24	2.81	23.11	4.64	11.27	1.394	8.96	1.125
Co17-38 garnetA - 8	129.1	0.0027	0.0027	0.0056	0.398	3.35	0.242	9.46	2.74	23.44	4.69	11.13	1.447	9.41	1.112
Co17-38 garnetA - 9	126.4	0.0105	0.013	0.0035	0.208	3.12	0.24	8.24	2.761	22.27	4.57	11.13	1.371	9.04	1.114

Co17-38 garnetA - 10	123.8	0.0014	0.0023	-6.23E-07	0.133	2.6	0.212	8.12	2.536	22.07	4.31	10.47	1.32	8.69	1.07
Co17-38 garnetA - 11	134.5	-2.3E-06	0.01	-5.96E-07	0.143	2.55	0.21	8.01	2.833	23.56	4.56	12.01	1.545	10.54	1.373
Co17-38 garnetA - 12	141.3	0.0031	0.021	0.0029	0.089	2.21	0.201	7.72	2.747	24.35	4.88	12.05	1.569	10.25	1.278
Co17-38 garnetA - 13	182.1	0.0081	0.0082	0.0032	0.153	3.23	0.275	9.79	3.44	30.76	6.44	16.28	2.056	14.35	1.781
Co17-38 garnetA - 14	180.9	-2.5E-06	0.0056	-4.79E-07	0.088	2.17	0.253	8.46	3.17	29.77	6.31	16.86	2.236	14.75	1.991
Co17-38 garnetA - 15	206.3	0.0083	0.025	0.0075	0.43	3.79	0.28	9.02	3.33	32.4	7.48	20.77	2.8	19.52	2.65
Co17-38 garnetA - 16	230.4	0.0031	-2.2E-06	0.0027	0.482	3.94	0.301	9.99	3.47	35.5	8.57	25.35	3.62	24.26	3.55
Co17-38 garnetA - 17	228.4	-2.7E-06	-2.1E-06	0.0022	0.295	3.66	0.298	9.01	3.27	34.37	8.62	25.91	3.75	25.46	3.74
Co17-38 garnetA - 18	240.4	-2.8E-06	0.0019	-3.39E-07	0.183	3.87	0.292	9.31	3.43	34.1	9.17	28.78	4.14	28.79	4.23
Co17-38 garnetA - 19	229.6	-3E-06	-2.4E-06	0.0006	0.309	3.58	0.35	9.24	3.2	33.65	8.91	28.32	3.99	28.4	4.26
Co17-38 garnetA - 20	230.2	-3.1E-06	-2.4E-06	-9.49E-08	0.217	3.97	0.319	9.24	3.21	33.87	8.94	28.37	4.06	28.79	4.34
Co17-38 garnetA - 21	225.2	-3.2E-06	0.0035	0.0017	0.334	4.07	0.31	9.26	3.21	33.1	8.47	27.37	3.93	27.8	4.18
Co17-38 garnetA - 22	206.7	-3.2E-06	0.0033	-1.48E-08	0.061	2.95	0.245	9.21	2.935	30.59	8.01	25.13	3.491	24.83	3.71
Co17-38 garnetA - 23	181.4	0.0059	0.0084	0.0011	0.035	1.79	0.211	8.03	2.73	27.52	7.04	21.88	3.04	20.7	3.07
Co17-38 garnetA - 24	169.7	-3.4E-06	-2.6E-06	5.91E-08	0.153	2.67	0.247	8.31	2.649	25.86	6.37	19.55	2.687	18.31	2.616
Co17-38 garnetA - 25	142.7	0.003	-2.6E-06	9.66E-08	0.124	2.71	0.261	7.62	2.305	22.23	5.5	15.44	2.102	14.61	1.994
Co17-38 garnetA - 26	131.3	0.004	0.0041	1.39E-07	0.114	2.88	0.281	7.69	2.316	20.97	4.9	14.07	1.895	12.79	1.762
Co17-38 garnetA - 27	128.3	-3.6E-06	-2.7E-06	1.72E-07	0.052	2.93	0.253	8.03	2.293	20.84	4.68	13.28	1.814	11.77	1.594
Co17-38 garnetA - 28	112.7	-3.7E-06	-2.8E-06	2.09E-07	0.08	2.71	0.22	7.82	2.157	18.42	4.04	10.84	1.479	9.61	1.325
Co17-38 garnetA - 29	114.5	-3.7E-06	-2.8E-06	2.47E-07	0.228	3.56	0.235	8.67	2.347	19.02	4.09	10.54	1.387	9.54	1.203

Co17-38 garnetA - 30	113.2	0.0022	0.01	0.0061	0.424	3.99	0.287	8.77	2.319	18.94	3.86	9.83	1.265	8.56	1.082
Co17-38 garnetA - 31	105.9	1.8	3.5	0.4	4.8	5.35	0.3	9.61	2.305	18.25	3.58	9.04	1.153	7.62	0.952
Co17-38 garnetA - 32	106.8	12.1	20	1.9	17	9.6	0.374	11.1	2.45	18.51	3.55	8.83	1.169	7.69	0.982
Co17-38 garnetA - 33	90.4	0.2	0.33	0.042	0.89	4.36	0.365	10.02	2.117	16.02	2.86	6.82	0.87	5.73	0.719
Co17-38 garnetA - 34	86.1	1.42	2	0.19	2.1	4.78	0.34	10.83	2.21	15.47	2.824	6.36	0.868	5.48	0.675
Co17-38 garnetB - 1	103.5	0.0021	-3.6E-06	0.0012	0.077	3.73	0.321	9.24	2.275	18.01	3.78	9.85	1.339	8.99	1.18
Co17-38 garnetB - 2	108.9	-4.7E-06	0.0047	6.94E-07	0.102	3.52	0.327	8.88	2.326	19.42	3.86	10.22	1.378	9.15	1.252
Co17-38 garnetB - 3	117.5	0.033	0.061	0.0062	0.164	2.84	0.274	9.08	2.467	20.7	4.3	11.31	1.444	10.08	1.333
Co17-38 garnetB - 4	121.2	0.65	1.11	0.113	0.76	3.83	0.314	9.21	2.567	21.47	4.41	11.72	1.546	10.58	1.367
Co17-38 garnetB - 5	122.8	0.0076	0.0084	7.53E-07	0.188	3.4	0.23	7.82	2.446	21.35	4.35	11.44	1.546	10.35	1.342
Co17-38 garnetB - 6	127.1	-4.8E-06	0.0073	0.0034	0.283	3.46	0.254	8.34	2.556	22.33	4.68	11.71	1.55	10.65	1.402
Co17-38 garnetB - 7	128.6	-4.9E-06	0.008	0.0024	0.55	3.23	0.206	8.39	2.65	23.39	4.69	12.18	1.577	10.91	1.413
Co17-38 garnetB - 8	129	-5E-06	0.0061	9.15E-07	0.25	3.04	0.268	7.84	2.67	22.49	4.56	12.06	1.562	10.55	1.42
Co17-38 garnetB - 9	131.3	4.4	8.6	0.97	6.1	4.7	0.268	8.55	2.61	23.39	4.68	12.17	1.63	11.15	1.381
Co17-38 garnetB - 10	130.1	0.0046	0.027	0.0031	0.136	2.44	0.211	7.61	2.686	22.41	4.77	12.08	1.667	10.52	1.474
Co17-38 garnetB - 11	136.3	0.0016	-3.8E-06	1.03E-06	0.215	3.01	0.238	7.88	2.708	24.05	4.91	12.38	1.649	11.31	1.428
Co17-38 garnetB - 12	133.2	-5.2E-06	0.0006	1.06E-06	0.218	3.01	0.217	8.16	2.672	23.19	4.82	11.97	1.635	11.05	1.401

APPENDIX H: WHOLE-ROCK GEOCHEMISTRY

Whole-rock chemical compositions were calculated for a total of twenty-two samples. Two samples were used in the calculation of metamorphic phase diagrams. These values were calculated at Franklin & Marshall College, Lancaster, Pennsylvania. Small representative blocks (50mm x 100mm) of each sample were sent away where they were crushed and homogenized using a tungsten carbide mill. Sending full blocks reduces the surface area of the sample, limiting the amount of oxidation that can take place before geochemical analysis. Major elements were analysed by fusing 0.1 g of the powdered sample with lithium metaborate before dissolution and analysis using inductively coupled plasma-optical emission spectroscopy (ICP-OES). Trace elements were analysed by digestion of the analytical pulp in HF acid before analysis using ICP-MS. Titration methods were used to determine the amount of FeO and Fe_2O_3.

Specimen	*Co17-37*	*Co17-38*	*Co17-41*		*Co17-37*	*Co17-38*	*Co17-41*
Major Oxides %				Trace Elements ppm			
SiO2	48.97	54.3	84.34	Rb	96	43.5	25.5
TiO2	0.75	1.14	0.3	Sr	138	46	39
Al2O3	34.43	26.6	7.94	Y	60.7	58.5	24.6
Fe2O3T	6.99	8.76	3.39	Zr	139	175	197
MnO	0.11	0.13	0.08	V	257	265	61
MgO	4.63	5.86	2.22	Ni	194	439	166
CaO	0.48	0.48	0.18	Cr	986	1025	549
Na2O	0.62	0.47	0.31	Nb	17.1	16.8	4.8
K2O	2.8	1.89	0.97	Ga	56.9	41.1	11.8
P2O5	0.04	0.03	0.03	Cu	41	36	34
Total	99.82	99.66	99.76	Zn	93	140	63
				Co	39	56	16
% LOI and FeO Titration values				Ba	646	216	201
LOI	0.93	0.93	0.57	La	28	12	21
FeO	5.83	5.95	2.72	Ce	43	17	37
Fe2O3	0.510841	2.147479	0.367133	U	<0.5	0.5	<0.5
				Th	6.9	8.8	15.9
				Sc	16	18	1
				Pb	2	<1	10

Bulk-rock geochemical data for the samples used in the study. Major oxides, LOI (loss on ignition) and FeO titration (relating to oxidation) are presented on the left, while trace elements are presented on the right.

APPENDIX I: EPMA ANALYSES RESULTS

Representative EPMA mineral oxide and halogen values. Appropriate elements are presented for each mineral.

	MgO	FeO	CaO	MnO	Na_2O	K_2O	Al_2O_3	Cl^-	F^-
Co17-37 garnet core	12.64	24.43	0.89	0.34	0.0232	0	22.6	-	-
Co17-37 garnet rim	9.80	27.31	1.27	0.47	0.0294	0.001	22.1	-	-
Co17-37 biotite incl.	22.49	4.63	-	-	0.3294	9.31	17.16	0.0103	0.722
Co17-37 matrix biotite	21.63	6.29	-	-	0.3728	9.08	18.26	0.0060	0.1985
Co17-38 garnet core	14.91	20.66	1.47	0.30	0.0203	0	22.75	-	-
Co17-38 garnet rim	9.38	28.57	1.23	0.61	0.0022	0	21.88	-	-
Co17-38 biotite incl.	23.02	3.53	-	-	0.7097	8.04	17.74	0.0086	0.861
Co17-38 matrix biotite	18.45	8.84	-	-	0.5209	8.49	17.03	0.017	0.113
Co17-38 plagioclase	-	-	-	-	8.327	0.019	-	-	-

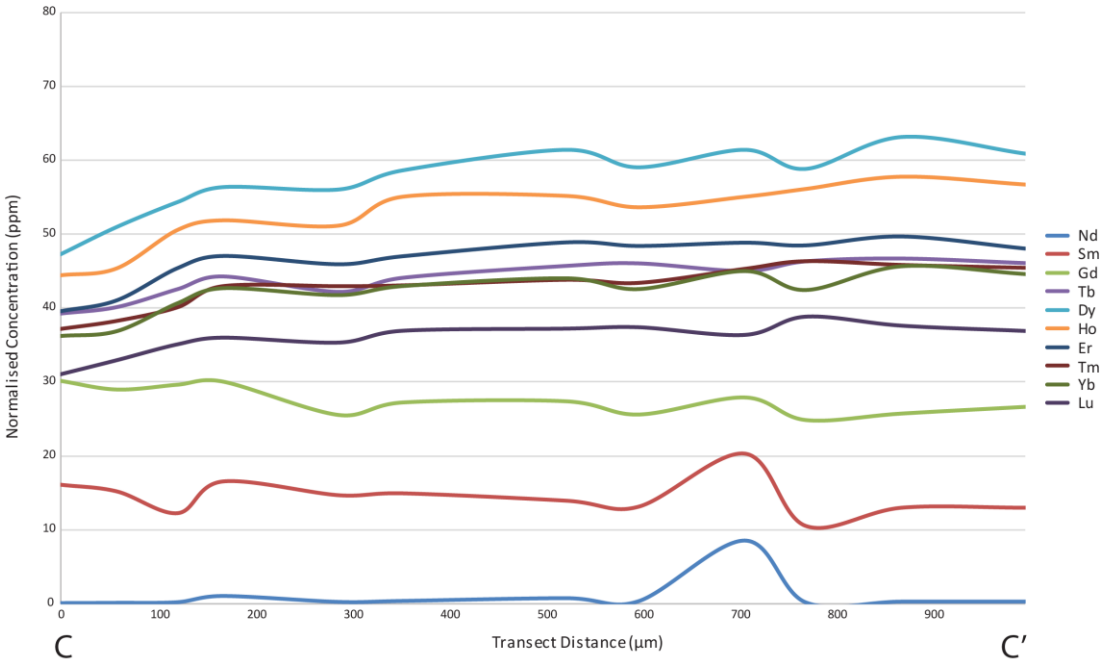

REE transect C–C' in garnet rim of Co17-38 (Fig. 5b). HREE are generally more enriched, while LREE are relatively depleted. MREE (middle-REE) are most enriched.

APPENDIX J: EXTENDED PHASE EQUILIBRIA FORWARD MODELLING METHODS

Prior to calculating a phase equilibrium pseudosection using THERMOCALC, the user must first use petrographic relationships to identify the stable assemblage within the sample to be modelled. The initial stable assemblage is determined by using a Gibbs energy minimization calculation at a set pressure–temperature (*P–T*) condition. The diagram is progressively built up from that initial assemblage, by the calculation of points and lines through trial and error to determine which phases appear or disappear as a function of pressure, temperature and composition. Lines represent the zero abundance of a phase and points signify the zero abundance of two phases, where four stability fields intersect. A good understanding of stable metamorphic assemblages across varying *P–T* space is required to predict the addition of new minerals into the assemblage, as the addition of accessory minerals can often be subtle and sometimes missed, resulting in the loss of many calculations. THERMOCALC software also needs to be understood in terms of how it calculates its 'starting guesses'. These are values for compositional variables of phases from which THERMOCALC commences its iterative least-squares calculation when calculating a point or line. This needs to be updated constantly, as calculations take place in differing parts of P–T–X (X = composition) space. The choice of starting guess can not only affect how a point or line plots, but also THERMOCALC's ability to calculate a point or line at all. The principal uncertainties on bulk composition for calculating mineral equilibria are H_2O and Fe_2O_3 (Johnson & White, 2011). $T–M_{H2O}$ and *P–Mo* diagrams are used to more accurately constrain the abundances of H_2O and Fe_2O_3 (oxidation state) as whole rock geochemical analyses are unreliable. Amounts of H_2O and Fe_2O_3 are selected from the $T–M_{H2O}$ and *P–Mo* diagrams for *P–T* modelling of samples as they correspond to the stable assemblage of the interpreted peak metamorphic assemblage observed in the rock. The choice of temperature to calculate the P–Mo is broadly estimating the pressure at which the observed peak metamorphic assemblage is stable. The pressure of the following $T–M_{H2O}$ is constrained by the peak field in the *P–Mo* diagram. These models are calculated by the same method as *P–T* phase equilibria models.

The contouring of phase equilibria models for the normalised abundances ('mode) of phases was calculated using Matlab-based, automated software TCInvestigator v2.0 (Pearce et al., 2015). Input to TCI requires THERMOCALC input files and executable (.exe) files as well as the finished P–T model from THERMOCALC.

APPENDIX K: EXTENDED GEOMORPHOLOGICAL ZIRCON ANALYSIS

CO17-37

In-situ zircons range in size from 10 µm to 120 µm, and are most commonly located in kyanite (Fig. 7a). Zircon grains are largely anhedral, with aspect ratios between 1–2. Most analysed grains display metamorphic textures, commonly observed in zircons grown from melt in ultra-high pressure (UHP) to upper granulite facies conditions (e.g. Stepanov et al., 2016). Fir-tree textures, associated with high-pressure metamorphism (e.g. Root et al., 2004) were also observed (Fig. 7a.2). Larger grains often preserve weakly concentric detrital cores, with overgrown metamorphic rims (Fig. 7a.1, a.4). These textures are widely reported to form during partial melting, particularly in the leucosomes of rocks of pelitic/arkosic compositions (Rubatto et al., 2001; Williams 2001). Ages from rims and cores are variable, with rims sometimes being older than cores (Fig. 7a.1). No relationship with Th and U concentrations between cores and rims was found.

CO17-38

In-situ zircons range in size from 10 µm to 120 µm and are found in a range of different phases (Fig. 7b). Grain mounted zircons are as large as 250 µm (Fig. 7c). This sample displayed variations in zircon morphology. Metamorphosed textures, largely associated with growth from melt in UHP to granulite facies conditions occur. These include fir-tree textures (Fig. 7b.1, 7b.2, 7c.5) and grains with characteristic textures of metamorphic growth around a detrital core (Fig. 7c.1, 7c.6). Zircons displaying metamorphic textures are often anhedral, with aspect ratios close to 1. These analyses provided ages < 3200 Ma. Euhedral to sub-rounded grains, with aspect ratios of 2–3, display concentric zoning patterns typically associated with igneous formation. These grains provide a range of ages, commonly > 3200 Ma (Fig. 7b.3, 7c.2, 7c.4). Five zircons were analysed within garnet, yielding ages between 3286–3120 Ma. These grains displayed mostly concentric zoning. Zircons in kyanite and biotite provided ages of 3156–2777 Ma, while a single zircon analysis within plagioclase returned an age of 2293 $\pm$ 39 Ma. Ages of rims and cores were again variable, with rims sometimes being older than cores (Fig. 7c.5). No relationship with Th and U concentrations between cores and rims was found.

CO17-41

In-situ zircons ranged in size from 10 µm to 180 µm and are predominately found in quartz and biotite (Fig. 7d). Grain mounted zircons are as large as 260 µm (Fig. 7e). A greater proportion of grains analysed appear to be inherited, and are euhedral to sub-

rounded in shape with concentric zoning patterns and aspect ratios between 2–3. These grains commonly provide ages > 3000 Ma, ranging up to 3800 Ma. (Fig. 7d.2, d.4, e.1, e.2, e.4). Zircons displaying metamorphic textures are mostly anhedral, with aspect ratios of 1–2. The textures that characterised the zircons are commonly associated with growth from melt in UHP to granulite facies conditions (e.g. Stepanov et al., 2016). Fir-tree textures (Fig. 7e.3) and metamorphic rims around inherited cores (Fig. 7d.1, 7d.3) are most common. For the most part, these grains provide ages < 3000 Ma (Fig. 7d, 7e). No relationship between mineral phase and age can be made from in-situ analyses (Fig. 7d). Ages in rims and cores are again variable, with rims sometimes older than cores (Fig. 7e.6). No relationship with Th and U concentrations between cores and rims could be identified.

APPENDIX L: SAMPLE CO17-37 P–M_O AND T–M_{H2O} PHASE EQUILIBRIA MODELS

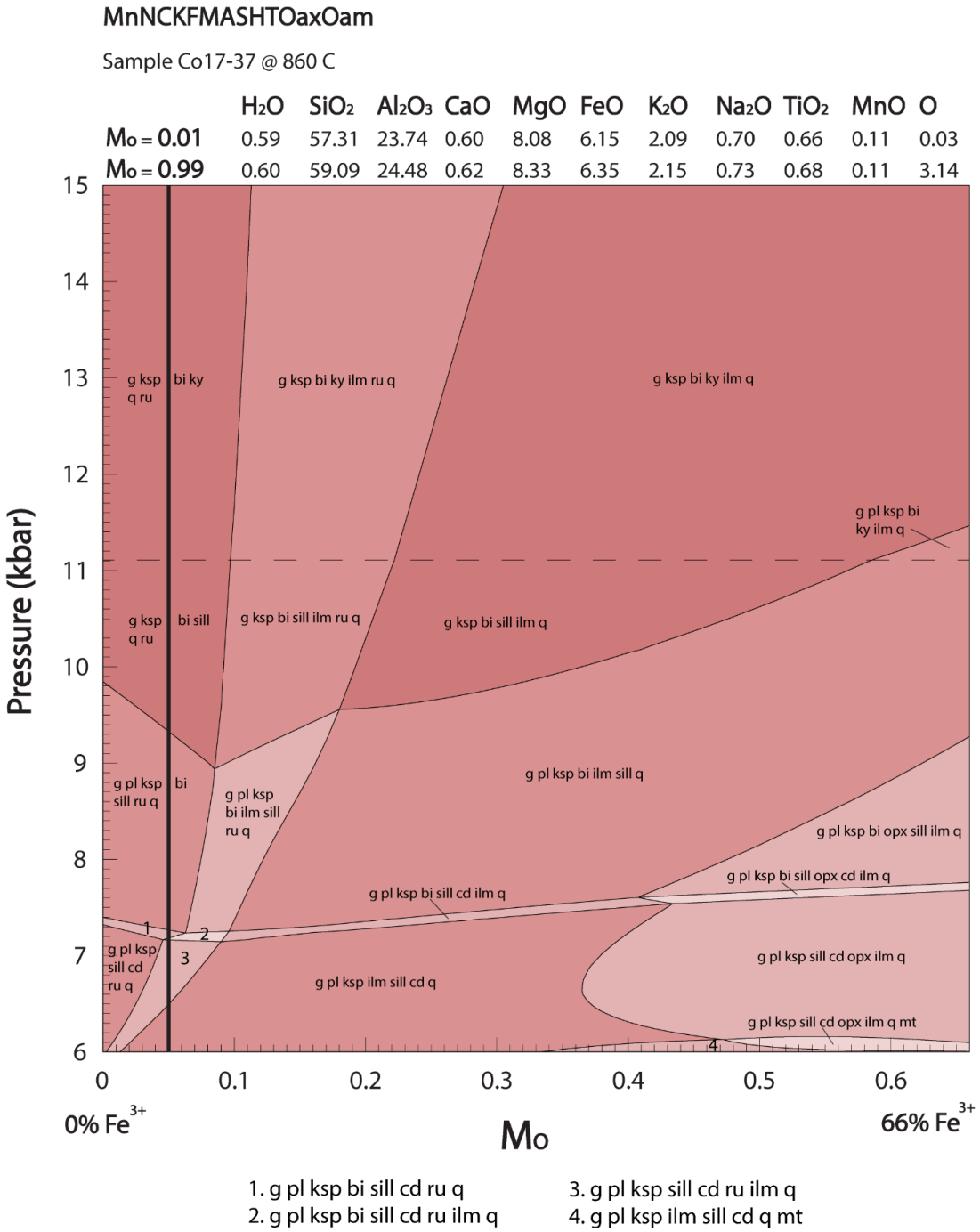

***P–Mo* diagram for sample Co17-37. The black line at M = 0.05 corresponds to the composition at which the *T–M_{H2O} and P–T* diagrams were calculated for Co17-37. This is constrained by the presence of rutile without ilmenite.**

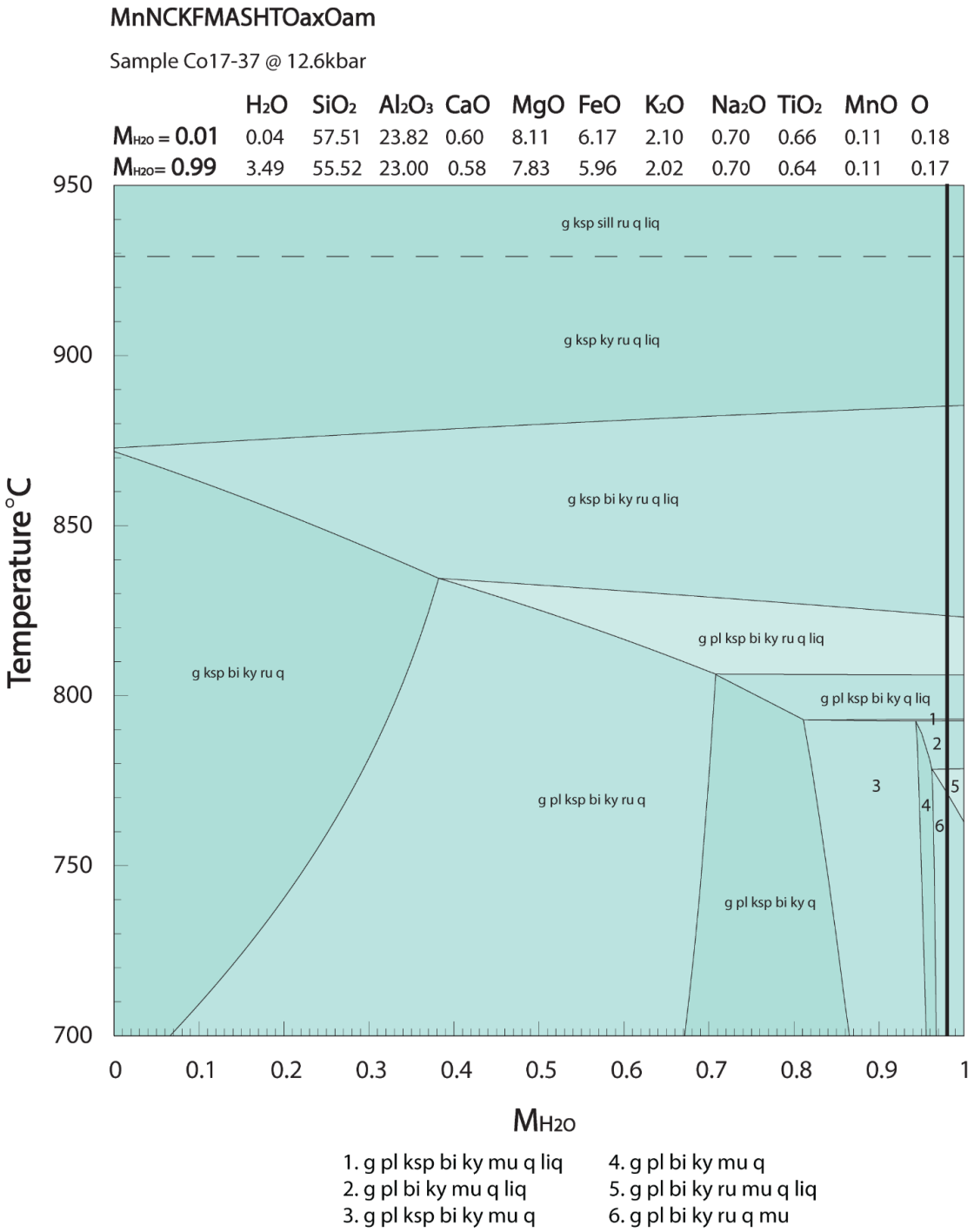

***T–M*$_{H2O}$ diagram for sample Co17-37. The black line at M = 0.98 corresponds to the composition at which the *P–T* diagram was calculated for Co17-37. This level of hydration is supported by EPMA data, where low halogen concentrations have been recorded in biotite.**

APPENDIX M: SAMPLE CO17-38 P–M_O, T–M_{H2O} AND *P–T* PHASE EQUILIBRIA MODELS

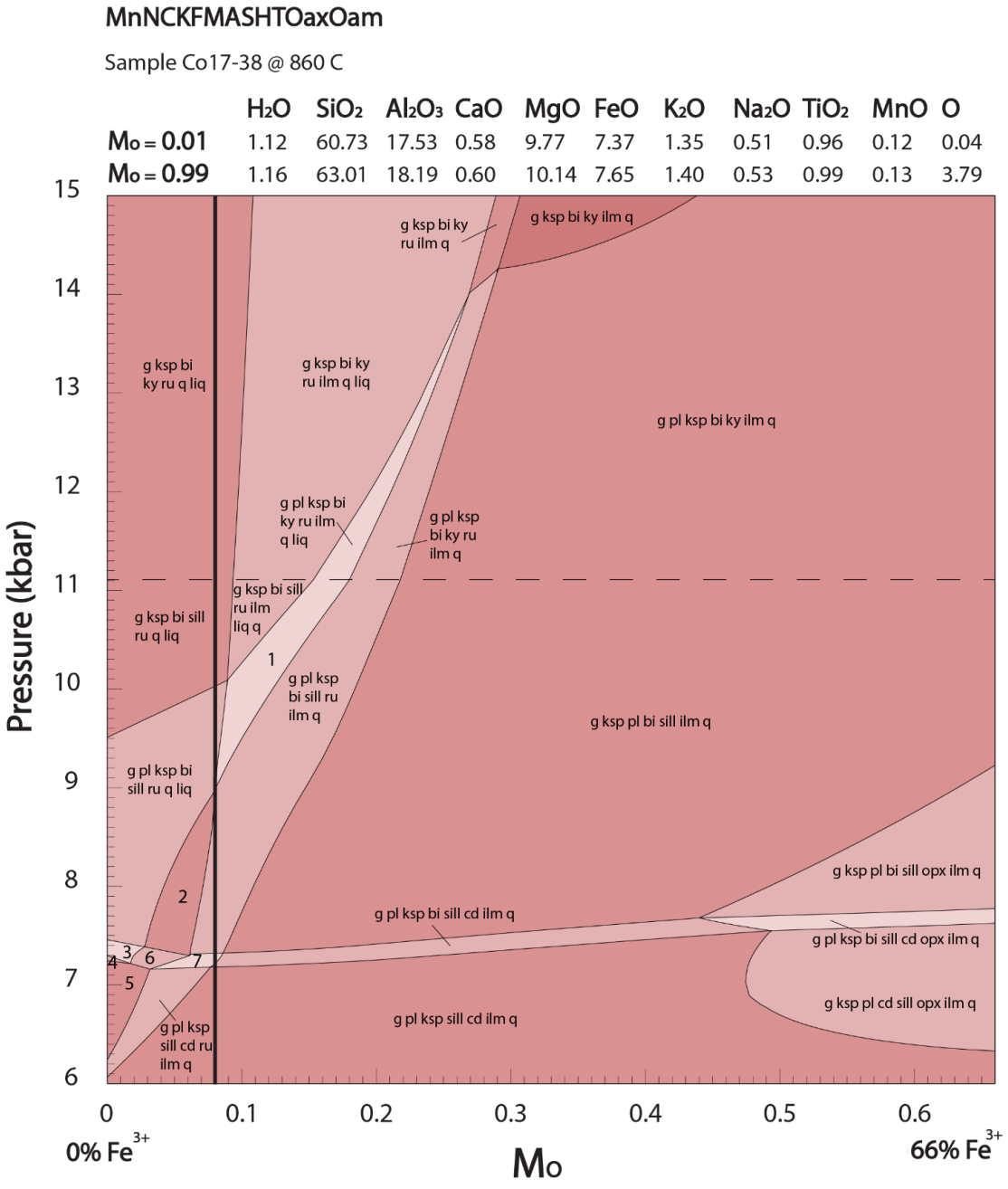

1. g pl ksp bi sill u ilm q liq
2. g pl ksp bi sill ru q
3. g pl ksp bi cd sill ru q liq
4. g pl ksp cd sill ru q liq
5. g pl ksp cd sill ru q
6. g pl ksp bi cd sill ru q
7. g pl ksp bi cd sill ru ilm q

***P–Mo* diagram for sample Co17-38. The black line at M = 0.08 corresponds to the composition at which the *T–*M_{H2O} and *P–T* diagrams were calculated for Co17-38. This is constrained by the presence of rutile without ilmenite.**

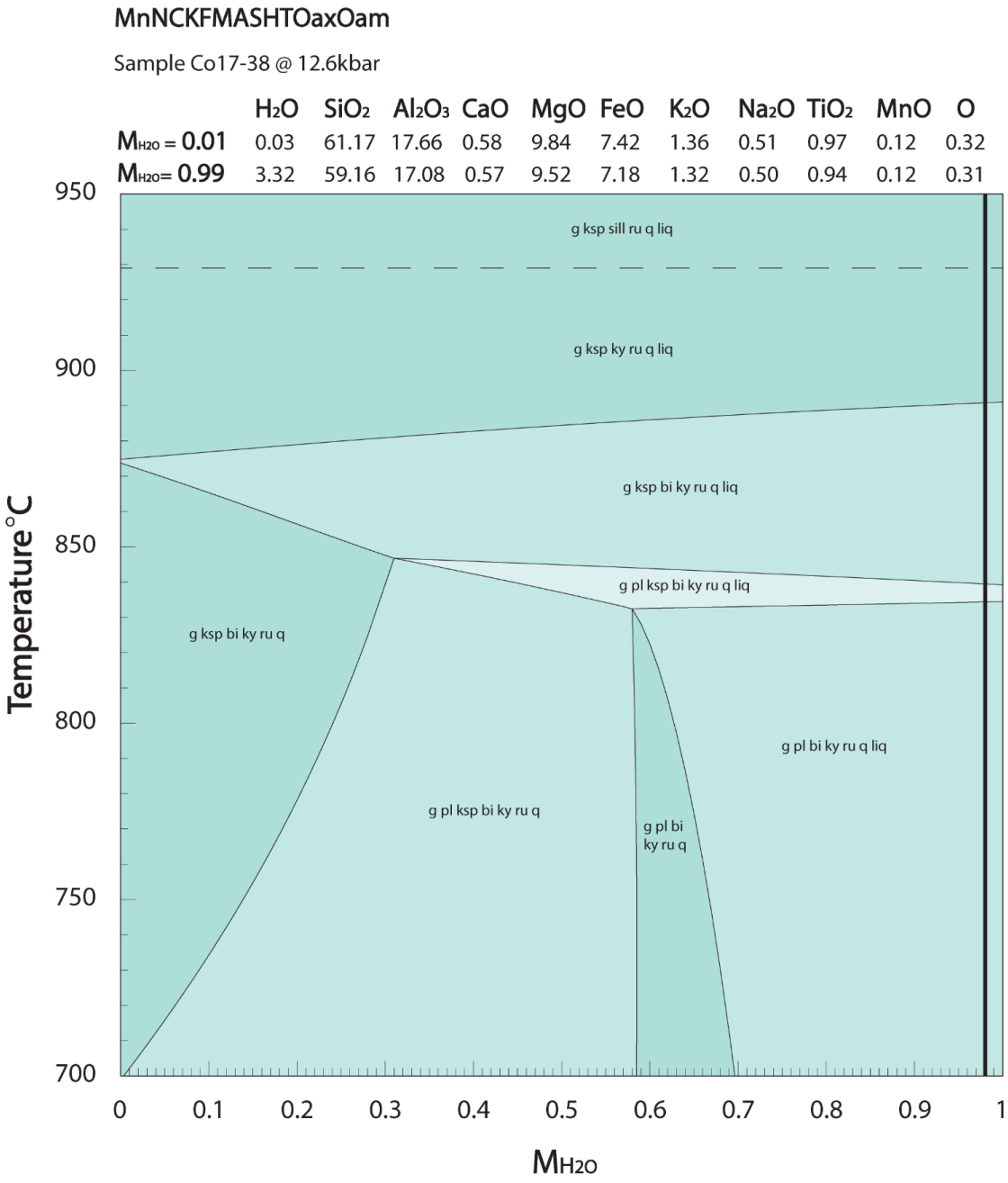

***T–M*$_{H2O}$ diagram for sample Co17-38. The black line at M = 0.98 corresponds to the composition at which the *P–T* diagram was calculated for Co17-38. This level of hydration is supported by EPMA data, where low halogen concentrations have been recorded in biotite.**

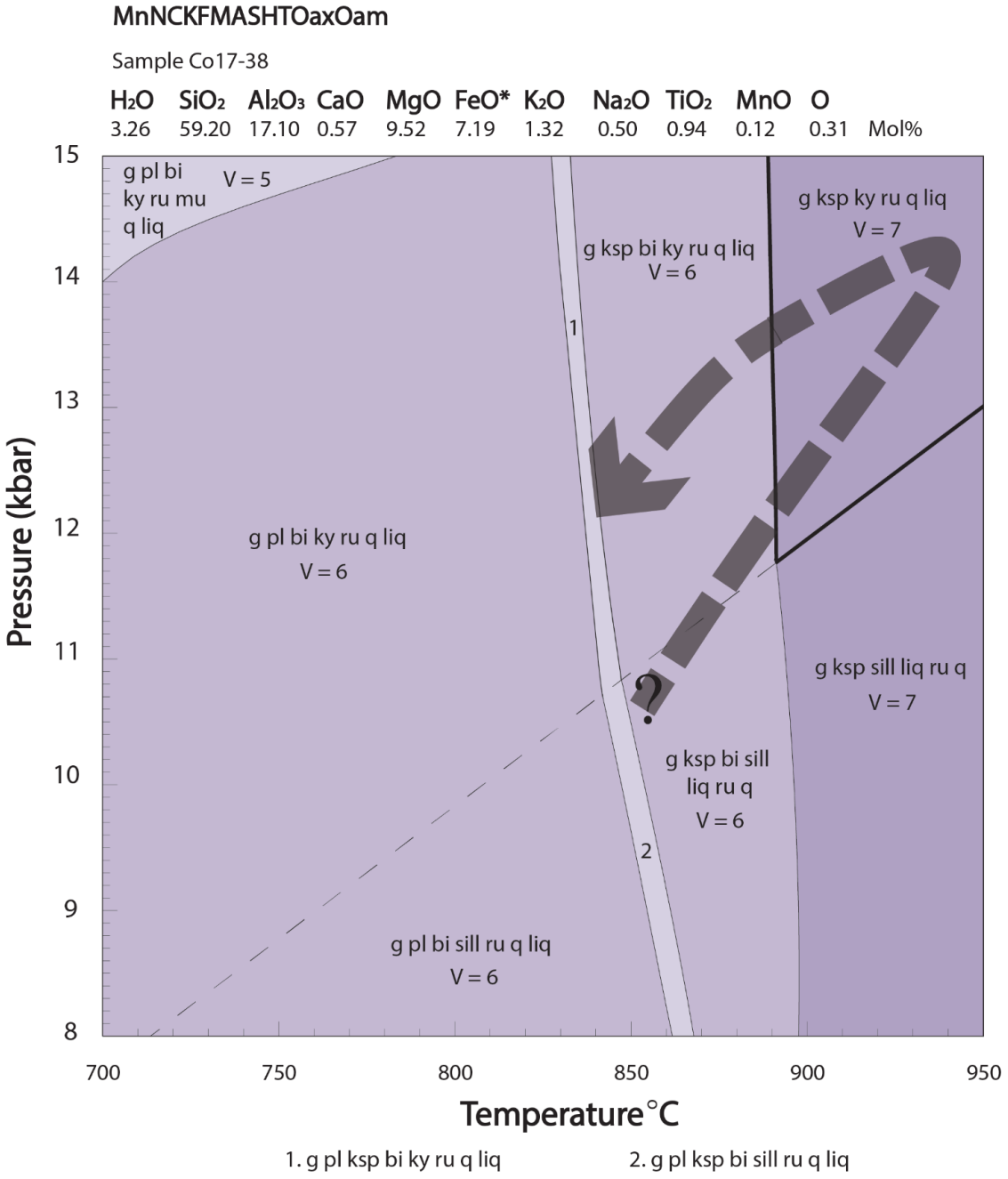

***P–T* diagram calculated for sample Co17-38, with the peak field highlighted by bold edges. An anticlockwise *P–T* path has been inferred, but is poorly constrained as the sample is too heavily retrogressed to accurately calculate the composition at the metamorphic peak.**

APPENDIX N: EXTENDED METHODS AND ASSUMPTIONS IN PEAK MODE CALCULATIONS

Peak mineral modes provided in Table 2 (main text) were calculated using EPMA data from near-peak sample Co17-37. This sample was interpreted as the best representation of the peak assemblage available, meaning that less extrapolation was required to calculate the modes of the peak metamorphic assemblage. A number of assumptions were made to calculate these mineral modes.
Assumptions and calculations are discussed below:

1. All biotite located in the matrix of the rock was formed at the expense of garnet, from a reaction between garnet and melt.
2. The most Mg-rich EPMA analysis of garnet is taken as the best representation of the composition of garnet at the metamorphic peak.

Therefore, based on assumptions 1 and 2, the proportion of garnet at the peak can be calculated by:
$MgO_{(bulk\text{-}rock)}$ / maximum $MgO_{(garnet)}$ (from EPMA data) = proportion of garnet at the metamorphic peak = 33.83wt% gt.

3. The LOI (loss on ignition) value provided by XRF geochemistry is purely attributed to biotite. This is assumed as it is (1) the only hydrous mineral in the assemblage (2) has virtually no halogens to contribute to the LOI value, and (3) the rock sample is from fresh quarry material and has no weathering or low-temperature alteration.

Therefore, based on assumption 3 and the average composition of biotite from EPMA analyses, 16.72wt% biotite was calculated for the preserved assemblage.

4. Assuming this amount of biotite and using the compositions calculated from EPMA data, collectively the biotite in the rock contains 1.53wt% K_2O.
5. As there is no EPMA data for K-feldspar, 14wt% K_2O is assumed for K-feldspar. This is a typical value if there is Na_2O in K-feldspar (Deer, Howie, & Zussman, 1992)

Therefore, based on assumptions 4 and 5, the proportion of K-feldspar can be calculated by:
$(K_2O_{(whole\text{-}rock)} - K_2O_{(biotite)}) / K_2O_{(K\text{-}feldspar)}$ = proportion of K-feldspar = 9.09wt% Ksp.

6. Following the assumption that biotite was produced in a reaction involving melt, it is assumed that:
   - the LOI value from geochemistry reflects the H_2O content of the melt
   - the K_2O in biotite came from the melt
   - the Na_2O in biotite came from the melt. However, 1.5% Na_2O is assumed to be in K-feldspar. This is a reasonable value provided there is no EPMA data for K-feldspar, while there is ample evidence for perthitic exsolution. Therefore $Na_2O_{(melt)} = Na_2O_{(bulk\text{-}rock)} - 1.5\%$.

Based on melt compositions calculated from THERMOCALC, which were converted from mole% to wt% for comparison with mineral chemistries, it is possible to estimate the amount of melt in three ways (i) using H_2O (ii) using K_2O and (iii) using Na_2O. However, because the concentrations of all three oxides vary within melt as a function of pressure and temperature, the most logical way to compute the melt proportion is to determine the point in *P–T* space where the proportion of melt calculated by the three different methods gives approximately the same melt proportion. This was found at ~13.2 kbar, 950ºC, where melt compositions from H_2O (18.34wt%), K_2O (20.46wt%) and Na_2O (21.39wt%) were calculated. Averaging these estimates suggests 20.07wt% melt at the peak.

7. It is assumed Al_2O_3 in the kyanite = 62wt%. This is slightly lower than usual, but its blue colour indicates that it contains Fe^{3+}, which substitutes for Al^{3+}.

Using the assumed kyanite composition from 7, and the sum of Al_2O_3 contained in the modal estimates previously calculated for garnet, K-feldspar and melt, the proportion of kyanite at the peak can be calculated. I.e.
$((Al_2O_{3(garnet)} + Al_2O_{3(K\text{-}feldspar)} + Al_2O_{3(melt)}) - Al_2O_{3(bulk\ rock)}) / Al_2O_{3(kyanite)}$ = proportion of kyanite at the peak = 35.57wt% ky.

Finally, quartz can be calculated by adding all the SiO_2 in the estimated modes for the peak, and subtracting that value from the bulk rock SiO_2. I.e.
$(SiO_{2(garnet)} + SiO_{2(K\text{-}feldspar)} + SiO_{2(kyanite)} + SiO_{2(melt)}) - SiO_{2(bulk\ rock)}$ = proportion of quartz at the peak = 3.2wt%.

The total value for the peak modes should not exceed 100%, especially since accessory phases are not considered in these calculations. However, based on the large number of assumptions that were made in these calculations, a total mode summation of 101.77% is quite reasonable. Furthermore, these calculations have produced peak mineral modes that are defendable, with overlapping modes in the peak field (Fig. 19). Although, assumptions could be reduced with EPMA data on K-feldspar and kyanite, which could potentially bring the total closer to 100%.